

INFORMATION TO USERS

This manuscript has been reproduced from the microfilm master. UMI films the text directly from the original or copy submitted. Thus, some thesis and dissertation copies are in typewriter face, while others may be from any type of computer printer.

The quality of this reproduction is dependent upon the quality of the copy submitted. Broken or indistinct print, colored or poor quality illustrations and photographs, print bleedthrough, substandard margins, and improper alignment can adversely affect reproduction.

In the unlikely event that the author did not send UMI a complete manuscript and there are missing pages, these will be noted. Also, if unauthorized copyright material had to be removed, a note will indicate the deletion.

Oversize materials (e.g., maps, drawings, charts) are reproduced by sectioning the original, beginning at the upper left-hand corner and continuing from left to right in equal sections with small overlaps.

Photographs included in the original manuscript have been reproduced xerographically in this copy. Higher quality 6" x 9" black and white photographic prints are available for any photographs or illustrations appearing in this copy for an additional charge. Contact UMI directly to order.

ProQuest Information and Learning
300 North Zeeb Road, Ann Arbor, MI 48106-1346 USA
800-521-0600

UMI[®]

University of Alberta

**DEPOSITION AND MODIFICATION OF GOLD NANOCRYSTALS ON
GLASSY CARBON ELECTRODES**

by

Michael Finot



A thesis submitted to the Faculty of Graduate Studies and Research in partial fulfillment of the requirements for the degree of Doctor of Philosophy

Department of Chemistry

Edmonton, Alberta, CANADA

Spring, 2000



National Library
of Canada

Acquisitions and
Bibliographic Services

395 Wellington Street
Ottawa ON K1A 0N4
Canada

Bibliothèque nationale
du Canada

Acquisitions et
services bibliographiques

395, rue Wellington
Ottawa ON K1A 0N4
Canada

Your file Votre référence

Our file Notre référence

The author has granted a non-exclusive licence allowing the National Library of Canada to reproduce, loan, distribute or sell copies of this thesis in microform, paper or electronic formats.

The author retains ownership of the copyright in this thesis. Neither the thesis nor substantial extracts from it may be printed or otherwise reproduced without the author's permission.

L'auteur a accordé une licence non exclusive permettant à la Bibliothèque nationale du Canada de reproduire, prêter, distribuer ou vendre des copies de cette thèse sous la forme de microfiche/film, de reproduction sur papier ou sur format électronique.

L'auteur conserve la propriété du droit d'auteur qui protège cette thèse. Ni la thèse ni des extraits substantiels de celle-ci ne doivent être imprimés ou autrement reproduits sans son autorisation.

0-612-59961-2

Canada

**University of Alberta
Library Release Form**

Name of Author: Michael Finot
Title of Thesis: Deposition and Modification of Gold
Nanocrystals on Glassy Carbon
Electrodes
Degree: Doctor of Philosophy
Year this Degree Granted: 2000

Permission is hereby granted to the University of Alberta Library to reproduce single copies of this thesis and to lend or sell such copies for private, scholarly, or scientific research purposes only.

The author reserves all other publication and other rights in association with the copyright in the thesis, and except as herein before provided, neither the thesis nor any substantial portion thereof may be printed or otherwise reproduced in any material form whatever without the author's prior written permission.



Michael Finot

6207 Thornaby Way N.W.
Calgary, Alberta, CANADA
T2K-5K7

April 10, 2000

*“You don’t have... to die and go to heaven,
or hang around to be born again,
just tune in to what this place has got to offer,
‘cause we may never be here again.”*

**E. Van Halen, A. Van Halen,
S. Hagar, and M. Anthony**

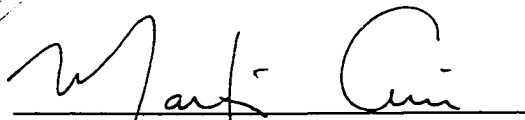
University of Alberta
Faculty of Graduate Studies and Research

The undersigned certify that they have read, and recommend to the Faculty of Graduate Studies and Research for acceptance, a thesis entitled "Deposition and Modification of Gold Nanocrystals on Glassy Carbon Electrodes" by Michael Finot in partial fulfillment of the requirements for the degree of Doctor of Philosophy.


Dr. Mark T. McDermott


Dr. Frederick F. Cantwell


Dr. D. Jed Harrison


Dr. Martin Cowie


Dr. Zhenghe Xu


Dr. Viola I. Birss, External
Examiner, University of Calgary

April 5th, 2000

*To my Mom...
who taught me that an education is important;
and my Dad...
who taught me that an education isn't everything.*

ABSTRACT

Chemically modified electrodes have been an intense area of research in the field of electroanalytical chemistry for the past 30 years. Since Lane and Hubbard first demonstrated that a platinum electrode could be chemically modified by the irreversible chemisorption of olefins, several diverse preparations of chemically modified electrodes have been described. Traditionally, there are four general methods which can be used to prepare chemically modified electrodes: 1) derivatization of existing surface functional groups, 2) non-specific adsorption of molecules, 3) coating with a thin polymer film, or 4) covalent attachment of chemical species. Electrode materials used in these preparations consist mainly of carbon or graphitic substrates, noble metals, or thin metal oxide films.

Another method, which has recently emerged, for the preparation of chemically modified gold electrodes is chemisorption of alkanethiols on gold. This approach provides an easy, well-characterized method for the preparation of self-assembled thin organic films. Unfortunately, an analogous self-assembly method does not exist for carbon/graphitic substrates. The objective of this research is to develop a method that takes advantage of gold/thiol chemistry in the preparation of chemically modified glassy carbon electrodes. Through the use of electrochemical metal deposition, a protocol for the deposition of small, well-dispersed, gold particle arrays on glassy carbon electrodes was established and

characterized. Results from scanning electron microscopy analysis show that it is possible to control the size and number density of electrochemically deposited gold particles by careful selection of either the deposition solution concentration or overpotential. These properties are also very sensitive to the electrode activation/pretreatment method employed. Gold deposits were then chemically modified using a variety of thiol molecules. Results from electrochemical and infrared studies show that it is possible to modify electrochemically deposited gold particles using self-assembly methods. A variety of functional groups have been attached to glassy carbon electrodes using this approach. Multiple deposition and modification steps have also been employed to attach more than one functional group to the glassy carbon surface. Thus, the self-assembly method can be used in the preparation of chemically modified carbon electrodes when coupled with gold deposition. It has also been demonstrated that it is possible to employ simple organic reactions to derivatize existing functional groups on chemically modified particles. This method has shown good potential for the attachment of biological molecules, such as enzymes and proteins, to carbon substrates.

ACKNOWLEDGMENTS

At this point I would like to take the opportunity to thank the many people who have helped me throughout my graduate career at the University of Alberta, and helped to make my stay at the U of A a pleasant one.

First of all, I would like to express my most sincere thanks and gratitude to my research advisor, Dr. Mark McDermott. Mark, regardless of what I write, I could never do justice to what a truly awesome boss, and great friend you have been to me. Thank you for providing me with an excellent opportunity to do research and learn from you. Thank you for your patience, as I am not always the easiest person to get along with, and thank you for the confidence you always displayed in me. It is an honor and a privilege for me to be your first grad student, and I will always be a proud member of the McDermott Group. Here's to many years of good friendship ahead, with you, and your wonderful family.

I would also like to express my most sincere thanks to my fellow group members, thank you for your help, and making the time I spent in the lab a most enjoyable one. Especially James, Truong, and Gregory, we have been together a long time and I will always look back fondly upon the truly good times we spent together. I am very fortunate to have had friends like you. An extra special thanks to Gregory; thank you for all of the intense work outs, you were an awesome coach. It was truly a blast to be able to train with you.

Thank you to my examining committee and faculty members of the Division of Analytical Chemistry, Department of Chemistry, University of Alberta. It was a privilege for me to be able to study under, teach for, and learn from such a distinguished group of scientists. Thank you also for your friendship.

Thank you to the Department of Chemistry, University of Alberta, and the Natural Science and Engineering Research Council of Canada (NSERC) for funding my research, as well as our group.

Thank you to the Department of Chemistry staff, and all members of the Glass Shop, Electronics Shop, and Machine Shop who were always willing to help me, no matter how small, or ridiculous the request.

Special thanks to George Braybrook, Department of Earth and Atmospheric Sciences, for his great work in obtaining the SEM images of gold particles. To Glen Fitzpatrick of the Alberta Microelectronics Corporation for numerous gold substrates, and the multitude of other kind and generous favors he provided for me, as well as my fellow group members. Glen, thank you for your generosity and patience, you were always willing to help me out and I will always be grateful for that. To Marc Porter, Iowa State University, for the gold substrates used in the tapping-mode studies, and the 16-MHDA, ODT- d_{37} , and FCUT adsorbates.

A special thank you also goes out to all of the wonderful friends I have made during my graduate career. Thanks for helping smooth out the bumps. I will not mention any names for fear of forgetting somebody, but you guys certainly know who you all are, thanks! Also, this way nobody can be contacted in the future for details pertaining to some wild, and highly exaggerated drinking story.

To Brian and Corrina, thank you for your generous hospitality during my final days at the U of A. You guys could never imagine how much you helped me out and I am very appreciative of this.

To the Tamburrino family, thank you for the many wonderful meals we shared together. You made me feel like family, when I was away from mine.

None of this would have ever been possible without the generous love, encouragement and support provided to me by my family. To all of my aunts, uncles, and cousins, both here and abroad; thank you for always taking the time to inquire about me, ask me how things are going, and for your kind words of encouragement.

To my loving Nonna and Nono, thank you for the generous love, encouragement, and support you have always shown me. Grazie delle vostre preghiere, il vostro affetto, la vostra generosità e i bes.

To my awesome brother Mark, thank you for always being there for me, and for your constant love, generosity, encouragement and support. Don't ever doubt the fact that I am extremely proud of you, and how truly fortunate I feel to have a brother like you. Your personality is golden, and the personal qualities you possess could never be attained through any degree of schooling or university.

Finally, a very emotional thank you to my Mom and Dad. Without your endless love and support I would not be a fraction of the person I am today. It is because of you that I have been able to achieve the success I have enjoyed in my life. Thank you for the countless opportunities you have provided me with that have allowed me to become the person I am today, and will allow me to become tomorrow. And finally, thank you for your never-ending encouragement, especially you Mom. For all of the times I have freaked out, and been stressed out, you have always been there to listen to me and make me feel better. When I look to the sky but can't see through the clouds, you show me the brightest star. When I think of giving up because I'm having my doubts, you tell me I have come so far; for this I will always be grateful. Mom and Dad, I love you very much, and thanks for everything you have ever done for me.

TABLE OF CONTENTS

CHAPTER I: GENERAL INTRODUCTION

Electrochemical Methods	1
Carbon Electrodes	16
Chemically Modified Electrodes	20
Research Objectives	36
References	39

CHAPTER II: CHARACTERIZATION OF ELECTROCHEMICALLY DEPOSITED GOLD PARTICLES ON GLASSY CARBON ELECTRODES

Introduction	48
Experimental	58
Results and Discussion	60
Conclusions	87
References	88

CHAPTER III: EFFECTS OF SURFACE OXIDE GROUPS ON THE ELECTROCHEMICAL DEPOSITION OF GOLD PARTICLES ON GLASSY CARBON ELECTRODES

Introduction	93
Experimental	100
Results and Discussion	102
Conclusions	118
References	119

CHAPTER IV: MODIFICATION OF SUPPORTED GOLD PARTICLES USING ALKANETHIOL SELF-ASSEMBLED MONOLAYERS

Introduction	123
Experimental	132
Results and Discussion	134
Conclusions	156
References	158

CHAPTER V: MODIFICATION OF SUPPORTED GOLD PARTICLES USING ω -TERMINATED ALKANETHIOL SELF-ASSEMBLED MONOLAYERS

Introduction	162
Experimental	167
Results and Discussion	170
Conclusions	194
References	195

CHAPTER VI: HIGH-RESOLUTION CHEMICAL MAPPING OF SURFACE BOUND FUNCTIONAL GROUPS WITH TAPPING-MODE SCANNING PROBE MICROSCOPY

Introduction	199
Experimental	202
Results and Discussion	203
Conclusions	209
References	210

CHAPTER VII: SUMMARY, CONCLUSIONS AND FUTURE WORK

Summary and Conclusions	212
Suggestions for Future Work	215
References	215

LIST OF TABLES

	Page
Table 2.1 Surface area determination of electrochemically deposited gold particles on GC via oxide reduction analysis, effect of deposition solution concentration.	74
Table 2.2 Surface area determination of electrochemically deposited gold particles on GC via oxide reduction analysis, effect of deposition overpotential.	74
Table 2.3 Results from scanning electron micrograph analysis for electrochemically deposited gold particles, effect of deposition solution concentration.	86
Table 2.4 Results from scanning electron micrograph analysis for electrochemically deposited gold particles, effect of deposition overpotential.	86
Table 3.1: Effect of electrode pretreatment on gold particle deposition, $[\text{AuCl}_4^-] = 100 \mu\text{M}$, $\eta = -800 \text{ mV}$.	105
Table 3.2 Results from scanning electron micrograph analysis for electrochemically deposited gold particles, effect of electrode pretreatment, $[\text{AuCl}_4^-] = 100 \mu\text{M}$, $\eta = -800 \text{ mV}$.	107
Table 3.3: Effect of electrode pretreatment on gold particle deposition and adhesion, $[\text{AuCl}_4^-] = 100 \mu\text{M}$, $\eta = -800 \text{ mV}$.	116
Table 4.1 Band positions and peak widths for the spectra shown in Figure 4.2. ODT on bulk gold film and chemically modified gold particles.	138
Table 4.2 ΔE_p values for catechol voltammetry on various electrode materials.	149
Table 4.3 ΔE_p values for catechol voltammetry on a single electrode, resulting from multiple gold particle deposition and modification steps.	153

LIST OF FIGURES

	Page
Figure 1.1 Schematic representations of (A) HOPG, and (B) GC.	18
Figure 1.2 Application of SAMs to GC electrodes.	37
Figure 1.3 Derivatizing GC with multiple functional groups.	38
Figure 2.1 Cyclic voltammetry of 200 μM AuCl_4^- in 0.5 M H_2SO_4 at a polished GC electrode, $v = 100$ mV/s.	61
Figure 2.2 Current response to a potential step of 1100 to 0 mV for a polished GC electrode, 200 μM AuCl_4^- in 0.5 M H_2SO_4 .	62
Figure 2.3 Representative current transients for gold deposition on GC from solutions of varying AuCl_4^- concentration, $\eta = -800$ mV.	64
Figure 2.4 Representative current transients for gold deposition on GC at varying overpotentials, $[\text{AuCl}_4^-] = 200$ μM .	66
Figure 2.5 Effect of oxide reduction current on a polycrystalline gold electrode as a function of anodization potential in 0.5 M H_2SO_4 .	69
Figure 2.6 Effect of oxide reduction current on a polycrystalline gold electrode as a function of anodization time in 0.5 M H_2SO_4 .	70
Figure 2.7 Linear sweep voltammograms for the reduction of gold surface oxides from electrochemically deposited gold particles. Deposition solution concentration series for $\eta = -800$ mV, $v = 200$ mV/s.	72
Figure 2.8 Linear sweep voltammograms for the reduction of gold surface oxides from electrochemically deposited gold particles. Overpotential series for $[\text{AuCl}_4^-] = 100\mu\text{M}$, $v = 200$ mV/s.	73
Figure 2.9 Linear sweep voltammograms for the stripping of underpotentially deposited lead from electrochemically deposited gold particles. Deposition solution concentration series for $\eta = -800$ mV, $v = 200$ mV/s.	77

Figure 2.10 Linear sweep voltammograms for the stripping of underpotentially deposited lead from electrochemically deposited gold particles. Overpotential series for $[\text{AuCl}_4^-] = 100 \mu\text{M}$, $v = 200 \text{ mV/s}$.	78
Figure 2.11 Scanning electron micrographs of electrochemically deposited gold particles on GC, $\eta = -800$.	81
Figure 2.12 Scanning electron micrographs of electrochemically deposited gold particles on GC, $[\text{AuCl}_4^-] = 100 \mu\text{M}$.	84
Figure 3.1: Schematic representation of a polishing layer, an EGO layer, and a surface oxide layer.	97
Figure 3.2 Cyclic voltammograms for electrochemically deposited gold on various GC substrates, $v = 100 \text{ mV/s}$, $[\text{AuCl}_4^-] = 100 \mu\text{M}$.	103
Figure 3.3 Scanning electron micrographs of electrochemically deposited gold particles on normal polished GC, $\eta = -800 \text{ mV}$, $[\text{AuCl}_4^-] = 100 \mu\text{M}$.	108
Figure 3.4 Scanning electron micrographs of electrochemically deposited gold particles on oxide free GC, $\eta = -800 \text{ mV}$, $[\text{AuCl}_4^-] = 100 \mu\text{M}$.	110
Figure 3.5 Scanning electron micrographs of electrochemically deposited gold particles on 1.0 M NaOH ECP GC, $\eta = -800 \text{ mV}$, $[\text{AuCl}_4^-] = 100 \mu\text{M}$.	112
Figure 3.6 Scanning electron micrographs of electrochemically deposited gold particles on 0.1 M H_2SO_4 ECP GC, $\eta = -800 \text{ mV}$, $[\text{AuCl}_4^-] = 100 \mu\text{M}$.	113
Figure 4.1 Scanning electron micrographs of electrochemically deposited gold particles on GC, $\eta = -800 \text{ mV}$.	135
Figure 4.2 Infrared reflectance spectra of ODT on a bulk gold film and electrochemically deposited gold particles, $\eta = -800 \text{ mV}$, $[\text{AuCl}_4^-] = 1 \text{ mM}$.	139

Figure 4.3 Linear sweep voltammograms for the reduction of gold surface oxides from chemically modified gold particles, $\eta = -800$ mV, $[\text{AuCl}_4^-] = 100$ μM , $\nu = 200$ mV/s.	141
Figure 4.4 Linear sweep voltammograms for the reduction of gold surface oxides from chemically modified bulk gold films, $\nu = 200$ mV/s.	144
Figure 4.5 Cyclic voltammograms for catechol on various electrode materials, $\nu = 200$ mV/s.	148
Figure 4.6 Cyclic voltammograms for catechol on chemically modified gold particles gold particles on GC, $\nu = 200$ mV/s, $\eta = -800$ mV, $[\text{AuCl}_4^-] = 100$ μM .	150
Figure 4.7 Cyclic voltammograms for catechol on electrochemically deposited on GC, $\eta = -800$ mV, $\nu = 200$ mV/s.	152
Figure 4.8 Cyclic voltammograms for catechol on chemically modified gold particles, multiple deposition and modification steps, $\eta = -800$ mV, $[\text{AuCl}_4^-] = 100$ μM , $\nu = 200$ mV/s.	154
Figure 5.1: Cyclic voltammogram of a NTP modified gold film electrode, initial reduction of the nitro group.	171
Figure 5.2: Cyclic voltammogram of a NTP modified gold film electrode, further oxidation of the amino group.	173
Figure 5.3: Cyclic voltammogram of NTP modified gold particles on GC.	175
Figure 5.4: IRRAS spectra of (a) a NTP modified bulk gold film, and (b) NTP modified gold particles on GC.	176
Figure 5.5: Cyclic voltammograms of FCUT adsorbed to polished GC Electrodes, before and after benzene rinse.	178
Figure 5.6: Cyclic voltammogram of FCUT modified gold particles, and a polished GC electrode.	179
Figure 5.7: Scan rate dependence study for a FCUT modified bulk gold film and supported gold particles.	181

Figure 5.8: Charge due to ferrocene oxidation as a function of $[\text{AuCl}_4^-]$ concentration.	183
Figure 5.9: Cyclic voltammogram of a FCUT modified gold film electrode.	184
Figure 5.10: Cyclic voltammograms of FCUT modified gold particles on GC. Before and after exposure to a potential step in 0.5 M H_2SO_4 supporting electrolyte.	186
Figure 5.11: Cyclic voltammogram of FCUT modified gold particles On GC after exposure to a second gold deposition step.	188
Figure 5.12: Cyclic voltammetry of FCUT modified gold particles After exposure to a second gold deposition step and subsequent Modification with NTP.	190
Figure 5.13: IRRAS spectra of ODT modified gold particles and MUDA modified gold particles on GC.	192
Figure 5.14: IRRAS spectra of cytochrome c attached to MUDA modified gold particles on GC, and activated MUDA modified particles	193
Figure 6.1 Schematic diagram of partial bilayers formed at Au(111) for SA a HDDA top layers.	201
Figure 6.2 Topographic (A, z-scale = 10 nm) and phase contrast (B, z-scale 20°) tapping-mode SFM images of a MHDA/SA partial bilayer.	204
Figure 6.3 Topographic (C, z-scale = 15 nm) and phase contrast (D, z-scale 20°) tapping-mode SFM images of a MHDA/HDDA partial bilayer.	206
Figure 6.4 Topographic (A, z-scale = 30 nm) and phase contrast (B, z-scale 30°) tapping-mode SFM images of a MHDA/SA partial bilayer.	208

LIST OF SYMBOLS

Roman Symbols

A	area
C_j^*	bulk concentration of electroactive species j
D_j	diffusion coefficient of electroactive species j
E	potential
E°	standard potential
$E^{\circ'}$	formal potential
E_{pa}	anodic peak potential
E_{pc}	cathodic peak potential
ΔE_p	$E_{pa} - E_{pc}$ in cyclic voltammetry
F	Faraday constant, 96485 C/mol
f	F/RT
f_o	resonance frequency
i	current
i_a	anodic component current
i_c	cathodic component current
i_d	diffusion limited current
i_{max}	current maximum, potential step
i_p	peak current
i_{pa}	anodic peak current
i_{pc}	cathodic peak current
j	current density
k	rate constant for a homogeneous reaction
k°	rate constant for a heterogeneous reaction
k_b	heterogeneous rate constant for oxidation
k_f	heterogeneous rate constant for reduction

L_a	intraplanar microcrystallite size
L_c	interplaner microcrystallite size
N	number density, metal particles
n	number of electrons
Q_{obs}	charge
R	gas constant
r_o	electrode radius
t	time
t_c	contact time
t_{max}	time that corresponds to current maximum, potential step
v_b	“backward” homogeneous reaction rate
v_f	“forward” homogeneous reaction rate
x	distance

Greek Symbols

α	transfer coefficient
β	1 - α
$\Delta\phi$	phase shift
v	scan rate
Γ_j	surface coverage of an electroactive adsorbate j
Γ_{sat}	saturation surface coverage
η	overpotential
ρ	density
Ψ	dimensionless parameter in CV

LIST OF ABBREVIATIONS

AFM	atomic force microscopy
CGA	chlorogenic acid
CME	chemically modified electrode
Cyc	cytochrome c
DCC	dicyclohexylcarbodiimide
DDT	dodecanethiol
DHB	dihydroxybenzaldehyde
DMF	dimethylformamide
ECP	electrochemical pretreatment
EDC	1-ethyl-3-[(dimethylamino)propyl] carbodiimide
EGO	electrochemical graphitic oxide
FCUT	11-ferrocene(carboxy) undecanethiol
FOA	free oscillation amplitude
FTIR	fourier transform infrared spectroscopy
FWHM	full width half maximum
GC	glassy carbon
hCG	human chorionic gonadotropin
HDDA	hexadecanedioic acid
HDT	hexadecane thiol
HOPG	highly ordered pyrolytic graphite
HT	hexanethiol
IA	imaging amplitude
IRRAS	infrared reflection absorption spectroscopy
MCT	mercury-cadmium-telluride
MHDA	16-mercaptohexadecanoic acid
MPC	monolayer protected cluster

MSEF	mean squared electric field
MUDA	11-mercaptoundecanoic acid
NADH	nicotinamide adenine dinucleotide
NHS	N-hydroxysuccinimide
NTP	4-nitrothiophenol
NTB	naphthoyl-Toluidine Blue O
ODT	octadecanethiol
OTF	organic thin film
PBS	phosphate buffered saline solution
PEM	proton exchange membrane
PG	pyrolytic graphite
PQQ	pyrroloquinolinequinone
SA	stearic acid
SDS	sodium dodecylsulfate
SEM	scanning electron microscopy
SFM	scanning force microscopy
SOD	superoxide dismutase
SPM	scanning probe microscopy
TM-SFM	tapping-mode scanning force microscopy
UPD	underpotential deposition
XPS	x-ray photoelectron spectroscopy

CHAPTER I

GENERAL INTRODUCTION

Electrochemical Methods.

Electroanalytical chemistry involves the use of an electrode to study an analyte in solution. Generally, the properties of the analyte induce a change in potential, the flow of current, or the accumulation of charge at the electrode surface. As the description implies, two important parameters in this process are potential and current, either of which can be held constant or varied during the course of an electrochemical experiment. Electrochemical behavior of such a species can be examined when the analyte is introduced into an electrochemical cell.

Two general types of electrochemical experiments can be performed; these are described as potentiometry or voltammetry. Potentiometry involves the measurement of cell potentials that develop between two electrodes in response to the concentration of the analytes. Measurements are made at currents that approach zero and in the complete absence of concentration polarization. Voltammetry, on the other hand, involves the measurement of current that arises as a result of the oxidation or reduction of an analyte by an applied potential. Also, measurements are made under the condition of complete concentration polarization. This is an important distinction that will be elaborated upon shortly. Use of voltammetric techniques is limited to the study of electroactive species, meaning that the analyte of interest must be able to take part in electron transfer reactions with the working electrode. Such species are often generically referred to as redox species. The main focus of this introduction is based on the discussion of voltammetric methods.

In voltammetric experiments, electrodes are immersed into a dilute solution of the redox species in the presence of a relatively high concentration of inert supporting electrolyte. Supporting electrolyte, such as potassium chloride, is used to render the solution conductive, thus minimizing the effects of solution resistance. If the solution possesses a relatively high resistance, then a significant voltage drop, also referred to as iR drop, will develop across the solution. This will result in errors in the applied potential at the working electrode. Furthermore, the effects of solution resistance may be mistaken for kinetic effects, rendering misleading information about the electrode mechanism [1].

The most common type of electrochemical cell configuration used in voltammetry experiments is the three-electrode cell. Electrodes consist of a working electrode, an auxiliary electrode, and a reference electrode. The working electrode is the electrode at which electron transfer with the redox species of interest occurs. The auxiliary electrode serves to conduct current between itself and the working electrode in order to maintain a constant potential at the working electrode. The auxiliary electrode also serves to eliminate current flow through the reference electrode and this prevents undesirable fluctuations in the potential of the reference electrode. The reference electrode serves as a potential reference for the electrochemical cell and accompanying instrumentation. In order to discuss these electrochemical experiments in a more quantitative manner, the concepts and nomenclature of Bard and Faulkner are employed [2].

A redox reaction may be represented using the following general expression.



O represents the oxidized form of the redox species and R the reduced form. n represents the number of electrons needed to reduce one molecule of O to R , and

vice versa. Reaction {1.1} has both forward and backward paths, as indicated by the double arrow, and in subsequent equations the subscripts f and b will be used. Forward and reverse reactions proceed at specific, but not necessarily equal, rates that must be proportional to the concentration of O and R at the surface of the electrode. These concentrations are expressed in terms of a specific distance from the electrode surface at a specific point in time during the experiment using the convention $C_O(x,t)$, in units of mol/cm^3 . x represents the distance from the electrode surface and t the elapsed time. To represent the concentration of O at the surface of the electrode x is defined as zero. The rates of reaction of the forward and reverse process are also related to the concentrations of O and R at the surface of the electrode via the heterogeneous rate constants of the two reactions, k_f and k_b respectively. Heterogeneous refers to the fact that an analyte in solution participates in an electron transfer reaction with a solid electrode surface. These reaction rates can be expressed mathematically as,

$$v_f = k_f C_O(0,t) = \frac{i_c}{nFA} \quad \{1.2\}$$

$$v_b = k_b C_R(0,t) = \frac{i_a}{nFA} \quad \{1.3\}$$

where F is Faraday's constant and A is the area of the working electrode in cm^2 . The forward reaction is a reduction and i_c is the cathodic current proportional to v_f . Conversely, the reverse process is an oxidation and i_a is the anodic current proportional to v_b . Currents are expressed in Amperes. It is important to recognize that if both O and R species are present at the electrode surface then both reactions will occur simultaneously. Therefore, the magnitude of the forward and reverse reaction rates will offset each other and a net current is observed.

Employing equation {1.2} and {1.3} one can easily derive an expression for the net current.

$$i = i_c - i_a = nFA[k_f C_O(0,t) - k_b C_R(0,t)] \quad \{1.4\}$$

From this expression it becomes obvious that the net current is proportional to the concentration of both O and R species at the electrode surface, in the absence of applied potentials.

In order to apply these concepts to a situation in which the potential of the working electrode is varied in a controlled manner, it is important to understand how the rate constants depend on the applied potential. The following equations represent the potential dependent rate constants of the forward and reverse reactions,

$$k_f = k^o e^{-\alpha n f (E - E^o')} \quad \{1.5\}$$

$$k_b = k^o e^{\beta n f (E - E^o')} \quad \{1.6\}$$

where $f = F/RT$, k^o is the standard rate constant, α and β ($\beta = 1 - \alpha$) are the cathodic and anodic transfer coefficients that represent the asymmetry of the energy barrier, and $(E - E^o')$ is the overpotential, where E^o' refers to the standard potential of the reaction. These expressions can be simplified by employing η in the place of $(E - E^o')$ to represent the applied overpotential. Substitution of the potential dependent rate constants into equation {1.4} yields the complete current-potential characteristic.

$$i = nFAk^o [C_O(0,t) e^{-\alpha n f \eta} - C_R(0,t) e^{-\beta n f \eta}] \quad \{1.7\}$$

When the applied potential, E , is not the equilibrium potential, $E^{o'}$, there will be a net current flow. Net current will be either anodic or cathodic, depending on the magnitude of η . Equation {1.7} is an important relationship, which can be used to mathematically treat any problem that requires heterogeneous electron transfer to be taken into account. However, such treatments are nearly always difficult.

Fortunately, in setting up an electrochemical experiment we are afforded the option of designing experiments such that the current-potential characteristic may be simplified to yield a more practical form. Several special cases have been identified [2, 3]: a) large-amplitude controlled-potential techniques, b) small-amplitude controlled-potential techniques, c) reversible (Nernstian) electrode processes, and d) totally irreversible electrode processes. In small-amplitude controlled potential techniques very small potential perturbations, typically on the order of 10 to 20 mV, are employed to induce small perturbations in the concentration profile of redox species at the electrode surface. Under these conditions the applied potential and resulting current are linearly related. This approach is based on the principle that a complex curve can be approximated by a series of small straight-line segments; the smaller the segments, the smaller the deviation from theoretical behavior. For reversible redox species, (i.e. $k^o \rightarrow \infty$) the current-potential characteristic simplifies to the Nernst equation.

$$E = E^{o'} + \frac{RT}{nF} \ln \frac{C_O(0,t)}{C_R(0,t)} \quad \{1.8\}$$

When electron transfer rates are very slow, as in irreversible systems, the anodic and cathodic terms of equation {1.7} are never simultaneously significant. That is, activation in one direction is so dominant (large overpotential) that the reverse reaction is totally inhibited. Such a system is said to display Tafel behavior and

can be described using the Tafel equation. Further discussion is focused on large-amplitude controlled-potential techniques and electrochemical reversibility.

Electrochemical methods employed during the course of this research consisted exclusively of large-amplitude controlled-potential techniques. These methods differ from small-amplitude controlled-potential techniques in that the applied overpotential is so large that the concentration of the redox species at the surface of the working electrode becomes essentially zero. Under these conditions, the observed current at the working electrode is totally controlled by mass transfer or diffusional processes. This category can be further subdivided into two subcategories: potential step techniques and potential sweep techniques. The major difference between these two methods resides in the nature of the excitation waveform that is applied to the working electrode.

Potential Step Methods. In potential step experiments, the excitation waveform consists of a potential step from an initial potential at which no electrolysis occurs, E_1 , to a final potential, E_2 , at which the redox species cannot exist at the electrode surface without being oxidized or reduced. Considering expression {1.1}, application of a sufficiently negative potential step ($E_1 > E_2$) to the working electrode will cause all of O to be reduced to R . This induces concentration polarization at the electrode surface in which $C_O(0, t) = 0$. Thus, a concentration gradient is established between a thin film of solution at the electrode surface and the bulk solution. This thin film is also referred to as the diffusion layer. The concentration gradient propagates outwards from the electrode surface into the bulk solution as time lapses. Current, due to the reduction of O to R , is monitored as a function of time for the duration of the potential step. Hence, this type of experiment is called chronoamperometry. Current is dictated by how efficiently O can diffuse from the bulk solution to the electrode surface, therefore, the observed current is defined as the mass transport limited current. As the diffusion layer becomes thicker with time it will take

progressively longer for molecules of O to diffuse to the electrode surface. Thus, the current is observed to decay with time. Duration of any one experiment is typically on the order of a few seconds. At longer times, perturbations due to convection or mechanical vibration tend to disrupt the concentration gradient at the electrode surface. Also, at longer times, the diffusion layer thickness approaches dimensions on the order of the electrode diameter. At this point the assumption of planar diffusion is no longer valid and current becomes independent of time. Since only a very small volume of solution is actually employed for any one experiment, the solution can be stirred, such that the bulk concentration of O is restored at the electrode surface. Therefore, several experiments can be performed using the same experimental set up.

In potential step experiments, electrode kinetics no longer influence the current at the electrode surface and ironically equation {1.7} is not needed at all. Current is independent of potential, provided a sufficiently large overpotential is employed, ensuring that experiments are performed in the mass transport limited region. Therefore, calculation of the diffusion limited current, i_d , and the concentration gradient, $C_O(x,t)$, involves searching for solutions of the linear diffusion equation,

$$\frac{\partial C_O(x,t)}{\partial t} = D_O \frac{\partial^2 C_O(x,t)}{\partial x^2} \quad \{1.9\}$$

adhering to the following boundary conditions:

$$C_O(x,0) = C_O^* \quad \{1.10\}$$

$$x \lim_{\infty} C_O(x,t) = C_O^* \quad \{1.11\}$$

$$C_O(0,t) = 0 \quad (\text{for } t > 0) \quad \{1.12\}$$

Equation {1.10} simply states that the solution is homogeneous and only contains the oxidized form of the redox species. Equation {1.11} states that the concentration of the bulk solution far away from the electrode surface at any time during the course of the experiment remains unchanged; this is referred to as the semi-infinite condition. Equation {1.12} states that upon application of the potential step program to the electrode, the concentration of the oxidized form of the analyte at the electrode surface becomes essentially zero and all of O has been converted to the reduced form. Thus, the experiment is performed in the mass transport limited region. At this point, the observed current is dependent upon diffusional mass transport of O to the electrode surface. This is the crux of the potential step experiment. Solution of equation {1.9}, adhering to the given boundary conditions, yields the following current-time response,

$$i(t) = i_d(t) = \frac{nFAD_i^{1/2}C_i^*}{\pi^{1/2}t^{1/2}} \quad \{1.13\}$$

known as the Cottrell equation, where C^* is the bulk concentration of electroactive species in solution and D is the diffusion coefficient. The subscript i can be O or R to indicate whether the redox species is in its oxidized or reduced form. The mathematics of this transformation are beyond the scope of this introduction; for a more detailed description one should consult Bard and Faulkner [2]. However, it is important to note that the observed current will vary as a function of $t^{-1/2}$ and this is characteristic of Cottrellian behavior.

The Cottrell equation is a very important equation in that it allows one to determine the geometric area of a working electrode provided that the diffusion coefficient of the redox species of interest is known. Similarly, one may determine the diffusion coefficient using an electrode of known area. The

calculations require generation of a Cottrell plot, a plot of i_d as a function of $t^{-1/2}$. Cottrell plots should be linear with a slope of:

$$m = \frac{nFAD_i^{1/2}C_i^*}{\pi^{1/2}} \quad \{1.14\}$$

Determination of the slope allows one to calculate the area of the electrode or diffusion coefficient of the redox species.

Potential Sweep Methods. In a potential sweep experiment, the excitation waveform is initiated at a potential at which no electrolysis occurs, E_1 . The potential is then swept in linear fashion to a final potential, E_2 , at which the redox species cannot exist at the electrode surface without being oxidized or reduced. The rate of change of the applied potential is defined as the scan rate and is given the symbol v . Scan rates are typically expressed in units of mV/s. Once the final potential has been reached the direction of the potential scan is reversed and the potential is swept back toward E_1 . Due to the nature of the potential program this technique is known as cyclic voltammetry. Cyclic voltammetry is a reversal technique and E_2 is referred to as the switching potential. Current is monitored as a function of potential, or time, and the resulting current transient is called a cyclic voltammogram. Experiments in which the potential scan is stopped at the switching potential are simply referred to as linear sweep voltammograms.

Due to the nature of the excitation waveform, interesting behavior is observed at the electrode/solution interface. Referring back to equation {1.1}; a cyclic voltammetry experiment is initiated at a potential at which reduction of O to R does not occur. As the potential is scanned negatively a cathodic peak current, i_{pc} , is observed at a potential, E_{pc} , between E_1 and E_2 . At potentials positive of E_{pc} , O is reduced, but not so effectively that its surface concentration becomes zero. Thus, the current continues to increase until a peak at E_{pc} is observed. At all

potentials negative of E_{pc} the onset of diffusional mass transport is observed and the current decays as a function of $t^{-1/2}$, as in chronoamperometry. The switching potential should be chosen such that oxidation of R back to O does not occur. A useful guideline quoted in the literature states that provided the switching potential is not less than $35/n$ mV past the peak current, then all subsequent curves should have the same relative shape [4]. As the potential is scanned positively an anodic peak current, i_{pa} is observed at a potential, E_{pa} between E_2 and E_1 . At potentials negative of E_{pa} , R is oxidized, but not so effectively that its concentration becomes zero, and again the current continues to increase until a peak at E_{pa} is observed. At potentials positive of E_{pa} diffusional mass transport of R to the electrode surface is observed and again the current decays as a function of $t^{-1/2}$. Return of the potential to E_1 signifies the end of the experiment or the start of another potential cycle. For a solution phase redox species, the peak current can be determined using the following expression, for a reversible system.

$$i_p = (2.69 \times 10^5) n^{3/2} A D_o^{1/2} v^{1/2} C_o^* \quad \{1.15\}$$

From this relationship it is important to note that the peak current is proportional to the square root of scan rate.

Referring back to the discussion of concentration gradients, as in the potential step experiment, one can visualize the build up of a concentration gradient of R at the electrode surface as the potential is swept from E_1 to E_2 . Conversely, once the potential scan is reversed, and oxidation of R back to O is initiated, yet another concentration gradient begins to develop. In this instance, a concentration gradient of O begins to develop within the previously established concentration gradient of R . This behavior gives rise to a dynamic concentration profile for the two redox species during the course of a cyclic voltammetry

experiment, close to the electrode surface. Illustrations of this behavior can be found in several textbooks [2, 3, 5].

Cyclic voltammetry possesses two major advantages over potential step techniques. First, it is possible to examine a fairly wide potential range in a relatively short period of time in order to identify the presence of redox species. A second advantage is the ability to vary the relative time scale of the experiment by changing the scan rate of the potential sweep. However, unlike chronoamperometry, cyclic voltammetry is used mainly as a qualitative or diagnostic tool [3]. Perhaps the most valuable aspect of cyclic voltammetry is realized in the study of heterogeneous electron transfer reactions that are coupled to homogeneous chemical reactions. From the qualitative description given above, it is emphasized that cyclic voltammetry is capable of generating a new species on the forward sweep, R , and then probing its fate on the reverse sweep.

As a simple example consider reaction {1.1}: now, suppose that R participates in a quick, chemically irreversible reaction, rendering an electrochemically inactive product, Z .



As a result, if R is consumed in a coupled chemical reaction, before it can be oxidized back to O , then the magnitude of the anodic peak current will be decreased on the reverse sweep. Thus, monitoring the peak currents, i_{pa} and i_{pc} , can provide valuable information in the diagnosis and study of the mechanisms of electrode reactions. For an electrochemical reaction in which no coupled chemical reactions occur, the ratio of the peak currents, i_{pa}/i_{pc} should be equal to one. If R is consumed before it can be oxidized back to O , then the ratio i_{pa}/i_{pc} will be less than one. Deviation of this ratio from unity is dependent on the rate of conversion of R to its inactive form. At slower scan rates R will have more time to undergo

conversion and i_{pa}/i_{pc} decreases as the scan rate is decreased. At sufficiently high scan rates however, conversion of R to Z may have relatively little time to occur and the presence of the chemical reaction is not detected. Thus, when probing complex reaction mechanisms that involve coupled chemical reactions, it is important to employ a range of scan rates such that these processes are not overlooked. The mechanism described above is a simple example of a following chemical reaction. Several, more complicated, reaction mechanisms exist that can be probed using cyclic voltammetry [4]. Nicholson and Shain used cyclic voltammetry to probe the reduction of p -nitrosophenol, which involves a chemical reaction interposed between two-electron transfer reactions [6].

Cyclic voltammetry can also be very useful in the determination of electrochemical reversibility, electron transfer rate constants, and the physical state of a redox species. Systems that display electrochemical reversibility are defined as systems in which the electrode potential can be related to the concentrations of redox species in solution via the Nernst equation, {1.8}. Thus, the rate constant for electron transfer is so large that the concentrations of O and R at the electrode surface readily adjust to reflect any change in potential at the working electrode. It is important to realize that when the concentration of O is equal to the concentration of R , the electrode potential is equal to the formal potential of the redox system.

One can probe the reversibility of a redox system using cyclic voltammetry by examining the separation of the anodic and cathodic peak currents, or ΔE_p . For a reversible system a ΔE_p value of $57/n$ mV is observed and $i_{pa}/i_{pc} = 1$. These values are independent of scan rate. At this point it is important to keep in mind that reversibility is a relative term. As illustrated earlier, using the example of a following chemical reaction, it is possible to increase or decrease the time scale of a reaction depending on the choice of scan rate. Hence, a reaction may “appear” to be reversible, provided the electron transfer rate constant is relatively large

compared to the time scale of the experiment. However, if the scan rate is increased sufficiently, a point may be reached at which the kinetics of electron transfer become competitive with the rate of potential change. At this point, anodic and cathodic peaks begin to broaden and peak separation, ΔE_p , begins to increase.

Reactions in which ΔE_p is observed to vary with scan rate are defined as quasi-reversible reactions. In 1965 Nicholson derived a useful method for estimating the rate constants or k^o values of quasi-reversible reactions by examining the variation in ΔE_p with scan rate [7]. This method involves the measurement of ΔE_p values of a particular redox system and using these to obtain suitable values of Ψ from a working curve of known Ψ versus ΔE_p values. Once a value of Ψ has been determined, a value of k^o can be obtained using the following expression.

$$\Psi = \frac{\left(\frac{D_O}{D_R}\right)^{\alpha/2} k^o}{[D_O \pi \nu (nF / RT)]^{1/2}} \quad \{1.17\}$$

In this work Nicholson evaluated this method by studying the reduction of cadmium. A number of scan rates were investigated that resulted in increased ΔE_p values with increased scan rate. However, similar k^o values were obtained for each case that were in good agreement with those of other workers. It should be realized that this technique is only valid for ΔE_p values smaller than ~212 mV. At larger peak separations, determination of an accurate value of Ψ becomes more difficult and less practical. In most cases this expression can be simplified by making the approximation $D_O = D_R$ [5]. For irreversible systems the electron transfer rate is so slow that excessive ΔE_p values are encountered. For example,

ΔE_p values as high as 1500 mV for $\text{Fe}(\text{CN})_6^{-3/4}$ have been observed on highly ordered pyrolytic graphite electrodes at a scan rate of 1000 mV/s [8].

Discussion thus far has been confined to redox species in the solution phase; however, the electrochemical response can be significantly altered by adsorption of O or R to the electrode surface. Adsorption of a redox species to the electrode surface can occur via one of two broad classes of mechanisms, physisorption or chemisorption. While physisorption occurs mainly via nonspecific intermolecular forces, such as dipole-dipole interactions or π - π interactions, chemisorption involves the actual linkage of the adsorbing species to the substrate surface via chemical bonding [9]. Theoretical treatment of this scenario becomes more complicated as one must introduce adsorption isotherms that describe the adsorption behavior of the species of interest. This is typically accomplished by employing Langmuir or linearized Langmuir isotherms. For this reason only a simple case is considered in which only adsorbed O is initially present on the electrode surface, as in the experiments presented in the following chapters. A rigorous mathematical description is not presented. For this scenario the peak current can be obtained using the following expression.

$$i_p = \frac{n^2 F^2}{4RT} v A \Gamma_O^* \quad \{1.18\}$$

Γ_O^* represents the surface coverage of oxidized species and this value is usually expressed in units of moles/cm². From this expression it is important to note that the peak current for an adsorbed redox species is proportional to the scan rate. This is in contradiction to Equation {1.15} in which the peak current of a solvated redox species is proportional to the square root of scan rate. Thus, cyclic voltammetry can be used to differentiate between solution phase and adsorbed redox species via a scan rate dependence study.

The appearance of adsorption waves differs from those of solution phase redox species. As one would expect, no effects of diffusion, or mass transport are observed in these cyclic voltammograms as the redox species is immobilized at the surface of the electrode. For a reversible system, the redox waves are symmetrical about the potential axis and display a peak width at half maximum, $\Delta E_{p,1/2}$, of $90.6/n$ mV (not to be confused with peak separation, ΔE_p). Also, when the sweep direction is reversed, the observed current is the mirror image of that observed on the forward sweep. Theory predicts a ΔE_p value of zero millivolts for an ideal case in which electron transfer rate is very fast between the electrode surface and surface modifier. It is possible to determine surface concentration of the adsorbate by integrating the area under the redox waves [10, 11]. Integration yields the charge under the wave, and this value can be used to calculate the surface concentration using the following expression,

$$Q = nFA\Gamma_o \quad \{1.19\}$$

where Q is the charge, in Coulombs. Similarly, if the surface coverage for a specific redox species is known, then the unknown surface area of an electrode can be determined using the same expression and solving for area. A major difference between this method of surface area determination and that using the Cottrell equation, {1.13}, is that the Cottrell equation renders the geometric electrode area while this method yields the real electrode area, the difference being that geometric area takes no account of surface roughness. Adsorption methods are used largely in the study of chemically modified electrodes in which the electroactive species has been covalently bound to the electrode surface. Laviron has published several studies dealing with the voltammetric behavior of adsorbed redox species, including a method for the determination of electron transfer rate constants based on anodic and cathodic peak separation [12-14].

Carbon Electrodes

Carbon made its debut as a working electrode in the work published by Lord and Rogers almost a half century ago [15]. In this work the authors compared the use of carbon to noble metal working electrodes of platinum and gold using polarographic techniques. Graphite electrodes were investigated because of their ability to easily render a fresh surface by cleaving with a razor blade. This feature was found to be particularly advantageous in the study of oxidations of organic molecules. Since this first investigation, carbon has found extensive use in a variety of electrochemical studies. More comprehensive reviews on carbon electrodes and carbon electrode materials can be found in the following references. [16-20]. The following discussion is based mainly on these reviews and the references therein.

Several “forms” of carbon are available for use as electrode materials; these materials have been grouped into one of two main categories; porous, and non-porous structures [16]. The major difference between these two categories resides in how the electrode material is employed. In porous carbon electrodes, electrochemical reaction occurs mainly in the pore structure of the electrode, and not at a prepared smooth interface, as for non-porous electrodes. The main advantage of porous electrodes over smooth, non-porous materials, is the high interfacial area that these materials possess. Porous carbon materials are generally used in the preparation of two main types of electrodes: flooded electrodes, and gas diffusion electrodes. The focus of this discussion will be based on non-porous structures.

Several types of non-porous carbon materials are available for use in the preparation of working electrodes. The most common types of these materials include: highly ordered pyrolytic graphite (HOPG), pyrolytic graphite (PG), glassy carbon (GC), carbon fibers, and various forms of carbon blacks or channel blacks [16-18]. A common characteristic of each of these materials is that they all

display extensive sp^2 hybridized structures. However, a difference in this sp^2 structure is the main factor that causes the bulk properties of these materials to vary so greatly from one another. Major differences in physical properties of these materials are manifested as a result of the microcrystal structure of these materials through the size and orientation of graphitic crystallites [17]. At this point, it is important to keep in mind that many forms of carbon mentioned above are all actually composed of microcrystalline single crystal graphite. Two main parameters used in describing the microcrystal structure of sp^2 hybridized carbon materials are intraplanar microcrystallite size, L_a , and interplanar microcrystallite size, L_c . Figure 1.1 (A) is a schematic representation of a single crystal of graphite. L_a defines the extent of the crystal in the plane of sp^2 hybridization, and, L_c defines the extent of the crystal in the plane perpendicular to sp^2 hybridization. Simply put, L_c is a measure of the thickness of the stacked sp^2 hybridized or hexagonal ring layers. These layers stack in an ABAB fashion. Values of L_a and L_c can vary between about 10 μm for HOPG to a few Angstroms for GC or carbon black [17].

The plane along the a-axis is commonly referred to as the basal plane while the plane perpendicular to the graphitic lattice is termed the edge plane. As the structure suggests, the physical properties of graphitic materials differ significantly depending along which axis the material is examined. Such materials are described as anisotropic. The most notable characteristic of graphitic material is the difference in resistivity along the a and c axes. Electrochemical behavior is also dependent on the crystallographic orientation of the electrode surface. For example, HOPG displays striking differences in the electron transfer behavior observed between basal plane, and edge plane orientations. McDermott and coworkers have investigated the kinetics of $\text{Fe}(\text{CN})_6^{-3/4}$ electron transfer on HOPG surfaces of varying defect density [8]. Higher defect densities reflect a

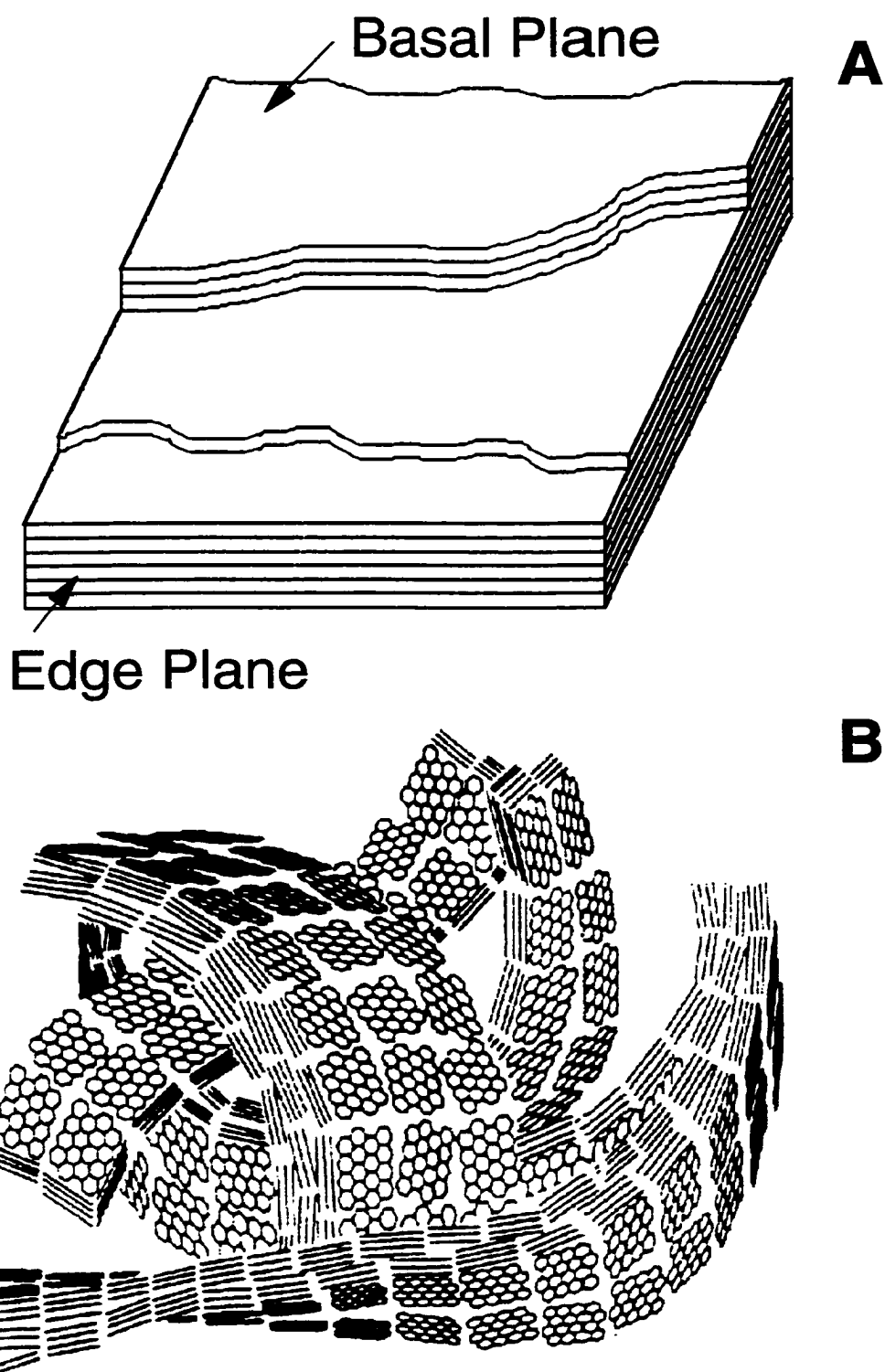


Figure 1.1: Schematic representations of (A) HOPG, and (B) GC.

higher proportion of edge plane to basal plane orientation. In this work the electron transfer rate constant was observed to vary over six orders of magnitude (8.0×10^{-7} to 0.130 cm/s) for HOPG electrodes of varying surface defect density.

GC, often referred to as vitreous carbon, is a hard, glossy, ceramic-like solid carbon material. Due to its many desirable properties GC has gained extreme popularity as a carbon electrode material. These properties include: impermeability to gases, resistance to chemical attack, electrical conductivity, availability in high purity, and favorable mechanical properties in terms of stability and machinability. Yamada and Sato first prepared GC in 1962 [21]. However, the first demonstration of GC as an electrode for voltammetry was that of Zittel and Miller published in 1965 [22]. In this work the authors revealed the wide potential range of GC in several electrolyte solutions. GC was also shown to be relatively insensitive to changes in pH, unlike PG. This observation was attributed to the isotropic nature of GC. More recently, van der Linden and Dieker have prepared a comprehensive literature review on the uses of GC electrodes in various electrochemical applications [19].

Preparation of GC is very different from that of other carbon materials such as carbon blacks, PG, and HOPG. GC is manufactured by employing a carefully controlled heating program under inert atmospheric conditions. The process involves slow thermal degradation of high molecular weight organic polymers such as phenol formaldehyde resins [19]. These polymers are first heated to 600 to 800 °C such that the starting material is cured and carbonized. At this point most of the noncarbon elements are volatilized, but the polymer backbone remains intact. Regions of sp^2 hybridized carbon are formed during this stage. The structure of GC was first determined by Jenkins and Kawamura using X-ray diffraction studies [23]. A schematic representation of the structure of GC is shown in Figure 1.1 (B). Due to the nature of the polymeric starting material, GC adopts an intertwined ribbon-like morphology that is composed of small

microcrystalline graphitic domains [19]. Use of a slow thermal degradation process allows the polymers to be transformed directly into a form of carbon that retains its original morphology. This morphology causes GC to display isotropic rather than anisotropic behavior. Once the initial pretreatment stage is complete the material is heated slowly under pressure to elevated temperatures, typically in the range of 1000 to 3000 °C. Three grades of GC are generally available, based on this final temperature: GC-10 (1000°C), GC-20 (2000°C), and GC-30 (3000°C). Physical properties of the final GC product are dependent upon this final temperature. The specific consequences of this final heat treatment are still not fully understood, however, they are usually generalized to imply greater ordering of the GC at higher temperature due to more complete graphitization [17, 23].

Electrode preparation or activation is a critical step in any experiment involving the use of carbon electrodes as the activation method employed may have a profound effect on the observed electron transfer behavior of the electrode surface. A more detailed discussion of electrode activation methods is deferred to Chapter III, however, some general details are provided below. As received GC electrodes are initially ground on silicon carbide or diamond grit paper to remove gross surface defects and impurities that result from the manufacturing process. Electrodes are then typically polished in alumina/water slurries of successively smaller particle size until a mirror like finish is achieved. This type of activation procedure is usually sufficient for most types of electroanalytical applications.

Chemically Modified Electrodes.

Chemically modified electrodes, CMEs, have been the topic of intense research over the past twenty-five years. Their preparation typically involves the immobilization of specific molecules or functional groups on electrode surfaces. These groups are usually electroactive and/or possess electron transfer mediator properties, or are able to enhance the selectivity or preference of an electrode for

one analyte over another. The motivation behind most CME studies stems from the desire to rationally design electrodes that display enhanced electrocatalytic properties, or electrochemical selectivity, for specific analytes. For example, oxidation of NADH at carbon electrodes has been the topic of numerous studies [24-32]. The main objectives of these studies have focused on the development of a surface modification procedure that serves to reduce the overpotential required to effect the electrochemical oxidation of NADH. Development of such a method would facilitate electrochemical detection and analysis of NADH, and contribute toward the development of a suitable biosensor. Another system that has been the focus of several CME and electrode activation studies is the detection of the neurotransmitter dopamine in the presence of large concentrations of ascorbic acid. Ascorbic acid becomes a particular problem in the biological analysis of dopamine as it possesses a similar redox potential, and is typically present in concentrations on the order of 1000 fold greater than that of dopamine [33]. The main focus behind these efforts has been the development of an electrode that displays enhanced selectivity for the analysis of dopamine in biological studies.

Perhaps the first demonstrations of CMEs were those of Lane and Hubbard [34, 35]. In this work the authors revealed the tendency of olefinic groups to chemisorb onto platinum electrodes. This phenomenon was exploited in an effort to attach a variety of reactive functional groups to the electrode surface. Furthermore, the attachment of chelating agents via olefinic side chains was employed in the selective adsorption of metals to the electrode surface. Elliott and Murray provided the first example of a chemically modified carbon electrode [36]. In these studies, organosilane chemistry was employed to immobilize amine, ethylenediamine, pyridine, and alkyl chloride groups to the surface of GC and graphite electrodes by silanization of surface oxide groups. Attachment to the electrode surface was confirmed by X-ray photoelectron spectroscopy and the modified electrodes displayed good electrochemical stability. Although Lane and

Hubbard were the first to explore the idea of immobilized reactive groups on electrode surfaces, Murray is usually credited for pioneering studies on CMEs.

Traditionally, CMEs have been prepared using one of three general methods, adsorption, covalent attachment, or application of a thin polymer film. Extensive studies have been published and a number of reviews can be consulted to obtain a more detailed background of CMEs [16, 37-44]. In more recent studies, electrode modification schemes are becoming increasingly more complex. The advent of self-assembled thiol monolayers on gold has also created numerous new possibilities. The use of multiple modification methods has become more common in the fabrication of CMEs. Current efforts often involve multiple step modification procedures, and synthetic methods, that result in the immobilization of enzymes, proteins, DNA, or other biologically active molecules. Such methods may consist of adsorption followed by derivatization, or application of a thin polymer film. Several examples are considered during the course of this discussion.

Adsorption. The simplest method available for immobilizing chemical species on the surface of an electrode is adsorption. This procedure typically involves incubation of the electrode in a solution of the desired adsorbate for a set period of time. Adsorbates may be either physisorbed, as in the case of anthraquinone 2,6-disulfonate on graphite, or chemisorbed, as in the case of ω -functionalized alkanethiols on gold. At this point it is important to make a distinction between chemisorption and covalent attachment. For the purpose of the discussions presented in this text, chemisorption will be used to describe scenarios in which bonding between a metal and nonmetal are implied, as in the self assembly of thiol monolayers on gold. Covalent attachment will be used to describe scenarios in which bonding between two non metal species is implied, such as an amide linkage or a carbon-carbon bond.

Several examples of CMEs prepared by the physisorption of specific molecules to carbon electrodes are presented in the literature [10, 11, 26, 27, 45-49]. Collman and coworkers have investigated a series of dimeric metalloporphyrins adsorbed on graphite electrodes for catalysis of the four electron reduction of oxygen to water [46]. Catalysis of this reaction is of particular importance in the development of fuel cell technology. One molecule, a dicobalt cofacial porphyrins, produced a catalyzed reduction almost exclusively to water at exceptionally positive potentials. Ye and Baldwin [47] were able to produce CMEs that displayed electrocatalytic activity toward myoglobin and hemoglobin. The CMEs were prepared by adsorbing methylene blue onto spectroscopic graphite electrodes. Modification of graphite electrodes in this manner allows the reduction of the hemoprotein to take place at the reduction potential of the mediator molecule. Use of these CMEs was tested in flow injection analysis and liquid chromatography detection systems, and their performance compared to that of a UV detector. Persson and Gorton used derivatives of phenothiazine [26], and 3,7-diaminophenoxazine [27] adsorbed on graphite in the electrocatalytic oxidation of NADH. Use of a 3- β -naphthoyl-Toluidine Blue O (3-NTB) modified graphite electrode resulted in a decrease of the overpotential required to oxidize NADH by about 500 mV compared with the direct oxidation of NADH at unmodified graphite electrodes. A 3-NTB modified electrode was tested in a flow through amperometric cell in a single channel, flow injection analysis system. The electrode response was shown to be linear over three decades of concentration and displayed good stability in alkaline (pH = 9) solutions. Finally, Chen and McCreery showed that adsorption of anthraquinone 2,6-disulfonate is able to catalyze electron transfer of the innersphere $\text{Fe}^{+2/+3}$ redox system at GC electrodes [48]. This system is very sensitive to the presence of surface oxide groups and the ΔE_p value decreases upon adsorption of anthraquinone 2,6-disulfonate.

Modification by adsorption is not exclusive to carbon electrodes however. Since it was first demonstrated that alkanethiol and disulfide molecules form well packed, self assembled monolayer films, organic thin films (OTFs), on gold substrates [50-58], these systems have been used extensively in the chemical modification of gold electrodes. Adsorbates usually consist of long chain alkanethiol molecules with a specific functional group, or molecule of interest, covalently attached at the terminal end of the alkane chain. Thus, one can easily control the surface chemistry of the monolayer by careful choice of the functional group present at the terminus or ω -position of the adsorbate molecule. These functional groups may be comprised of specific electroactive groups, electron transfer mediators, or receptor molecules. Zhong and Porter have presented an excellent overview of the development and application of self assembled OTFs in analytical chemistry [59].

Electroactive self-assembled monolayer systems have recently emerged in a number of electrochemical studies [59-69]. Electroactive monolayers are produced by tethering electroactive groups, such as ferrocene or ruthenium pentaamine, to the surface of gold electrodes via long alkane chains. The main focus of these studies has been on the investigation of electron transfer at the metal/electrolyte interface through an impermeable monolayer structure of hydrocarbon chains. Determinations of rate constants, tunneling parameters, and reorganization energies have been presented for several systems.

Chidsey and coworkers have studied the rate constant for electron transfer between a gold electrode and bound ferrocene groups at different temperatures and reaction free energies [61], as well as the effects of mixed monolayer formation [60]. It was observed that by diluting the ferrocene terminated adsorbates with a normal alkanethiol of similar chain length, voltammograms that displayed nearly ideal electron transfer behavior were obtained. The voltammograms of non-diluted ferrocene monolayers tended to be extremely broadened and not well

defined. This behavior is attributed to repulsive interactions between closely packed ferrocene groups. It was also demonstrated that ferrocenyl adsorbate coverage decreases with increasing length of the diluent thiol. This behavior is attributed to the greater affinity of longer adsorbates for adsorption and self-assembly due to higher free energy and lower solubility in ethanol.

Finklea and coworkers used similar adsorbates in their studies of electron transfer. In these studies the adsorbates consisted of a long alkanethiol chain terminated with electroactive ruthenium pentaamine groups [64, 65, 69]. A significant difference between these adsorbates and the ferrocenyl adsorbate is that ideal electron transfer behavior is observed for the ruthenium pentaamine monolayers; diluent thiol is not needed in order to achieve ideal behavior. In a more recent study, diluent thiols have been used to influence the surrounding medium of the terminal electroactive group [69]. Employing adsorbates of varying chain lengths it was possible to create three different scenarios: a matched case in which the electroactive adsorbate was the same length as the diluent, an exposed case in which the electroactive adsorbate was longer than the diluent, and a buried case in which the electroactive adsorbate was shorter than the diluent. In each case, the position of the terminal electroactive group with respect to the supporting electrolyte is altered. As a result, it was demonstrated that the tunneling parameter is influenced by the position of the redox center with respect to its surrounding medium. The buried case displayed a much lower tunneling parameter than the exposed case, and the matched case displayed the highest tunneling parameter. Effects of the terminal group of the diluent thiol have also been considered [64].

Perhaps the earliest investigation of the use of self-assembled monolayers in the preparation of CMEs was that of Taniguchi and coworkers [70]. In this study the authors report the enhancement of electron transfer rates for the protein cytochrome c at gold electrodes modified by the chemisorption of

bis(4-pyridyl)disulfide. Modified electrodes displayed well-defined voltammetry for cytochrome c while no redox waves were observed at bare gold electrodes. More recent studies have emerged that examine the effects of similar adsorbates on cytochrome c electron transfer [71, 72]. In each case, modification of gold electrodes with bis(4-pyridyl)disulfide and 4-mercaptopyridine yields quasi-reversible electron transfer of cytochrome c. Improvement in the observed voltammetry is attributed to a more favorable configuration of the adsorbed protein on the modified electrodes compared with a bare gold electrode [71]. Adsorbed pyridine derivatives display no apparent charge transfer mediation ability. Lisdat and Scheller recently demonstrated the use of oligonucleotide modified gold electrodes for fast electron transfer to cytochrome c [73]. Electrode modification was carried out using 11-mer oligonucleotides that were modified at the 3' end with a $-(\text{CH}_2)_3\text{-SH}$ group. When the oligonucleotide-modified electrode was exposed to a cytochrome c solution, quasi-reversible behavior for the redox protein was observed.

Malem and Mandler have demonstrated that modification of gold electrodes with ω -mercapto carboxylic acid monolayers is able to induce electrochemical differentiation between dopamine and ascorbic acid [74]. The oxidation wave of dopamine is shifted to less positive potentials and that of ascorbic acid is shifted to more positive potentials, compared to a bare gold electrode, when electrodes were modified with $\text{HS}(\text{CH}_2)_2\text{CO}_2\text{H}$. The shift in peak potentials is attributed to more favorable electrostatic interactions between dopamine and the negatively charged monolayer surface. Ascorbic acid is essentially repelled from the electrode surface due to its negative charge at physiological pH. It is worth noting that no difference in the electron transfer rate for dopamine or ascorbic acid is observed at pH values at which the carboxylic acid monolayer is protonated, i.e. no longer charged. Also, a trade off is observed when adsorbates possessing longer alkane chains are used. While the terminal

carboxylic acid group improves the electrode selectivity for dopamine, a decrease in the electron transfer rate is observed due to more effective blocking by the longer, better ordered monolayers. Aside from their utility as adsorbates, OTFs can also be used as a foundation for further chemical modification through derivatization of the terminal functional groups. This scenario is considered below.

Covalent Attachment. Covalent attachment results in the formation of a covalent bond between the electrode surface and the modifier of interest. Two methods of covalent attachment can be employed in the chemical modification of carbon electrodes: derivatization of existing functional groups, and covalent attachment directly to the carbon backbone via a carbon-carbon bond. Derivatization of existing functional groups is often employed in conjunction with electrochemical pretreatment procedures, such as oxidation, in an effort to augment the density of surface oxide groups available for derivatization. Several derivatization methods have been described for the modification of carbon electrode surfaces. These methods include amidation [24, 25, 31, 75-80], esterification [16, 37], silanization [36, 81], and ether bond formation [82, 83]. However, these methods are not exclusive to carbon electrodes, as the derivatization of tin oxide [84-90], titanium oxide [85], and ruthenium oxide [91] electrodes by silanization has also been investigated.

As described earlier, Elliott and Murray provided the first example of chemically modified carbon electrodes employing organosilane chemistry to attach specific chemical groups to the surfaces of GC electrodes [36]. Tse and Kuwana demonstrated that *o*-quinoidal structures, such as catechols, appear to be rather specific electron transfer mediators for the electrochemical oxidation of NADH [24]. Thus, immobilization of dopamine and 3,4-dihydroxybenzylamine was attempted via amidization of the amino groups and GC surface oxide groups in the presence of the coupling agent dicyclohexylcarbodiimide (DCC).

3,4-dihydroxybenzylamine modified GC electrodes displayed the most effective catalytic activity toward NADH oxidation. However, the activity of these electrodes could not be maintained due to fouling by the products of NADH oxidation. The same modification procedure was employed in the electrocatalytic oxidation of ascorbic acid [25]. In contrast to NADH, the oxidation of ascorbic acid showed good reproducibility between scans and no appreciable deactivation with repeated cycling was observed. The overpotential for ascorbic acid oxidation was reduced by 200 – 300 mV through the use of surface bound redox mediators. Bourdillon and coworkers have used similar methods to immobilize glucose oxidase on the surface of GC electrodes [92]. This procedure involves activation of surface carboxylic acid groups with an appropriate carbodiimide-coupling agent. The activated electrode is then exposed to a solution of glucose oxidase and the enzyme is covalently attached to the electrode surface via amide linkages to amino groups on the enzyme. Cass and coworkers have employed this method to immobilize glucose oxidase in the construction of a ferrocene mediated enzyme electrode for the amperometric determination of glucose [79]. Hayes and Kuhr have used a similar, yet more complicated multistep procedure in the preparation of enzyme modified carbon fiber electrodes for NADH detection [31].

It has also been reported that reaction of a freshly polished GC surface with *N*-hydroxysuccinimide (NHS) esters provides a facile method for covalent attachment to a GC electrode surface. Anne and coworkers have proposed a two step strategy for the covalent attachment of biomolecules at a short distance from the electrode surface [80]. The first step involves derivatization of an electrode surface with a NHS ester of a molecule possessing a protected amino group at the ω -position. This amino group can then be deprotected and reacted further with the NHS ester of a suitable biomolecule. However, this method may potentially lose its initial appeal as the electrode activation step requires polishing of the GC

electrode in the presence of 1.0 M ammonia in an effort to augment the density of surface amino groups.

Surface derivatization can also be accomplished through direct covalent attachment to carbon electrodes. Mazur and coworkers first demonstrated that an olefinic addition reaction could be used in the preparation of derivatized oxide free graphite electrodes [93]. Acrylyl chloride was shown to react with the oxide free surface of carbon fibers in good yield. This procedure gives rise to reactive acid chloride groups on the electrode surface that can be used in further derivatization reactions. Nowak and coworkers demonstrated that mechanical abrasion of an oxide free GC surface under inert atmosphere and in the presence of olefinic reagents, such as vinyl ferrocene or vinyl pyridine, could also be used to introduce electroactive groups onto the surface of oxide free carbon substrates [94]. More recently, the electrochemical oxidation of amine containing compounds has been shown to be a useful method for the attachment of functional groups to carbon surfaces [95, 96]. This method involves the electrooxidation of amines to their analogous cation radicals to form a chemically stable covalent linkage between the nitrogen atom of the amine and a carbon surface.

Most of the derivatization methods described thus far require oxidation (or some other form of activation) of the carbon surface in an effort to augment the density of surface oxide groups available for derivatization. A drawback to this approach is that oxidation results in etching of the electrode surface accompanied by the observation of large background current [97]. More recently, a new method for the covalent attachment of functional groups directly to carbon electrodes has been described. This method involves the attachment of functionalized aryl radicals, generated by the electrochemical reduction of diazonium salts. The first demonstration of this technique was reported by Delamar and coworkers [98]. In this work the authors used (4-nitrophenyl)diazonium tetrafluoroborate in the modification of various carbon electrodes. Attachment of 4-nitrophenyl groups

was investigated by electrochemistry and X-ray photoelectron spectroscopy (XPS). Results from these experiments confirm the covalent attachment of the 4-nitrophenyl groups on the carbon surface as opposed to adsorption.

Several investigations involving this new approach have recently been reported [99-105]. Bourdillon and coworkers have demonstrated that it is possible to use this method to graft functional groups onto a carbon surface for the purpose of further chemical derivatization [99]. In this work GC electrodes were prepared by the attachment of 4-phenylacetic acid groups by reduction of the corresponding diazonium salt. Glucose oxidase was then immobilized on the surface via amidization through activation of the 4-phenylacetic acid groups using a carbodiimide-coupling agent. Attachment of the protein was confirmed by XPS. Electron transfer properties of these films have also been investigated [101, 104]. GC electrodes modified with 4-nitrophenyl and 4-carboxyphenyl groups were studied in aqueous solutions of $\text{Fe}(\text{CN})_6^{-3}$ and $\text{Ru}(\text{NH}_3)_6^{+3}$ at $\text{pH} = 7$. The 4-carboxyphenyl modified electrode showed good electron transfer kinetics for $\text{Ru}(\text{NH}_3)_6^{+3}$ but completely blocked $\text{Fe}(\text{CN})_6^{-3}$. These observations are attributed to electrostatic interactions. While the negatively charged carboxylic acid layer is able to repel $\text{Fe}(\text{CN})_6^{-3}$ from the electrode surface, it is also able to attract $\text{Ru}(\text{NH}_3)_6^{+3}$, thus, reversible behavior is observed for $\text{Ru}(\text{NH}_3)_6^{+3}$. The 4-nitrophenyl modified electrode was able to completely block both $\text{Fe}(\text{CN})_6^{-3}$ and $\text{Ru}(\text{NH}_3)_6^{+3}$. These observations are attributed to the blocking properties of the film. Kariuki and McDermott have studied the nucleation and growth behavior of functionalized aryl films on graphite electrodes using electrochemistry, atomic force microscopy, and scanning tunneling microscopy [105]. The authors conclude that film growth initiates at cleavage steps and atomic scale defects on the basal plane of HOPG electrodes. Film growth then propagates in both two and three dimensions through the binding of aryl radicals to aryl groups already

present on the surface. This description implies that multilayer formation is possible and this growth mechanism is under further investigation.

Covalent attachment has also been used in the modification of gold electrodes that have been previously modified using self-assembled monolayers. In this case, functional groups that have been introduced onto the gold surface are employed in further derivatization steps. Self-assembly methods permit introduction of a high density of surface functional groups to a gold surface in a controlled manner that can be made available for further derivatization. The most popular derivatization methods involve modification of a gold surface with carboxylic acid terminated thiol molecules. The carboxylic acid group is then activated using a suitable carbodiimide catalyst, such as dicyclohexylcarbodiimide (DCC) or 1-ethyl-3-[(dimethylamino)propyl]carbodiimide (EDC). Exposure of the activated carboxylic acid groups to amino groups results in the formation of an amide linkage. This method has been used to attach a variety of biological molecules such as amino acids, proteins, and antibodies to gold electrode surfaces [106-111].

Duan and Meyerhoff have used self-assembled monolayers of thioctic acid on the surface of a gold-coated microporous nylon membrane in the development of a separation-free, electrochemical sandwich, enzyme immunoassay [107]. Capture antibodies toward model protein analytes were immobilized on a gold-coated membrane via amidization using EDC as the coupling agent. In this case, the solid phase on which the sandwich is formed also serves as the electrochemical detector, i.e. gold working electrode. Preparation of the separation-free immunoassay sandwich electrode requires incubation of an immobilized capture anti-hCG antibody in the presence of the model analyte protein, human chorionic gonadotropin, (hCG) and alkaline phosphatase labeled anti-hCG (ALP-Ab). The enzyme substrate, 4-aminophenyl phosphate, is then introduced through the backside of the porous membrane such that it first encounters bound ALP-Ab at

the gold surface. Enzymatically generated product, aminophenol, is then immediately detected by oxidation at the gold electrode held at the appropriate potential. The magnitude of the anodic current is directly proportional to the concentration of hCG in the sample. A detection limit of 2.5 units/L hCG (in blood) was obtained, comparable to most heterogeneous enzyme immunoassays that require multiple washing steps.

Willner and Riklin have demonstrated that it is possible to use multiple modification steps in the preparation of an amperometric biosensor for malic acid [108]. Gold electrodes were first modified by immersion into an aqueous solution of cystamine dihydrochloride, resulting in a monolayer of surface amino groups. Exposure of the modified electrode to a solution of pyrroloquinolinequinone (PQQ) in the presence of EDC results in the covalent attachment of PQQ to the electrode surface. The resulting PQQ modified electrode provides a catalytic interface for the electrooxidation of NAD(P)H. Anodic currents that depend on the concentration of NADH added to solution were observed. A linear relationship between anodic current and NADH concentration was obtained in the range of 3.0×10^{-4} to 1.0×10^{-2} M NADH. Therefore, the PQQ modified electrode could be used for quantitative analysis of NADH in aqueous solutions. PQQ possesses multiple carboxylic acid functional groups. Therefore, further chemical modification procedures may be attempted based on derivatization of these groups. In this case the authors attempted to attach malic enzyme; an enzyme that is able to oxidize malic acid in the presence of NAD(P)^+ , to the PQQ modified electrode surface via amidization. Further modification was accomplished by exposing a PQQ modified electrode to a solution of malic enzyme in the presence of EDC. Oxidation of malic acid by malic enzyme in the presence of NADP^+ results in the generation of NADPH. In turn, NADPH can be regenerated by oxidation by immobilized PQQ functionalities. Thus, the concentration of malic acid present in the sample is proportional to the current that arises due to NADPH

oxidation. In these studies a linear relationship over a broad range of malic acid concentration was observed (10^{-7} to 10^{-3} M) using such an electrode. The authors have used a similar scheme in the preparation of a CME for the electrooxidation of glucose at an “unprecedentedly high rate” [109].

More recent studies have examined the stepwise self-assembly of multiple layers of thionine and horseradish peroxidase in the development of a hydrogen peroxide biosensor [110]. In this system thionine serves as an electron transfer mediator; its responsibility is to regenerate the active form of the enzyme. Modified electrodes used in the quantification of superoxide dismutase (SOD) activity have also been prepared by immobilization of cytochrome c onto carboxylic acid terminated monolayers using similar amidization methods [111].

Polymer Coatings. Modification of electrode surfaces with thin polymer films can be achieved employing a number of different methods. These methods include: dip coating, spin coating, solution casting, electrochemical polymerization, and electrochemical precipitation. Some advantages of this technique are realized over other immobilization methods. For example, greater stability of immobilized redox species is realized as these molecules tend to be trapped or covalently bound within the polymer matrix. The thickness of the deposited film can be controlled in a reliable and reproducible manner. Polymer films also display good chemical stability in contacting solvents; thus, loss of material from the electrode surface is not a problem. Finally, due to the thickness of the polymer film, a higher concentration of immobilized redox species can be achieved over covalent attachment or adsorption methods using thin polymer films. For example, consider a polymer film with a thickness of ten Angstroms that contains a particular redox species at a concentration of 2×10^{-10} mol/cm². This value translates into a concentration of 2.0 mmol/L in an equivalent volume of solution [16].

Three general types of polymer films have been identified in the modification of electrode surfaces [41]. A major distinction between these types of films has been made based on the mechanism of charge transport within the film. Polymer films that possess redox sites as part of the polymer backbone are known as redox polymers; for example, poly(vinylferrocene) [112] and poly(*p*-nitrostyrene) [113]. Charge transfer through redox polymers typically occurs via electron hopping between oxidized and reduced sites. The second type of polymer film includes the electronically conducting polymers. Electronically conducting polymers are able to conduct electricity more efficiently than redox polymers due to their delocalized, metal-like band structures [114]. These materials have also been referred to as organic metals [40, 114]. Poly(pyrrole), an example of an electronically conducting polymer; is easily formed by electrochemical polymerization from solution, and is useful for the entrapment of electrocatalysts and redox mediators within the polymer matrix [41, 114-120]. The third type of polymer film is comprised of the ion exchange polymers. Examples of such polymers include Nafion[®], a commercially available ion exchange polymer from Dupont[™], and pyridine based polymers such as poly(vinylpyridine) [121-125]. Ion exchange polymers themselves are not electroactive; however, they can be made electroactive by ion exchange of a suitable redox counter ion. Exchange of $\text{Ru}(\text{NH}_3)_6^{+2/+3}$, $\text{Ru}(\text{bpy})_3^{+2/+3}$, or methylviologen (MV^{+2}) into Nafion films are such examples [126-129]. Physical diffusion of electroactive counter ions within the polymer matrix accounts for the main method of charge transport within these polymer films. Unlike electroactive and electronically conducting polymers that possess fixed or entrapped redox centers, ion exchange polymers have a tendency to lose their electroactivity when employed in solutions that are free of the electroactive counterion. An advantage of this behavior is that it is possible to exchange a number of electroactive counterions into the same film. Extensive work has been published on the use of

polymer films as electrode modifiers, and some recent examples are considered below.

Pariante and coworkers have recently investigated the electrodeposition of a number of redox active films of dihydroxybenzaldehydes and related analogs [28-30]. Not only do these electropolymerized films display redox behavior that is consistent with that of an immobilized species, but some of them also display electrocatalytic activity toward NADH oxidation. Voltammetric behavior and electrocatalytic activity is attributed to the high density of *o*-quinone functionalities within the electrochemically polymerized film. NADH oxidation typically occurs at potentials close to the redox potential of the polymer film. Thus, the modifying film serves as an electron transfer mediator. GC electrodes modified with films of 2,3-dihydroxybenzaldehyde (2,3-DHB) and 3,4-DHB display the best catalytic activity for the electrooxidation of NADH [29]. A linear response for anodic current as a function of NADH concentration was obtained over a range of 0.01 to 1.2 mM and 0.01 to 0.9 mM for films derived from 3,4-DHB and 2,3-DHB respectively.

Zare and Golabi have studied the electrocatalytic oxidation of NADH [32] and hydrazine [130] at chlorogenic acid (CGA) modified GC electrodes. CGA also possesses an *o*-quinone functional group and is deposited onto GC electrodes by electrochemical polymerization. CGA films display voltammetry that is consistent with an immobilized redox couple and the redox waves are attributed to the voltammetry of the *o*-quinone group. Modification with CGA films was able to reduce the overpotential for NADH and hydrazine oxidation by 430 mV and 600 mV respectively. Oxidation of NADH and hydrazine occurs at the redox potential of the immobilized film, indicative of electron transfer mediator behavior. For NADH analysis, a linear response in concentration from 0.1 to 1.0 mM NADH was observed. Ciszewski and Milczarek have recently investigated the use of poly(eugenol) modified platinum electrodes for the

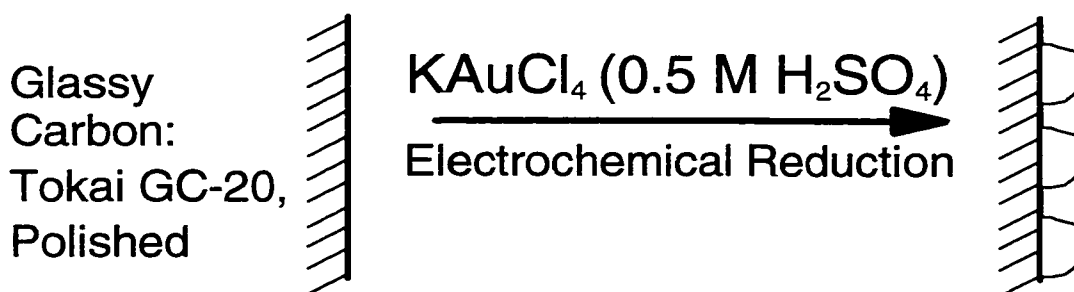
selective analysis of dopamine in the presence of large concentrations of ascorbic acid [33]. Poly(eugenol) films were applied to platinum electrodes via electropolymerization. It was observed that the relative sensitivity of the electrode for dopamine over ascorbic acid is dependent upon polymerization potential. The high selectivity for dopamine was attributed to electrostatic repulsion of negatively charged ascorbate from the electrode surface by the poly(eugenol) film.

Research Objectives

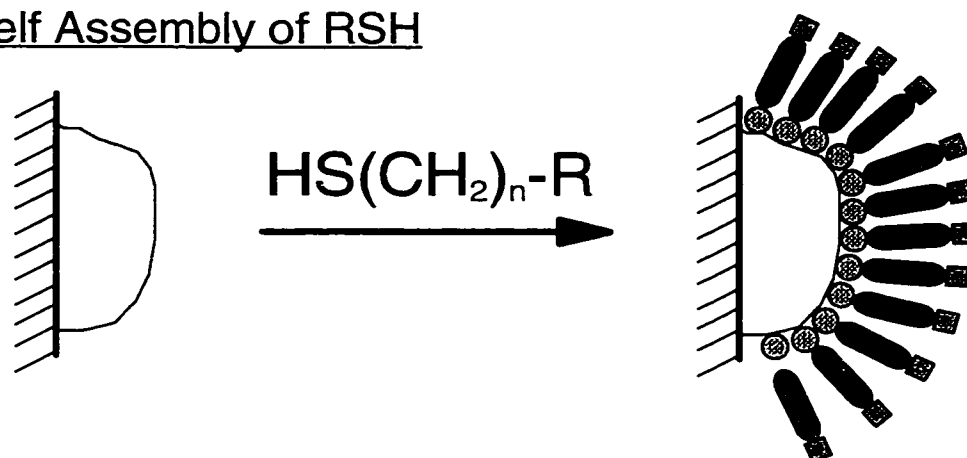
Self assembled monolayer techniques possess several advantages over other electrode modification methods such as physisorption, covalent attachment or polymer films. These advantages include: stability and integrity of the monolayer structure, flexibility and control of surface chemistry, uniformity of surface coverage, and ease of preparation. Unfortunately, a similar modification method does not exist for carbon electrodes. The main objective of this research is to devise a method in which self-assembly methods can be extrapolated to include modification of GC electrodes.

The experiments employed during the course of this dissertation were designed and geared towards the exploration of a potentially new method for the preparation of chemically modified electrodes. This method entails the use of metal deposition and self-assembly techniques in an effort to introduce multiple functional groups onto carbon electrodes. This can be accomplished employing a two step approach as illustrated in Figure 1.2. The first step (a) is the production of an array of small, well-dispersed, supported gold particles on a GC substrate. This is achieved by potential step deposition of gold onto a polished GC electrode. In the second step of this process (b), the supported gold particles are chemically modified by taking advantage of the self-assembly of thiol molecules on gold. Coupling of multiple gold deposition and particle modification steps should permit

a. Electrochemical Deposition of Gold Nanoparticles



b. Self Assembly of RSH



c. Segregated Domains Next to Electron Transfer Sites

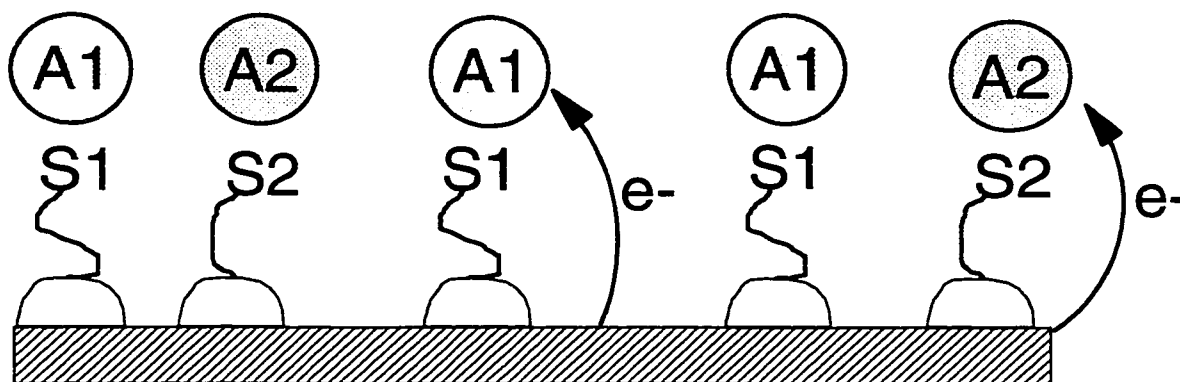


Figure 1.2: Application of SAMs to GC electrodes. (a) metal deposition, (b) modification of gold particles by self-assembly of thiols, (c) segregated domains of specific surface chemistry situated next to electron transfer sites.

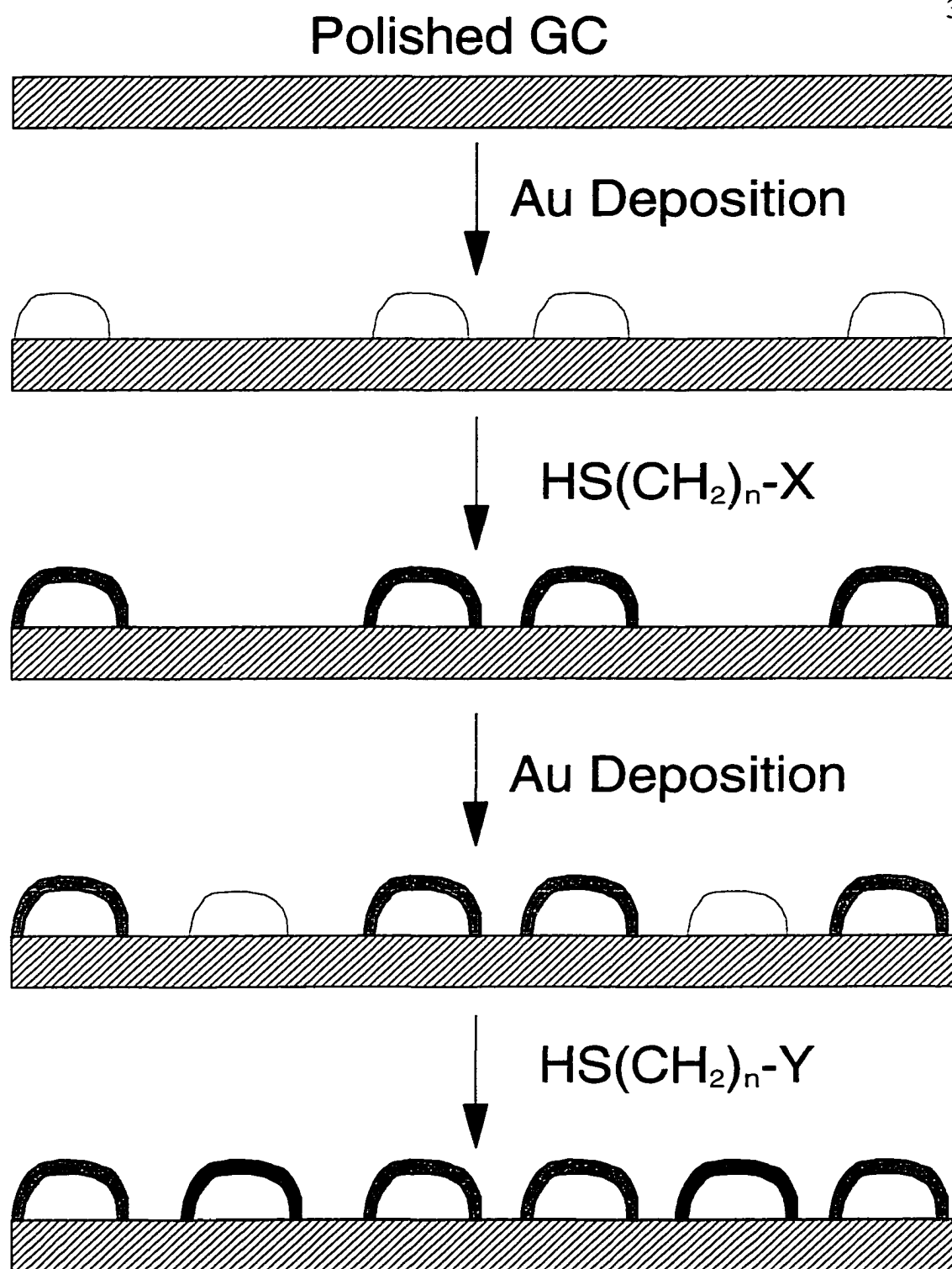


Figure 1.3: Derivatizing GC with multiple functional groups.

the introduction of multiple functional groups onto the surface of a GC electrode, as illustrated in Figure 1.3. This method can be extended to include the attachment of specific receptors or electron transfer mediators to the electrode surface as a means of preparing an electrode of analytical utility.

There are some perceived advantages to the development of such modified electrodes, these are illustrated in Figure 1.2 (c). Firstly, this method provides us with a means of producing segregated domains of specific surface chemistry situated on a conductive carbon support. Employing this method it may eventually be possible to produce an electrode that is selective to multiple analytes. Secondly, these segregated domains may be situated adjacent to electron transfer sites present on regions of the exposed carbon surface. This may provide for more facile electron transfer between the analyte and electrode, eliminating the need for tunneling through the monolayer. The work presented herein describes our efforts and progress toward achieving this goal.

References

1. R. S. Nicholson, *Anal. Chem.*, **37**, 667, (1965).
2. A. J. Bard and L. R. Faulkner, *Electrochemical Methods: Fundamentals and Applications*, John Wiley & Sons, Inc., New York, (1980).
3. W. R. Heineman and P. T. Kissinger, in *Laboratory Techniques In Electroanalytical Chemistry* (P. T. Kissinger and W. R. Heinemann, eds.), Marcel Dekker, Inc., New York, (1996), p. 51.
4. R. S. Nicholson and I. Shain, *Anal. Chem.*, **36**, 706, (1964).
5. P. H. Rieger, *Electrochemistry*, Chapman & Hall, Inc., New York, (1994).
6. R. S. Nicholson and I. Shain, *Anal. Chem.*, **37**, 190, (1965).
7. R. S. Nicholson, *Anal. Chem.*, **37**, 1351, (1965).

8. M. T. McDermott, K. Kneten, and R. L. McCreery, *J. Phys. Chem.*, **96**, 3124, (1992).
9. A. W. Adamson, *Physical Chemistry of Surfaces*, John Wiley & Sons, Inc., New York, (1990).
10. A. P. Brown and F. C. Anson, *J. Electroanal. Chem.*, **83**, 203, (1977).
11. A. P. Brown and F. C. Anson, *Anal. Chem.*, **49**, 1589, (1977).
12. E. Laviron, *J. Electroanal. Chem.*, **52**, 355, (1974).
13. E. Laviron, *J. Electroanal. Chem.*, **52**, 395, (1974).
14. E. Laviron, *J. Electroanal. Chem.*, **101**, 19, (1979).
15. S. S. Lord and L. B. Rogers, *Anal. Chem.*, **26**, 284, (1954).
16. K. Kinoshita, *Carbon: Electrochemical and Physiochemical Properties.*, Wiley, New York, (1988).
17. R. L. McCreery, in *Electroanalytical Chemistry*, Vol. 17, Marcel Dekker, New York, (1991), p. 221.
18. R. L. McCreery and K. K. Cline, in *Laboratory Techniques in Electroanalytical Chemistry* (P. T. Kissinger and W. R. Heineman, eds.), Marcel Dekker, Inc., New York, (1996), p. 293.
19. W. E. van der Linden and J. W. Dieker, *Anal. Chim. Acta*, **119**, 1, (1980).
20. J. O. Bessenhard and H. P. Fritz, *Angew. Chem. Int. Ed. Engl.*, **22**, 950, (1983).
21. S. Yamada and H. Sato, *Nature*, **193**, (1962).
22. H. E. Zittel and F. J. Miller, *Anal. Chem.*, **37**, 200, (1965).
23. G. M. Jenkins and K. Kawamura, *Nature*, **231**, 175, (1971).
24. D. C. Tse and T. Kuwana, *Anal. Chem.*, **50**, 1315, (1978).
25. C. Ueda, D. C. Tse, and T. Kuwana, *Anal. Chem.*, **54**, 850, (1982).

26. B. Persson, *J. Electroanal. Chem.*, **287**, 61, (1990).
27. B. Persson and L. Gorton, *J. Electroanal. Chem.*, **292**, 115, (1990).
28. F. Pariente, E. Lorenzo, and H. D. Abruna, *Anal. Chem.*, **66**, 4337, (1994).
29. F. Pariente, F. Tobalina, M. Darder, E. Lorenzo, and H. D. Abruna, *Anal. Chem.*, **68**, 3135, (1996).
30. F. Pariente, F. Tobalina, G. Moreno, L. Hernandez, E. Lorenzo, and H. D. Abruna, *Anal. Chem.*, **69**, 4065, (1997).
31. M. A. Hayes and W. G. Kuhr, *Anal. Chem.*, **71**, 1720, (1999).
32. H. R. Zare and S. M. Golabi, *J. Electroanal. Chem.*, **464**, 14, (1999).
33. A. Ciszewski and G. Milczarek, *Anal. Chem.*, **71**, 1055, (1999).
34. R. F. Lane and A. T. Hubbard, *J. Phys. Chem.*, **77**, 1401, (1973).
35. R. F. Lane and A. T. Hubbard, *J. Phys. Chem.*, **77**, 1411, (1973).
36. C. M. Elliott and R. W. Murray, *Anal. Chem.*, **48**, 1247, (1976).
37. R. W. Murray, in *Electroanalytical Chemistry*, Vol. 13 (A. J. Bard, ed.), Marcel Dekker, Inc., New York, (1984), p. 191.
38. C. R. Martin and C. A. Foss, in *Laboratory Techniques in Electroanalytical Chemistry* (P. T. Kissinger and W. R. Heineman, eds.), Marcel Dekker, Inc., New York, (1996), p. 404.
39. M. S. Wrighton, *Science*, **231**, 32, (1986).
40. C. E. D. Chidsey and R. W. Murray, *Science*, **231**, 25, (1986).
41. R. W. Murray, A. G. Ewing, and R. A. Durst, *Anal. Chem.*, **59**, 379A, (1987).
42. J. E. Frew and H. A. O. Hill, *Anal. Chem.*, **59**, 933A, (1987).
43. R. P. Baldwin and K. N. Thomsen, *Talanta*, **38**, 1, (1991).

44. A. J. Bard, H. D. Abruna, C. E. D. Chidsey, L. R. Faulkner, S. W. Feldberg, K. Itaya, M. Majada, O. Melroy, R. W. Murray, M. D. Porter, M. P. Soriaga, and H. S. White, *J. Phys. Chem.*, **97**, 7147, (1993).
45. A. P. Brown, C. Koval, and F. C. Anson, *J. Electroanal. Chem.*, **72**, 379, (1976).
46. J. P. Collman, P. Denisevich, Y. Konai, M. Marrocco, C. Koval, and F. C. Anson, *J. Am. Chem. Soc.*, **102**, 6027, (1980).
47. J. Ye and R. P. Baldwin, *Anal. Chem.*, **60**, 2263, (1988).
48. P. Chen, M. A. Fryling, and R. L. McCreery, *Anal. Chem.*, **67**, 3115, (1995).
49. P. Chen and R. L. McCreery, *Anal. Chem.*, **68**, 3958, (1996).
50. R. G. Nuzzo and D. L. Allara, *J. Am. Chem. Soc.*, **105**, 4481, (1983).
51. M. D. Porter, T. B. Bright, D. L. Allara, and C. E. D. Chidsey, *J. Am. Chem. Soc.*, **109**, 3559, (1987).
52. H. O. Finklea, S. Avery, and M. Lynch, *Langmuir*, **3**, 409, (1987).
53. R. G. Nuzzo, F. A. Fusco, and D. L. Allara, *J. Am. Chem. Soc.*, **109**, 2358, (1987).
54. C. D. Bain and G. M. Whitesides, *J. Am. Chem. Soc.*, **110**, 3665, (1988).
55. C. D. Bain, E. B. Troughton, Y. Tao, J. Evall, G. M. Whitesides, and R. G. Nuzzo, *J. Am. Chem. Soc.*, **111**, 321, (1989).
56. R. G. Nuzzo, L. H. Dubois, and D. L. Allara, *J. Am. Chem. Soc.*, **112**, 558, (1990).
57. C. E. D. Chidsey and D. N. Loiacono, *Langmuir*, **6**, 682, (1990).
58. A. Ulman, *An Introduction to Ultrathin Organic Films: From Langmuir-Blodgett to Self-Assembly.*, Academic Press, Inc., Boston, (1991).
59. C. J. Zhong and M. D. Porter, *Anal. Chem.*, 709A, (1995).

60. C. E. D. Chidsey, C. R. Bertozzi, T. M. Putvinski, and A. M. Majsce, *J. Am. Chem. Soc.*, **112**, 4301, (1990).
61. C. E. D. Chidsey, *Science*, **251**, 919, (1991).
62. G. K. Rowe and S. E. Creager, *Langmuir*, **7**, 2307, (1991).
63. M. M. Walczak, D. D. Popenoe, R. S. Deinhammer, B. D. Lamp, C. Chung, and M. D. Porter, *Langmuir*, **7**, 2687, (1991).
64. H. O. Finklea and D. D. Hanshew, *J. Am. Chem. Soc.*, **114**, 3173, (1992).
65. H. O. Finklea, M. S. Ravenscroft, and D. A. Snider, *Langmuir*, **9**, 223, (1993).
66. L. Tender, M. T. Carter, and R. W. Murray, *Anal. Chem.*, **66**, 3173, (1994).
67. K. Weber and S. E. Creager, *Anal. Chem.*, **66**, 3164, (1994).
68. L. A. Hockett and S. E. Creager, *Langmuir*, **11**, 2318, (1995).
69. H. O. Finklea, L. Liu, M. S. Ravenscroft, and S. Punturi, *J. Phys. Chem.*, **100**, 18852, (1996).
70. I. Taniguchi, K. Toyosawa, Y. H., and K. Yasukouchi, *J. Electroanal. Chem.*, **140**, 187, (1982).
71. T. Sagara, K. Niwa, A. Sone, C. Hinnen, and K. Niki, *Langmuir*, **6**, 254, (1990).
72. B. D. Lamp, D. Hobara, M. D. Porter, K. Niki, and T. M. Cotton, *Langmuir*, **13**, 736, (1997).
73. F. Lisdat, B. Ge, and F. W. Scheller, *Electrochem. Comm.*, **1**, 65, (1999).
74. F. Malem and D. Mandler, *Anal. Chem.*, **65**, 37, (1993).
75. B. F. Watkins, J. R. Behling, E. Kariv, and L. L. Miller, *J. Am. Chem. Soc.*, **97**, 3549, (1975).
76. J. F. Evans, T. Kuwana, M. T. Henne, and G. P. Royer, *J. Electroanal. Chem.*, **80**, 409, (1977).

77. C. A. Koval and F. C. Anson, *Anal. Chem.*, **50**, 223, (1978).
78. N. Oyama, A. P. Brown, and F. C. Anson, *J. Electroanal. Chem.*, **87**, 435, (1978).
79. A. E. G. Cass, G. Davis, G. D. Francis, H. A. O. Hill, W. J. Aston, I. J. Higgins, E. V. Plotkin, L. D. L. Scott, and A. P. F. Turner, *Anal. Chem.*, **56**, 667, (1984).
80. A. Anne, B. Blanc, J. Moiroux, and J. M. Saveant, *Langmuir*, **14**, 2368, (1998).
81. L. Netzer and J. Sagiv, *J. Am. Chem. Soc.*, **105**, 674, (1983).
82. A. W. C. Lin, P. Yeh, A. M. Yacynych, and T. Kuwana, *J. Electroanal. Chem.*, **84**, 411, (1977).
83. A. M. Yacynych and T. Kuwana, *Anal. Chem.*, **50**, 640, (1978).
84. P. R. Moses, L. Wier, and R. W. Murray, *Anal. Chem.*, **47**, 1882, (1975).
85. P. R. Moses and R. W. Murray, *J. Am. Chem. Soc.*, **98**, 7435, (1976).
86. D. G. Davis and R. W. Murray, *Anal. Chem.*, **49**, 194, (1977).
87. G. J. Leigh and C. J. Pickett, *J. Chem. Soc. Dalton. Trans.*, 1797, (1977).
88. A. Diaz, *J. Am. Chem. Soc.*, **99**, 5838, (1977).
89. D. C. Bookbinder and M. S. Wrighton, *J. Electrochem. Soc.*, **130**, 1080, (1983).
90. T. Tatsuma, Y. Okawa, and T. Watanabe, *Anal. Chem.*, **61**, 2352, (1989).
91. P. R. Moses and R. W. Murray, *J. Electroanal. Chem.*, **77**, 393, (1977).
92. C. Bourdillon, J. P. Bourgeois, and D. Thomas, *J. Am. Chem. Soc.*, **102**, 4231, (1980).
93. S. Mazur, T. Matusinovic, and K. Cammann, *J. Am. Chem. Soc.*, **99**, 3888, (1977).

94. R. Nowak, F. A. Schultz, M. Umana, H. Abruna, and R. W. Murray, *J. Electroanal. Chem.*, **94**, 219, (1978).
95. B. Barbier, J. Pinson, G. Desarmot, and M. Sanchez, *J. Electrochem. Soc.*, **137**, 1757, (1990).
96. R. S. Deinhammer, M. Ho, J. W. Andereg, and M. D. Porter, *Langmuir*, **10**, 1306, (1994).
97. G. K. Kiema, G. Fitzpatrick, and M. T. McDermott, *Anal. Chem.*, **71**, 4306, (1999).
98. M. Delamar, R. Hitmi, J. Pinson, and J. M. Saveant, *J. Am. Chem. Soc.*, **114**, 5883, (1992).
99. C. Bourdillon, M. Delamar, C. Demaille, R. Hitmi, J. Moiroux, and J. Pinson, *J. Electroanal. Chem.*, **336**, 113, (1992).
100. Y. Liu and R. L. McCreery, *J. Am. Chem. Soc.*, **117**, 11254, (1995).
101. C. Saby, B. Ortiz, G. Y. Champagne, and D. Belanger, *Langmuir*, **13**, 6805, (1997).
102. Y. Liu and R. L. McCreery, *Anal. Chem.*, **69**, 2091, (1997).
103. P. Allongue, M. Delamar, B. Desbat, O. Fagebaume, R. Hitmi, J. Pinson, and J. M. Saveant, *J. Am. Chem. Soc.*, **119**, 201, (1997).
104. B. Ortiz, C. Saby, G. Y. Champagne, and D. Belanger, *J. Electroanal. Chem.*, **455**, 75, (1998).
105. J. K. Kariuki and M. T. McDermott, *Langmuir*, **15**, 6534, (1999).
106. E. Katz, A. Riklin, and I. Willner, *J. Electroanal. Chem.*, **354**, 129, (1993).
107. C. Duan and M. E. Meyerhoff, *Anal. Chem.*, **66**, 1369, (1994).
108. I. Willner and A. Riklin, *Anal. Chem.*, **66**, 1535, (1994).
109. I. Willner, V. Heleg-Shabtai, R. Blonder, E. Katz, and G. Tao, *J. Am. Chem. Soc.*, **118**, 10321, (1996).

110. C. Ruan, F. Yang, C. Lei, and J. Deng, *Anal. Chem.*, **70**, 1721, (1998).
111. F. Lisdat, B. Ge, E. Ehrentreich-Forster, R. Reszka, and F. W. Scheller, *Anal. Chem.*, **71**, 1359, (1999).
112. A. Merz and A. J. Bard, *J. Am. Chem. Soc.*, **100**, 3222, (1978).
113. M. R. Van De Mark and L. L. Miller, *J. Am. Chem. Soc.*, **100**, 3223, (1978).
114. K. K. Kanazawa, A. F. Diaz, R. H. Geiss, W. D. Gill, J. F. Kwak, J. A. Logan, J. F. Rabolt, and G. B. Street, *J. Chem. Soc. Chem. Comm.*, 854, (1979).
115. G. P. Kittlesen, H. S. White, and M. S. Wrighton, *J. Am. Chem. Soc.*, **106**, 7389, (1984).
116. R. A. Bull, F. Fan, and A. J. Bard, *J. Electrochem. Soc.*, **131**, 687, (1984).
117. B. J. Feldman, P. Burgmayer, and R. W. Murray, *J. Am. Chem. Soc.*, **107**, 872, (1985).
118. R. A. Saraceno, J. G. Pack, and A. G. Ewing, *J. Electroanal. Chem.*, **197**, 265, (1986).
119. S. M. Hendrickson, M. Krejcik, and C. M. Elliott, *Anal. Chem.*, **69**, 718, (1997).
120. J. Wang, M. Jiang, and B. Mukherjee, *Anal. Chem.*, **71**, 4095, (1999).
121. N. Oyama and F. C. Anson, *J. Am. Chem. Soc.*, **101**, 739, (1979).
122. N. Oyama and F. C. Anson, *J. Electrochem. Soc.*, **127**, 247, (1980).
123. H. D. Abruna, P. Denisevich, M. Umana, T. J. Meyer, and R. W. Murray, *J. Am. Chem. Soc.*, **103**, 1, (1981).
124. D. J. Harrison, K. A. Daube, and M. S. Wrighton, *J. Electroanal. Chem.*, **163**, 93, (1984).
125. K. Doblhofer and R. Lange, *J. Electroanal. Chem.*, **229**, 239, (1987).
126. D. A. Buttry and F. C. Anson, *J. Am. Chem. Soc.*, **104**, 4824, (1982).

127. C. R. Martin, I. Rubinstein, and A. J. Bard, *J. Am. Chem. Soc.*, **104**, 4817, (1982).
128. C. R. Martin, T. A. Rhoades, and J. A. Ferguson, *Anal. Chem.*, **54**, 1639, (1982).
129. D. J. Harrison, *Chem 415 Lab Manual, Experiment #4, Rotating Disk Voltammetry*, University of Alberta, (1996).
130. S. M. Golabi and H. R. Zare, *J. Electroanal. Chem.*, **465**, 168, (1999).

CHAPTER II

CHARACTERIZATION OF ELECTROCHEMICALLY DEPOSITED GOLD PARTICLES ON GLASSY CARBON ELECTRODES

Introduction

The work presented herein concentrates on the electrochemical deposition of small gold particles on glassy carbon (GC) electrodes. Our efforts are motivated by the potential utility of these supported gold particles as future modification sites in the preparation of chemically modified electrodes. Ultimately, our goal is to exploit gold-sulfur chemistry to modify the carbon electrode surface with electron transfer mediators in an effort to produce a customized carbon electrode surface with potentially useful analytical applications. However, before such modifications can be attempted, it is important to develop a procedure for introducing small gold particles onto the electrode surface. Ideally, the particles should be small, well dispersed, and present in large number densities. This has prompted us to study the nucleation and growth behaviour of gold on GC, and how this behaviour can be manipulated experimentally to produce gold particles of desired size and shape. In this work we have studied the effects of deposition solution concentration and overpotential on the nature of the gold deposits obtained. We have also developed electrochemical methods to determine the surface area and probe the microcrystalline structure of the resulting gold particles through the use of surface oxidation and underpotential deposition of lead. Scanning electron microscopy was employed to gain a visual representation of the gold deposits and correlations are made between the information obtained from scanning electron micrographs and the observed electrochemical behaviour of the gold particles. Gold was

employed because thiol molecules spontaneously self-assemble on gold substrates. We feel that this approach has promise as a new method for preparing chemically modified carbon electrodes and attaching functional groups to GC.

Interest in the study of small metal particles is due, in large part, to their valuable catalytic properties. An important modern day example of such an application is the use of small supported platinum particles as a catalyst in the membrane-electrode-assemblies of proton exchange membrane (PEM) fuel cells. Several other metals also display catalytic properties including: palladium, ruthenium, rhodium, iridium, and nickel. Often times the metal is supported on a solid substrate, such as carbon, as small particles. The reasons for employing small metal particles are two fold. Firstly, due to the high cost of most of these metals it not economically feasible to employ large quantities of metal in the preparation of, say, a fuel cell electrode. Secondly, heterogeneous catalysis involves specific surface phenomena and chemisorption of reactants to the catalyst usually plays an important role in this function [1]. A dramatic increase in catalyst utilization is realized with smaller particles, as smaller particles result in a larger active surface area [2]. However, catalytic activity is usually dependent on particle size and smaller particles may not necessarily serve as better catalysts. Small metal particles can be prepared on solid substrates using a variety of methods; this is called loading. Such methods include impregnation, ion exchange, adsorption, the use of organic macrocycles, and electrochemical deposition [3]. Further discussion will focus on electrochemical deposition.

The electrochemical deposition of metal particles onto carbon electrodes has been the subject of a large number of investigations [4-21]. Interest is sparked, in most cases, by the utility of this type of interface in electrocatalysis and as model systems for electroplating. The focus of many of these studies has been on the early stages of electrochemical deposition in an effort to elucidate the nucleation and growth mechanism of the metal phase on the substrate. Some

common experimental procedures for studying these nucleation and growth mechanisms will now be discussed. This discussion is based largely on the work of Gunawardena and co-workers [4-9]. These studies are of particular relevance because they deal mainly with the electrochemical nucleation and growth of various metals on GC electrodes.

An advantage of studying electrochemical nucleation and growth, over other nucleation and growth methods, i.e. precipitation, is the ability to control the degree of supersaturation by controlling the potential applied to the working electrode [4]. In order for nucleation and growth to proceed at an appreciable rate, an overpotential must be applied to the working electrode. This is known as the activation overpotential [22] because it is required to drive the heterogeneous process at a rate reflected by the current. As will be illustrated in these studies, overpotential has a profound effect on the nucleation and growth behaviour of gold particles on GC.

There are three main electrochemical methods that may be employed to study the nucleation and growth of electrochemically deposited metal particles [4]. The first of these is a linear potential sweep or cycle. This method is used mainly as a qualitative indicator or diagnostic of nucleation and growth behaviour. Cyclic voltammograms for metal deposition display a characteristic cross-over of the current in the cathodic branch [5]. Cross-over is due to more facile metal deposition on the bulk metal than on the carbon substrate. Thus, once initial nucleation sites are established, greater current is observed due to further growth, and the increasing area of these nuclei. Successive potential cycles are not reproducible as metal deposition occurs more readily on the second and successive cycles, due to the presence of existing nuclei [5]. The second method is called the current step method. It is also a useful means for detecting the presence of nucleation behavior, but not used extensively enough in the literature to warrant a detailed discussion. The third, and most widely used technique is the potential

step method. This method has been used by several authors to characterize the nucleation and growth of a variety of metals on a number of substrates [4-10, 12, 21].

As alluded to previously, overpotential is analagous to the degree of supersaturation in the consideration of nucleation and growth from concentrated solutions. Thus, it is important to consider how changes in overpotential can affect the nucleation and growth behavior of metal nuclei on an electrode surface. Previous studies have shown that an increase in number density is realized with increasing overpotential for a variety of metals on GC [4-9]. For instantaneous nucleation, the number of nuclei N_n can be related to the current density j at time t using the following expression,

$$j = \lambda A(t) N_n \quad \{2.1\}$$

where,

$$\lambda = zFk \exp(-\alpha zF\eta/RT) C_M \quad \{2.2\}$$

and C_M is the concentration of metal ions in solution. Substituting Equation {2.2} into Equation {2.1} for λ and rearranging, one may obtain an equation that relates number density to the applied overpotential. As overpotential is increased, an increase in number density is expected be observed.

When a potential step is applied to the working electrode, the resulting current transients can be evaluated to obtain information such as induction times, nucleation rate constants, nuclear number densities, and nucleation and growth mechanism. The two main features of these transients are a rising portion, which corresponds to the increase in electroactive area as established nuclei grow and new nuclei are formed, and the position of the current maximum in terms of the

current and time maxima, i_{max} and t_{max} . From these values it is possible to predict the nucleation and growth mechanism using the following equations,

$$i_{max}^2 t_{max} = 0.2598(nFC^*)^2 D \quad \{2.3\}$$

for progressive nucleation, and,

$$i_{max}^2 t_{max} = 0.1629(nFC^*)^2 D \quad \{2.4\}$$

for instantaneous nucleation. The distinction between these two mechanisms is that in the case of instantaneous nucleation, all of the available sites for nucleation at a specific overpotential are readily exhausted. In progressive nucleation, new nucleation sites are formed continuously, as long as the diffusion layer immediately next to the electrode surface is not so depleted in metal ions that planar diffusion becomes predominant [4]. When the overpotential is sufficiently high, Cottrellian behaviour is observed, and it is possible to determine the diffusion coefficient of the aqueous metal ions/complexes in solution.

For systems that obey the instantaneous nucleation and growth model, current, i can be plotted as a function of $t^{1/2}$ according to the following equation for the rising portion of the transient.

$$i(t) = nF\pi(2DC^*)^{3/2} M^{1/2} N t^{1/2} / \rho^{1/2} \quad \{2.5\}$$

where nF is the molar charge of the depositing species, D is the diffusion coefficient, C^* is the concentration (in mol/cm³), M is the molecular weight, and ρ is the density of the metal. A straight line results and thus it is possible to determine the number density, N of particles growing by hemispherical diffusive

flux, from the slope of this line. The limiting factor imposed on N is mainly that of overlapping diffusion zones, i.e., when planar diffusion to the electrode surface becomes predominant [4].

In recent studies, Zoval and co-workers applied this method to the determination of the number density of silver [10] and platinum [12] nuclei on the basal plane of HOPG electrodes. The results obtained differ significantly for the two metals studied. For silver nuclei, number density values obtained using Equation {2.5} were compared to those estimated from noncontact atomic force microscopy images of the graphite electrode surface and were found to be in good agreement. For platinum nuclei, however, the current transients for platinum deposition do not display the initial rising portion and resemble Cottrellian behavior. Thus, it was not possible to predict the number density of this system using the i vs. $t^{1/2}$ method of Equation {2.5}. The reason for this, as stated by the authors, is that the number density values obtained from image analysis (3.0×10^9 to $6.0 \times 10^9 \text{ cm}^{-2}$) translate into an average interparticle distance of 140 to 200 nm. Thus, due to the small interparticle spacing, hemispherical diffusion zones quickly coalesce, and a planar diffusion controlled response is observed. In principle, if the microsecond time domain were experimentally accessible, then a rising portion of the transient that is linear with $t^{1/2}$ would be observed at very short times as predicted by Equation {2.5} [4].

Comparing the results of these two studies, it should be pointed out that for silver nuclei on HOPG, a number density of $2.7 \times 10^9 \text{ cm}^{-2}$ was obtained [10]. Theoretically, this value should give rise to similar interparticle spacings as those determined for platinum, yet, a rising portion in the deposition current transients is still observed. This would suggest that the explanation is more complicated than a simple transition from hemispherical to planar diffusion. Perhaps this behaviour is due to a difference in the rate of growth of the particles upon their initial nucleation, with platinum particle growth proceeding at a larger rate than silver

particle growth. From these studies, it has been determined that both systems obey the instantaneous nucleation and growth model. Thus, while these two systems may theoretically possess similar characteristics, the behaviour they actually exhibit in practice is strikingly different.

Studies examining the electrochemical deposition of gold onto various carbon substrates have recently emerged [23-27]. The main focus of these reports was to study the electrodeposition of gold with specific emphasis on electroplating applications. These reports suggest that electrochemical deposition of gold from a variety of electrolytes occurs via a nucleation and growth process on carbon, and results in three-dimensional gold particles. Because of our desire to spontaneously adsorb specific functional groups to supported gold particles, the size, structure, and distribution of these particles must be controlled. Ideally, small, well-dispersed gold particles are desired as precursors for chemical modification. The experiments presented herein are aimed at characterizing the overall gold surface area deposited, as well as the microcrystal structure, size, and spatial density of the resulting particles. Results of these experiments provide us with a standard procedure for preparing gold particles supported on GC of known size and number density for the purpose of further chemical modification.

Determination of gold surface area is important because it gives an indication of the fraction of the electrode surface that has been made available for further modification; however, it is not a simple matter. Since both gold and GC are active electrode materials it is not possible to perform a simple experiment such as chronoamperometry in $K_3Fe(CN)_6$ to obtain the electrode area. Such an experiment renders the geometric area of the gold and GC combined. Therefore, methods that are selective to the gold particles must be employed. An alternative method that can be used to determine electrode area is to examine the electron transfer behavior of an adsorbed redox species. As discussed in Chapter I, adsorbed redox species display significantly different electron transfer behavior

than those in solution. The behavior of a redox species in solution is dictated by diffusional mass transport to the electrode surface. As adsorbed species are already present at the electrode surface, such mass transport effects are not observed. Brown and Anson showed that integration of the charge under a voltammetric wave is proportional to the amount of adsorbed material using Equation {1.19} [28, 29]. Therefore, one can experimentally obtain a value of the saturation coverage, Γ_{sat} , for an adsorbate on an electrode of known area, and then this value may be used along with Equation {1.19} to obtain the unknown area of an electrode by integrating the charge under the adsorption wave. There is an important distinction to be made between this method and that of chronoamperometry using the Cottrell equation. Since this method involves redox species adsorbed/bound directly to the electrode surface, the real electrode area is obtained and the roughness factor of the electrode surface must be taken into account. Chronoamperometry renders the geometric electrode area, which is independent of surface roughness. The roughness factor of an electrode is defined as the ratio of its real area to its geometric area. In order to apply this method to gold particles a suitable adsorbate that is selective for gold is needed.

The use of hydrogen adsorption and surface oxidation has been investigated as a method for determining the surface area of noble metal electrodes such as platinum, palladium, rhodium, and gold [30, 31]. Rand and Woods derived a method for obtaining the real surface areas of rhodium, palladium, and gold electrodes by determination of the stoichiometry of chemisorbed oxygen on these metals. While rhodium displays both hydrogen and oxygen adsorption, no analogous hydrogen adsorption is observed for palladium or gold [30]. It was also demonstrated that oxygen adsorption approaches a limiting value on rhodium, even at high anodization potentials, however, this is not the case for platinum, palladium or gold. Beyond a brief plateau, anodization at higher potentials causes severe roughening of a gold electrode surface accompanied by the irreversible

formation of “phase oxide” which causes permanent damage to the electrode surface [30, 32-35].

The electrochemical oxidation of gold electrodes has been the focus of many studies [30, 32-41], perhaps, in part, due to the fact that gold has no stable surface oxides at open circuit. When a gold electrode is cycled at sufficiently anodic potentials, anodic and cathodic waves due to oxidation and reduction of the gold surface appear. It has been shown that the exact position and appearance of these waves is dependent upon the supporting electrolyte used, due to the effects of adsorbed anions [35-37]. The magnitude of the reduction wave is also dependent upon the magnitude of the anodic potential limit, and anodization time [30, 32, 33]. Thus, in order to apply this method to the determination of gold surface area, anodization of the gold surface must be carefully controlled in order to ensure reproducible coverage. Ideally, monolayer coverage is desired. Several authors have attempted to derive the charge required for the reduction of a monolayer of gold surface oxide groups [32, 33, 35]. Agreement between these values is generally quite good with values ranging between 427 and 482 $\mu\text{C}/\text{cm}^2$. Thus, it seems reasonable to conclude that use of the gold oxide reduction peak would be an acceptable method for determination of the surface area of gold particles on GC.

Underpotential deposition (UPD) of lead is another electrochemical system that displays selectivity for gold, as UPD of lead on GC is not observed. It involves the deposition of a monolayer of metal adatoms at potentials more positive than the reduction potential for bulk deposition of the metal, i.e. at potentials more positive than those predicted by the Nernst equation [22]. The formation of UPD monolayers is related to the energetics of the foreign metal (M) and substrate (S) bonding. Underpotential deposition occurs when the M-S bonding is more favorable than M-M bonding in the bulk metal [42]. Some

examples of systems that display this behaviour are lead on gold, copper on gold, lead on silver and copper on platinum.

UPD of lead on gold has been studied extensively by a number of researchers [43-51]. The majority of these studies have been performed using gold single crystal electrodes of specific crystallographic orientation, particularly Au(111), (110), and (100) faces. Cyclic and linear sweep voltammograms demonstrate that the desorption potential of UPD lead is dependent upon the crystallographic orientation of the underlying substrate. Hamelin and Lipkowski have determined the Gibbs free energy of adsorption (ΔG_A) for the (111), (100), (100), faces and several monatomic steps on the gold surface [50]. This information has been employed to assess the crystallographic orientation of polycrystalline gold electrodes [43, 52]. Walczak and coworkers have demonstrated how the polycrystalline nature of a gold thin film is influenced based on the underlying substrate [43]. Evaporative deposition onto mica gives rise to larger Au(111) terraces than either glass or silicon. We have also adopted this method as a tool to gauge the microcrystalline structure of the resulting gold particles.

Our interest in the rational design of chemically modified carbon electrodes has prompted us to consider supported metal particles as sites for future modification steps. The large body of recent literature on the modification of gold electrodes and colloids by the spontaneous chemisorption of alkanethiols ($X(\text{CH}_2)_n\text{SH}$) guided us to explore the electrochemical deposition of gold particles. The results presented in Chapter II concentrate on characterizations of gold particles electrochemically deposited on GC substrates, and development of a standardized method for the preparation of supported gold particle arrays.

Experimental

Chemicals. Potassium tetrachloroaurate(III) (Aldrich), lead oxide (Certified, Fisher), sodium fluoride (Analytical Grade, BDH), potassium hexacyanoferrate(III) (Certified, Caledon), potassium chloride (Anachemia), sulfuric acid (Fisher), perchloric acid (Caledon) were all used as received. All solutions were prepared using Nanopure water (18 M Ω /cm) and purged with prepurified argon prior to use.

Electrode Preparation. GC electrodes (Tokai GC-20, Electrosynthesis Company, NY) were prepared by polishing on Micropolish polishing cloth (Buehler) in alumina/water slurries. Two grades of polishing alumina were employed, 1.0 micron alpha alumina, and 0.3 micron alpha alumina (Buehler). Upon polishing, the electrodes were rinsed, sonicated for ten minutes, rinsed, sonicated further for ten minutes, rinsed, and stored in a beaker of water. This procedure was repeated after polishing with each size of alumina. Nanopure water was used throughout the polishing process and the electrodes were used immediately after being polished.

Polycrystalline gold electrodes consisted of 3 mm diameter gold wire embedded into a teflon electrode body. Electrical contact to the gold wire is made through a brass rod and silver epoxy. Gold electrodes were polished using the same procedure as GC electrodes.

Electrochemistry. All electrochemical experiments were performed in an inverted three-electrode cell or glass beaker. The electrodes were connected to a Pine Model AFCBP1 bipotentiostat with platinum auxiliary and Ag/AgCl (sat'd KCl) reference electrodes. All cyclic voltammograms were collected using PineChem version 2.5.2 software. The auxiliary electrode was separated from the bulk solution using a glass frit. All potentials in the text are referred to the Ag/AgCl reference electrode unless stated otherwise. The GC electrodes were mounted into the inverted cell between a viton o-ring and a metal plate and held in

place by the use of a metal clip. The geometrical electrode area is defined by the circumference of the o-ring and forms the bottom of the inverted cell.

Determination of Electrode Area. Chronoamperometry of 1 mM $\text{Fe}(\text{CN})_6^{-3/4}$ in 0.1 M KCl yielded a working electrode area of $0.31 \text{ cm}^2 \pm 0.02 \text{ cm}^2$ for the viton o-ring in the inverted cell. A 5 second potential step from 0 mV to 800 mV was employed. The geometric electrode area was then determined using the Cottrell equation {1.13} and the slope of i vs. $t^{-1/2}$ plots. The first 200 ms of the experiment are disregarded due to charging of the double layer. A value of $6.32 \times 10^{-6} \text{ cm}^2/\text{s}$ was employed for the diffusion coefficient of $\text{Fe}(\text{CN})_6^{-3/4}$.

As the charge due to gold surface oxide reduction is dependent on time and potential, a value for the reduction of a monolayer of adsorbed oxygen was initially determined using polycrystalline gold electrodes of known surface area and roughness factor under standardized anodization conditions. Gold particle surface areas were then determined using this value in Equation {1.19} under identical conditions.

Capacitance Measurements. The capacitance of polycrystalline gold electrodes was measured in 0.1 M NaF. Differential capacitance was determined using a 63 Hz, 20 mV peak-to-peak triangle wave centered at -0.6 V . The peak-to-peak current of the output waveform is proportional to the capacitance [53].

Metal deposition. Gold particles were electrochemically deposited on GC electrodes by potential step from 1100 mV to some final deposition potential for a period of 5 seconds. A series of AuCl_4^- deposition solution concentrations and deposition overpotentials were investigated.

SEM Imaging. Scanning electron microscopy analysis of the gold deposits was carried out using a JEOL model 6301FXV scanning electron microscope at an acceleration voltage of 15 to 20 kV and a working distance of 4 to 5 mm. Image analysis was performed visually (i.e., manually counting particles) or with the aid

of commercial software (Image Tool, version 2.00, University of Texas Health Science Center in San Antonio) for particle counting and diameter measurement.

Results and Discussion

The objectives of these studies were focused on controlling the size, density and structure of electrochemically deposited gold particles on GC. Once a protocol has been developed for producing well dispersed gold particle arrays, the gold particles can be subjected to further chemical modification by self-assembly. Toward this end, gold particles formed via potential step as a function of the initial bulk AuCl_4^- concentration, and overpotential (η) at constant concentration, have been studied. It was desirable to produce arrays of well-dispersed, nanometer-sized gold particles; thus, the deposition concentrations used here, 10 μM to 200 μM , are significantly lower than those employed in previous studies [23-27]. Characterization of the gold particles is aimed at elucidating the surface area and crystal structure of the electrochemically deposited gold, as well as the size and number density of the particles. Because both GC and gold are active electrode materials, methodologies which could distinguish between the two materials were employed.

Gold Particle Deposition. Gold particles were deposited on GC substrates from 0.5 M H_2SO_4 solutions of KAuCl_4 by employing a 5 second potential step from 1100 mV to some final potential. An overview of the electrochemical behavior of this system is provided in Figures 2.1 and 2.2. Figure 2.1 is a current-potential curve for a cyclic voltammetric experiment at a polished GC electrode in 200 μM AuCl_4^- . This wave exhibits an initial cathodic current at ~ 800 mV and a sharp peak at ~ 500 mV, corresponding to the reduction of solvated Au(III) to Au(0). The initial wave at 800 mV is attributed to the reduction of adsorbed AuCl_4^- . Voltammetric evidence for the adsorption of gold complexes to carbon electrodes similar to Figure 2.1 has been observed previously [23, 27]. Crossover

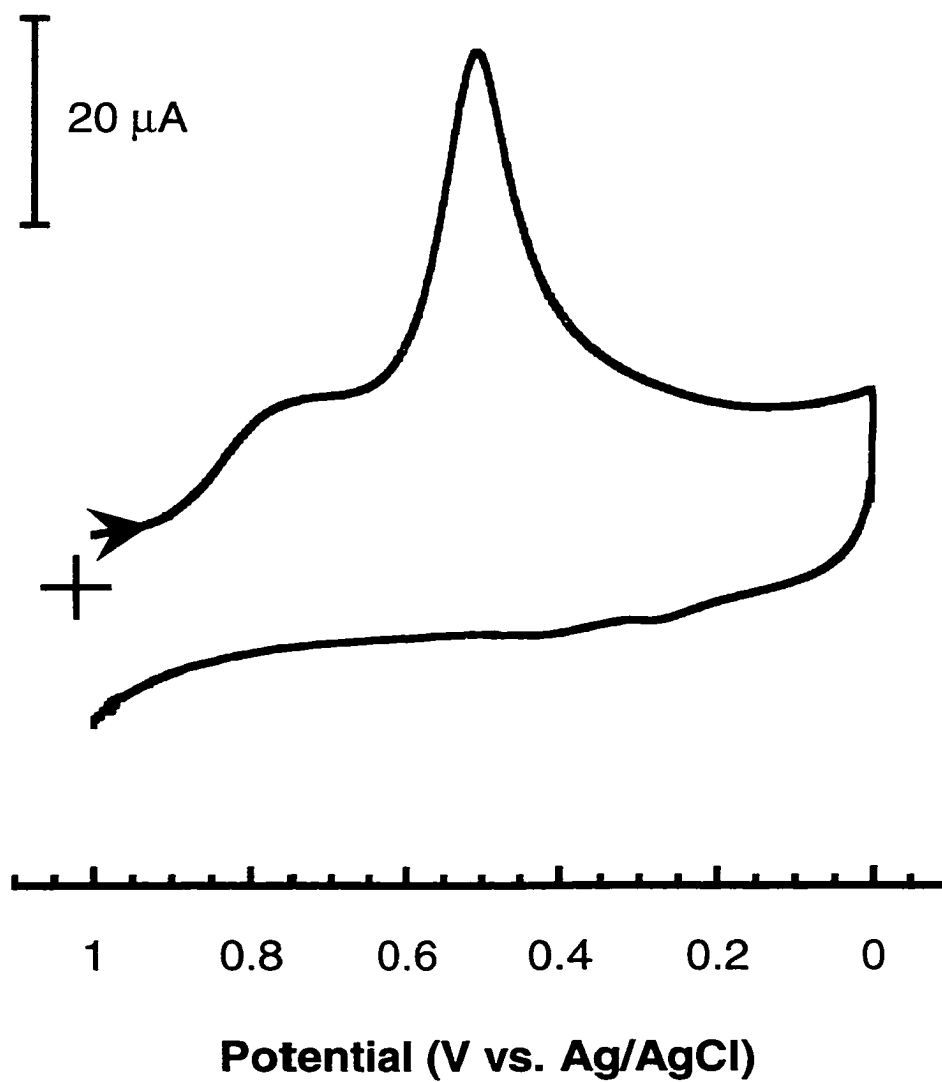


Figure 2.1: Cyclic voltammetry of 200 μM AuCl_4^- in 0.5 M H_2SO_4 on a polished GC electrode, $\nu = 100$ mV/s.

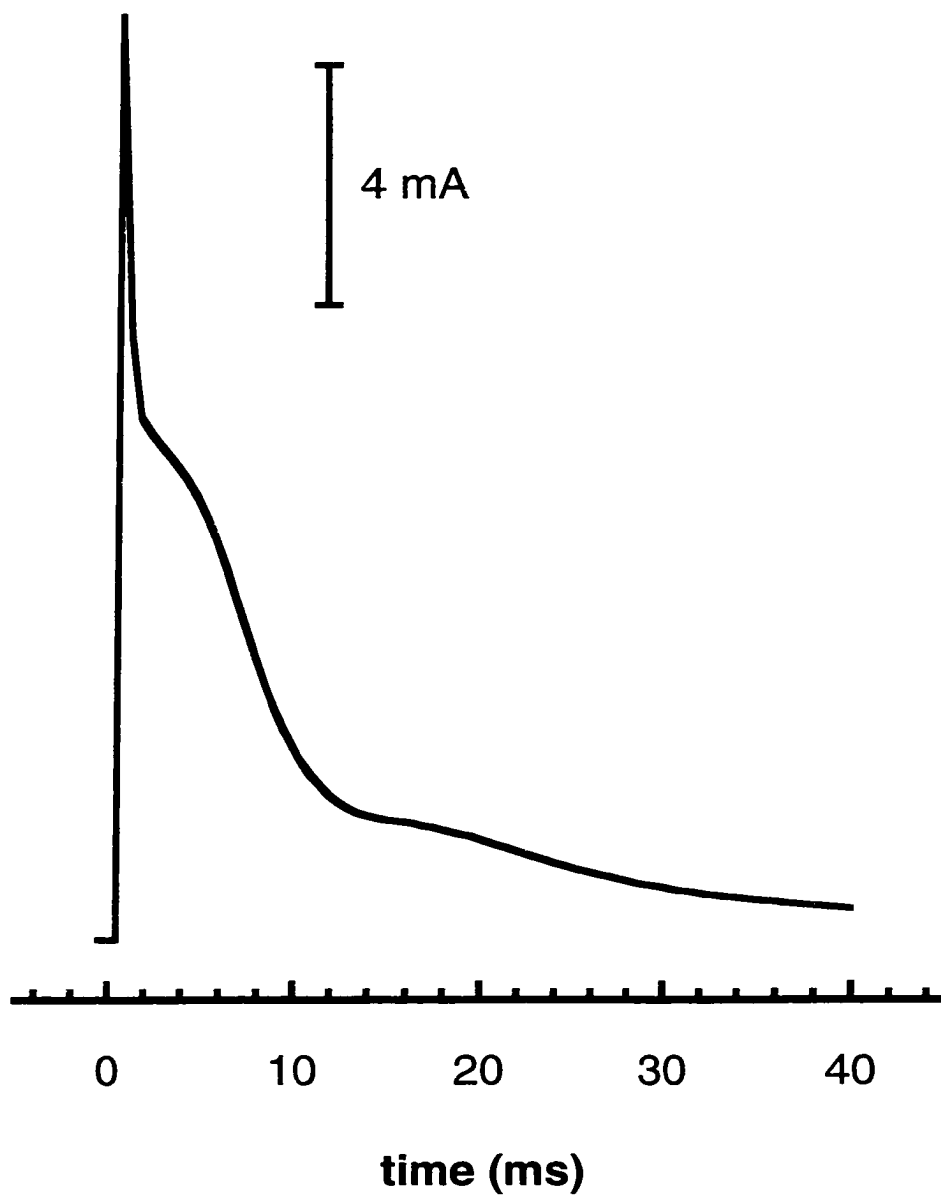


Figure 2.2: Current response to a potential step of 1100 to 0 mV on a polished GC electrode, 200 μM AuCl_4^- in 0.5 M H_2SO_4 .

of the cathodic branch, reflective of metal nucleation and growth, is not observed at the scan rate employed in Figure 2.1 [4, 5]. Voltammetry which more closely resembles reported current-potential curves for nucleation and growth is observed at scan rates slower than 5 mV/s [23]. Furthermore, no anodic current is observed on the reverse sweep indicating the irreversibility of the reduction of AuCl_4^- . In 0.5 M H_2SO_4 , the electrochemical dissolution of deposited gold is not observed within the potential limits employed in these characterizations, 1500 to -400 mV. All overpotentials stated here are relative to the standard potential for AuCl_4^- reduction to $\text{Au}(0)$ which is 800 mV vs. Ag/AgCl (sat'd KCl). Note that from Figure 2.1, gold deposition on GC requires an overpotential of about -300 mV.

The first 50 ms of a representative current response to a potential step from 1100 mV to 0 mV in 200 μM AuCl_4^- is shown in Figure 2.2. The initial sharp current spike is due to the charging of the double-layer. The curve then exhibits a humped shaped response following the charging current spike. The position and size of these humps varies with overpotential and thus is likely the tail of a current peak commonly observed for the electrochemical nucleation and three dimensional growth of metal crystallites [23]. Similar behavior is observed for the electrochemical deposition of platinum on GC [13]. After the second hump, a current decay is observed which is linear with $t^{-1/2}$ reflecting a planar diffusion regime. This situation develops due to overlap of growing hemispherical diffusion layers which initially provide mass transport for particle growth [4]. The position of the hump in Figure 2.2 within the first 10 ms argues that the growth of the Au nuclei is relatively rapid. Because the rising portion of the peak is experimentally inaccessible under our conditions, an analysis of the nucleation mechanism (i.e., instantaneous vs. progressive) is not possible from current transients [4].

Figure 2.3 contains a series of current transients obtained from a deposition solution concentration study. The concentrations employed were 200, 100, 50 and 10 μM AuCl_4^- , shown in traces (a) to (d) respectively. Two important

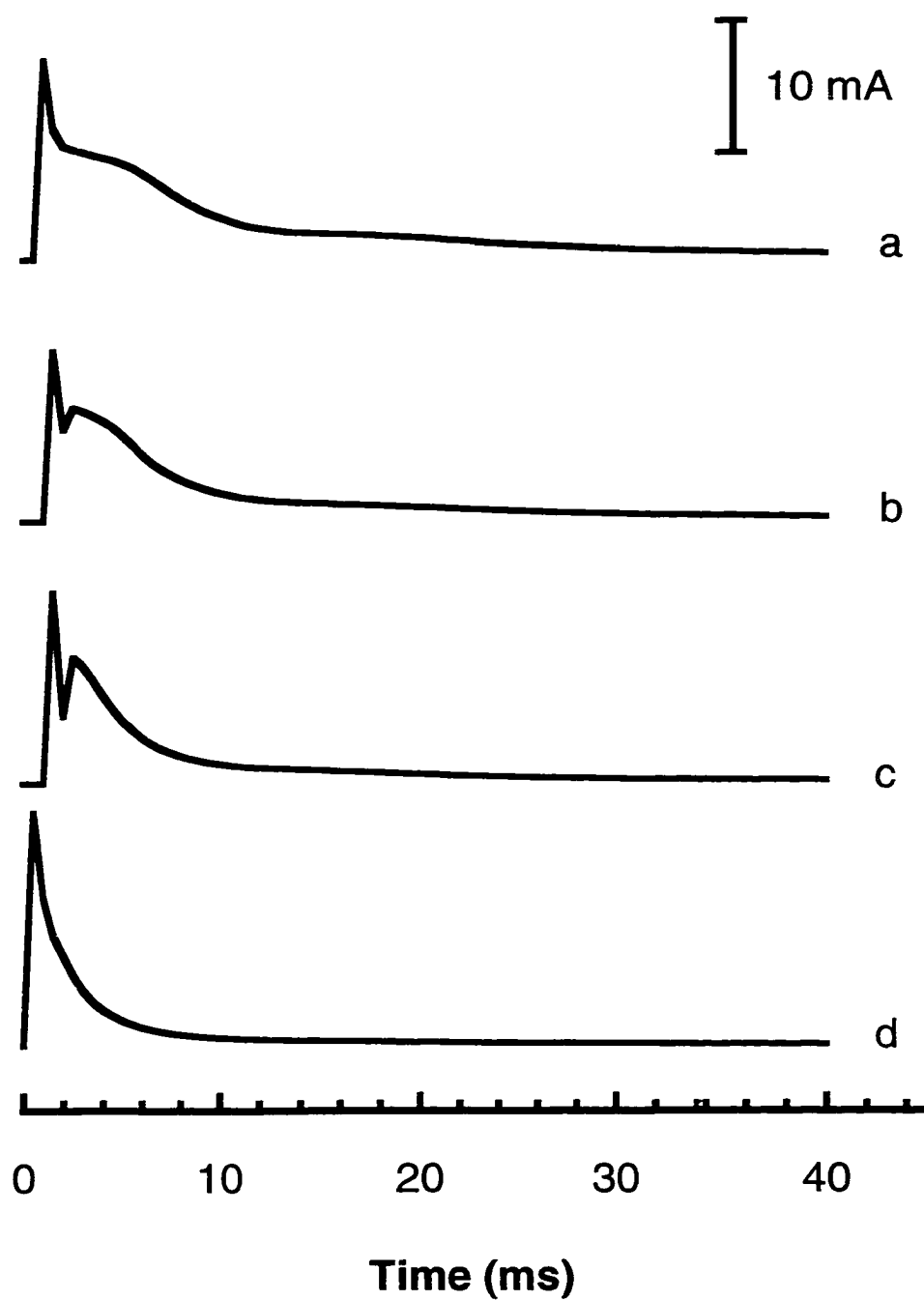


Figure 2.3: Representative current transients for gold deposition on GC from solutions of varying AuCl_4^- concentration, $\eta = -800 \text{ mV}$. (a) $200 \mu\text{M}$, (b) $100 \mu\text{M}$, (c) $50 \mu\text{M}$, (d) $10 \mu\text{M}$, in $0.5 \text{ M H}_2\text{SO}_4$.

observations can be made upon close examination of this set of current transients. Firstly, it is important to observe the presence of a rising portion in the current transients. This is most evident in traces (b) and (c). As discussed previously, this feature is indicative of nucleation and growth behavior. In most cases, it was very difficult to capture this behavior on the current transients obtained during these experiments; however, these examples clearly illustrate its presence. The elusive nature of this feature is attributed to fast nucleation and growth behavior on the experimental time scale. As observed in the figure, the rising portion is surpassed within the first 10 to 15 ms of the experiment, and often superimposed with double layer charging current. Zoval encountered similar difficulties while studying platinum deposition on graphite [12]. An interesting explanation of this behaviour may be attributed to the nature of the metal ions in solution. Simple metal ions such as Ag^+ [4, 5, 10], Hg_2^{2+} [4, 6], Cu^{2+} [8], Cd^{2+} [9], Sn^{2+} [20], and In^{3+} [7], all display significant rising portions in their deposition transients. For complex metal ions such as AuCl_4^- [55] and PtCl_6^{2-} [12], observation of this behavior has proven to be more elusive. The second feature one may observe from this set of transients is that the charge under the current transient increases with increasing deposition solution concentration. As expected, this is indicative of increased gold deposition due to higher concentrations of AuCl_4^- .

Figure 2.4 contains a series of current transients obtained from a deposition overpotential study. As observed in previous studies, nucleation and growth behavior is very sensitive to overpotential [4-10]. The overpotentials employed here were -1000, -800, -600, and -400 mV, for traces (a) to (d) respectively. Unfortunately, no rising portion is observed in any of these transients, hence it is difficult to locate the current maximum, i_{max} , and t_{max} values. Regardless of this, it is still observed that the maximum shifts to longer times as the overpotential is decreased, and the transients become broadened. This behavior is consistent with results of previous studies for gold deposition on GC [23]. A possible explanation

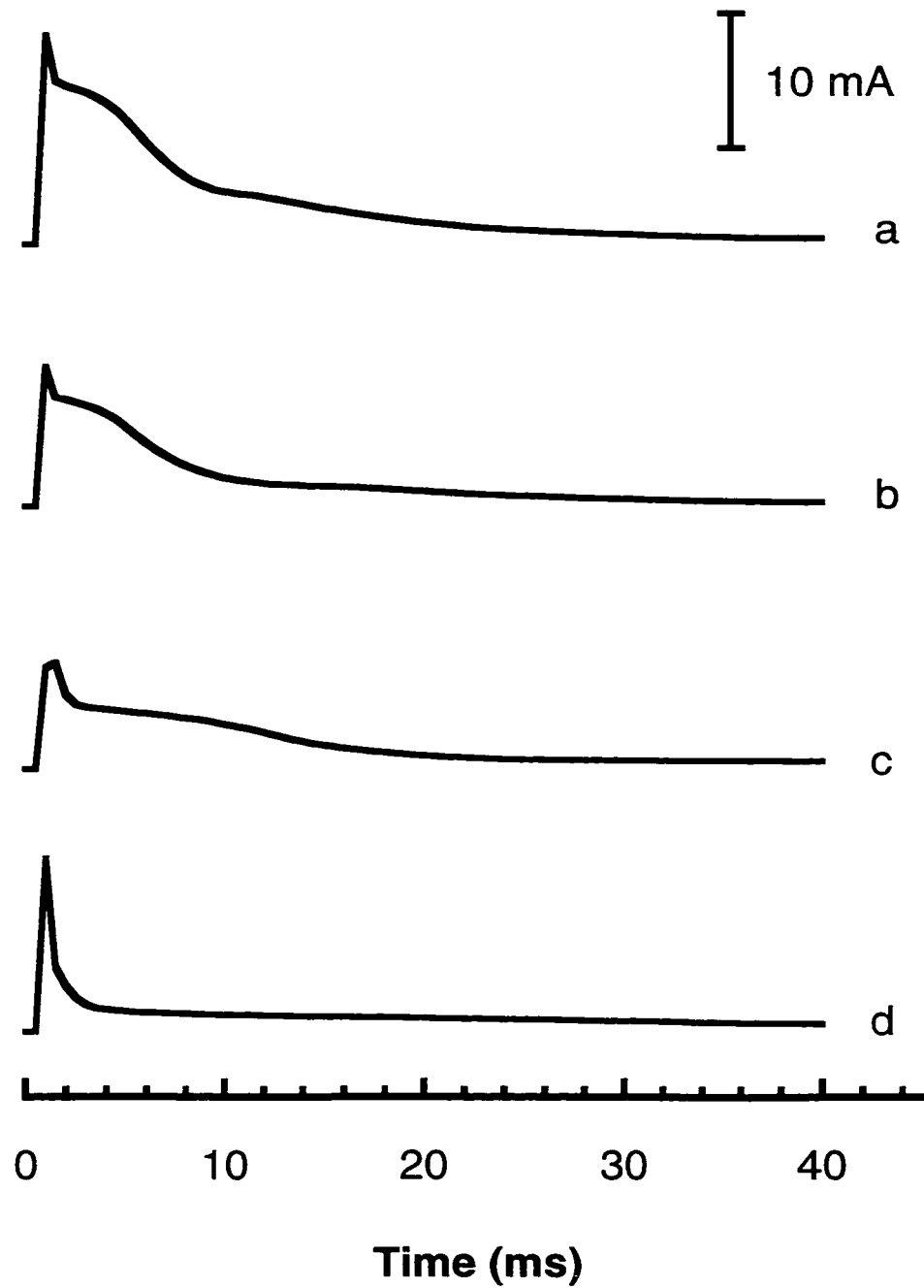


Figure 2.4: Representative current transients for gold deposition on GC at varying overpotentials, $[\text{AuCl}_4^-] = 200 \mu\text{M}$. (a) -1000 mV , (b) -800 mV , (c) -600 mV , (d) -400 mV , in $0.5 \text{ M H}_2\text{SO}_4$.

for this behavior is that at lower overpotential fewer nucleation sites are accessed and hence smaller number densities are observed. This behavior gives rise to larger particles. With fewer growing nuclei on the electrode surface, it will take longer for the hemispherical diffusion layers of individual particles to overlap; thus, hemispherical diffusive flux of metal ions to the growing nuclei is sustained for a longer period of time before planar diffusion begins to predominate.

$$i_d(t) = nFA D_O C_O^* \left[\frac{1}{(\pi D_O t)^{1/2}} + \frac{1}{r_o} \right] \quad \{2.6\}$$

Equation {2.4} can be used to describe the combined effects of planar and radial diffusion on current at a microelectrode [22]. When an array of microelectrodes, such as uniformly dispersed gold particles, is considered, three diffusion regimes can arise depending on the extent of electrolysis. Considering the case where electrolysis is exhaustive, as in metal deposition, the diffusion layer thickness, defined as $(\pi D_O t)^{1/2}$, becomes much larger than the radius of the microelectrodes (r_o) or metal particles in this case. Under these circumstances the diffusion layers of the gold particles begin to overlap, and Cottrell behavior, i.e. planar diffusion, is observed. For larger and fewer particles it will take a longer period of time for the individual diffusion layers to overlap due to the greater distance between the growing metal nuclei. Thus, it is possible that the humps observed in the gold deposition transients are a result of this hemispherical diffusive flux, and hence, indicative of growth of the gold nuclei.

Gold Oxide Reduction. The extent to which a GC electrode surface can be chemically modified will ultimately depend on the surface area of gold particles. Insights into this parameter are provided by the electrochemical reduction of gold surface oxides [30, 32-37]. Following the deposition of gold

particles, the surface was oxidized by a potential step from 0 mV to 1400 mV in 0.5 M H₂SO₄ for 5 seconds. Although it is likely that both the GC surface and gold particles are oxidized at this potential, the oxide film on the gold particles can be selectively reduced by a potential sweep [30, 32-37]. Before this system can be applied to surface area determinations, it is important to develop a standardized method to oxidize the gold particles, as gold oxidation is dependent on both anodization potential and anodization time. This is demonstrated in both the literature [30, 32, 35-37] and control experiments.

Figure 2.5 illustrates the effects of anodization potential on surface oxide coverage for a 5 second potential step on a polycrystalline gold electrode. As observed in this figure, the charge due to surface oxide reduction increases with larger anodization potentials. Figure 2.6 illustrates the effects of anodization time on surface oxide coverage for a potential step to 1400 mV on a polycrystalline gold electrode. Under these conditions, surface oxide coverage is not observed to change dramatically with increased anodization time. The charge due to oxide reduction remains essentially constant after 5 seconds of anodization, even though the logarithmic growth of a layer of surface oxides is observed. Based on the results of these experiments, suitable conditions were chosen such that monolayer coverage of surface oxides could be achieved. Thus, the potential program employed for gold surface area determination consisted of a potential step to 1400 mV for 5 seconds, immediately followed by a linear potential sweep from 1400 to 500 mV at a scan rate of 200 mV/s.

Gold oxidation conditions were assessed on polycrystalline gold electrodes and shown to achieve ~1 monolayer of gold surface oxides [33-36]. For example, integration of the cathodic stripping wave yields a charge of 930 $\mu\text{C}/\text{cm}^2$. The same electrode exhibits a double layer capacitance of 42 $\mu\text{F}/\text{cm}^2$ at -600 mV in 0.1 M NaF. Assuming a capacitance of 22 $\mu\text{F}/\text{cm}^2$ for a metallic electrode with a roughness factor of 1 [33], a value of ~1.9 was estimated as the roughness factor

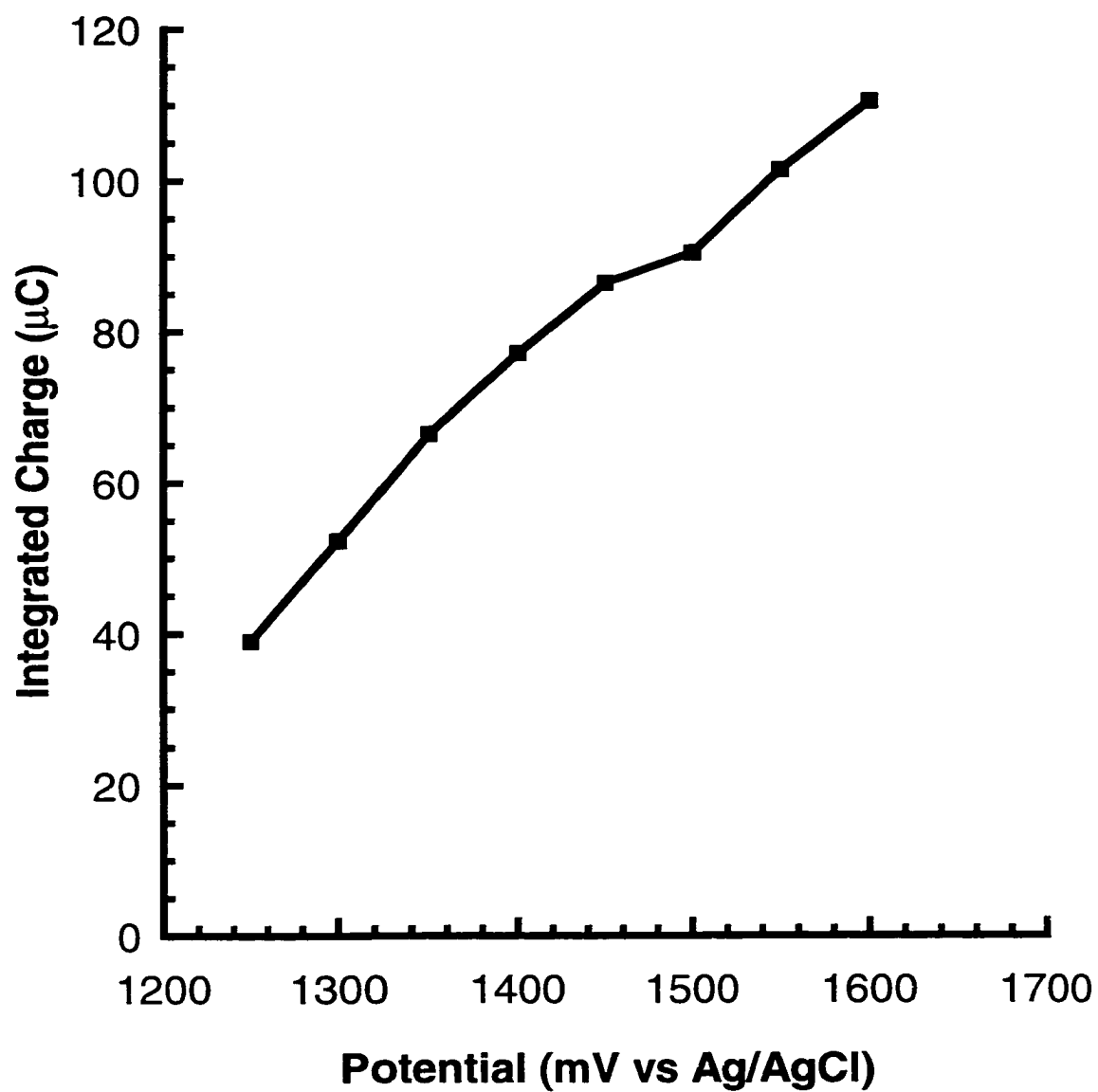


Figure 2.5: Effect of oxide reduction current on a polycrystalline gold electrode as a function of anodization potential in 0.5 M H₂SO₄, anodization time = 5s. Electrode area = 0.1 cm².

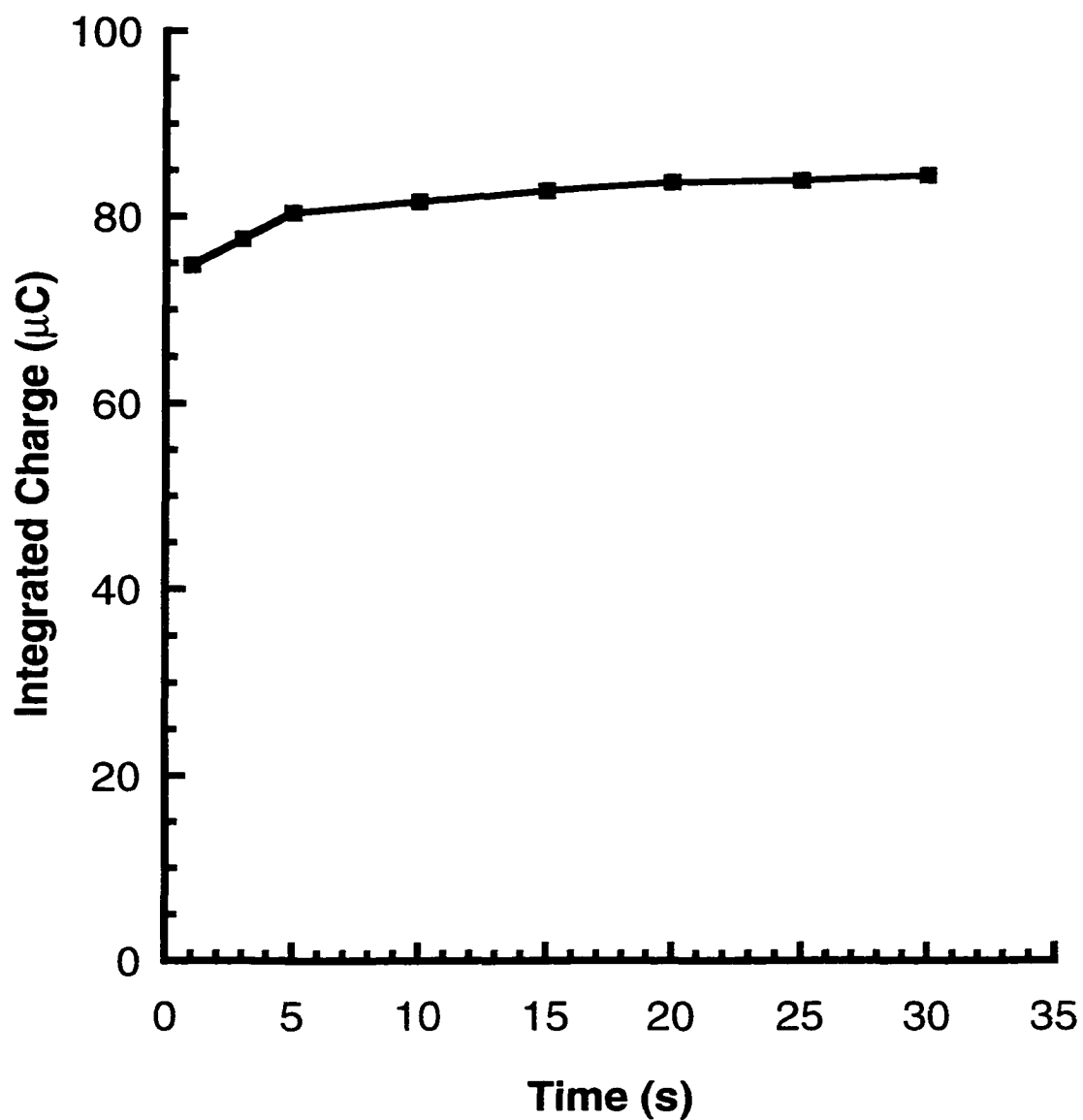


Figure 2.6: Effect of oxide reduction current on a polycrystalline gold electrode as a function of anodization time in 0.5 M H_2SO_4 , anodization potential equals 1400 mV. Electrode area = 0.1 cm^2 .

of the polycrystalline gold electrode. Thus, a roughness corrected value of $489 \mu\text{C cm}^{-2}$ is obtained which agrees well with the theoretically determined value of $482 \mu\text{C cm}^{-2}$ for the reduction of a monolayer of gold surface oxides [33, 34].

Figure 2.7 contains the linear sweep voltammograms for oxide reduction on gold particles deposited from a series of AuCl_4^- solutions of varying concentration at an overpotential of -800 mV . Figure 2.8 shows a similar study for oxide reduction on gold particles deposited at a series of overpotentials for a solution of $100 \mu\text{M AuCl}_4^-$. The sharp wave appearing at $\sim 935 \text{ mV}$ in all the voltammograms is consistent with the reduction of an oxide film on gold. The observation of this wave confirms the deposition of metallic gold onto GC under the conditions employed. The area under the oxide reduction waves for repeated oxidation cycles varies by no more than 5%, implying that roughening of the gold particles is negligible [33].

An assessment of the amount of gold deposited by electroless means was made based upon the gold oxide reduction currents observed at GC electrodes exposed to AuCl_4^- at open circuit. Specific chemical groups present on the GC surface may act as reducing agents resulting in the nucleation of small gold particles in the absence of an applied potential step. Shimazu and coworkers have observed that exposure of a polished GC electrode to a solution of hexachloroplatinate(IV) results in electrodes that become active toward hydrogen evolution [13]. This result is attributed to the electroless deposition of small platinum particles on the GC surface. It is important to understand to what extent electroless deposition contributes to overall gold particle deposition in order to gain control of this process. Electroless deposition of gold was found to constitute no more than 5% of the amount of gold deposited electrochemically. In addition, poisoning the GC electrode at 1100 mV prior to, and during its initial exposure to AuCl_4^- has no effect on the amount of electrochemically deposited gold. Thus, the

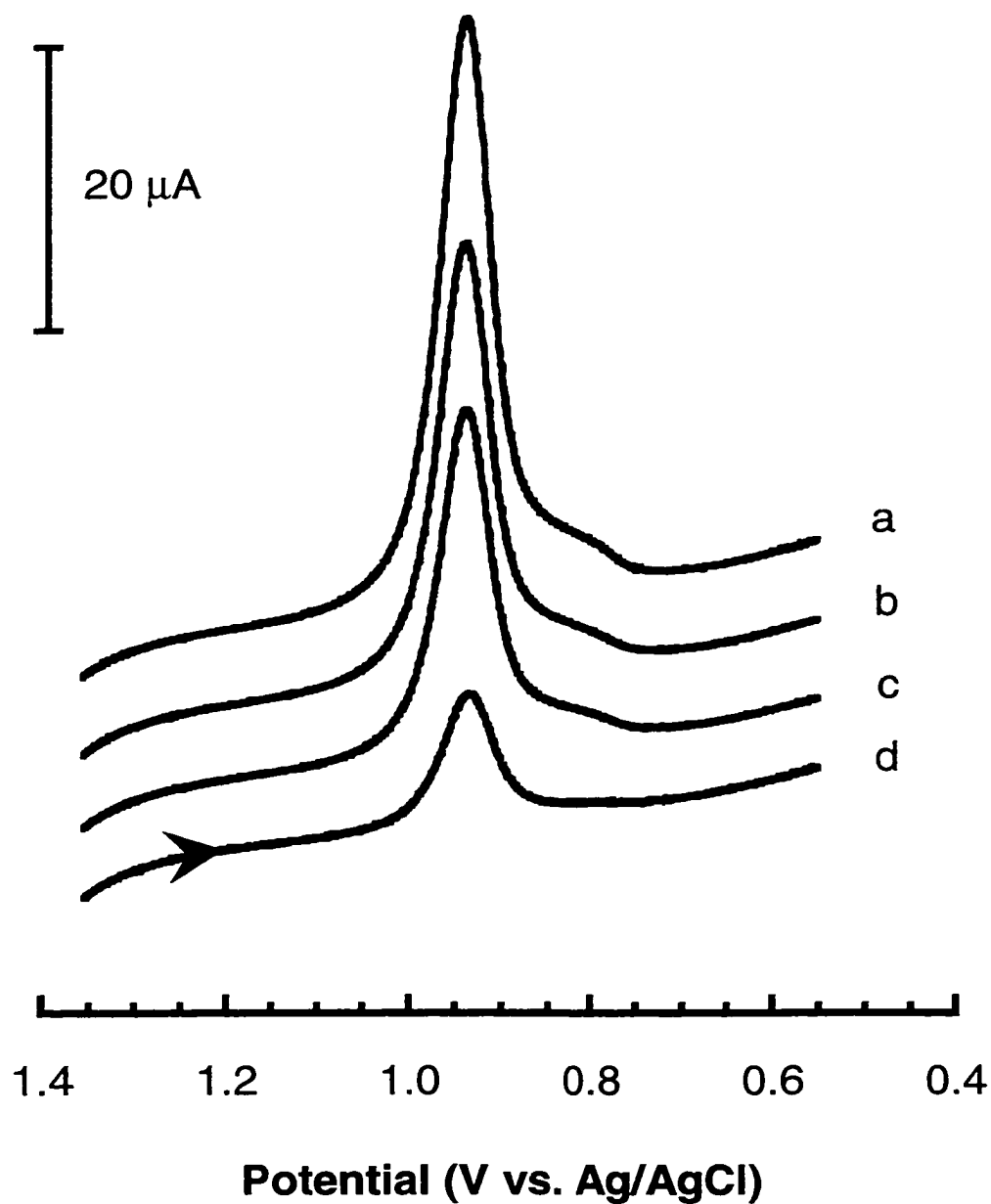


Figure 2.7: Linear sweep voltammograms for the reduction of gold surface oxides from electrochemically deposited gold particles in 0.5 M H₂SO₄. Deposition solution concentration series for $\eta = -800$ mV, $v = 200$ mV/s, $t = 5$ s. (a) 200 μ M, (b) 100 μ M, (c) 50 μ M, (d) 10 μ M, AuCl₄⁻.

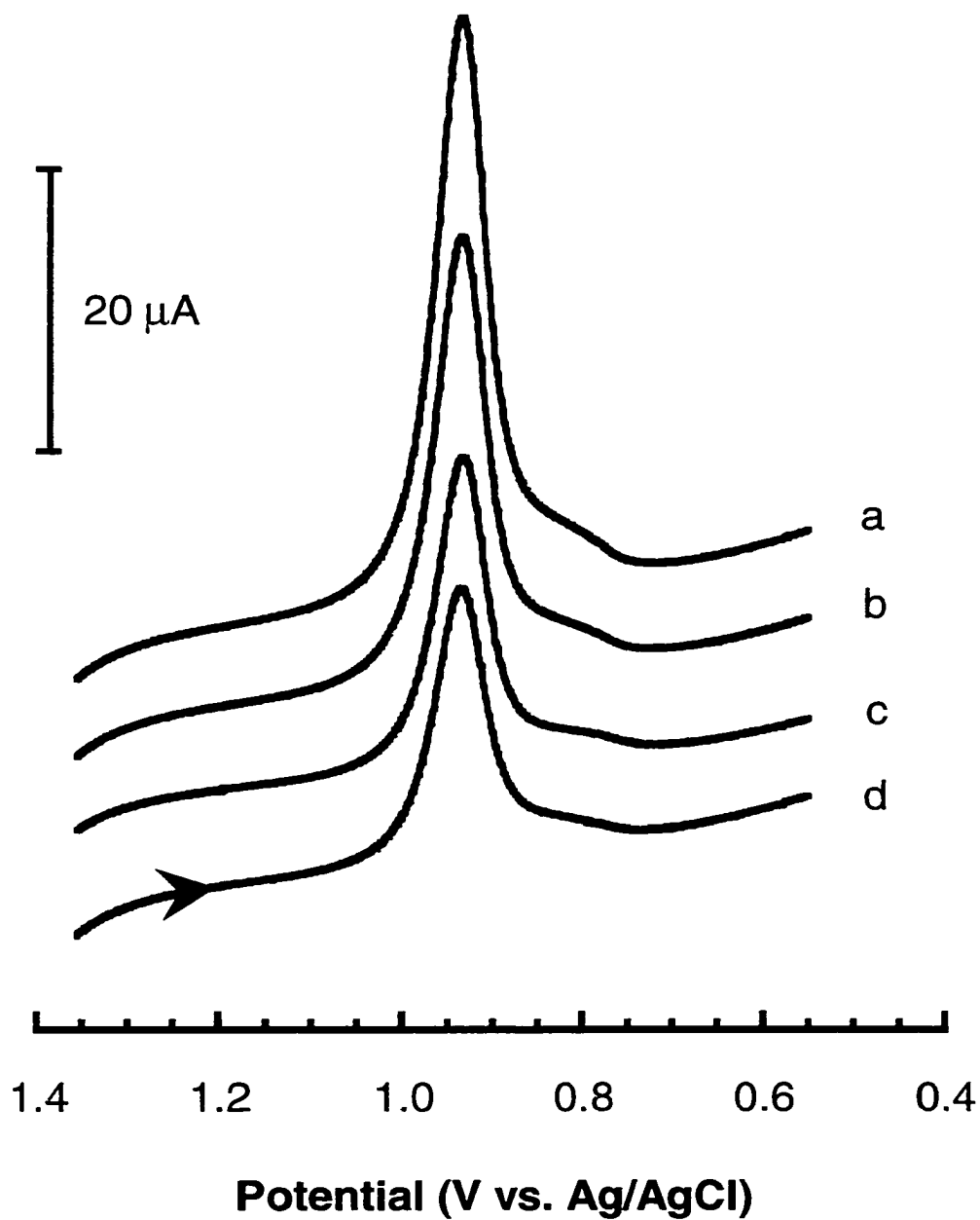


Figure 2.8: Linear sweep voltammograms for the reduction of gold surface oxides from electrochemically deposited gold particles in 0.5 M H_2SO_4 . Overpotential series for $[\text{AuCl}_4^-] = 100 \mu\text{M}$, $\nu = 200 \text{ mV/s}$, $t = 5 \text{ s}$. (a) -1000 mV , (b) -800 mV , (c) -600 mV , (d) -400 mV .

Table 2.1: Surface area determination of electrochemically deposited gold particles on GC via oxide reduction analysis. Effect of deposition solution concentration.

[AuCl ₄ ⁻] (μM)	Q_{obs} (μC)	Gold Area (cm^2) ^b	% Geometric Area
200	$15.0 \pm 1.6^{\text{a}}$	0.031 ± 0.003	10.0 ± 1.1
100	11.8 ± 1.0	0.024 ± 0.002	8.1 ± 0.7
50	8.9 ± 1.1	0.018 ± 0.002	6.0 ± 0.7
10	2.9 ± 0.8	0.006 ± 0.002	2.0 ± 0.5

- a. Statistics based on six measurements for each concentration.
 b. A value of $489 \mu\text{C}/\text{cm}^2$ was used as the charge required to reduce a monolayer of surface oxides on a polycrystalline gold surface.

Table 2.2: Surface area determination of electrochemically deposited gold particles on GC via oxide reduction analysis. Effect of deposition overpotential.

η (mV)	Q_{obs} (μC)	Gold Area (cm^2) ^b	% Geometric Area
-1000	$16.6 \pm 0.6^{\text{a}}$	0.034 ± 0.001	10.9 ± 0.3
-800	11.8 ± 1.0	0.024 ± 0.002	7.7 ± 0.6
-600	9.7 ± 0.7	0.020 ± 0.001	6.5 ± 0.3
-400	7.4 ± 0.2	0.015 ± 0.0004	4.8 ± 0.1

- a. Statistics based on three measurements for each overpotential.
 b. A value of $489 \mu\text{C}/\text{cm}^2$ was used as the charge required to reduce a monolayer of divalent oxygen on a polycrystalline gold surface.

currents observed for the reduction of gold oxide reflects the surface area of electrochemically deposited gold particles.

The trend in Figure 2.7 reveals higher peak currents for oxide reduction as the bulk AuCl_4^- concentration increases. This result is not unexpected and implies that the surface area of deposited gold particles tracks solution concentration for a given deposition potential and time. A similar trend is observed as a function of overpotential, Figure 2.8, where greater overpotentials achieve higher gold surface area. Using the observed charge, Q_{obs} , obtained by integrating the area under each of the waves in Figures 2.7 and 2.8, and the charge expected for complete monolayer coverage as described above, quantitative surface areas can be determined for each deposition condition. Tables 2.1 and 2.2 contain quantitative results from the analysis of the data in Figures 2.7 and 2.8. As illustrated in Tables 2.1 and 2.2, areas corresponding to 2% to 11% of the geometrical area of the GC electrode can be made available for future chemical modification by varying either the bulk AuCl_4^- concentration, or the overpotential.

Sample Calculation. A sample calculation for the surface area of electrochemically deposited gold particles on GC from a 200 μM AuCl_4^- solution follows. First, the charge due to surface oxide reduction from a polycrystalline gold electrode was determined using an electrode of known area.

$$93 \mu\text{C} / 0.1 \text{ cm}^2 = 930 \mu\text{C cm}^{-2}$$

A roughness corrected value was then determined by dividing by the roughness factor. The roughness factor was derived with the use of capacitance measurements, as discussed above

$$930 \mu\text{C cm}^{-2} / 1.9 = 489 \mu\text{C cm}^{-2}$$

This value was then used along with the charge for oxide reduction from gold particles on GC to determine the surface area of the gold particles.

$$15.0 \mu\text{C} / 489 \mu\text{C cm}^{-2} = 0.031 \text{ cm}^2$$

All calculations of gold surface area were performed in this manner.

Stripping UPD Lead. A monolayer of lead adatoms will form on gold surfaces at potentials slightly more positive than for bulk deposition of lead [43-52, 56]. This UPD lead monolayer can be subsequently stripped from the gold surface by oxidation. Similar to the case of the oxide reduction experiments, control experiments indicate that lead UPD occurs solely on the gold particles. Contrary to a recent report, we do not observe lead stripping currents from the unmodified GC substrate [57]. The stripping of UPD lead has been used by several authors to characterize the surface of gold substrates [43, 52, 56], and was employed here to assess the microcrystal structure of electrochemically deposited gold particles.

Lead was deposited onto supported gold particles by stepping the potential from open circuit to -400 mV for a period of 5 seconds. Figures 2.9 and 2.10 contain lead stripping voltammograms from gold particles deposited under the various concentration and overpotential conditions. The sloping background current in these voltammograms is due mainly to the GC substrate. Two oxidative stripping waves are observed; a sharp wave at -200 mV which is diagnostic of lead stripping from the Au(111) crystal plane and a broader wave at 25 mV corresponding to lead stripping from the Au(110)/Au(100) crystal planes [44-51]. Closer examination of the Au(111) wave for some of the voltammograms (i.e., Figure 2.9 , curves c and d; Figure 2.10, curves a, b, c) reveals the presence of a shoulder at a slightly more positive potential, -170 mV. This feature has been attributed to lead stripping from Au(111) terraces of extended lengths, greater than 11 Au atoms [49-52]. Close observation of all the voltammograms in these figures suggests that the gold particles deposited on GC under the present conditions are

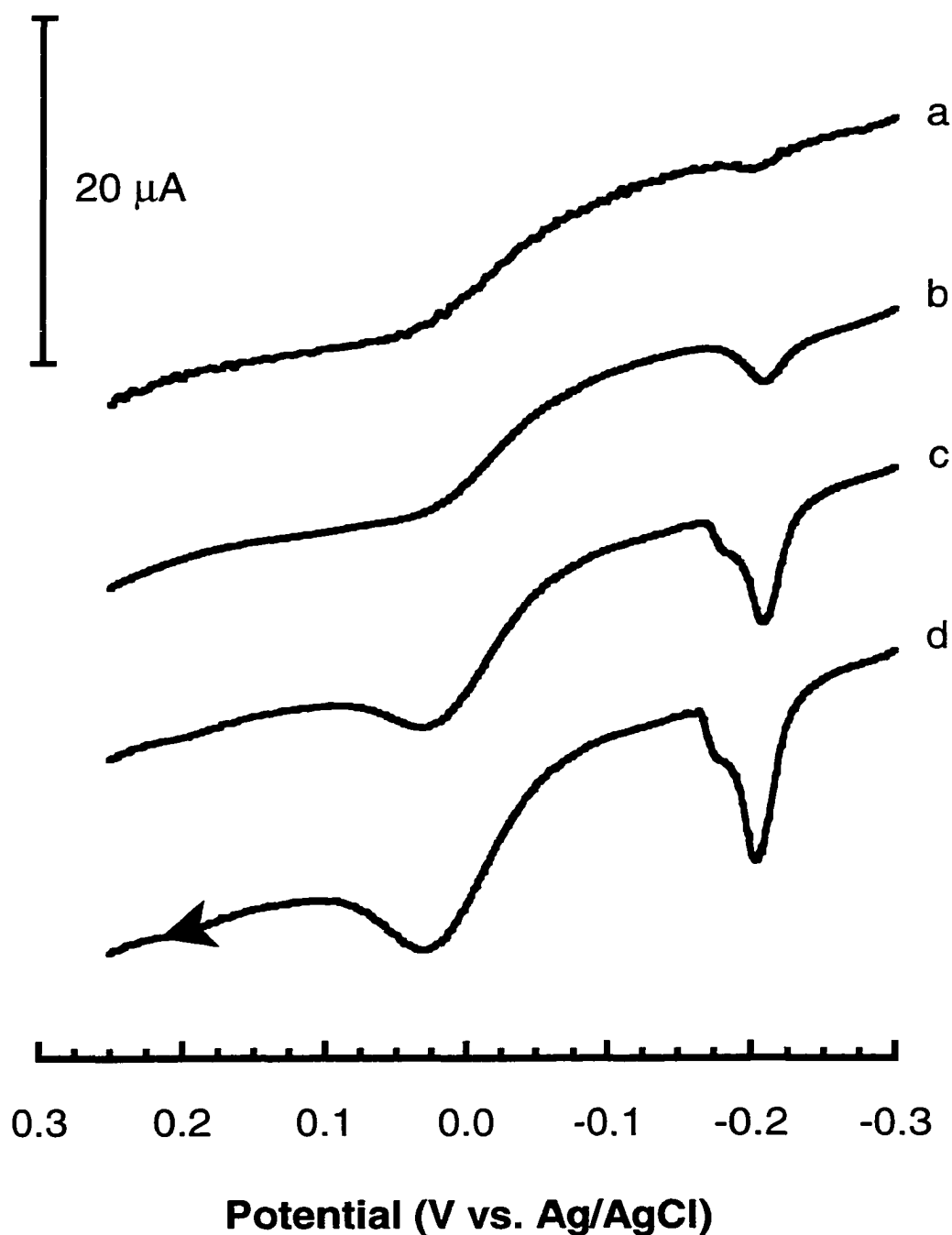


Figure 2.9: Linear sweep voltammograms for the stripping of underpotentially deposited lead from electrochemically deposited gold particles. Deposition solution concentration series for $\eta = -800$ mV, $\nu = 200$ mV/s. (a) 10 μM , (b) 50 μM , (c) 100 μM , (d) 200 μM , AuCl_4^- .

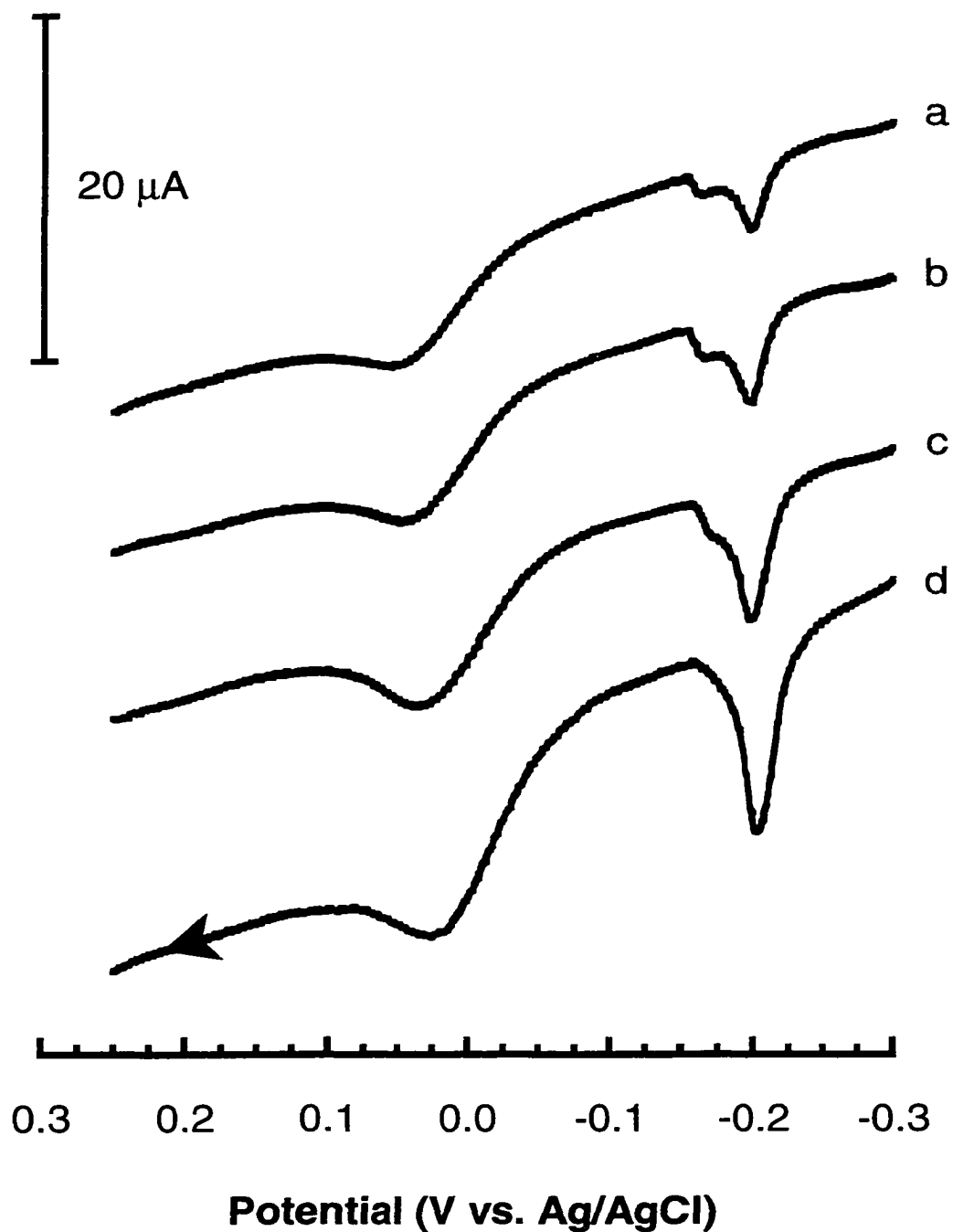


Figure 2.10: Linear sweep voltammograms for the stripping of underpotentially deposited lead from electrochemically deposited gold particles. Overpotential series for $[\text{AuCl}_4^-] = 100 \mu\text{M}$, $v = 200 \text{ mV/s}$. (a) -400 mV , (b) -600 mV , (c) -800 mV , (d) -1000 mV .

polycrystalline with a combination of (111), (110) and (100) sites. Additionally, in some cases, particles are composed of Au(111) terraces of extended length.

Two trends are apparent in Figure 2.9 as the bulk concentration of AuCl_4^- is increased (a to d). First, the observed current for each lead stripping wave tracks deposition solution concentration. This observation mirrors the oxide reduction in Figure 2.7 and confirms the increase in overall gold particle surface area resulting from depositions from higher concentration solutions. Gold surface area determination by lead stripping is risky due to the uncertainty associated with the integration and summation of several waves, and the variation in the values of charge associated with desorption of a monolayer of adsorbed lead atoms reported in the literature (225 to 362 $\mu\text{C}/\text{cm}^2$) [43, 46, 47, 51]. Secondly, the microstructure of the deposited particles evolves with bulk concentration as gauged by the shoulder on the Au(111) peak at -170 mV. This wave becomes more pronounced on nanocrystals deposited from 100 and 200 μM solutions indicating the formation of larger Au(111) terraces. From rough integration of the waves, the percentage of the Au(111) crystal face area for the 200 μM solution (28%) is similar to that of polycrystalline gold [43].

The dependence of overpotential on the microstructure of electrochemically deposited gold particles is deduced from Figure 2.10. Lead stripping currents increase as the deposition overpotential for gold deposition increases (a to d), reflecting the increase in gold surface area shown in Table 2.2. However, the stripping signature for particles deposited at low overpotential (e.g., curve a in Figure 2.10) includes a significant shoulder on the Au(111) wave arguing that, although a relatively small amount of gold is deposited at low overpotential (Table 1), the resulting particles exhibit a significant (111) texture which is comprised of larger terraces. For higher overpotentials, although the total stripping current increases, the wave at -170 mV becomes less prominent, indicating smaller (111) planes. These observations taken together suggest that at low overpotentials, a

small number of gold particles nucleate and grow to significant sizes during deposition. In this case, the applied overpotential provides sufficient driving force to activate only certain nucleation sites and gold particle growth is favored. Higher overpotentials access more nucleation sites and a larger density of smaller particles results. This model is confirmed by the scanning electron micrograph analysis presented in the next section.

Scanning Electron Microscopy. Oxide reduction and lead stripping indicate that the amount of gold deposited onto GC tracks both the bulk AuCl_4^- concentration and the deposition overpotential. Although these analyses yield a quantitative perspective, they do not provide insights into the manner in which the change in gold surface area is manifested in terms of the interfacial architecture. That is, oxide reduction and lead stripping results cannot resolve whether the variation in surface area is due to changes in particle size, particle density, or a combination of these two scenarios. Stripping of UPD lead provides some insights, particularly for variations in overpotential. To build upon these insights a visual representation of the gold particles was obtained with scanning electron microscopy (SEM).

SEM was employed because it provides superior images to those obtained with scanning force microscopy (SFM). Imaging in contact mode SFM results in a large number of particles being dislodged from the surface. Also, convolution of tip shape with particle shape introduces large errors in particle size. Tapping-Mode, or intermittent contact SFM imaging is more delicate in that it does not dislodge the supported particles, but convolution of tip shape is still a major problem.

Figure 2.11 contains representative scanning electron micrographs illustrating the effect of bulk AuCl_4^- concentration while Figure 2.12 contains representative scanning electron micrographs illustrating the effect of overpotential. Gold particles in the micrographs appear as circular bright spots

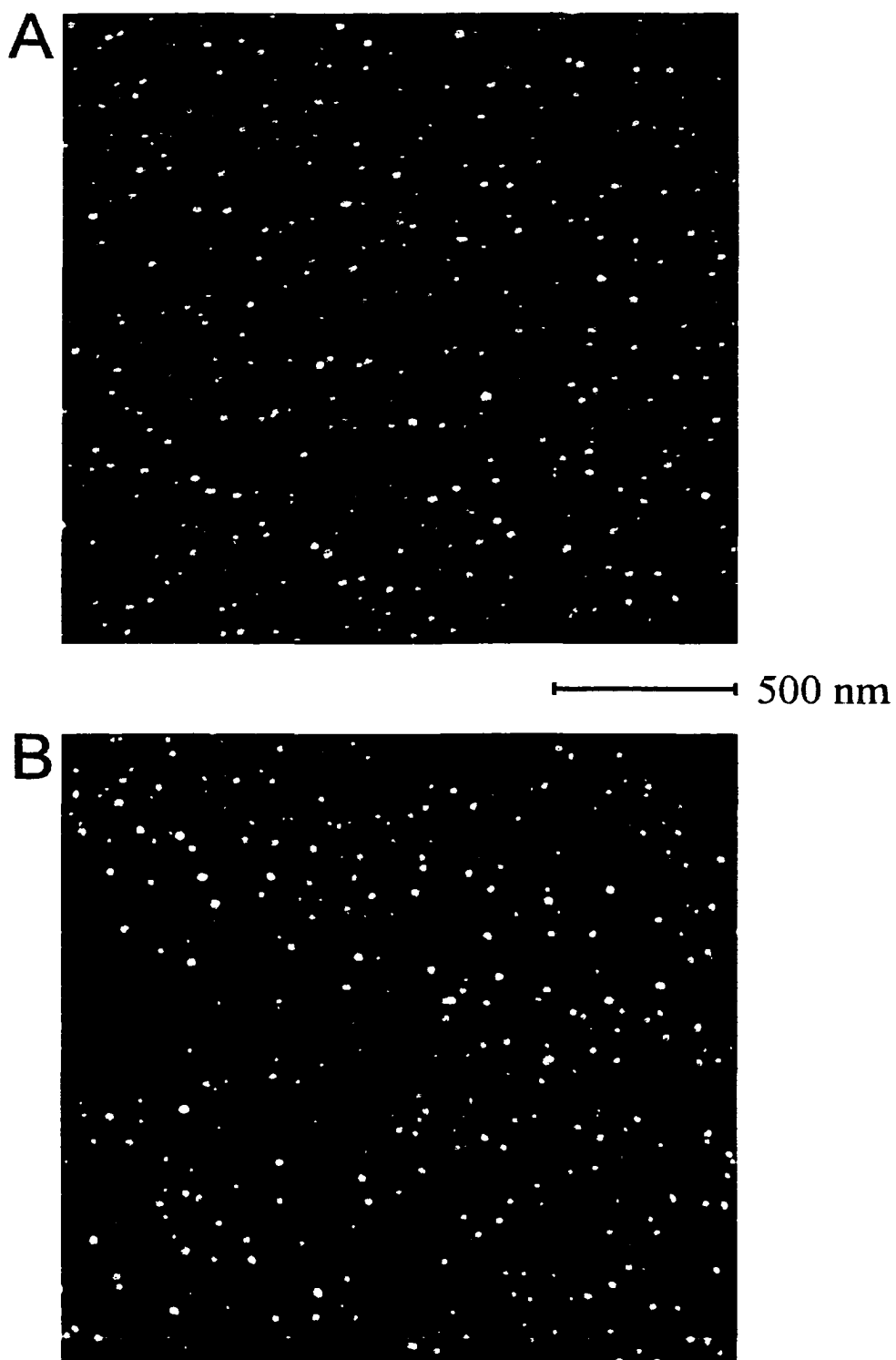


Figure 2.11: Scanning electron micrographs of electrochemically deposited gold particles on GC, $\eta = -800$ mV. (A) 200 μM , (B) 100 μM , (C) 50 μM , (D) 10 μM , AuCl_4^- .

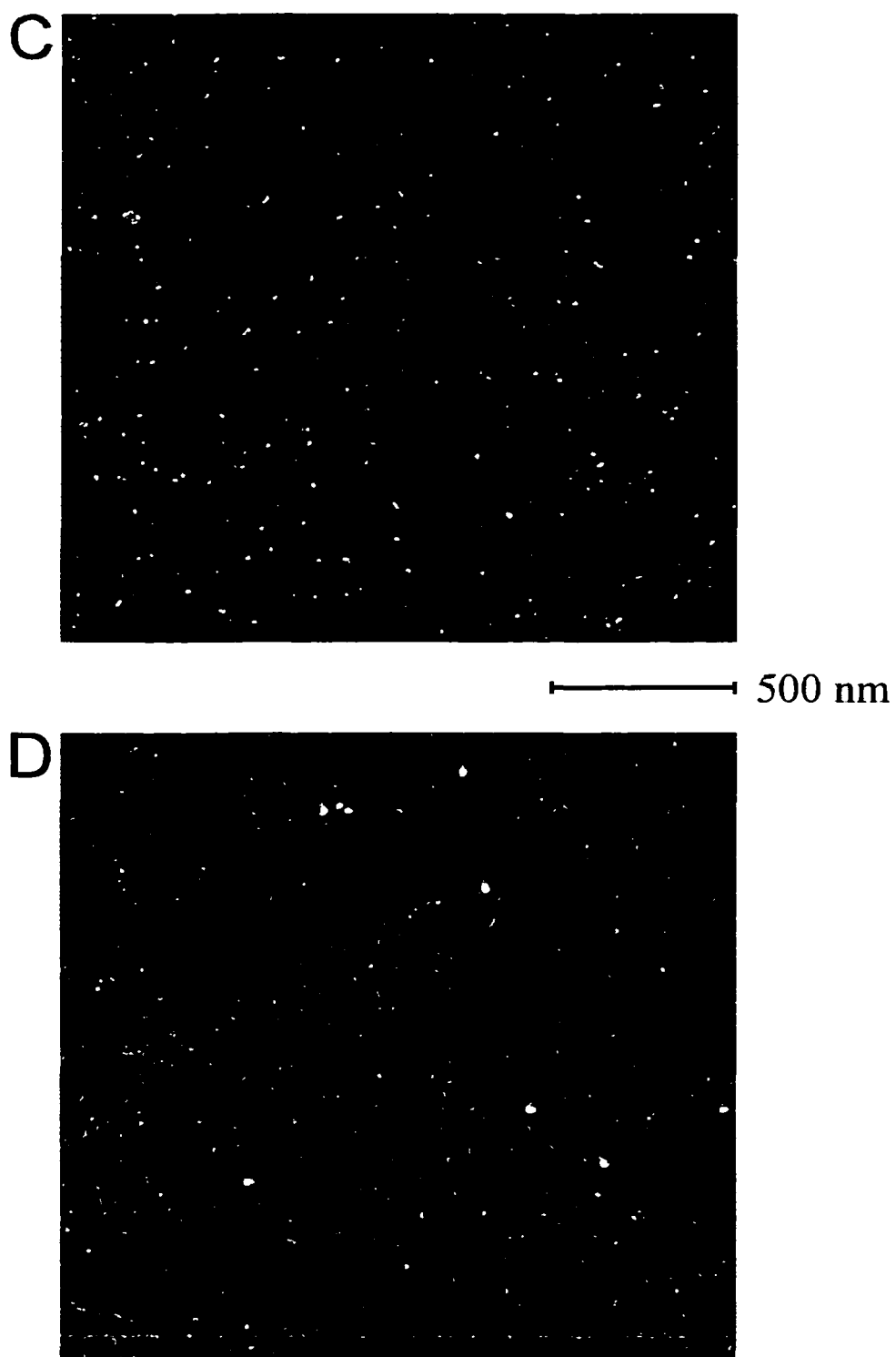


Figure 2.11: (continued)

surrounded by a textured background of darker GC substrate. The difference in contrast between the two materials is due to the difference in atomic number between carbon and gold. The heavier gold atoms are more effective at reflecting/scattering the electron beam than carbon, and thus appear brighter. As shown in Figure 2.11-D, deposition at low concentration, 10 μM , yields a low number of small particles. Figure 2.11-A illustrates that at higher concentrations, 200 μM , a high density of relatively monodisperse particles are deposited. Quantitative results from SEM image analysis for particle number density, which reflects the number of nucleation sites on the GC electrode, and particle diameter, which represents particle growth, are listed in Tables 2.3 and 2.4.

Results presented in Table 2.3 show that both number density and diameter of electrochemically deposited gold particles on GC electrodes increase with bulk AuCl_4^- concentration. These trends are responsible for the increase in electrochemically deposited gold surface area indicated by gold oxide reduction (Figure 2.7 and Table 2.1). If the gold particles are modeled as hemispheres a value for gold surface area can be estimated using the diameters and number densities in Table 2.3. Comparison of surface area values calculated from SEM data with those determined by oxide reduction yields a range of correlation from a 10% difference to a difference by a factor of 2. However, use of a hemisphere as a model for the shape of a particle may not be a valid assumption. As observed in the SEM micrographs gold particles may adopt a variety of complex shapes. In addition, we note that the scanning electron micrographs likely do not reveal gold particles of very small diameters $< 5\text{nm}$.

Figure 2.12 illustrates the effect of overpotential on gold particle distribution and size. At low overpotentials, Figure 2.12-D, a number of large (50 to 80 nm) particles are observed coexisting with smaller ones. Higher overpotentials (Figure 2.12-A) yield an array of evenly distributed, relatively monodisperse particles.

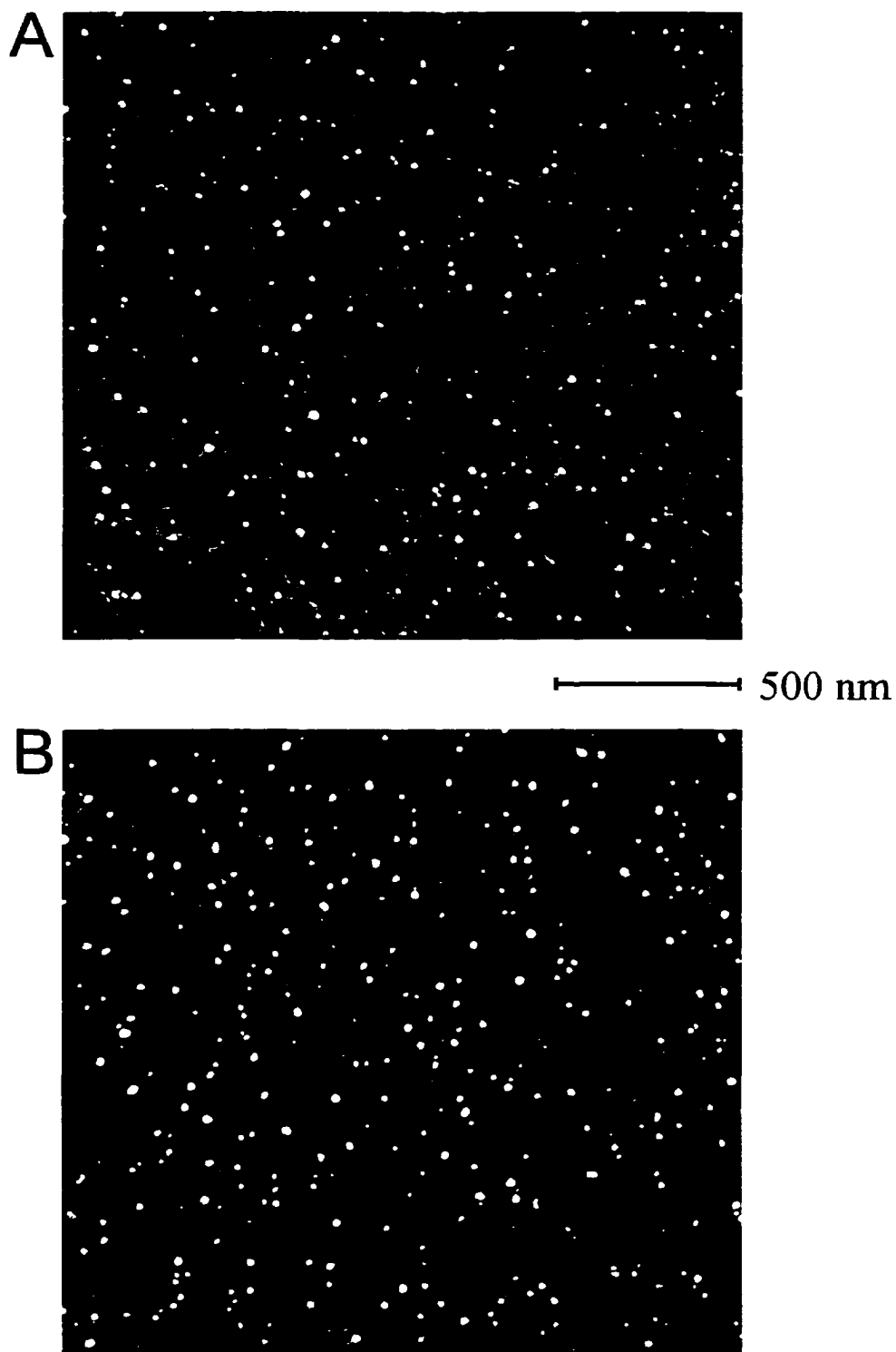


Figure 2.12: Scanning electron micrographs of electrochemically deposited gold particles on GC, $[\text{AuCl}_4^-] = 100 \mu\text{M}$. (A) -1000 mV, (B) -800 mV, (C) -600 mV, (D) -400 mV.

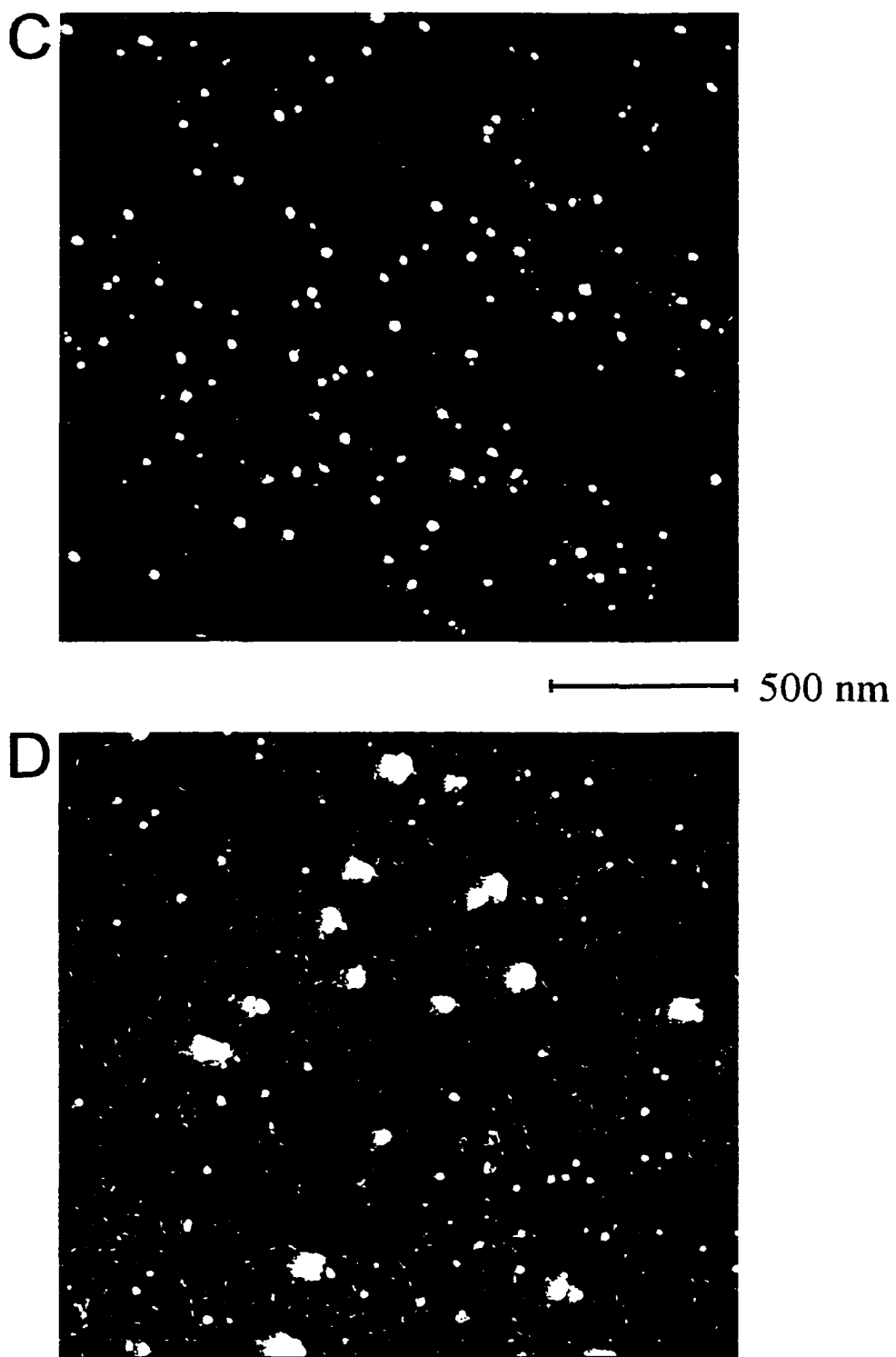


Figure 2.12: (continued)

Table 2.3: Results from scanning electron micrograph analysis for electrochemically deposited gold particles. Effect of deposition solution concentration.

$[\text{AuCl}_4^-]^a$ (μM)	Number Density (particles/ μm^2)	Diameter (nm)	% Area ^d
200	135 ± 16^b	20 ± 5^c	8.5 ± 0.9
100	89 ± 7	18 ± 4	4.5 ± 0.3
50	68 ± 7	13 ± 3	1.8 ± 0.2
10	15 ± 3	10 ± 3	0.2 ± 0.1

- a. $\eta = -800$ mV.
 b. Based on measurements of at least 20, $1\mu\text{m}^2$ areas.
 c. Based on measurements of at least 80 particles.
 d. Calculated using hemisphere model, $A = 2\pi r^2$.

Table 2.4: Results from scanning electron micrograph analysis for electrochemically deposited gold particles. Effect of deposition overpotential.

η^a (mV)	Number Density (particles/ μm^2)	Diameter (nm)	% Area ^d (nm)
-1000	140 ± 15^b	17 ± 4^c	6.4 ± 0.7
-800	89 ± 7	18 ± 4	4.6 ± 0.4
-600	54 ± 8	24 ± 5	4.9 ± 0.7
-400	28 ± 6	34 ± 24	5.1 ± 1.1

- a. $[\text{AuCl}_4^-] = 100 \mu\text{M}$.
 b. Based on measurements of at least 20, $1\mu\text{m}^2$ areas.
 c. Based on measurements of at least 80 particles.
 d. Calculated using hemisphere model, $A = 2\pi r^2$.

Table 2.4 quantitatively lists the values for gold particle number density and diameter as a function of overpotential. The increase in number density with overpotential implies that the number of active sites on GC for gold particle nucleation increases with overpotential. This observation is consistent with a recent report [23]. For lower overpotentials, the growth of a small number of initial nuclei is favored over the establishment of new nucleation sites as indicated by the large size of the particles apparent in Figure 2.12–D. This mechanism is also consistent with the lead stripping results which indicate a relatively low gold surface area comprised of larger Au(111) terraces. Taken together, the data in Tables 2.3 and 2.4 imply that the size, density, and structure of gold particles on GC electrodes can be systematically controlled via variations in deposition solution concentration and overpotential. This control will be exploited in future work aimed at the chemical modification of gold particles via self-assembly.

The magnitude of the number density values observed here (10^9 to 10^{10} cm^{-2}) are larger than those reported for gold nucleation on polished GC from concentrated LiCl solutions [23] and agree well with the number density of other metals electrochemically deposited on GC [58]. However, a direct comparison with particle number densities from previous reports is clouded because of inconsistencies in electrode handling and preparation procedures from lab-to-lab. Further studies indicate that the number of electrochemically deposited gold particles also depends strongly on the initial GC surface preparation. The results of these studies are discussed in Chapter III.

Conclusions

Traditional gold electrochemistry and microscopic analysis have been applied to characterize gold particles electrochemically deposited on GC. Results show that the overall surface area of gold as well as the particle size, density, and surface texture, can be controlled by rational variation of deposition conditions.

As stated above, we are interested in producing sites for attaching functional groups to GC surfaces using thiol self-assembly which exhibit analytical selectivity and are located adjacent to electron transfer sites. From the analyses presented here, high density arrangements of monodisperse, nanometer sized gold particles which will serve as foundations for the self-assembly of alkanethiolate monolayers can be deposited from solutions containing 100 to 200 μM AuCl_4^- at overpotentials of -800 to -1000 mV. These conditions provide sufficient gold surface area, as well as the site segregation desired for our purpose.

References

1. A. W. Adamson, *Physical Chemistry of Surfaces*, John Wiley & Sons, Inc., New York, (1990).
2. K. Kinoshita, in *Modern Aspects of Electrochemistry*, Vol. 14, Bockrus, Conway, and White, eds.
3. K. Kinoshita, *Carbon: Electrochemical and Physiochemical Properties.*, Wiley, New York, (1988).
4. G. Gunawardena, G. Hills, I. Montenegro, and B. Scharifker, *J. Electroanal. Chem.*, **138**, 225, (1982).
5. G. Gunawardena, G. Hills, and I. Montenegro, *J. Electroanal. Chem.*, **138**, 241, (1982).
6. G. Gunawardena, G. Hills, I. Montenegro, and B. Scharifker, *J. Electroanal. Chem.*, **138**, 255, (1982).
7. G. Gunawardena, D. Pletcher, and A. Razaq, *J. Electroanal. Chem.*, **164**, 363, (1984).
8. G. Gunawardena, G. Hills, and I. Montenegro, *J. Electroanal. Chem.*, **184**, 357, (1985).
9. G. Gunawardena, G. Hills, and I. Montenegro, *J. Electroanal. Chem.*, **184**, 371, (1985).

10. J. V. Zoval, R. M. Stiger, P. R. Biernacki, and R. M. Penner, *J. Phys. Chem.*, **100**, 837, (1996).
11. J. M. Zoval, P. R. Biernacki, and R. M. Penner, *Anal. Chem.*, **68**, 1585, (1996).
12. J. V. Zoval, J. Lee, S. Gorer, and R. M. Penner, *J. Phys. Chem. B*, **102**, 1166, (1998).
13. K. Shimazu, D. Weisshaar, and T. Kuwana, *J. Electroanal. Chem.*, **223**, 223, (1987).
14. K. Shimazu, K. Uosaki, H. Kita, and Y. Nodasaka, *J. Electroanal. Chem.*, **256**, 481, (1988).
15. A. Milchev, E. Vassileva, and V. Kertov, *J. Electroanal. Chem.*, **107**, 323, (1980).
16. A. Milchev, E. Vassileva, and V. Kertov, *J. Electroanal. Chem.*, **107**, 337, (1980).
17. N. Georgolios, D. Jannakoudakis, and P. Karabinas, *J. Electroanal. Chem.*, **264**, 235, (1989).
18. Z. Chen, J. Li, and E. Wang, *J. Electroanal. Chem.*, **373**, 83, (1994).
19. B. U. Yoon, K. Cho, and H. Kim, *Analytical Sciences*, **12**, 321, (1996).
20. E. Gomez, E. Guaus, F. Sanz, and E. Valles, *J. Electroanal. Chem.*, **465**, 63, (1999).
21. M. Palomar-Pardave, M. T. Ramirez, I. Gonzalez, A. Serruya, and B. R. Scharifker, *J. Electrochem. Soc.*, **143**, 1551, (1996).
22. A. J. Bard and L. R. Faulkner, *Electrochemical Methods: Fundamentals and Applications*, John Wiley & Sons, Inc., New York, (1980).
23. U. Schmidt, M. Donten, and J. G. Osteryoung, *J. Electrochem. Soc.*, **144**, 2013, (1997).
24. H. Martin, P. Carro, A. Hernandez Creus, S. Gonzalez, R. C. Salvarezza, and A. J. Arvia, *Langmuir*, **13**, 100, (1997).

25. Y. G. Li and A. Lasia, *J. Electrochem. Soc.*, **144**, 1979, (1997).
26. X. Wang, N. Isaev, and J. G. Osteryoung, *J. Electrochem. Soc.*, **143**, 1201, (1996).
27. G. Trejo, A. F. Gil, and I. Gonzalez, *J. Electrochem. Soc.*, **142**, 3404, (1995).
28. A. P. Brown and F. C. Anson, *Anal. Chem.*, **49**, 1589, (1977).
29. A. P. Brown and F. C. Anson, *J. Electroanal. Chem.*, **83**, 203, (1977).
30. D. A. J. Rand and R. Woods, *J. Electroanal. Chem.*, **31**, 29, (1971).
31. T. Biegler, D. A. J. Rand, and R. Woods, *J. Electroanal. Chem.*, **29**, 269, (1971).
32. S. B. Brummer and A. C. Makrides, *J. Electrochem. Soc.*, **111**, 1122, (1964).
33. U. Oesch and J. Janata, *Electrochimica Acta*, **28**, 1237, (1983).
34. U. Oesch and J. Janata, *Electrochimica Acta*, **28**, 1247, (1983).
35. H. Angerstein-Kozłowska, B. E. Conway, A. Hamelin, and L. Stoicoviciu, *J. Electroanal. Chem.*, **228**, 429, (1987).
36. H. Angerstein-Kozłowska, B. E. Conway, A. Hamelin, and L. Stoicoviciu, *Electrochimica Acta*, **31**, 1051, (1986).
37. H. Angerstein-Kozłowska, B. E. Conway, B. Barnett, and J. Mozota, *J. Electroanal. Chem.*, **100**, 417, (1979).
38. J. K. Lee, R. N. Adams, and C. E. Bricker, *Analytica Chimica Acta*, **17**, 321, (1957).
39. A. Hickling, *Trans. Faraday Soc.*, **42**, 518, (1946).
40. T. F. Buehrer and W. E. Roseveare, *J. Am. Chem. Soc.*, **49**, 1989, (1927).
41. R. H. Gerke and M. D. Rourke, *J. Am. Chem. Soc.*, **49**, 1855, (1927).

42. W. Obertenov, U. Schmidt, W. J. Lorenz, G. Staikov, E. Budevski, D. Carnal, U. Muller, H. Siegenthaler, and E. Schmidt, *J. Electrochem. Soc.*, **140**, 692, (1993).
43. R. Adzic, E. Yeager, and B. D. Cahan, *J. Electrochem. Soc.*, **121**, 474, (1974).
44. J. W. Schultze and D. Dickertmann, *Surf. Sci.*, **54**, 489, (1976).
45. K. Engelsmann, W. J. Lorenz, and E. Schmidt, *J. Electroanal. Chem.*, **114**, 1, (1980).
46. K. Engelsmann, W. J. Lorenz, and E. Schmidt, *J. Electroanal. Chem.*, **114**, 11, (1980).
47. A. Hamelin, *J. Electroanal. Chem.*, **101**, 285, (1979).
48. A. Hamelin and A. Katayama, *J. Electroanal. Chem.*, **117**, 221, (1981).
49. A. Hamelin, *J. Electroanal. Chem.*, **165**, 167, (1984).
50. A. Hamelin and J. Lipkowski, *J. Electroanal. Chem.*, **171**, 317, (1984).
51. R. Parsons and G. Ritzoulis, *J. Electroanal. Chem.*, **318**, 1, (1991).
52. M. M. Walczak, C. A. Alves, B. D. Lamp, and M. D. Porter, *J. Electroanal. Chem.*, **396**, 103, (1995).
53. E. Gileadi, N. Tshernikovski, and M. Babai, *J. Electrochem. Soc.*, **119**, 1018, (1972).
54. A. L. Horvath, *Handbook of Aqueous Electrolyte Solutions*, Ellis Harwood, New York, 1985.
55. M. O. Finot, G. D. Braybrook, and M. T. McDermott, *J. Electroanal. Chem.*, **466**, 234, (1999).
56. O. Melroy, K. Kanazawa, J. G. Gordon, and D. Buttry, *Langmuir*, **2**, 697, (1986).
57. S. Dong and Q. Qui, *J. Electroanal. Chem.*, **314**, 331, (1991).

58. P. Allongue and E. Souteyrand, *J. Electroanal. Chem.*, **286**, 217, (1990).

CHAPTER III

EFFECTS OF SURFACE OXIDE GROUPS ON THE ELECTROCHEMICAL DEPOSITION OF GOLD PARTICLES ON GLASSY CARBON ELECTRODES

Introduction

In Chapter II, the interfacial properties of gold particles electrochemically deposited onto GC electrodes were characterized. Scanning electron microscopy (SEM) as well as electrochemical methods were employed to systematically examine the effects of deposition solution concentration and overpotential on the resulting gold particles. The results of these studies show that it is possible to control the gold surface area, particle number density, particle size, and microcrystal structure, by variation of the deposition conditions employed. In these studies gold was deposited on polished GC electrodes. The main focus of the following study was to examine the effects of different electrode pretreatment procedures on the deposition of gold particles on GC electrodes. Different pretreatment procedures may result in a difference in surface chemistry of the GC electrodes, thus influencing nucleation and growth behavior of the resulting gold particles. Surface chemistry may also influence the adhesion of gold particles to the GC surface.

The first step in any electrochemical procedure involving the use of solid electrodes is pretreatment of the electrode surface. In the case of carbon electrodes, a loss of activity upon exposure to a working solution or the ambient environment is generally observed. Pretreatment procedures that enhance the electron transfer rate between the electrode surface and electroactive species in solution are known as activation procedures. Following application of these

methods electron transfer between the electrode and electroactive species becomes more facile resulting in increased electron transfer rates. Accelerated electron transfer rates give rise to more well-defined voltammetric behavior, resulting in better resolution of voltammetric waves. It has been proposed that improvement of electron transfer properties of carbon electrodes may be realized through a number of effects: (a) removal of contaminants from the electrode surface; (b) increasing the density of surface functional groups that may act as electron transfer catalysts or mediators; (c) increasing the electrode surface area by roughening; and (d) exposure of fresh edge planes or surface defects that may act as preferred sites for electron transfer [1, 2]. These effects combined contribute to the preparation of a more reproducible electrode surface, and serve to enhance the electrocatalytic activity and selectivity of the electrode.

An important point, which should be stressed, is that the main objective of electrode pretreatment is the preparation of a reproducible electrode surface. Reproducibility is important because it allows one to gain a certain degree of control over electron transfer. Fast electron transfer is not necessarily as important as control. For example, one of the most desirable properties of carbon electrodes is that the reduction of H^+ to H_2 is very slow, resulting in a wide working potential window for these electrodes.

The most widely used method of pretreatment is mechanical polishing of the GC electrode surface. Several such procedures are described in the literature [2-6]. A new electrode is initially ground on a piece of fine grain silicon carbide or diamond grit paper to remove gross surface defects and impurities that result from the manufacturing process. The electrode is then polished to a mirror-like finish using a series of successively smaller particle size abrasive powders, such as 1.0, 0.3, and 0.05 μm alumina. Use of powders containing deagglomerating agents should be avoided, as they tend to deactivate the electrode. The use of latex gloves is also recommended to minimize contamination from the hand and

fingers. Polishing is achieved by the use of repetitive circular motions of the electrode surface in an alumina/water slurry against polishing cloth or a glass plate. Extensive sonication and rinsing with nanopure water are employed between each particle size to remove polishing alumina and debris from the electrode surface. Although sonication is effective at removing excess polishing debris from the surface of the electrode [4], it has been shown that a thin layer of polishing debris comprised of finely divided carbon microparticles, alumina particles, and water remains on the electrode surface [5]. Figure 3.1 shows an artistic representation of the ubiquitous layer of finely divided polishing debris that remains on the electrode surface.

Conventional polishing procedures described herein are adequate for most electroanalytical work. Electrochemistry of the $\text{Fe}(\text{CN})_6^{-3/4}$ redox system has been used extensively to gauge the effectiveness of polishing, and a range of electron transfer constants have been reported in the literature for various polishing procedures [2-4, 7, 8]. Hu and coworkers were able to achieve a level of activity comparable to that of active platinum by careful polishing of a GC electrode on a glass plate [2]. Work by Thornton and coworkers also demonstrates how the rate constant for $\text{Fe}(\text{CN})_6^{-3/4}$ progresses towards greater reversibility as finer abrasives are used in the preparation of the electrode surface [8]. This work also demonstrates that the actual electrode area approaches the geometric area as polishing progresses to smaller particle sizes attributed to a decrease in the surface roughness. While polishing may be performed on either polishing cloth or a glass plate, some authors have debated the use of polishing cloth stating that it contributes to deactivation of the electrode surface [2].

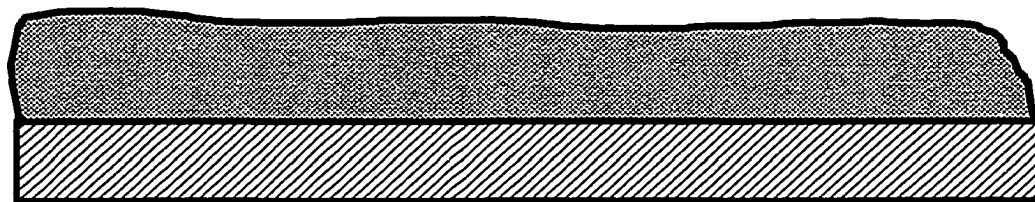
Aside from polishing, several other methods of electrode pretreatment have been studied. These methods include thermal treatments [3, 4, 9-11], radio frequency plasma treatment [12, 13], laser activation [14-16], and electrochemical pretreatment [7, 17-28]. Although not as simple and inexpensive to implement as

mechanical polishing, these methods offer the advantage of preparation of a cleaner, more reproducible surface. Some of these pretreatment methods are effective at removing the thin layer of finely divided carbon that remains upon polishing [5, 15, 20]. Further discussion will focus on electrochemical pretreatment (ECP) methods.

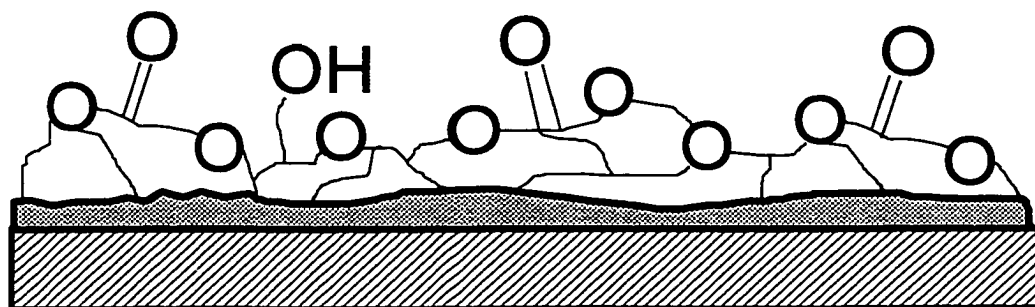
ECP of GC has been used extensively as an electrode pretreatment method. The first demonstration of ECP of carbon electrodes dates back to the work of Lord and Rogers [29]. In this work the authors report that the anodization of a graphite electrode, a pencil lead in this case, greatly changes the shape of a slow scan voltammetric curve for the reduction of Fe(III) in 0.1M HCl. ECP methods can involve either anodization or cathodization of the electrode surface. It is not uncommon to come across procedures in which both anodization and cathodization are employed as a means of electrode activation. ECP can be performed in either acidic [9, 21, 22, 24], basic [19, 20], or buffered/salt solutions [3, 7, 22, 23, 25, 30]. Each of these methods has markedly different physical effects on the underlying GC substrate [20, 31]. However, the end result remains constant, as an increase in the density of surface oxide groups is realized. This has been demonstrated using X-ray photoelectron spectroscopy (XPS) [7, 22] and electrochemical techniques [20, 25]. It is postulated that the majority of these surface oxide groups are present as phenolic and quinonal functionalities [7, 13, 25, 32].

Increased oxygen to carbon ratios of GC surfaces electrochemically pretreated in acidic or neutral media are attributed to the formation of electrochemical graphitic oxide (EGO) layers upon anodization of the GC surface. An artistic representation of the EGO layer that is generated upon ECP of a GC electrode in acidic media is illustrated in Figure 3.1. This EGO layer is generally thought of as an oxygen-rich, hydrated, porous, nonconducting, nonstoichiometric compound [33]. Work by Kepyly and coworkers has shown that EGO layers can

a. Polished GC



b. 0.5 M H_2SO_4 ECP GC



c. 1.0 M NaOH ECP GC

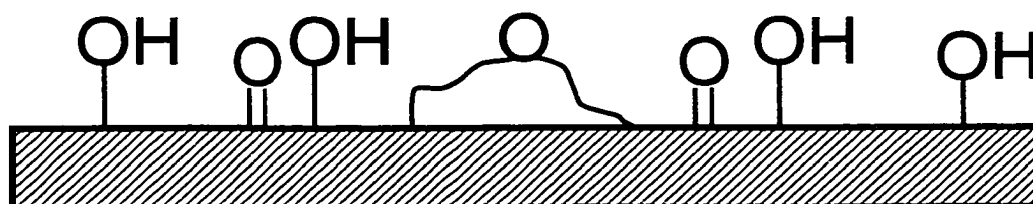


Figure 3.1: Schematic representation of (a) polishing layer, (b) EGO layer, and (c) surface oxide layer.

continually grow thicker at increased anodization times [24]. In this study optical ellipsometry was used to monitor the in situ growth of EGO on a GC electrode. EGO appears as a colored film on the electrode surface. Several different colors have been reported [20, 22, 26]. The intensity and shade of the color have been attributed to optical interference in the transparent EGO layer [24, 26]. Work by McDermott and coworkers has demonstrated that the presence of surface oxide groups generated by ECP serve as important electron transfer catalysts for certain inner sphere electrochemical systems [18]. The electron transfer rate constants for aquated metal ions on GC are shown to increase dramatically upon pretreatment in 0.1 M H₂SO₄, compared to a fractured or oxide free GC surface.

Cabaniss and coworkers realized a two-fold increase in the surface oxygen content of a GC electrode upon electrochemical pretreatment in 0.1 M H₂SO₄ [22]. This result produced a marked effect on the voltammetry of certain proton coupled electron transfer systems compared to their behavior on unactivated electrodes. Engstrom also observed a significant increase in the oxygen carbon ratio of GC electrodes anodized in 0.1 M KNO₃ compared to polished electrodes, 0.22 versus 0.084 respectively [7]. This ratio did not change upon cathodization of the electrode, indicating that while the surface oxides groups may be reduced electrochemically, they are not removed from the surface upon further cathodization. This result is consistent with the appearance of a surface bound redox couple upon electrochemical pretreatment [34].

ECP in basic solutions has significantly different effects than pretreatment in acidic or buffered/salt solutions [17, 20]. Results from a previous study support the idea of the formation of different chemical species on the electrode surface with changes in pH [17]. Electrochemical pretreatment in basic solution tends to dissolve away the products of anodization, making the appearance of polishing scratches more pronounced [20]. Figure 3.1 illustrates the results of ECP of a GC electrode in basic media. Unlike ECP in acid, EGO is dissolved in basic solution,

resulting in a thin layer of surface oxides, as opposed to a relatively thick layer of EGO, as illustrated in Figure 3.1. Work by Kiema and coworkers has demonstrated that it is possible to selectively etch specific regions of a GC electrode [31]. In this work “wells” of varying depth were etched onto the surface of a GC electrode by first patterning the surface using lithography techniques. It was also shown that the depths of these wells could be controlled by varying the anodization time, longer anodization times giving rise to deeper wells. Also, work by Anjo and coworkers has demonstrated that GC electrodes that have been electrochemically pretreated in basic solution demonstrate superior performance in the analysis of dopamine to those that have been electrochemically pretreated in acidic media [19]. Electrodes anodized in basic solution display lower capacitance values and significantly reduced dopamine adsorption compared to electrodes anodized in acidic solution. From these observations one may conclude that no accumulation or growth of EGO film occurs upon ECP in basic solution. The extent of the EGO layer is limited to the presence of a thin layer of surface oxide groups (Figure 3.1).

Some studies have been undertaken in an effort to determine the effects of surface chemistry on electrochemical metal deposition. Shimazu and coworkers have studied the effects of ECP of a GC electrode in 0.5 M H₂SO₄ at 1800 mV for 15 minutes [35]. Platinum particles electrochemically deposited on such a pretreated electrode surface exhibited lower catalytic activity toward hydrogen generation compared to unoxidized heat-treated electrodes. Milchev and coworkers have examined the effects on anodic pretreatment of GC on the nucleation and growth behavior of silver particles on GC electrodes [36]. SEM images show that an increase in silver particle number density is achieved when the electrode is subjected to anodic ECP at a potential of 900 mV for 30 minutes in silver nitrate solution. As anodic pretreatment procedures typically result in the formation of anionic surface oxide groups, or an EGO layer, on the surface of the

electrode, the increased number density may result from favorable electrostatic interactions between positively charged Ag^{+} ions in solution and anionic surface oxide groups.

In this work, the deposition of gold on a variety of pretreated GC electrode surfaces was studied. Four different electrode activation methods were employed; these include polishing in a water/alumina slurry, referred to as polished GC; polishing in a cyclohexane/alumina slurry, referred to as cyclohexane polished GC; electrochemical pretreatment in 1.0 M NaOH, and electrochemical pretreatment in 0.1 M H_2SO_4 . A series of samples were prepared by the electrochemical deposition of gold particles on a number of pretreated GC surfaces. These samples were then analyzed employing SEM and oxide stripping voltammetry. As stated previously, GC and gold are both active electrode materials, thus, it is important to employ electrochemical methods that are selective to gold only.

The purpose of these experiments was to study the effects of GC surface chemistry on the electrochemical deposition of gold particles. Variations in chemistry were induced by application of various ECP and polishing procedures. Specific investigations are aimed at their effect on number density, particle size, surface area, and adhesion.

Experimental Section

Reagents. Potassium tetrachloroaurate(III) (Aldrich), lead oxide (Certified, Fisher), sodium hydroxide (Fisher), sulfuric acid (Fisher), perchloric acid (Caledon), and cyclohexane (Certified A.C.S. Fisher) were all used as received. All solutions were prepared using Nanopure[®] (18 M Ω /cm) water and purged with prepurified argon prior to use.

Electrode Preparation. GC electrodes (Tokai GC-20, Electrosynthesis Company, NY) consisted of either 12mm x 12 mm x 3mm plates or 3 mm sections

of a 6 mm diameter GC rod heat pressed into a teflon electrode housing. Electrical contact to the GC is made through an aluminum rod and silver epoxy. These electrodes were polished on a glass plate following the procedure described in detail in Chapter II. For polishing in cyclohexane, a similar procedure was followed using cyclohexane instead of water. Polished electrodes were used in a normal three-electrode electrochemical cell configuration with a coiled platinum auxiliary electrode and a Ag/AgCl reference electrode. The geometrical electrode area was determined by chronoamperometry in 1 mM $\text{Fe}(\text{CN})_6^{-3/-4}$ and yielded a working electrode area of 0.30 cm², as described in detail in Chapter II. Electrodes were used immediately after polishing, or were subjected to further ECP prior to gold deposition. Electrodes employed for SEM analysis consisted of GC plates and were prepared as described in Chapter II.

ECP procedures consisted of anodization of the GC electrode in either 0.1 M H₂SO₄ or 1.0 M NaOH employing a potential step for a set period of time. For pretreatment in acidic media the potential was stepped from 0 mV to 2000 mV for a period of 60 s. For pretreatment in basic media the potential was stepped from 0 mV to 1800 mV for a period of 30 s. Polishing of the electrodes in a series of alumina/water slurries always preceded any ECP steps.

Electrochemistry. Electrochemical deposition of gold particles and oxide stripping experiments were performed as described in detail in Chapter II.

Gold Particle Adhesion Studies. Gold particles were electrochemically deposited on a pretreated GC substrate. The surface area of the gold deposit was then immediately determined by oxide stripping voltammetry in 0.5 M H₂SO₄. At this point the electrode was removed from the cell, rinsed, and sonicated in a beaker of nanopure water for a period of 30 seconds. Once sonicated, the electrode was removed from the beaker of water, rinsed, dried under a stream of prepurified argon, and replaced within the electrochemical cell. Further oxide stripping voltammetry was then run to determine the remaining gold surface area.

Adhesion was gauged by comparing the area of the gold deposit before and after sonication.

SEM Imaging. SEM analysis of the gold deposits and image analysis of the resulting scanning electron micrographs was performed as described in detail in Chapter II.

Results and Discussion

The objective of these experiments was to determine the effect of various electrode pretreatment methods on the nucleation and growth of gold particles on GC electrodes. Because of our desire to produce arrays of small gold particles for further chemical modification it is important to understand the effects of GC surface chemistry on the resulting gold deposits. This will ensure preparation of the most desirable gold deposits to be used in further chemical modification steps. Ideally, gold particles should be small (10 to 20 nm), well-dispersed, present in large numbers, and display good adhesion to the GC surface. Gold particles are evaluated in terms of their number density, particle size, surface area, and adhesion to the GC substrate.

Cyclic Voltammetry. To assess the effect of GC electrode pretreatment on gold deposition, a series of cyclic voltammograms in 100 μM AuCl_4^- were obtained on each substrate. These voltammograms are displayed in Figure 3.2 and the results of this study are summarized in Table 3.1. Voltammograms are for (a) polished GC, (b) cyclohexane polished GC, (c) base ECP GC, and (d) acid ECP GC (d), electrodes respectively. One concern was whether the various pretreatments employed would influence the overpotential and thus the electron transfer rate for gold deposition. The heterogeneous rate constant for the transition of AuCl_4^- to the metallic state obeys the following equation for irreversible electron transfer [37] where $(E - E^{\circ'})$ is the overpotential.

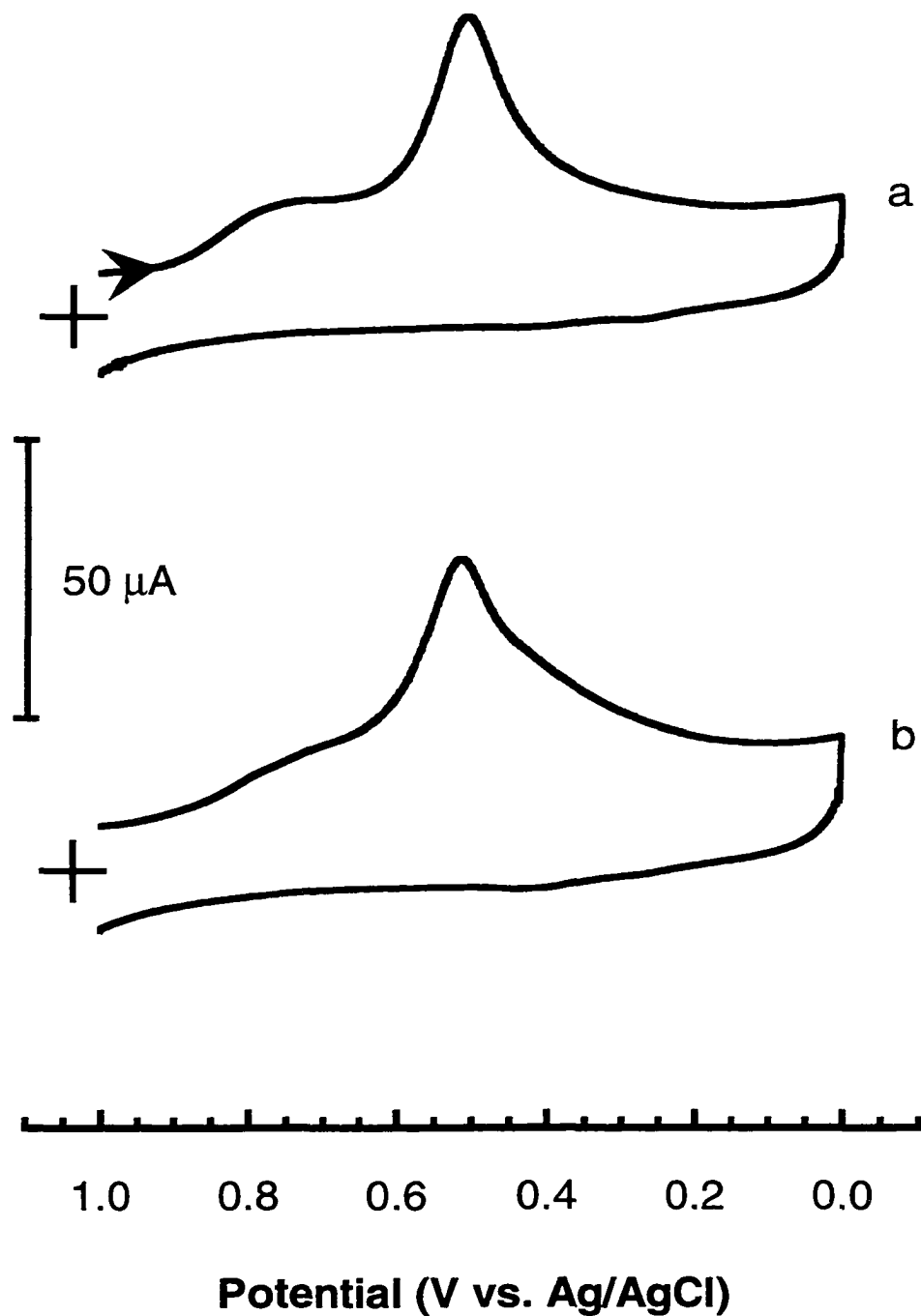


Figure 3.2: Cyclic voltammograms for electrochemically deposited gold on various GC substrates. $v = 100 \text{ mV/s}$, $[\text{AuCl}_4^-] = 100 \mu\text{M}$. (a) normal polished GC, (b) cyclohexane polished GC, (c) 1.0 M NaOH ECP GC, (d) 0.1 M H_2SO_4 ECP GC.

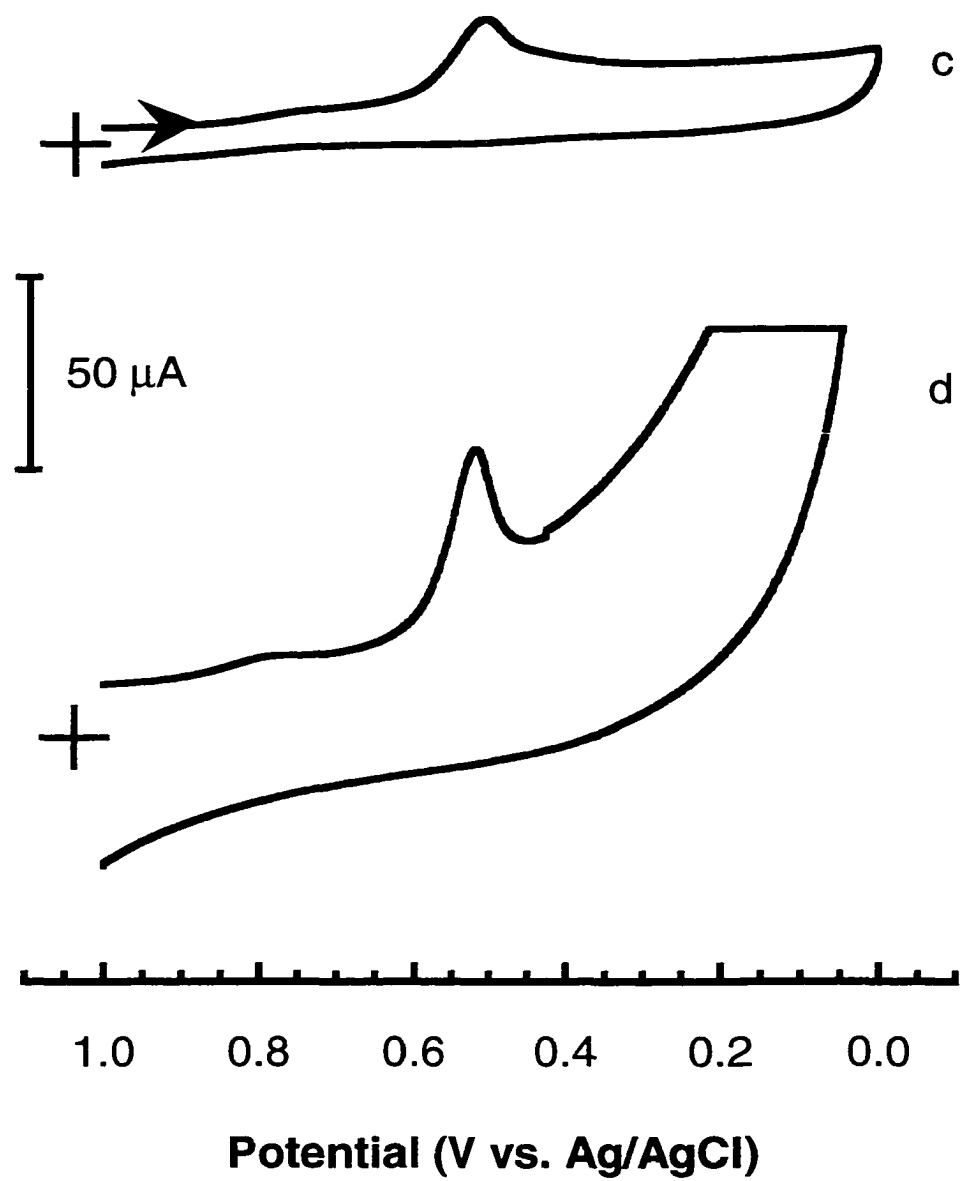


Figure 3.2: (continued)

$$k_c = k^o \exp \left[-\frac{\alpha n F (E - E^{o'})}{RT} \right] \quad \{3.1\}$$

In the case of the voltammograms in Figure 3.2, the cathodic peak potential $E_{p,c}$ was used as a measure of the overpotential. As noted in Table 3.1, $E_{p,c}$ for gold deposition occurs at roughly the same potential on each of the substrates examined, within a range of about 16 mV. Thus, no significant differences in the electron transfer rate for gold deposition on GC is observed as a result of the various electrode pretreatment procedures used.

Table 3.1: Effect of electrode pretreatment on gold particle deposition, $[\text{AuCl}_4^-] = 100 \mu\text{M}$, $\eta = -800 \text{ mV}$.

Electrode Pretreatment	$E_{p,\text{cath}}$ (mV)	Q_{obs}^b (μC)
Polish, water	504 ± 4^a	$10.0 - 10.4^a$
Polish, cyclohexane	502 ± 5	$4.5 - 5.6$
ECP, 1.0 M NaOH	504 ± 5	$4.1 - 4.5$
ECP, 0.1 M H_2SO_4	518 ± 8	$4.7 - 5.3$

- a. Based on measurements of at least 5 samples.
 b. For surface oxide reduction in 0.5 M H_2SO_4 .

Effects of electrode pretreatment are discerned by direct observation of the background capacitive currents in Figure 3.2. Both polished substrates display similar background currents. This is not unexpected due to the layer of fine polishing debris that remains on the electrode surface. Although not studied directly, polishing in cyclohexane may also result in a layer of polishing debris on the electrode surface. This is not an unreasonable assumption given the similarity

in background current of a cyclohexane polished electrode to that of a polished electrode. Upon rinsing with water, these electrodes are also observed to be hydrophobic in nature, possibly due to the presence of cyclohexane on the GC surface that has been incorporated into the layer of polishing debris. As one of the electrodes is pretreated with an aqueous alumina/water suspension and the other with an organic solvent/alumina suspension one would expect a variation in the physical properties of the polishing layer. ECP in base (c) displays the lowest background current, as the layer of polishing debris is etched away in basic media, only a thin layer of surface oxide groups remain [31]. ECP in acid (d) displays the highest background current due to the anodic EGO layer [24]. In this case the current is observed to go offscale during a gold deposition experiment, due to the reduction of surface oxide groups generated during pretreatment.

Gold Oxide Reduction. The use of gold oxide reduction was employed in Chapter II to determine the surface area of electrochemically deposited gold particles. The integrated area of the gold oxide reduction wave was also used here to gauge gold deposition on the various pretreated GC substrates. The results are summarized in Table 3.1. Gold deposition onto a polished GC electrode resulted in a Q_{obs} value for gold oxide reduction that is consistent with that observed for similar substrates under similar conditions in Chapter II. However, Q_{obs} values for gold oxide reduction on cyclohexane polished, base ECP, and acid ECP GC electrodes were observed to be roughly half of that observed on polished GC. This result suggests that only half of the gold surface area obtained on polished electrodes is being generated via gold deposition onto the other pretreated electrodes. This decrease in surface area is likely a result of altered nucleation and growth behavior due to the pretreatment method employed. One method used to investigate this phenomenon is SEM. A possibility for the observed differences in gold surface area may be poor electrical contact of the gold particles with the GC

surface, resulting from the pretreatment method employed. This will be addressed in the last section of this chapter on adhesion.

Scanning Electron Microscopy. The first step in this investigation was to obtain SEM micrographs of gold deposits on the various pretreated surfaces. This approach was taken because it allows a direct qualitative comparison to be made on the effects of electrode pretreatment on gold deposition. A series of gold deposits were prepared for SEM analysis, all depositions were performed using a deposition solution concentration of $100 \mu\text{M AuCl}_4^-$ and a deposition overpotential of -800 mV . Figures 3.3 to 3.6 contain SEM micrographs of gold particles electrochemically deposited on a variety of pretreated GC substrates. As expected for a polished GC substrate, an array of small, uniformly dispersed gold particles is obtained, Figure 3.3. Table 3.2 contains the values of number density and particle size derived from SEM image analysis. Observation of these images reveals that the electrode pretreatment method employed has a profound effect on the nucleation and growth behavior of gold particles on GC.

Table 3.2: Results from scanning electron micrograph analysis for electrochemically deposited gold particles, effect of electrode pretreatment, $[\text{AuCl}_4^-] = 100 \mu\text{M}$, $\eta = -800 \text{ mV}$.

Electrode Pretreatment	Number Density (particles/ μm^2)	Diameter (nm) ^c
Polish, water	89 ± 7^a	13 ± 3
Polish, cyclohexane	78 ± 7^a	20 ± 4
ECP, 1.0 M NaOH	22 ± 4^a	35 ± 8
ECP, 0.1 M H ₂ SO ₄	4 ± 2^b	70 ± 28

- a. Based on measurements of at least 25, $1 \mu\text{m}^2$ areas.
- b. Average values based on measurements of three, $12 \mu\text{m}^2$ areas.
- c. Based on measurements of at least 40 particles.

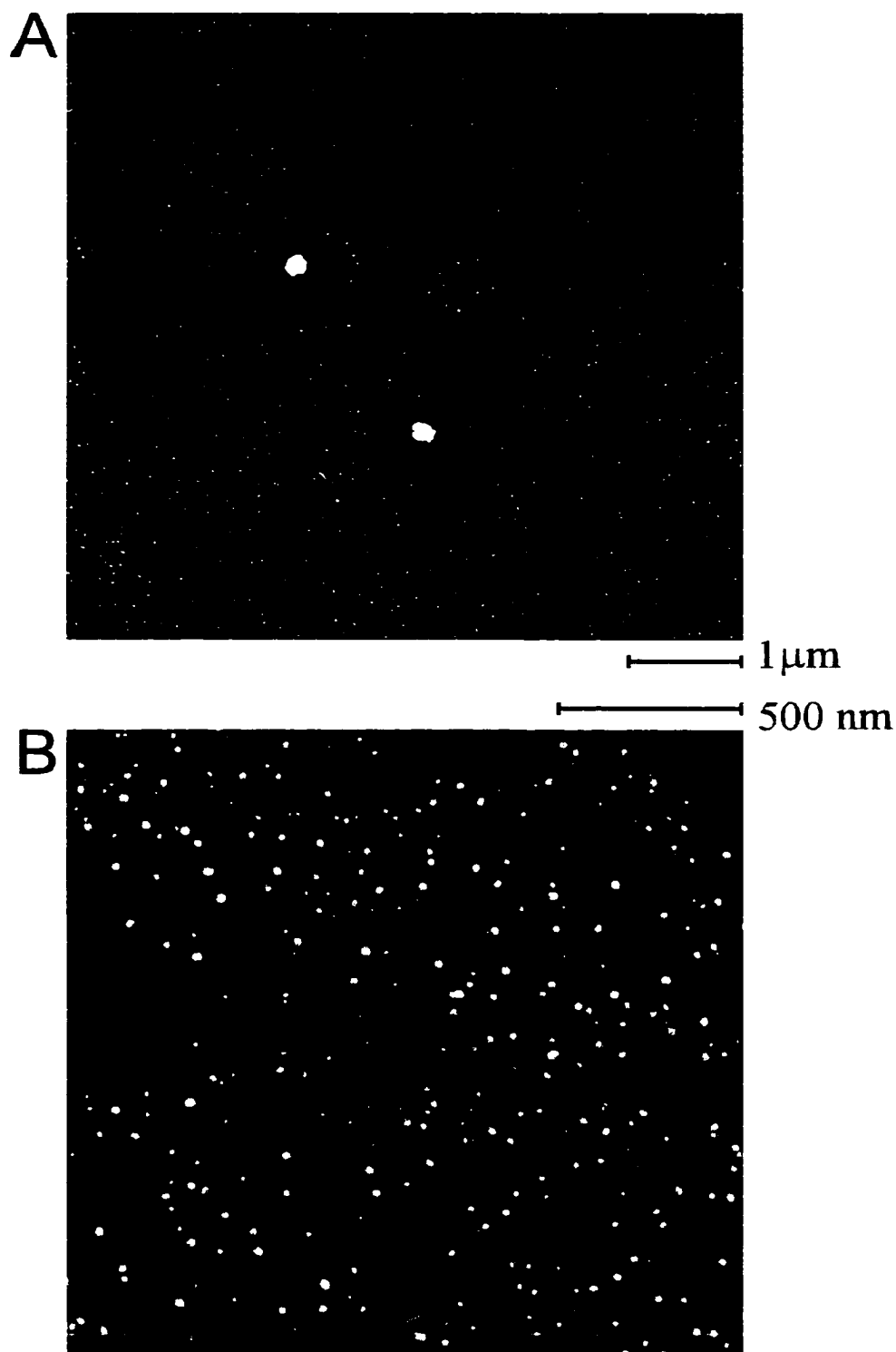


Figure 3.3: Scanning electron micrographs of electrochemically deposited gold particles on normal polished GC. $\eta = -800$ mV, $[\text{AuCl}_4^-] = 100$ μM . (A) 15000x, (B) 50000x, magnification.

Polishing in cyclohexane renders an electrode surface that is considerably devoid of surface oxide groups compared to a GC electrode polished in water [38]. Control experiments using the $\text{Fe}^{+2/+3}$ redox system were employed to evaluate the effects of this pretreatment method. Cyclic voltammograms of the $\text{Fe}^{+2/+3}$ system typically displayed a peak separation of 600 to 700 mV, indicative of a surface that is relatively free of surface oxide groups. Figure 3.4 contains SEM micrographs of gold particles deposited on a cyclohexane polished GC electrode. Again, an array of small, uniformly dispersed gold particles is obtained. Table 3.2 shows that the values of number density and particle diameter obtained on a cyclohexane polished electrode are very similar to those obtained on a polished GC electrode. However, this observation is in contradiction with that expected from the results presented in Table 3.1.

Results from gold oxide reduction experiments suggest that roughly half of the gold surface area is obtained on a cyclohexane polished GC electrode relative to a polished GC electrode under similar deposition conditions. A possible explanation for the inconsistency in these two observations is that a fraction of the gold particles become dislodged or are in poor electrical contact with the underlying GC substrate, and cannot be addressed using gold oxide reduction experiments. At this point, judging from the scanning electron micrographs, it is concluded that the presence of surface oxide groups does not affect the nucleation and growth behavior of gold particles on GC. However, as the cyclohexane polished electrodes are observed to become hydrophobic upon pretreatment in cyclohexane/alumina slurries, physical differences in the nature of the polishing layer may cause these particles to lose electrical contact, or become detached from the underlying GC substrate. Another possible reason for the increased surface area may be the presence of small (< 5 nm) gold particles on the polished GC surface. It is not possible to observe such small particles using SEM.

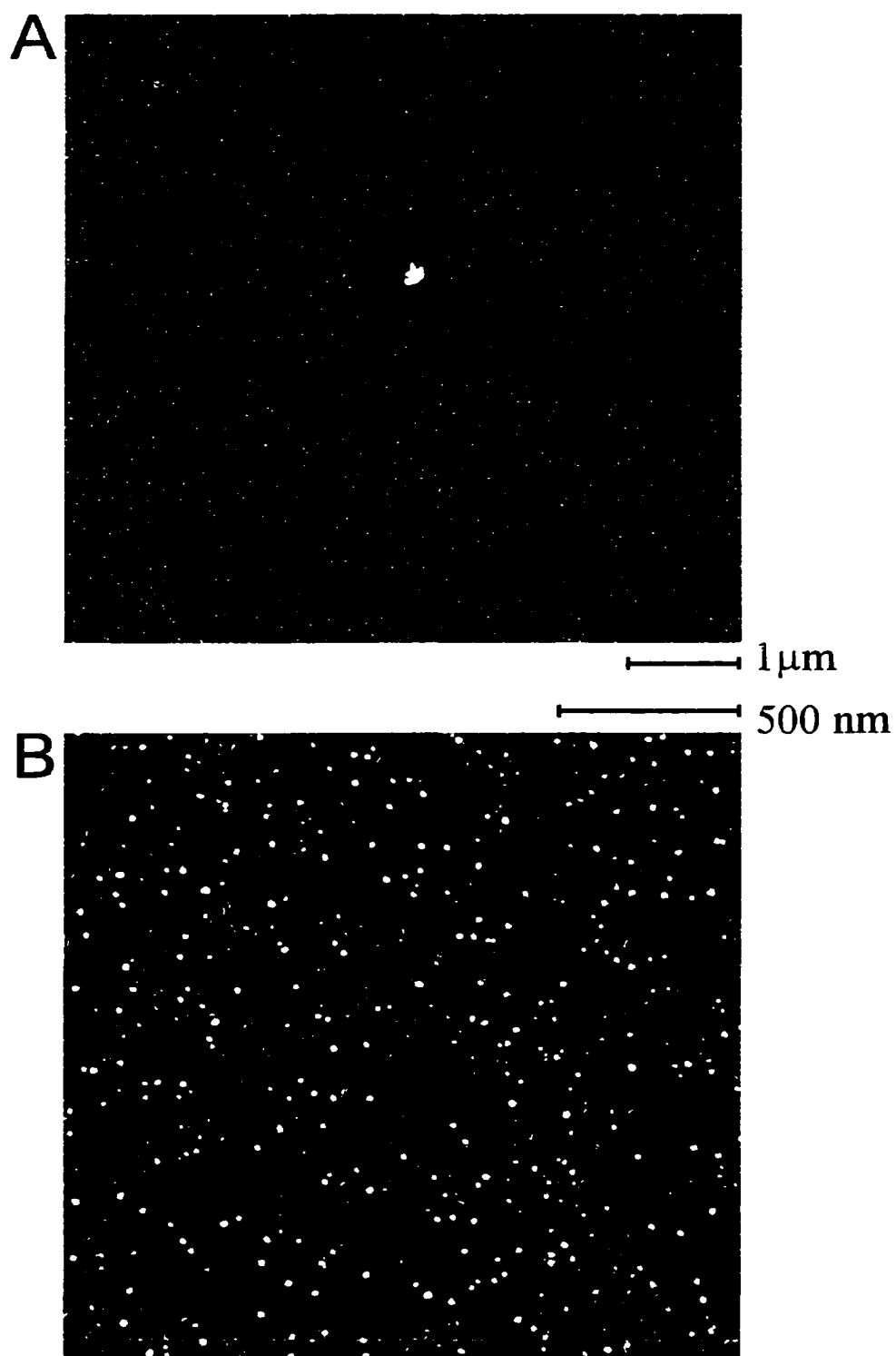


Figure 3.4: Scanning electron micrographs of electrochemically deposited gold particles on cyclohexane polished GC. $\eta = -800$ mV, $[\text{AuCl}_4^-] = 100$ μM . (A) 15000x, (B) 50000x, magnification.

Incorporation of cyclohexane into the polishing layer may prevent the deposition of such small particles on cyclohexane polished GC electrodes.

Figure 3.5 contains SEM micrographs of gold particles deposited on a GC electrode that has been electrochemically pretreated in 1.0 M NaOH. Worthy of note is the predominant appearance of enlarged polishing scratches that result from ECP and dissolution of EGO. In terms of the effects on nucleation and growth behavior, number density is observed to decrease while gold particle size increases. Quantitative values from image analysis contained in Table 3.2 confirm these observations. Distribution of the gold particles remains fairly uniform. A possible explanation for this behavior is that ECP of the electrode has served to reduce the number of nucleation sites available on the electrode surface for gold particle deposition. These sites are blocked by the presence of a thin layer of surface oxide groups. It has been demonstrated that the anodization of GC under basic conditions causes the polishing debris and EGO layer to be dissolved away [20, 31]. While most of the oxidized material is removed during this process a very thin layer of surface oxides remain on the GC surface. This thin layer serves to block most of the electrode surface toward gold deposition. When these electrodes are removed from the electrochemical cell the pretreated surface appears gray in color, and polishing scratches are somewhat visible when the electrode is tilted against direct light. This behavior may result from electrostatic interactions. Surface oxide groups are anionic in nature, and thus electrostatic repulsion of negatively charged AuCl_4^- ions from the vicinity of the electrode surface serves to inhibit nucleation and growth. Since fewer nucleation sites become available, larger particles are obtained, as observed in Figure 3.5, because a greater proportion of gold in solution is directed toward particle growth.

Figure 3.6 contains SEM micrographs of gold particles deposited on a GC electrode that has been electrochemically pretreated in 0.1 M H_2SO_4 . As illustrated in Figure 3.1, ECP of GC in acidic media is accompanied by the

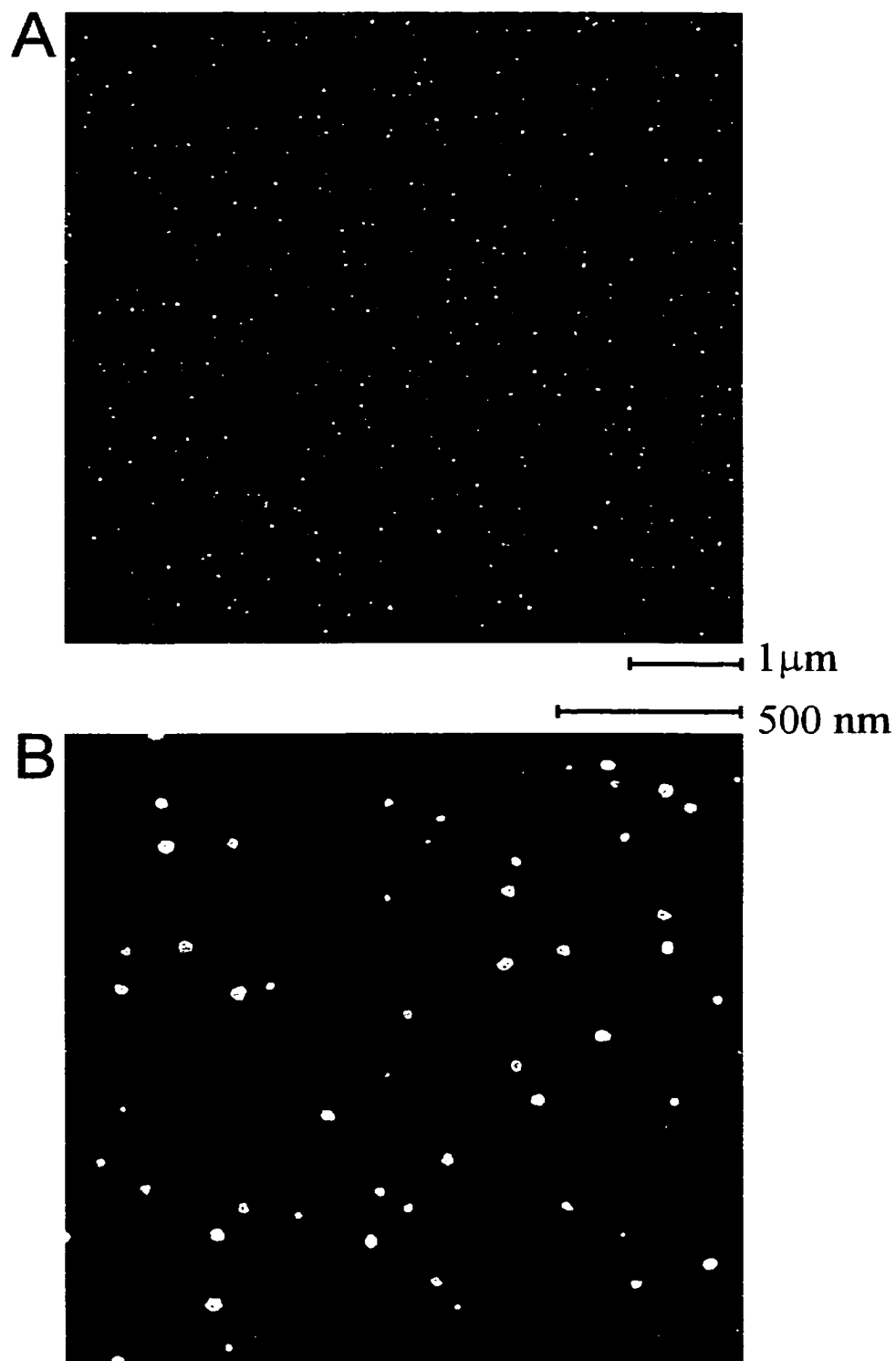


Figure 3.5: Scanning electron micrographs of electrochemically deposited gold particles on 1.0 M NaOH ECP GC. $\eta = -800$ mV, $[\text{AuCl}_4^-] = 100$ μM. (A) 15000x, (B) 50000x, magnification.

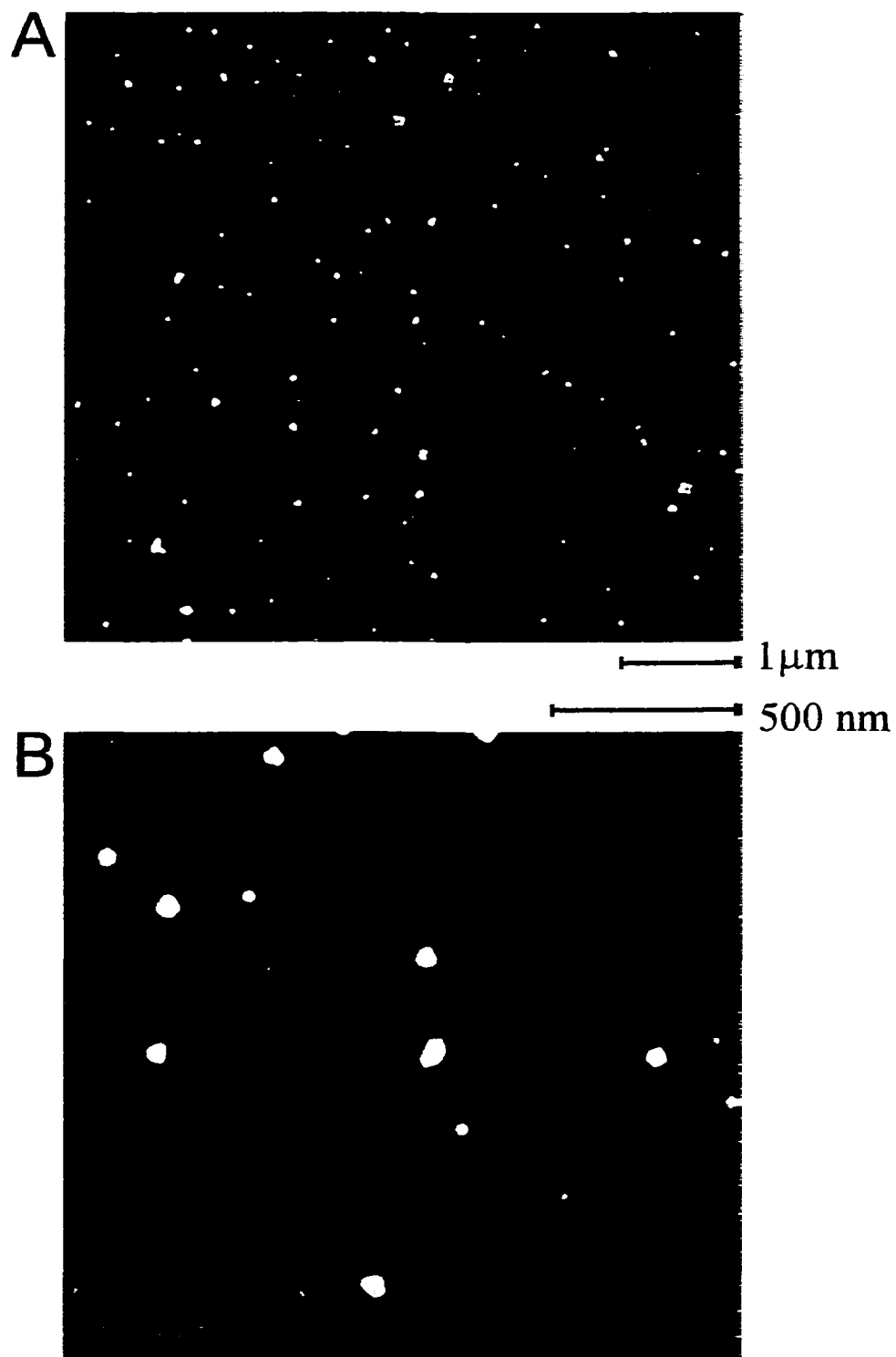


Figure 3.6: Scanning electron micrographs of electrochemically deposited gold particles on 0.1 M H_2SO_4 ECP GC. $\eta = -800$ mV, $[\text{AuCl}_4^-] = 100$ μM. (A) 15000x, (B) 50000x, magnification.

formation of a thick EGO layer. [20, 22, 24, 26]. In these samples, the observed differences in particle size, number density and distribution are even more dramatic. Quantitative values from image analysis listed in Table 3.2 reflect the dramatic reduction in number density and increase in particle size observed on these electrodes. Larger and fewer particles are observed with a somewhat random distribution. Also, larger particles possess irregular as opposed to circular shapes, as seen in Figure 3.6 and Table 3.2. These results are attributed to the effects of ECP on the electrode surface and the presence of a thick EGO layer, which effectively blocks gold particle nucleation. Firstly, the EGO layer has been described as nonconducting except for the region immediately adjacent to the electrode surface [24]. Therefore EGO may serve to insulate or shield the GC surface from gold deposition. Secondly, due to the buildup of EGO in acidic media as opposed to basic media, the thick EGO layer may also electrostatically repel AuCl_4^- from the electrode surface, further restricting particle nucleation.

Anodization under acidic conditions produces a stable EGO film on the surface of GC electrodes that continues to grow deeper with increased anodization times [24]. It has also been demonstrated that this EGO layer is capable of blocking ferricyanide voltammetry [23, 25]. In Figure 3.6 polishing scratches remain relatively unchanged from those observed on a polished electrode. This is indicative of accumulation and growth of an EGO layer. When removed from the electrochemical cell the graphitic oxide layer appears blue in color, a result of optical interference due to the thickness of the transparent layer [24]. For ECP in acidic media the resulting EGO layer is thicker in contrast to the layer of surface oxides generated in basic media (Figure 3.1) and hence more efficient at blocking gold deposition on GC electrodes, either by insulation or electrostatic repulsion. Thus, even fewer and larger particles are observed, due to the reduced number of available nucleation sites, as observed in Figure 3.6.

In summary, the differences observed in the nucleation and growth behavior between the polished and electrochemically pretreated GC substrates are attributed mainly to the presence of surface oxides and EGO layers that form upon ECP of the GC substrates [20]. Thus, the presence of surface oxides or an EGO layer may block active sites for gold particle nucleation, limiting deposition to defects or discontinuities in these layers. Electrostatic considerations may also be partly responsible for inhibiting nucleation of gold particles on the electrode surface. As previously discussed, anodization in either acidic or basic media results in significantly different effects on the GC surface. Differences in the two anodization processes (Figure 3.1) can be used to explain the variations observed in gold particle deposition on these two electrodes. We propose that gold particle deposition occurs mainly on exposed regions of the carbon substrate, and, to a lesser extent, on surface oxide and EGO layers. Polishing serves to expose nucleation sites, while surface oxides and EGO block them.

Adhesion Studies. As already discussed, different electrode preparation methods have diverse impacts on the physical nature of the prepared electrode surface. Polishing procedures give rise to a thin layer of finely divided polishing debris on the electrode surface while ECP imparts layers of EGO or surface oxides onto the GC substrate. The adhesion of metal particles to carbon supports often arises as a major issue in catalysis studies. The sintering of platinum particles on fuel cell electrodes is one such example [1]. The ultimate goal of this research is to be able to use electrochemically deposited gold particles as sites for the attachment of specific functional groups to GC by taking advantage of well characterized self-assembly methods. If this method is to be successful, then the gold particles should display good adhesion to the carbon substrate such that they are not dislodged or rinsed from the surface, or lose electrical contact with the substrate during preparation and regular usage of the electrode. The following

study was aimed at the determination of the effects of surface pretreatment on gold particle adhesion.

Gold particles were electrochemically deposited on a series of pretreated GC substrates. Adhesion of the gold particles was evaluated by determination of the total gold surface area, as determined by gold oxide reduction, before and after sonication in water for 30 seconds. Results from these experiments are tabulated in Table 3.3. Polishing in water renders a surface that favors the formation of high surface area gold deposits. Surface areas obtained on this electrode were a factor of two greater than those obtained for any of the other GC pretreatment methods. This is not surprising in the case of the ECP electrodes as the particle sizes are larger and the number densities are significantly reduced (Table 3.2). However, polished GC and cyclohexane polished GC display very similar number densities and particle sizes, yet, a large difference in surface area is observed. It is postulated that the difference in observed surface area might be due to poor electrical contact of the gold particles deposited on cyclohexane polished electrodes.

Table 3.3: Effect of electrode pretreatment on gold particle deposition and adhesion, $[AuCl_4^-] = 100 \mu M$, $\eta = -800 \text{ mV}$.

Electrode Pretreatment	Q_{obs} (μC) ^a	Au Retained (%) ^a
Polish, water	10.0 – 10.4	45 - 91
Polish, cyclohexane	4.5 – 5.6	24 - 34
ECP, 1.0 M NaOH	4.1 – 4.5	5 - 14
ECP, 0.1 M H ₂ SO ₄	4.7 – 5.3	60 - 97

a. Based on measurements of at least 5 samples.

As observed in Table 3.3, the polished GC surface displays significantly better gold particle adhesion than cyclohexane polished GC. Cyclohexane polished electrodes maintain a maximum of 34 percent of their gold surface area upon sonication whereas polished electrodes maintain 45 to 91 percent. Whether the differences in adhesion are due to the presence of surface oxide groups or a thin film of polishing debris cannot be determined at this point. Gold particles are more easily dislodged during sonication on a cyclohexane polished electrode than on a polished electrode. The poor adhesion of gold particles to cyclohexane polished electrodes suggests that these particles may lose electrical contact with the GC substrate more readily than on a polished GC electrode; thus, a decrease in surface area is observed. The differences in adhesion may be due to physical differences in the nature of the thin layer of polishing debris. As one is generated from an aqueous alumina suspension and the other is generated from an organic solvent/alumina suspension their physical properties may differ, directly affecting adhesion and electronic connectivity to the electrode surface.

Electrochemically pretreated GC electrodes render similar gold surface areas; however, adhesion to these surfaces differs significantly as observed in Table 3.3. On a base pretreated surface, a large percentage of the original gold surface area is lost upon sonication, only 5 to 14 percent of the observed surface area is maintained upon sonication. For an acid pretreated surface a much larger percentage of the original gold surface area remains after sonication, in most cases, upwards of 80 percent of the original surface area is maintained. Since both surfaces possess surface oxide groups, it is difficult to attribute these differences in adhesion solely on the presence or absence of surface oxide groups. Differences in adhesion are attributed to the nature of the EGO layer present on the acid ECP electrode surface. As alluded to previously, it has been demonstrated that electrochemical pretreatment in basic media dissolves away most of the EGO layer that is generated during pretreatment [20, 31]. Thus, it is suspected that only

a very thin film of surface oxides remains on these electrodes. Two scenarios may arise to account for the significant loss of gold surface area. Firstly, adhesion of gold particles to surface oxides is poor and the particles are readily dislodged from the GC surface upon sonication. Alternatively, adhesion of the gold particles to surface oxides may be good, but they are so loosely bound to the GC substrate that the particles are easily dislodged upon sonication.

Electrochemical pretreatment in acid results in a thick EGO layer on the GC electrode. This layer continues to form as long as a potential is applied to the GC substrate in acidic media [24]. EGO is also hydrated, porous, anionic, and permits ion exchange and uptake of ions in solution to take place [25, 32]. Due to the porous nature of this layer, it may be better suited to trapping electrochemically deposited gold particles onto the GC surface, making them difficult to remove by sonication. The results of this investigation suggest that the best method of electrode pretreatment is polishing in an alumina/water slurry. Gold particles obtained are small, well dispersed, and display good adhesion to the GC surface.

Conclusions

From the results of these studies it is difficult to attribute the differences observed for gold deposition on the four different surfaces studied solely on the presence or absence of surface oxide groups. In fact, cyclic voltammetry suggests that the presence of surface oxide groups do not play an important role in terms of the kinetics of gold deposition. Major differences in gold deposition behavior are encountered when electrochemically pretreated substrates are employed. Thus, the differences observed are attributed mainly to the nature of the layer of surface oxide groups or EGO that accumulates on the electrode surface. As the EGO layer is much thicker than a layer of surface oxide groups it may be more efficient at electrostatically repelling AuCl_4^- ions from the electrode surface and trapping the

particles that do manage to nucleate. Differences observed in the two polished substrates may be attributed to the polishing media employed, polishing in water vs. cyclohexane, and the nature of the resulting layer of polishing debris. To attribute the observed differences solely to the presence of surface oxide groups would be risky at this point and further experimentation is needed. Some suggestions for future experiments include; SEM analysis as a function of pretreatment time, SEM analysis after sonication, and a study of the effect of the application of a cathodization step immediately following the anodization step. Use of metal cations, such as Ag^+ or Cu^{2+} , may also be used to test whether or not electrostatic repulsion plays an important role in nucleation and growth behavior. Recall from the introduction that an increase in number density is observed for silver particle nucleation on anodically pretreated GC electrodes.

From these results it was concluded that the best method of electrode preparation to employ for future work is polishing in an alumina/water slurry. The gold deposits obtained possess large surface areas and a large number of small, uniformly dispersed particles that generally display good adhesion to the GC substrate. Gold particle arrays prepared in this manner serve as desirable precursors for further chemical modification in the preparation of chemically modified electrodes.

References

1. K. Kinoshita, *Carbon: Electrochemical and Physicochemical Properties.*, Wiley, New York, (1988).
2. I. F. Hu, D. H. Karweik, and T. Kuwana, *J. Electroanal. Chem.*, **188**, 59, (1985).
3. R. M. Wightman, M. R. Deakin, P. M. Kovach, W. G. Kuhr, and K. J. Stutts, *J. Electrochem. Soc.*, **131**, 1578, (1984).
4. G. N. Kamau, W. S. Willis, and J. F. Rusling, *Anal. Chem.*, **57**, 545, (1985).

5. B. Kazee, D. E. Weisshaar, and T. Kuwana, *Anal. Chem.*, **57**, 2736, (1985).
6. D. E. Weisshaar and T. Kuwana, *Anal. Chem.*, **57**, 378, (1985).
7. R. C. Engstrom and V. A. Strasser, *Anal. Chem.*, **56**, 136, (1984).
8. D. C. Thornton, K. T. Corby, V. A. Spendel, J. Jordan, A. Robbat, D. J. Rutstrom, M. Gross, and G. Ritzler, *Anal. Chem.*, **57**, 150, (1985).
9. G. W. Hance and T. Kuwana, *Anal. Chem.*, **59**, 131, (1987).
10. D. T. Fagan, I. F. Hu, and T. Kuwana, *Anal. Chem.*, **57**, 2759, (1985).
11. K. J. Stutts, P. M. Kovach, W. G. Kuhr, and R. M. Wightman, *Anal. Chem.*, **55**, 1632, (1983).
12. J. F. Evans and T. Kuwana, *Anal. Chem.*, **51**, 358, (1979).
13. J. F. Evans, T. Kuwana, M. T. Henne, and G. P. Royer, *J. Electroanal. Chem.*, **80**, 409, (1977).
14. E. Hershenhart, R. L. McCreery, and R. D. Knight, *Anal. Chem.*, **56**, 2256, (1984).
15. M. Poon and R. L. McCreery, *Anal. Chem.*, **58**, 2745, (1986).
16. R. Rice, C. Allred, and R. L. McCreery, *J. Electroanal. Chem.*, **263**, 163, (1989).
17. A. L. Beilby, T. A. Sasaki, and H. M. Stern, *Anal. Chem.*, **67**, 976, (1995).
18. C. A. McDermott, K. R. Kneten, and R. L. McCreery, *J. Electrochem. Soc.*, **140**, 2593, (1993).
19. D. M. Anjo, M. Kahr, M. M. Khodabakhsh, S. Nowinski, and M. Wanger, *Anal. Chem.*, 2603, (1989).
20. A. L. Beilby and A. Carlsson, *J. Electroanal. Chem.*, **248**, 283, (1988).
21. E. Theodoridou, J. O. Besenhard, and H. P. Fritz, *J. Electroanal. Chem.*, **122**, 67, (1981).

22. G. E. Cabaniss, A. A. Diamantis, W. R. Murphy, R. W. Linton, and T. J. Meyer, *J. Am. Chem. Soc.*, **107**, 1845, (1985).
23. R. C. Engstrom, *Anal. Chem.*, **54**, 2310, (1982).
24. L. J. Kely and A. J. Bard, *Anal. Chem.*, **60**, 1459, (1988).
25. T. Nagaoka and T. Yoshino, *Anal. Chem.*, **58**, 1037, (1986).
26. A. Rojo, A. Rosenstratten, and D. Anjo, *Anal. Chem.*, **58**, 2988, (1986).
27. N. Cenas, J. Rozgaite, A. Pocius, and J. Kulys, *J. Electroanal. Chem.*, **154**, 121, (1983).
28. W. J. Blaedel and R. A. Jenkins, *Anal. Chem.*, **47**, 1337, (1975).
29. S. S. Lord and L. B. Rogers, *Anal. Chem.*, **26**, 284, (1954).
30. M. S. Freund, A. Brajter-Toth, T. M. Cotton, and E. R. Henderson, *Anal. Chem.*, 1047, (1991).
31. G. K. Kiema, G. Fitzpatrick, and M. T. McDermott, *Anal. Chem.*, **71**, 4306, (1999).
32. T. Nagaoka, T. Fukunaga, T. Yoshino, I. Watanabe, T. Nakayama, and S. Okazaki, *Anal. Chem.*, **60**, 2766, (1988).
33. P. T. Kissinger and W. R. Heineman, *Laboratory Techniques in Electroanalytical Chemistry, Second Edition.*, Marcel Dekker, New York, (1996).
34. D. Laser and M. Ariel, *J. Electroanal. Chem.*, **52**, 291, (1974).
35. K. Shimazu, K. Uosaki, H. Kita, and Y. Nodasaka, *J. Electroanal. Chem.*, **256**, 481, (1988).
36. A. Milchev, E. Vassileva, and V. Kertov, *J. Electroanal. Chem.*, **107**, 323, (1980).
37. J. Koryta, J. Dvorak, and L. Kavan, *Principles of Electrochemistry*, John Wiley & Sons, Inc., New York, (1993).

38. P. Chen and R. L. McCreery, *Anal. Chem.*, **68**, 3958, (1996).

CHAPTER IV

MODIFICATION OF SUPPORTED GOLD PARTICLES USING ALKANETHIOL SELF ASSEMBLED MONOLAYERS

Introduction

In the preceding chapters, the electrochemical deposition of gold onto GC was studied. The main objective of these studies was to develop a protocol for producing arrays of supported gold particles for future chemical modification using thiol molecules. In Chapter II, the effects of deposition solution concentration and deposition overpotential were investigated. It was found that the most desirable arrays of small, well dispersed, gold particles can be prepared using dilute solutions, 100 to 200 μM AuCl_4^- , and overpotentials of -800 to -1000 mV. The number density, surface area, and microcrystal structure of these particle arrays were also determined. In Chapter III, the effects of electrode surface pretreatment on gold particle deposition were investigated. It was found that the various surface pretreatment methods employed in this study each have a profound effect on the nature of the gold particles obtained. Particle size, number density, and gold surface area were most notably affected. Some insight into the adhesive properties of the gold particles was also obtained. From the results of these studies it was determined that the most desirable gold deposits are produced on surfaces that are prepared by polishing in water/alumina slurries. These electrodes are referred to as normal polished surfaces.

From the results of Chapters II and III combined, a suitable protocol for the preparation of small supported gold particle arrays was established. Thus, subsequent experiments were performed employing gold particles prepared using

these conditions, except where stated otherwise. The next generation of experiments was focused on the chemical modification of these gold particles using self-assembled alkanethiolate monolayers. More specifically, in this chapter the properties of alkanethiolate monolayers on electrochemically deposited gold particles were investigated using electrochemical and spectroscopic techniques. Also, the feasibility of successive deposition and modification steps on a single electrode was explored. The purpose of these studies was to evaluate these supported gold particles as sites for chemical modification of the GC surface. We feel that this technique has good potential as a method for the preparation of chemically modified electrodes.

Self-assembled monolayers of long-chain alkanethiols or disulfides on gold have been an area of intense research over the past fifteen years. The popularity of this system can be attributed to its numerous attractive properties. These properties include: the strength and stability of the gold-sulfur interaction which allows monolayer formation to proceed in the presence of many functional groups, the flexibility afforded with respect to surface chemistry obtained by simply changing the tail group on the disulfide or thiol molecule, well-defined structural order and integrity of self-assembled films due to favorable van der Waals interactions between the long alkane chains, the stability of the films in the presence of strongly acidic or basic electrolytes and applied potentials, and the ease of preparation and analysis of film samples. These model systems have been extensively studied and characterized using techniques such as optical ellipsometry, X-ray photoelectron spectroscopy, reflectance infrared spectroscopy, surface Raman scattering, contact angle measurements, surface plasmon resonance, scanning probe microscopy, and electrochemistry [1-15].

A more traditional method of preparing thin organic films has been the use of the Langmuir-Blodgett technique [16]. However, self-assembly offers significant advantages over this method. Unlike the labor-intensive Langmuir-

Blodgett technique, preparation of these thin organic films involves the spontaneous solution adsorption of thiol or disulfide molecules onto gold substrates. Also, due to the nature of the Langmuir-Blodgett method, the types of bifunctional molecules that can be employed to produce thin organic films is restricted to those containing only one polar group. This limitation is not encountered when employing the self-assembly method, further expanding the number and types of films that may be prepared. These advantages are among the main reasons for the increasing popularity of this sample preparation technique.

Nuzzo and Allara were the first to demonstrate the ability of sulfur containing molecules to bind to gold substrates [1]. In this work they showed that it was possible to prepare supported, oriented monolayers of polyfunctional organic molecules with a variety of molecular structures. In particular, they demonstrated that it is possible to control the surface chemistry at the interface by simply varying the functional group at the opposite end, or terminus of the disulfide molecule. In this study a series of samples of disulfide monolayers were prepared and analyzed using optical ellipsometry, reflectance infrared spectroscopy, and contact angle measurements. Film thicknesses obtained by ellipsometry were slightly less than the estimated values obtained for an arrangement of molecules having bulk packing densities and full vertical chain extensions away from the substrate surface. This discrepancy may be attributed to the fact that the alkyl chains are not oriented normal to the substrate surface, and display some degree of tilt in their orientation. Results obtained from infrared reflection experiments indicate that the chains are at full extension with a planar zigzag conformation [17, 18]. In addition, the various contact angle measurements for water on the different samples studied display variation in a manner that is consistent with the polarity of the terminal functional group, i.e. not the disulfide group. This observation provides additional strong evidence for adsorption of the disulfide group at the gold substrate.

Thiol molecules display similar self-assembly behavior to that of disulfides on gold [2, 5-7, 9-12] and other metals [9, 10, 19]. In fact, it has been observed that thiols and disulfides give rise to similar monolayer species even though their kinetics of adsorption and place exchange may differ [6]. Infrared spectroscopic and ellipsometric data show that long-chain thiols form a densely packed, crystalline-like assembly with fully extended alkyl chains exhibiting tilt angles of 20 to 40 degrees vs. the surface normal [2, 6, 7]. Scanning tunneling microscopy [11] and atomic force microscopy [12] studies confirm that for alkyl chain lengths of four carbon atoms or longer these adsorbates adopt a $(\sqrt{3} \times \sqrt{3})R30^\circ$ adlayer structure on Au(111) substrates. It is speculated that tilting of the chains occurs in order to maximize the van der Waals interactions between them.

An extensive study of the structural characterization of normal alkanethiolate monolayers on gold was first presented by Porter and co-workers [2]. In this study, monolayer assemblies of *n*-alkanethiols of varying chain length, $\text{CH}_3(\text{CH}_2)_n\text{SH}$, were characterized by optical ellipsometry, reflectance infrared spectroscopy, and electrochemistry. The results of these studies reveal distinct differences in the properties between long and short-chain alkanethiolate monolayers. Transition from a densely packed, highly ordered, crystalline-like assembly for longer chains ($n > 9$) to an increasingly disordered, less densely packed structure is observed to occur for alkyl chains less than ten carbon atoms in length. Ellipsometric measurements of film thickness give rise to lower values than those theoretically predicted for the shorter chain lengths, ($n < 8$). This observation suggests that the alkyl chains are not fully extended or as densely packed and adopt a more disordered liquid-like orientation. It is generally accepted in the literature that this transition occurs for chain lengths less than ten carbon atoms long ($n < 9$).

Infrared spectroscopic data reveal that the asymmetric methylene stretching mode (ν_a, CH_2) absorption intensity is directly proportional to the number of

methylene groups per alkyl chain [2]. This result suggests that the self-assembly process renders reasonably uniform quality monolayers for all alkyl chain lengths. However, upon closer examination, the spectra reveal subtle, but important effects of alkyl chain length on packing density, crystallinity, and orientation of the monolayer. Comparison of the position of the peak frequency for $\nu_{\text{a,CH}_2}$ in the monolayer spectra reveals a shift toward higher energy as the length of the alkyl chain is decreased. Thus, a shift to higher energy is indicative of decreased order in the monolayer structure. Peak broadening (FWHM) is also observed for less ordered samples. These analyses and conclusions are based on previous work by Snyder and coworkers on the infrared investigation of single crystal and liquid state polymethylene chains [17, 18].

The structure of self-assembled monolayers may also be probed using electrochemical methods. While ellipsometry and infrared spectroscopy provide a more general idea of the average structure of these assemblies, electrochemistry is highly sensitive to defects and imperfections in the monolayer structure. In their investigations, Porter and co-workers compared the blocking effects of monolayers of various chain lengths on the redox behavior of the $\text{Fe}^{+2/+3}$ and $\text{Fe}(\text{CN})_6^{-3/4}$ redox systems at gold electrodes [2]. At bare gold electrodes, both systems display nearly reversible electron transfer behavior. On electrodes modified with butanethiol ($n = 3$) the electron transfer kinetics become severely affected, giving rise to large peak separations. In fact, the anodic peak for the $\text{Fe}^{+2/+3}$ system is no longer observed. However, the observed current is attributed to electron transfer at defects in the monolayer. Electrodes modified with octanethiol ($n = 7$) completely block electron transfer for both systems, indicative of a structure that is low in defects and impermeable to ions.

Capacitance measurements can also be used as a diagnostic of film thickness. If the electrode/monolayer/solution interface is modeled as a capacitor, then the monolayer can be thought of as the dielectric material between the two

plates of the capacitor. As the separation between the plates is increased, capacitance decreases as a function of the distance between the plates. Hence, this method may also be employed to probe monolayer film thickness. For alkyl chains longer than nine carbon atoms the capacitance was found to be inversely proportional to the length of the alkyl chain [2]. This is also a good indication of the structural integrity of these monolayers. For monolayers consisting of nine carbon atom or less this behavior is not observed. This suggests that supporting electrolyte ions are participating in some manner in the charge redistribution process. This was attributed to either permeation of ions into the monolayer structure or a contribution from structural defects.

Further studies have emerged whose main focus has been on the effects of different functional groups, other than methyl, at the terminus of the alkane chain. As already mentioned, changing the tail group affords the ability to control the surface chemistry of the film. It has been shown that this will affect the properties of the thin film in terms of its wettability [5, 6], and may also induce changes in ordering or packing density depending on the size of the terminal group. Chidsey and coworkers have examined the effects of various tail groups on the defectiveness and permeability of long chain organic monolayers [8]. As long as the terminal group is relatively small, the structure of the monolayer is dominated by the van der Waals interactions between the methylene chains. Infrared studies reveal that monolayers terminated with $-OH$ and $-CN$ groups have nearly crystalline packing and $-COOH$ terminated monolayers more disordered or liquid like packing. This result was confirmed by observing the electrochemical blocking behavior of these films on the $Fe(CN)_6^{-3/-4}$ and $Ru(NH_3)_6^{+2/+3}$ redox systems. It has also been demonstrated that the capacitance of a modified gold electrode will change depending on the nature of the terminal functional group [13]. Since all monolayers in this study were formed from similar chain lengths ($n = 11$) and small terminal groups, ($-CH_3$, $-OH$, $-CN$, and $-Cl$) the differences in

capacitance of the samples were attributed to the difference in dielectric behavior of the terminal functional groups. Monolayers containing electroactive moieties as the tail group have also been prepared using the self-assembly method. Discussion of these types of monolayers will be deferred to Chapter V.

The large body of recent literature on the preparation of gold colloids modified by the spontaneous chemisorption of alkanethiols has guided us to explore the electrochemical deposition and modification of supported gold particles on GC [20-35]. Brust and coworkers were the first to demonstrate that it is possible to synthesize modified gold colloids by employing a two-phase liquid-liquid system [20, 21]. Tetrachloroaurate(III), (AuCl_4^-) is transferred from aqueous solution into toluene using an appropriate phase transfer reagent. Gold is then reduced with aqueous sodium borohydride in the presence of the desired thiol molecule. This procedure results in thiol derivatized metal nanoparticles that can be handled and characterized as a simple chemical compound. Materials prepared in this manner are extremely stable and do not show any signs of decomposition such as particle growth or loss of solubility. Colloidal solutions of these particles are also very stable and show no signs of decomposition or aggregation over a period of several weeks [21]. Transmission electron microscopy shows that the modified metal particles have diameters in the range of 1 to 3 nm and possess either cuboctahedral or icosahedral shapes. It is also possible to obtain infrared spectra of these materials by dropcasting a film of the modified colloids onto a NaCl or KBr disc. Transmission spectra of the modified particles look similar to those of the bulk thiol used for modification. This provides evidence that the colloids have indeed been modified with thiol monolayers. It is also possible to further react the modified colloids using simple organic reactions such as esterification of surface bound phenolic hydroxy groups [21]. The reaction was monitored using infrared spectroscopy which provides further evidence that the thiols are attached to the surface of the gold colloids.

Several interesting studies have recently emerged which focus on the study of modified colloids. The majority of these studies are focused on the investigation of monolayer structure and properties. It is believed that the properties of the monolayers are affected mainly by the high radius of curvature of particles in the 1 to 5 nm range. The small gold core radius causes the attached hydrocarbon chains to fan out on average away from the gold core. Therefore, the average ligand packing density is necessarily higher near the gold core and becomes considerably less dense at the chain termini [30].

It has been demonstrated that core sizes can be finely adjusted by varying the gold:thiol ratio and the temperature at which the colloids are prepared [32]. The ability to vary the size of these colloids presents significant opportunities in chemistry, as catalytic, optical, magnetic, and electronic properties can be dimensionally sensitive. Due to their physical properties: small size, large surface area, and solubility, these modified colloids can be investigated using techniques that are not sufficiently sensitive for study of a monolayer on a flat surface [22]. This has prompted researchers to redefine these systems as “monolayers in three dimensions”. Such techniques include ^1H and ^{13}C NMR spectroscopy, elemental analysis, differential scanning calorimetry, thermogravimetry, UV visible spectroscopy, and diffusion ordered NMR spectroscopy. More conventional techniques such as electrochemistry, scanning probe microscopy, small angle X-ray scattering, X-ray photoelectron spectroscopy, transmission electron microscopy, and contact angle measurements have also been employed. Some interesting results from these studies will now be discussed.

Infrared spectroscopic studies of modified colloids suspended in a KBr pellet show that the monolayers exhibit similar crystalline structure to those obtained on planar gold substrates [25, 28]. This is a surprising result since some disorder is expected due to the decreased packing density of alkane chains at the outermost region of the monolayer. However, the authors caution that this

observation may be an artifact of sample preparation. Firstly, order may be induced in the alkane chains due to the applied pressure during pellet fabrication [32]. Also, interdigitation at the terminal regions of the alkane chains may contribute to ordering in the bulk sample [22, 26, 30-32]. It has been shown by transmission electron microscopy that the distance between two modified particles can be considerably less than twice the length of the alkane chains used for modification. From this observation interdigitation is inferred [31]. Much of the observed disorder in these monolayers is attributed to gauche defects present at the chain termini [25, 32].

Results from NMR studies further support the idea that packing density decreases toward the outermost regions of the monolayer. Since these samples are prepared as dilute solutions of modified colloids, ordering should be minimal due to solvation of the chain termini [30]. Proton and ^{13}C NMR linewidths tend to become broadened as the positions of the atoms become closer to the gold core [22, 26, 30, 32]. This observation is largely attributed to the fact that chain packing near the gold core is more dense. Therefore, methylene groups closest to the gold core experience faster spin relaxation from dipolar interactions [32]. ^{13}C spectra of modified colloids reveal that linewidths vary systematically with carbon site position relative to the gold core surface [22, 26, 32].

The results presented in Chapter IV focus on the chemical modification of small supported gold particles with long chain alkanethiolate molecules. The modified particles have been studied by scanning electron microscopy (SEM), infrared reflection absorption spectroscopy (IRRAS) and electrochemistry. While this system differs significantly from that of chemically modified gold colloids, the results of studies performed on chemically modified gold colloids proved useful in the interpretation of the experimental data. Chemically modified gold particles present an intermediate scenario between those of monolayers on planar gold substrates and those on small gold colloids. While the supported particles are

large enough in diameter to be considered “planar” substrates, some effects due to their small size and shape are reflected in the observed monolayer structure and properties. The results of these studies will now be presented.

Experimental Section

Chemicals. Potassium tetrachloroaurate (Aldrich), hexanethiol, HT, (Aldrich), dodecanethiol, DDT, (Aldrich), catechol (Aldrich), potassium ferricyanide (Certified, Caledon), potassium chloride (Anachemia), ethanol (punctilious grade, Millennium Petrochemicals), cyclohexane (Certified, Fisher) sulfuric acid, (Fisher), and perchloric acid, (Caledon) were all used as received. Octadecanethiol, ODT, (Aldrich) was recrystallized three times from ethanol, and octadecanethiol- d_{37} was a gift from Marc Porter (Iowa State University).

Electrode Preparation. GC electrodes (Tokai GC-20, Electrosynthesis Company, NY) consisted of either 12mm x 12 mm x 3mm plates or 3 mm sections of a 6 mm diameter GC rod heat pressed into a teflon electrode housing. Electrical contact to the GC is made through an aluminum rod and silver epoxy. For infrared measurements, 3 cm x 6 cm x 1 mm GC plates were employed. The backside of these plates was coated with a thick film of poly(ethylene)/poly(vinylacetate) 60:40 (Aldrich) to block electrochemical activity. Electrode surfaces were prepared by polishing on a glass plate in alumina/water or alumina/cyclohexane slurries. Two grades of polishing alumina were employed, 1.0 micron alpha alumina, and 0.3 micron alpha alumina (Buehler). Upon polishing, the electrodes were rinsed, sonicated for ten minutes, rinsed, sonicated for a further ten minutes, rinsed, and stored in a beaker of water or cyclohexane. This procedure was repeated after polishing with each size of alumina and electrodes were used immediately after being polished. Polycrystalline gold electrodes consisted of either a 1 mm diameter gold disk electrode (Bio-Analytical Systems) or glass

slides sputter coated with 500 nm of gold, primed with 30 nm of titanium for adhesion. Supported gold particles were prepared by potential step deposition from solutions of AuCl_4^- in 0.5 M sulfuric acid, as described in Chapter II. Monolayer samples were prepared by immersion of the electrodes into millimolar solutions of the desired alkanethiol in ethanol for a set period of time.

Electrochemical Measurements. Electrochemical experiments were carried out using a Pine Model AFCBP1 bipotentiostat with a coiled platinum wire auxiliary electrode and Ag/AgCl (sat'd KCl) reference electrode. The auxiliary electrode was separated from the bulk solution using a glass frit. All potentials in the text are referred to the Ag/AgCl reference electrode unless stated otherwise. All solutions were purged with prepurified argon prior to use.

SEM Imaging. Scanning electron microscopy analysis of the gold deposits was carried out by George Braybrook, Department of Earth and Atmospheric Sciences, using a JEOL model 6301FXV scanning electron microscope at an acceleration voltage of 15 to 20 kV and a working distance of 4 to 5 mm.

IRRAS Studies. IRRAS spectra were obtained on an ATI Mattson Infinity Series FTIR spectrometer equipped with an external sample module and liquid nitrogen cooled mercury-cadmium-telluride (MCT) detector. Spectra were taken at 2 cm^{-1} resolution with a mirror speed of 50 kHz. Typically, 1000 scans and 5000 scans were averaged to yield spectra with acceptable signal-to-noise ratios for bulk gold films and supported gold particles respectively. The interferograms were Fourier transformed using triangular apodization. Reference spectra were obtained with bulk gold films and supported gold particles modified with octadecanethiol- d_{37} under the same conditions.

Results and Discussion

In Chapter II it was demonstrated that it is possible to control the size and number density of electrochemically deposited gold particles on GC by varying the deposition solution concentration or deposition overpotential. The result of this work is that we now have a reproducible method of producing arrays of well dispersed, nanometer sized supported gold particles. The results presented herein focus on the use of alkanethiols to chemically modify supported gold particles. The goals of these studies are two fold. Firstly, we wish to investigate the feasibility of modifying these supported gold particles using self-assembled monolayers. The ability to modify the existing particles by taking advantage of gold-sulfur chemistry provides a potentially new method for introducing functional groups onto the surface of GC electrodes in a controlled manner. Secondly, we wish to examine the monolayers formed, and draw some conclusions about their structure and physical properties.

Gold particles were electrochemically deposited onto polished GC electrodes via potential step, as described in Chapter II. The existing particles were then chemically modified by placing these electrodes into dilute solutions of the desired alkanethiol for a predetermined period of time. Various electrochemical and spectroscopic experiments were then employed to probe the properties of these modified particles.

SEM Imaging. In Chapter II scanning electron microscopy (SEM) was employed to obtain a visual perspective of gold particles electrochemically deposited onto GC substrates. From SEM image analysis it was possible to obtain values of number density and particle diameter for the various deposition conditions studied. In this chapter the range of deposition solution concentrations was expanded to include more concentrated AuCl_4^- solutions. Concentrations as high as 1 mM AuCl_4^- were used in the preparation of infrared samples in an effort to obtain better signal-to-noise ratios for the infrared spectra. SEM imaging was

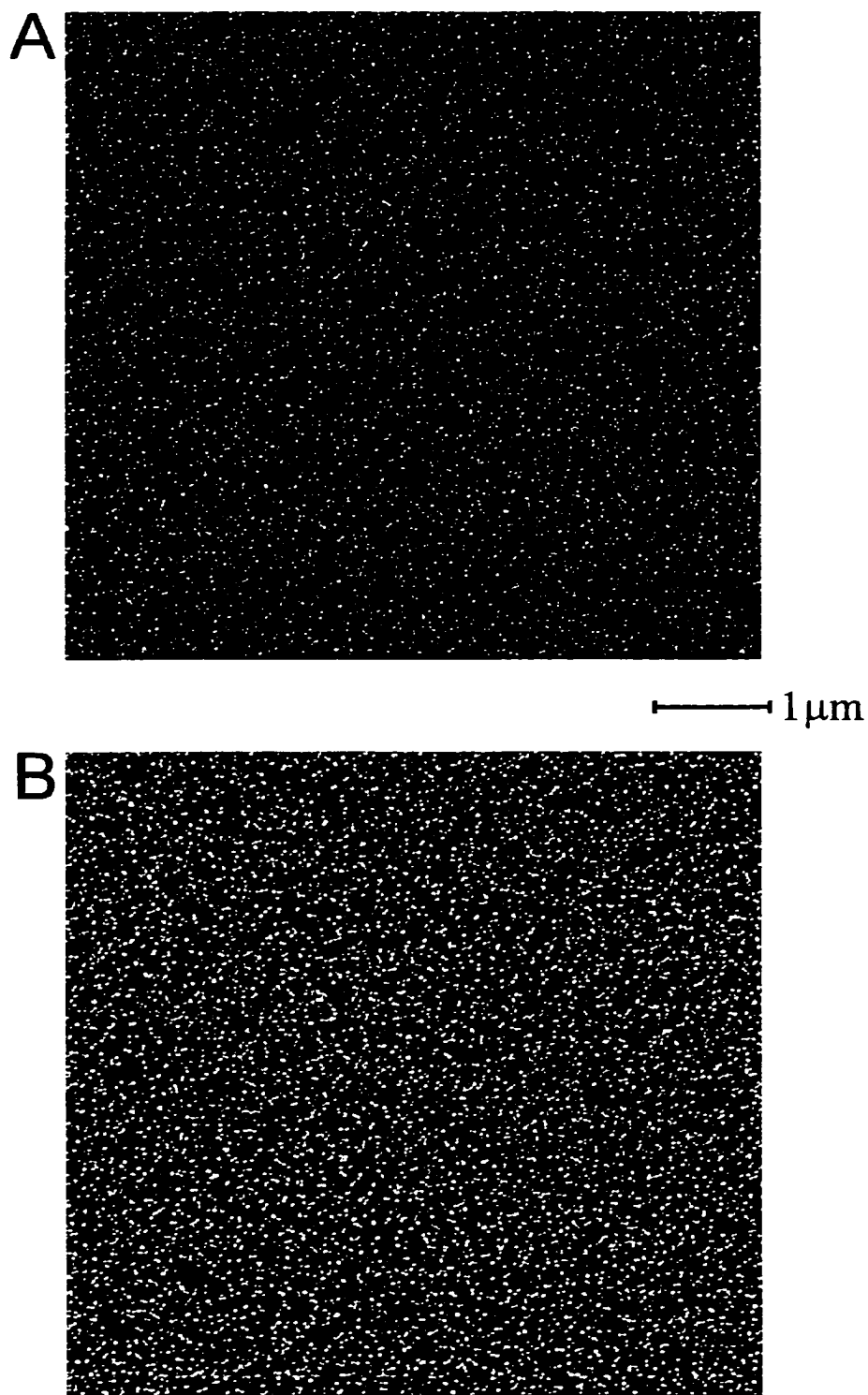


Figure 4.1: Scanning electron micrographs of electrochemically deposited gold particles on GC, $\eta = -800$ mV, $t = 5$ s. (A) 500 μM , (B) 1 mM , AuCl_4^- .

employed to confirm that individual, well-dispersed gold particles are obtained at the higher deposition solution concentrations. Parts A and B of Figure 4.1 contain SEM images of gold particles electrochemically deposited on GC from solutions of 500 μM , and 1 mM AuCl_4^- . Gold particles appear as circular bright spots surrounded by a background of darker GC substrate. The SEM images confirm that it is still possible to obtain good distributions of individually supported gold particles from more concentrated deposition solutions.

IRRAS Studies. IRRAS has been used extensively to study and characterize self-assembled monolayers of various thiol molecules on bulk gold films [1, 2, 7, 8]. From these studies it is possible to gain information about monolayer order, packing density, coverage, surface chemistry, and orientation. In this investigation the focus was to obtain infrared reflectance spectra of supported octadecanethiol (ODT) modified gold particles. Several studies have shown that it is possible to obtain infrared spectra of chemically modified gold colloids [20, 21, 25, 28, 30, 32]. However, the samples employed in these studies typically consist of modified colloids drop cast onto a salt plate or pressed into a KBr pellet. Spectra were obtained by transmission infrared spectroscopy. The primary goal of this study was to test the feasibility of modifying supported gold particles with alkanethiol molecules and to probe the structure of the resulting monolayer using IRRAS. Herein, the first infrared spectrum of chemically modified gold particles supported on a GC substrate is presented. This sample allows for spectroscopic interrogation of the modified gold particles without the possible consequences encountered from drop casting or pressing them into a KBr matrix. Such consequences may include alteration of the monolayer structure, such as induced ordering of the alkane chains due to the applied external pressure during pellet fabrication [32]. It is also possible for the long alkane chains to intercalate or interdigitate at their termini to produce well-ordered, crystalline,

hydrocarbon domains [22, 26, 30-32], even when the sample is prepared by drop casting a film of modified colloids on a KBr plate.

A major stumbling block associated with this analysis is the inherent low infrared reflectivity of the GC substrate. This results in a very low mean-squared electric field (MSEF) for GC compared to that of metallic gold [36]. Also, the optimal angle of incidence for GC, that is, the angle of incidence at which the MSEF on GC is a maximum, is significantly different from that of gold. The respective values are $\sim 60^\circ$ for GC and $\sim 79^\circ$ for gold. At an angle of incidence of $\sim 75^\circ$, as used in our study, the MSEF on GC is approximately one seventh of that on gold [36]. An advantage of this is that interference from molecules adsorbed to the GC should be minimized. A major concern is whether these small gold particles can provide enough surface area to obtain a discernable infrared reflectance spectrum.

The particles in this study were electrochemically deposited by potential step from a solution of 1 mM AuCl_4^- . Self-assembly of ODT was allowed to occur for at least 20 hours. Figure 4.2 contains two infrared reflectance spectra for ODT on gold. Trace (a) is representative of an ODT monolayer on a bulk gold film and is consistent with previous observations [1, 2, 4, 7, 8], as illustrated in Table 4.1. Trace (b) represents the reflectance spectrum of supported gold particles that have been chemically modified with ODT. Note that trace (b) has been plotted on a more sensitive scale compared to trace (a), thus, background noise becomes more pronounced. All of the characteristic symmetric and asymmetric methyl and methylene stretches are easily discerned for both modified gold particle and bulk gold film spectra (Table 4.1). This is an interesting result in itself as all of the electric field enhancement experienced by the ODT molecules is due to the small gold particles, and not the GC substrate. From these spectra it is possible to extract some detail about monolayer structure.

Table 4.1: Band positions and peak widths for the spectra shown in Figure 4.2. ODT on bulk gold film, modified gold particles, and literature values, from ref [2].

IR Band Assignment	Gold Film	Gold Particles on GC	Gold Film Lit. Values [2]
$\nu_a(\text{CH}_3, \text{FR})$	2964 cm^{-1}	2970 cm^{-1}	2965 cm^{-1}
$\nu_a(\text{CH}_2)$	2918 cm^{-1}	2924 cm^{-1}	2917 cm^{-1}
$\Delta\nu_{1/2}$ for $\nu_a(\text{CH}_2)$	12.0 cm^{-1}	15.2 cm^{-1}	N/A
$\nu_s(\text{CH}_3)$	2877 cm^{-1}	2881 cm^{-1}	2878 cm^{-1}
$\nu_s(\text{CH}_2)$	2850 cm^{-1}	2852 cm^{-1}	2850 cm^{-1}

As observed in Table 4.1, comparison of the asymmetric methylene stretch for the bulk gold sample to that for supported gold particles reveals a shift to higher energy for ODT on gold particles by approximately 6 cm^{-1} . Previous infrared studies have shown that the location of this peak is a sensitive indicator for lateral interactions between long *n*-alkane and polymethylene chains [2, 7, 17, 18]. This peak is also broadened compared to that obtained on the bulk gold film. Taken together, a shift to higher energy and peak broadening, is indicative of a less ordered, more loosely packed ODT monolayer. Possible explanations for the observed disorder include disruption of the monolayer structure by a large number of surface defects such as step edges and grain boundaries, or surface roughness of the gold particles. Also, the effect of the radius of curvature of the particles on the packing of the alkane chains, particularly toward the chain termini, should be considered. These explanations are explored in more detail below.

Attempts to obtain reflectance spectra from particles deposited from less concentrated solutions, or adsorbates of shorter chain lengths, did not render as well defined spectra. This is most likely a consequence of the low surface area of electrochemically deposited gold. However, it is still possible to discern the

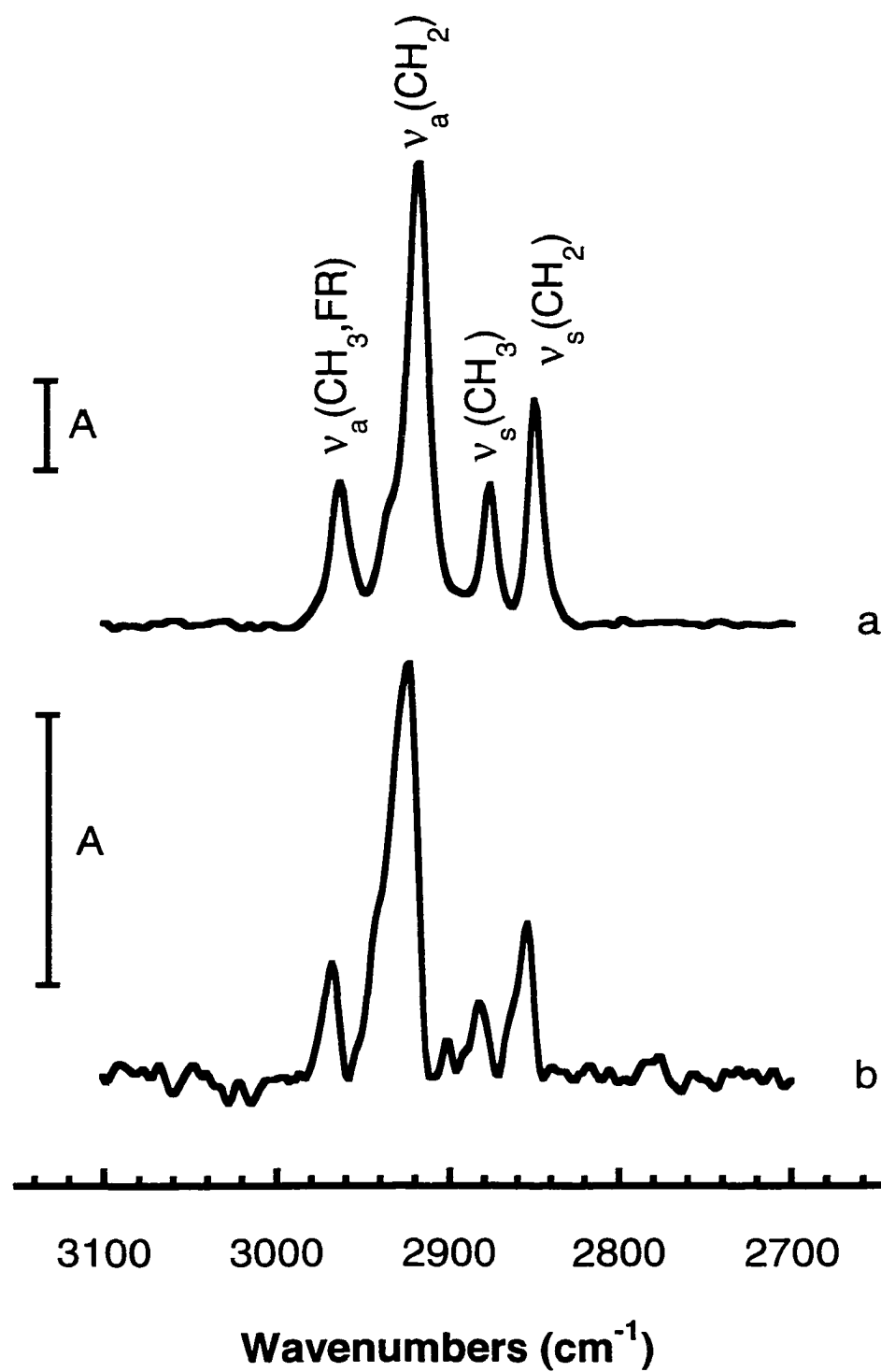


Figure 4.2: Infrared reflectance spectra of ODT on, (a) bulk gold film, (b) electrochemically deposited gold particles, $\eta = -800$ mV, $[\text{AuCl}_4^-] = 1$ mM.

asymmetric methylene stretch (ν_a , CH_2) of ODT for modified gold particles deposited from less concentrated deposition solutions, as low as $100\ \mu\text{M}$. This observation confirms the presence of modified gold particles supported on the GC surface. Further investigations are aimed at electrochemical characterization of the modified gold particles.

Oxide Blocking. Gold particles were deposited from a $100\ \mu\text{M}$ AuCl_4^- solution onto polished GC electrodes by potential step. The gold particles were then modified using self assembled monolayers of alkanethiols of varying chain length, hexanethiol (HT), dodecanethiol (DDT), and octadecanethiol (ODT). Particle modification was then evaluated based on the ability of these monolayers to block surface oxidation of the gold particles. In Chapter II surface oxidation was used to probe the surface area of the gold deposits obtained. In these investigations the objective was to probe gold particle modification, and the stability of the resulting monolayers by examining their ability to block oxidation of the gold surface.

Figure 4.3 contains linear sweep voltammograms for gold oxide reduction on gold particles modified with alkanethiols of varying chain length: HT, DDT, and ODT. The reduction of a gold oxide film appears as a sharp wave at $\sim 935\ \text{mV}$ on unmodified gold particles, as observed for trace (a) of Figure 4.3. This result also confirms the presence of gold particles on the GC surface. Integrating the area under the oxide wave gives the charge associated with reduction of the oxide film. From this value and using $489\ \mu\text{C}/\text{cm}^2$ for the reduction of a monolayer of chemisorbed divalent oxygen from a gold surface [37-39] an area of $\sim 0.025\ \text{cm}^2$ was determined for the gold deposit. This constitutes approximately 8 percent of the macroscopic electrode area as determined by chronoamperometry. The area of the gold deposit obtained in each deposition step is reproducible and did not vary by more than 5 percent between successive experiments.

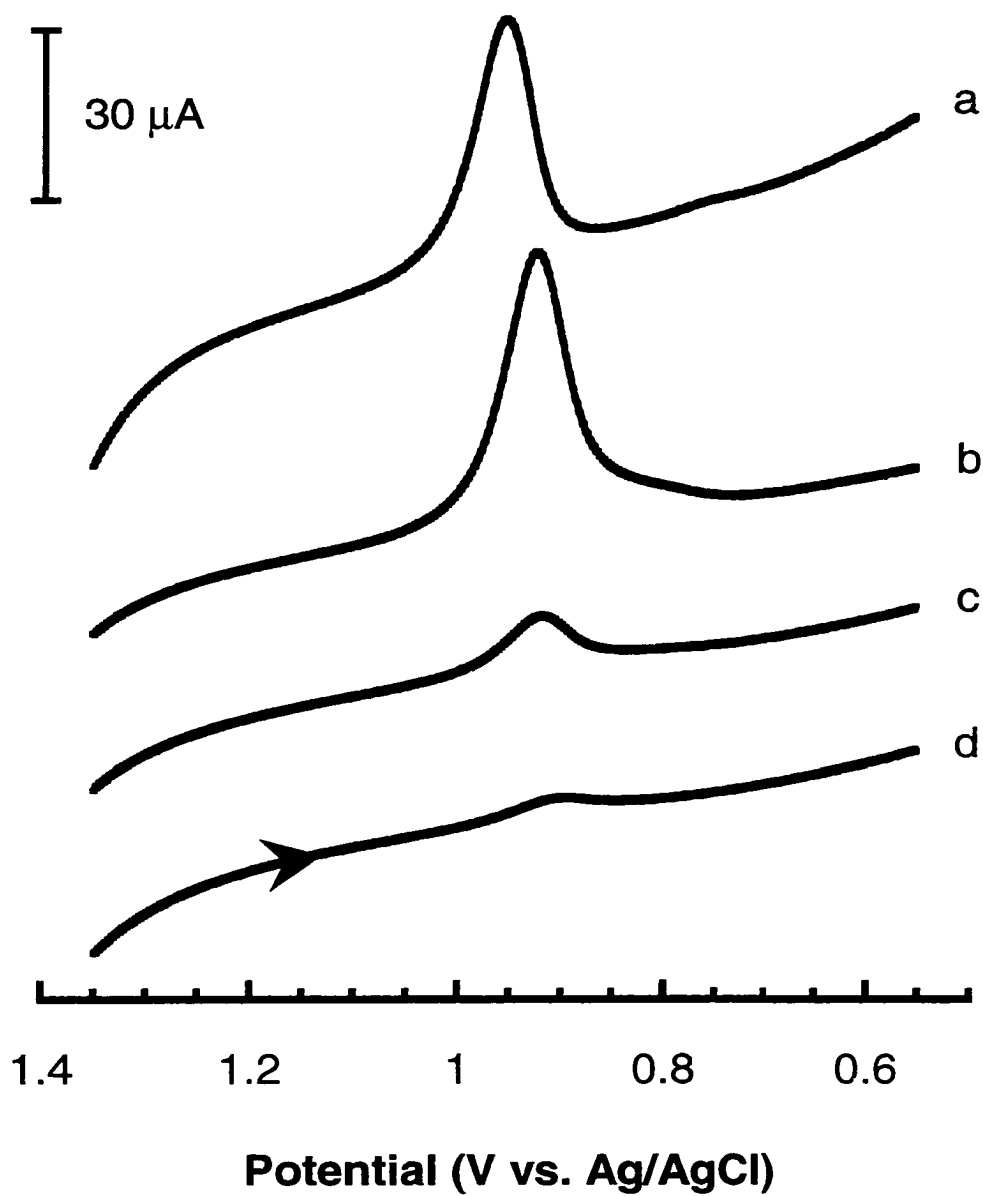


Figure 4.3: Linear sweep voltammograms for the reduction of gold surface oxides from chemically modified gold particles in 0.5 M H_2SO_4 , $\eta = -800$ mV, $[\text{AuCl}_4^-] = 100$ μM , $v = 200$ mV/s: (a) unmodified particles, (b) HT, (c) DDT, (d) ODT.

Traces (b), (c), and (d) of Figure 4.3 represent the blocking of surface oxidation of gold particles modified with HT, DDT, and ODT respectively. The first linear sweep for each experiment is displayed in the figure. For ODT modified particles, trace (d), virtually no oxide reduction wave is observed on the first potential sweep. As observed in Figure 4.3, the longer ODT chain most effectively blocked surface oxidation. As the alkanethiol chain length is decreased, the surface of the particles becomes more susceptible to surface oxidation. This is evident in Figure 4.3 for traces (b) and (c) by the increasing magnitude of the oxide reduction waves for particles modified with the shorter chain lengths. As expected, the observed trend reveals that longer alkane chains are more effective at blocking particle surface oxidation than shorter ones. It is also noted that the oxide stripping waves for modified particles are shifted to more negative potentials by ~ 20 mV; this behavior was also observed by Malem and Mandler in their investigations of carboxylic acid terminated monolayers [40]. Upon repeated potential cycling, the ability of the monolayers to block surface oxidation is quickly disrupted. For ODT modified particles, significant oxide reduction current is observed after only three potential cycles. As expected, the magnitude of the oxide reduction wave increases more rapidly for particles modified with shorter chain lengths, as they are not as effective at blocking surface oxidation.

We attribute the decreasing blocking ability of the monolayers on gold particles to disruption and damage of the monolayer structure upon surface oxidation. Chidsey and coworkers observed similar degradation in the study of oxide blocking on bulk gold films [8]. Shorter chain lengths also experienced quicker, more pronounced degradation. Oxidation may result in the increased exposure of gold particle surface area via turn over and place exchange processes that are thought to occur upon gold surface oxidation [37, 41]. Oxidative desorption of thiol molecules should also be considered [42]. Similarly, one must

also be aware of the consequences of reducing potentials on these monolayer assemblies as the reductive desorption of thiol molecules from gold electrodes has also been well documented [42-44]. However, we believe that the first potential cycle serves as a good indicator for structural integrity of the monolayer, and can be useful in revealing subtle differences in monolayer structure that arise as a consequence of alkyl chain length.

The ability of self-assembled monolayers to block surface oxidation of gold particles was compared to their blocking ability on a two-dimensional polycrystalline gold film electrode. As illustrated in Figure 4.4, ODT and DDT monolayers, traces (c) and (b) respectively, are able to completely block surface oxidation of a polycrystalline gold film electrode. These monolayers are also very stable toward continuous potential cycling. For example, the third potential sweep for each electrode is shown in Figure 4.4 and further potential sweeps had little effect on the observed current. The small currents observed are attributed to small defects in the monolayer structure. For the HT monolayer however, trace (a), effective blocking was not observed and the surface of the electrode was readily oxidized. This result is not unexpected due to the poor packing and disordered or liquid-like nature of short chain monolayers, even for long assembly times. The results presented in Figure 4.4 are consistent with previous studies [3].

Insights into the structure of monolayers adsorbed on GC supported gold particles can be gained by comparing Figures 4.3 and 4.4. From these figures it is apparent that shorter chain length monolayers (HT) are not effective at blocking gold oxidation. Also, the blocking ability of long chains (ODT) is roughly equivalent on both substrates; however, a significant difference is observed between DDT monolayers on polycrystalline gold films and those on supported gold particles. Previous SEM studies reveal that bulk gold thin films that have been prepared by thermal evaporation possess rolling hill-like variations with relatively smooth topography [4, 45]. Based on models and analyses it is

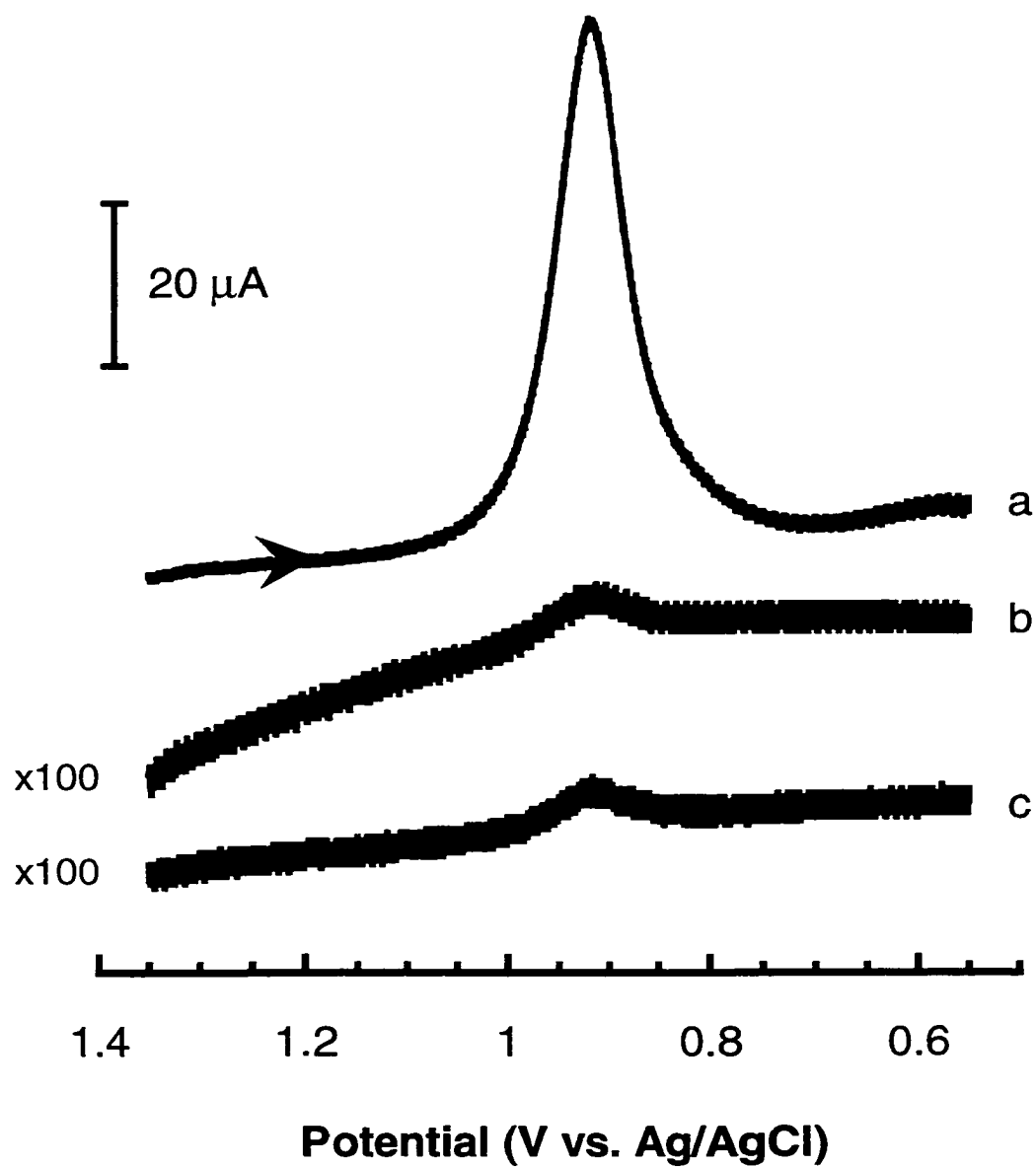


Figure 4.4: Linear sweep voltammograms for the reduction of gold surface oxides from chemically modified bulk gold films, $v = 200 \text{ mV/s}$: (a) HT, (b) DDT, (c) ODT. Third linear sweep in $0.5 \text{ M H}_2\text{SO}_4$.

estimated that at least 80 to 90 percent of these samples exhibit the preferred Au(111) or flat terrace orientation [4]. Sputtered gold films used in this study exhibit similar properties based on SPM and UPD lead analysis. These observations are consistent with a surface that has a low density of surface defects. Therefore stable, resistant monolayers are readily formed on the bulk gold films and, as expected, no difference is observed between DDT and ODT samples.

The reduced ability of DDT to block the oxidation of gold particles likely stems from a disordered monolayer structure. Two properties of electrochemically deposited gold particles on GC may result in monolayers with a higher density of defects than monolayers on planar substrates. First, the radius of curvature of the gold particles may cause a decrease in packing density towards the outer regions of the monolayer. This result has been confirmed by NMR studies [22, 26, 30, 32]. This will introduce some disorder into the monolayer, primarily in the form of gauche kinks at the terminus of the alkane chains. This may also be a contributing factor to the disordered monolayer structure inferred from the infrared spectra of ODT monolayers on gold particles and their inability to block gold particle surface oxidation. "Fanning out" of the alkane chains inhibits their ability to adopt a more crystalline orientation and renders the monolayer more permeable to electrolyte solution, and therefore gold surface oxidation. It is expected that fanning out of the alkane chains becomes a more pronounced problem for smaller gold particles, less than 5 nm in diameter, and longer alkane chains. However, given the size of electrochemically deposited gold particles, monolayer samples are thought to be more consistent with a two dimensional, i.e. planar system [23, 32]. Thus, the radius of curvature of the gold particles is not expected to be a major contributor to the disordered monolayer structures observed in this study.

Another factor that may be responsible for monolayer disorder is the polycrystalline morphology, geometry, or topography of electrochemically deposited gold particles, hereupon generically referred to as surface defects.

Creager and coworkers have demonstrated that the density of defects in monolayer structure is highly dependent on the morphology and degree of surface roughness of the underlying substrate [45]. Macroscopic roughness, even when quite prominent, appears to be less important. Harrison and coworkers have been able to form highly impermeable hexadecanethiol (HDT) monolayers on the surfaces of static mercury drop electrodes [19]. In these studies the capacitance of a HDT modified mercury drop electrode remains constant across a wide range of ionic strength. This result is indicative of an impermeable, pinhole free monolayer that protects the mercury surface. Since mercury is a liquid it is capable of forming homogeneous, defect free surfaces. The high quality of these monolayers is attributed to the essentially defect free mercury surface.

In Chapter II it was demonstrated that supported gold particles possess significant polycrystalline architecture. UPD and stripping of lead experiments reveal that a significant portion of the gold particle surface exists in the Au(110)/(100) orientation. The Au(110) face itself is a stepped surface [46], and these results may account for a gold substrate that possesses particularly complex polycrystalline geometry, and hence, a high density of surface defects. Creager and coworkers used similar methods to evaluate the surface structure of the gold substrates used in their experiments [45]. The method of preparation and general shape and size of the gold particles themselves is conducive to an architecture that displays a particularly high density of surface defects. A high density of surface defects will surely disrupt monolayer packing and orientation, leading to a more disordered monolayer structure. This result is indeed observed in the infrared spectrum for ODT modified particles, Figure 4.2. It has also been observed for silver and copper substrates that monolayers appear to adopt a more disordered structure on substrates that have been exposed to air prior to derivatization [10]. This observation is partially attributed to roughening of the surface due to oxidation.

In summary, the decreased blocking ability of monolayers on gold particles is attributed to the high density of surface defects of electrochemically deposited gold particles, and, to a lesser extent, the radius of curvature of these particles. It has been proposed that surface defects can be partially protected by collapse of the monolayer structure about these features [3, 15]. Octadecanethiol monolayers are more effective at blocking surface oxidation than DDT and HT due to their longer chain length, making them more effective and efficient at collapsing about surface defects. HT however, is not able to block surface oxidation due to its short chain length and disordered or liquid-like monolayer structure.

Catechol Blocking. Results of oxide blocking experiments presented above examine the ability of the monolayers to block the voltammetry of a surface-bound redox process. For completeness, the electrochemical blocking of a solution bound redox system was also studied. Since both gold and GC are active electrode materials, the choice of redox probe is crucial. Ideally, a redox probe that exhibits fast electron transfer at gold and slow electron transfer at GC is desired. Unfortunately, this prerequisite greatly limited the number of redox probes available for this study. A system that we found applicable for this investigation is the catechol redox system. However, it was necessary to modify the polishing procedure to obtain the desired behavior. As observed in Figure 4.5, trace (a), catechol displays quasi-reversible electron transfer kinetics on polycrystalline gold electrodes with ΔE_p values in the range of 38 to 42 mV at a scan rate of 200 mV/s. However, catechol also displays quasi-reversible electron transfer on GC, as observed in trace (b), due to catalysis by surface bound oxide groups [47]. This behavior can be circumvented by polishing the electrode in cyclohexane. Polishing GC using cyclohexane/alumina slurries produces an electrode surface that is relatively free of surface oxide groups [48]. As discussed in Chapter III, such treatment has been shown to produce GC surfaces with an oxygen/carbon (O/C) ratio similar to that obtained for vacuum heat treated GC

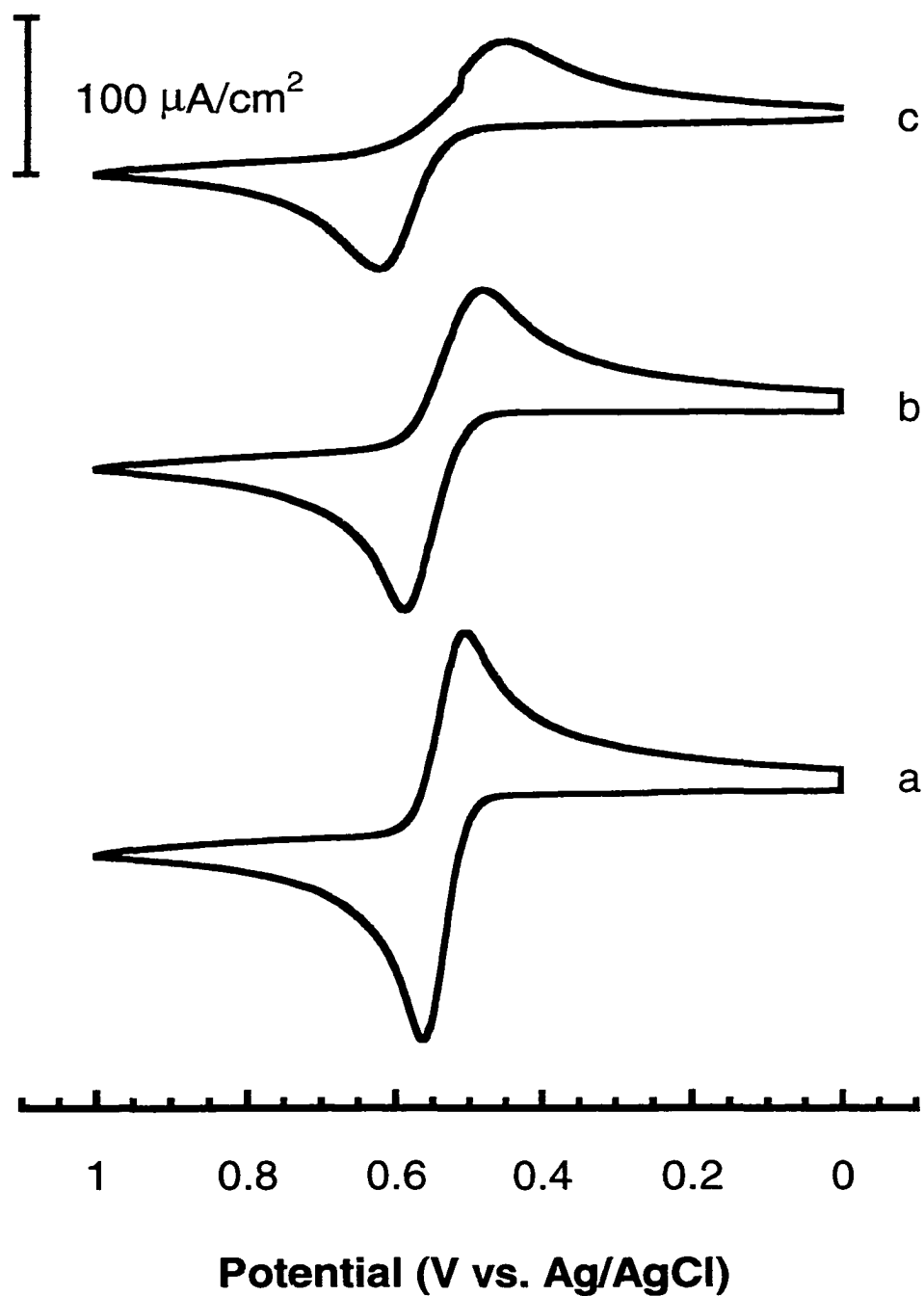


Figure 4.5: Cyclic voltammograms for 1 mM catechol in 0.5 M H_2SO_4 on various electrode materials, $\nu = 200 \text{ mV/s}$: (a) polycrystalline gold, (b) GC, (c) oxide free GC.

[48]. As observed in trace (c) of Figure 4.5, cyclic voltammetry of catechol on GC electrodes polished in cyclohexane renders slow electron transfer kinetics. Typical ΔE_p values in the range of 180 to 200 mV for successive experiments are observed. The difference in electron transfer between these two electrode materials, gold and oxide free GC, provides a sufficient difference in electron transfer behavior to be able to study the effects of monolayer blocking on catechol voltammetry; these results are summarized in Table 4.2.

Table 4.2: ΔE_p values for catechol voltammetry on various electrode materials.

Electrode Material	ΔE_p (mV)
Oxide free GC	184
GC	95
Gold	40

Figure 4.6 displays cyclic voltammograms for catechol blocking at modified gold particles. The particles have been modified with HT, DDT, and ODT, traces (a), (b), and (c) respectively. Modification of the gold particles with alkanethiolate monolayers causes the voltammetry to revert back to that observed on oxide free GC, and ΔE_p values in the range of 180 to 220 mV are observed. This is an interesting result in that while oxide blocking was observed to decrease with decreasing alkane chain length, all chain lengths are able to block catechol voltammetry with equal effectiveness. One possible explanation is that the catechol molecule may be sterically hindered from approaching defects in the monolayer structure by the alkyl chains, and thus is prevented from undergoing efficient electron transfer. Modification of the gold particles may serve to inhibit this proton transfer step. Control experiments show that HT, DDT, and ODT all

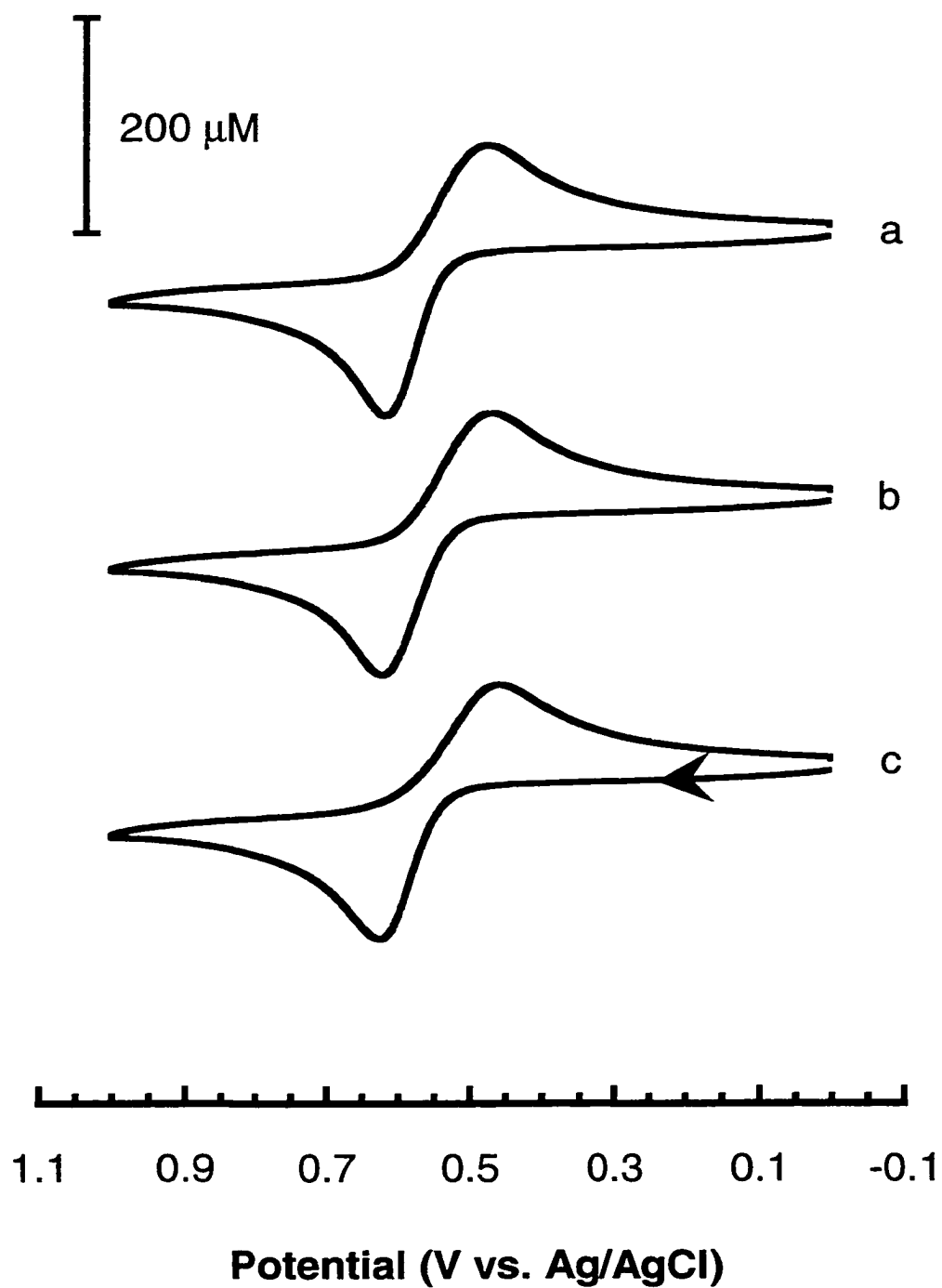


Figure 4.6: Cyclic voltammograms for 1 mM catechol in 0.5 M H_2SO_4 on chemically modified gold particles, $\eta = -800$ mV, $[\text{AuCl}_4^-] = 100$ μM , $\nu = 200$ mV/s: (a) HT, (b) DDT, (c) ODT.

completely block catechol on polycrystalline gold. This result confirms that the observed voltammetry for the modified particles is due to catechol voltammetry at the carbon surface. Given this observation, it may be possible to employ the catechol redox system to study the effects of multiple deposition and modification steps as described below.

A single wave is usually observed for catechol voltammetry upon gold particle deposition on oxide free GC electrodes. In some cases, quasi-reversible waves from catechol voltammetry at the gold particles are superimposed on the irreversible waves of catechol voltammetry at oxide free GC. Figure 4.7 illustrates two such scenarios. Trace (a) represents catechol voltammetry on gold particles that have been prepared from a 500 μM AuCl_4^- deposition solution; similarly, trace (b) represents particles that have been prepared from a 100 μM AuCl_4^- deposition solution. Note that the quasi-reversible waves obtained in trace (a) are of greater magnitude than the reversible waves obtained in trace (b) due to larger surface area of gold obtained from the more concentrated deposition solution. In some instances, we fail to observe two sets of waves. Supported gold particles may be considered as an array of gold microelectrodes. However, when the distance between the gold particles is sufficiently small, and scan rates are relatively slow, as those employed in these studies, then hemispherical diffusion zones are quick to overlap and macroelectrode behavior is observed

Multiple Deposition and Modification. The results presented thus far demonstrate our ability to successfully modify supported gold particles by taking advantage of the strength and stability of thiol adsorption to gold particles. From these experiments we wish to extend our capabilities to be able to perform multiple deposition and modification steps on a single GC substrate. It has been demonstrated that modification of an electrode surface with gold colloids alone is sufficient to improve electron transfer kinetics and selectivity [49, 50]. As seen in

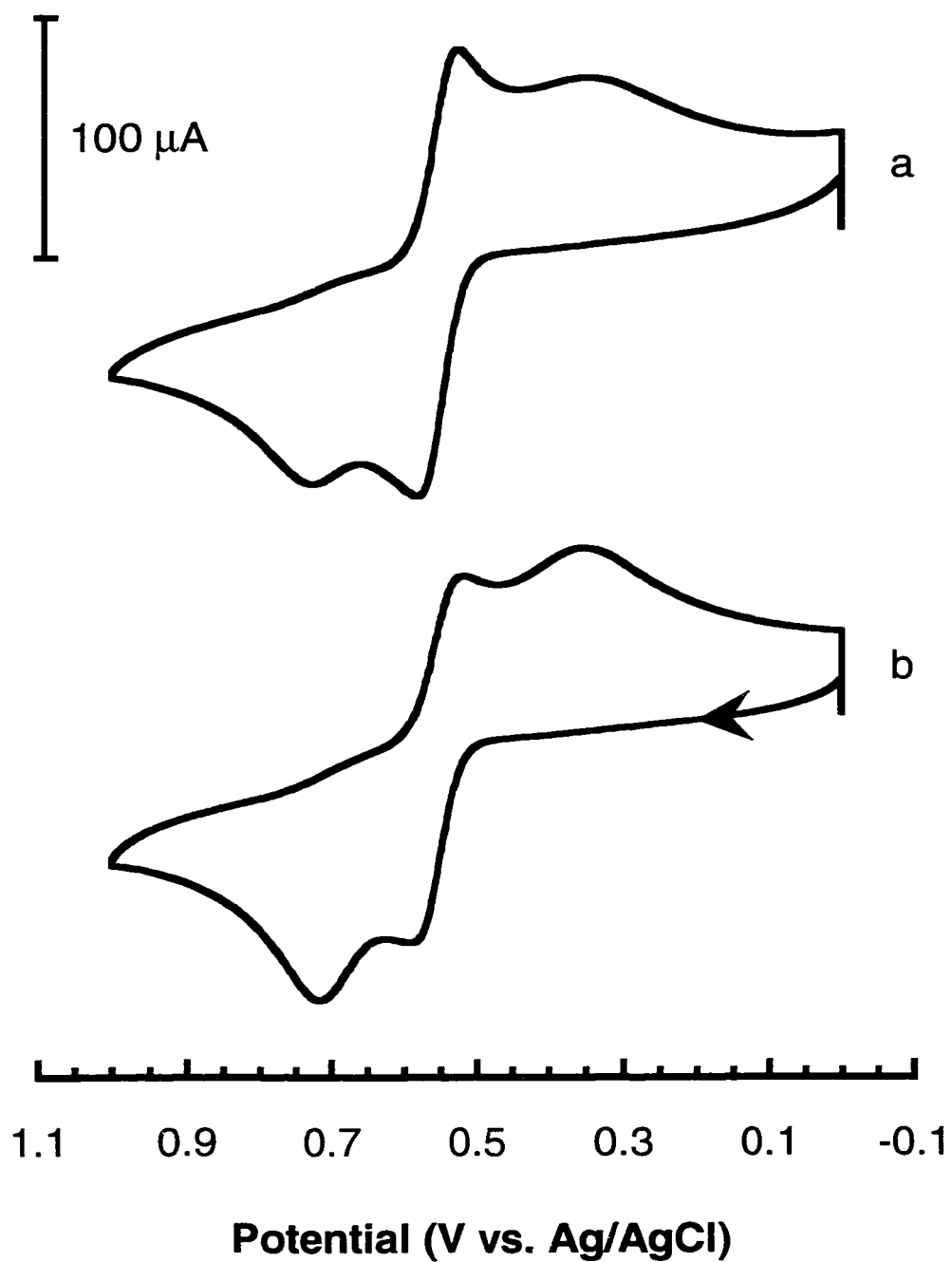


Figure 4.7: Cyclic voltammograms for 1 mM catechol in 0.5 M H_2SO_4 on electrochemically deposited gold particles on GC, $\eta = -800$ mV, $\nu = 200$ mV/s: (a) 500 μM , (b) 100 μM , AuCl_4^- .

Figure 4.7 the electron transfer behavior of catechol readily improves upon deposition of gold particles onto cyclohexane polished GC, rendering ΔE_p values in the range of 45 to 55 mV. Thus, deposition of gold particles alone is sufficient to activate oxide free GC toward catechol voltammetry.

Our first objective was to study the stability of the modified particles toward further gold deposition steps. Electrodes were prepared by polishing in cyclohexane, followed by deposition of gold particles and modification with ODT; catechol voltammetry was monitored after each step. Modified particles were then exposed to multiple blank deposition steps in order to test monolayer stability on the modified particles. Blank potential step experiments in 0.5 M H_2SO_4 had no effect on catechol electron transfer. This result confirms that the modified particles are stable toward further potential step programs employed in further gold particle deposition steps. Further experiments were designed to study the feasibility of multiple deposition and modification steps.

Table 4.3: ΔE_p values for catechol voltammetry on a single electrode, resulting from multiple gold particle deposition and modification steps.

Electrode Modification	ΔE_p , (mV)
Oxide free GC	184
1 st gold deposition	47
Modification, ODT	174
2 nd gold deposition	53
Modification, ODT	188
3 rd gold deposition	52

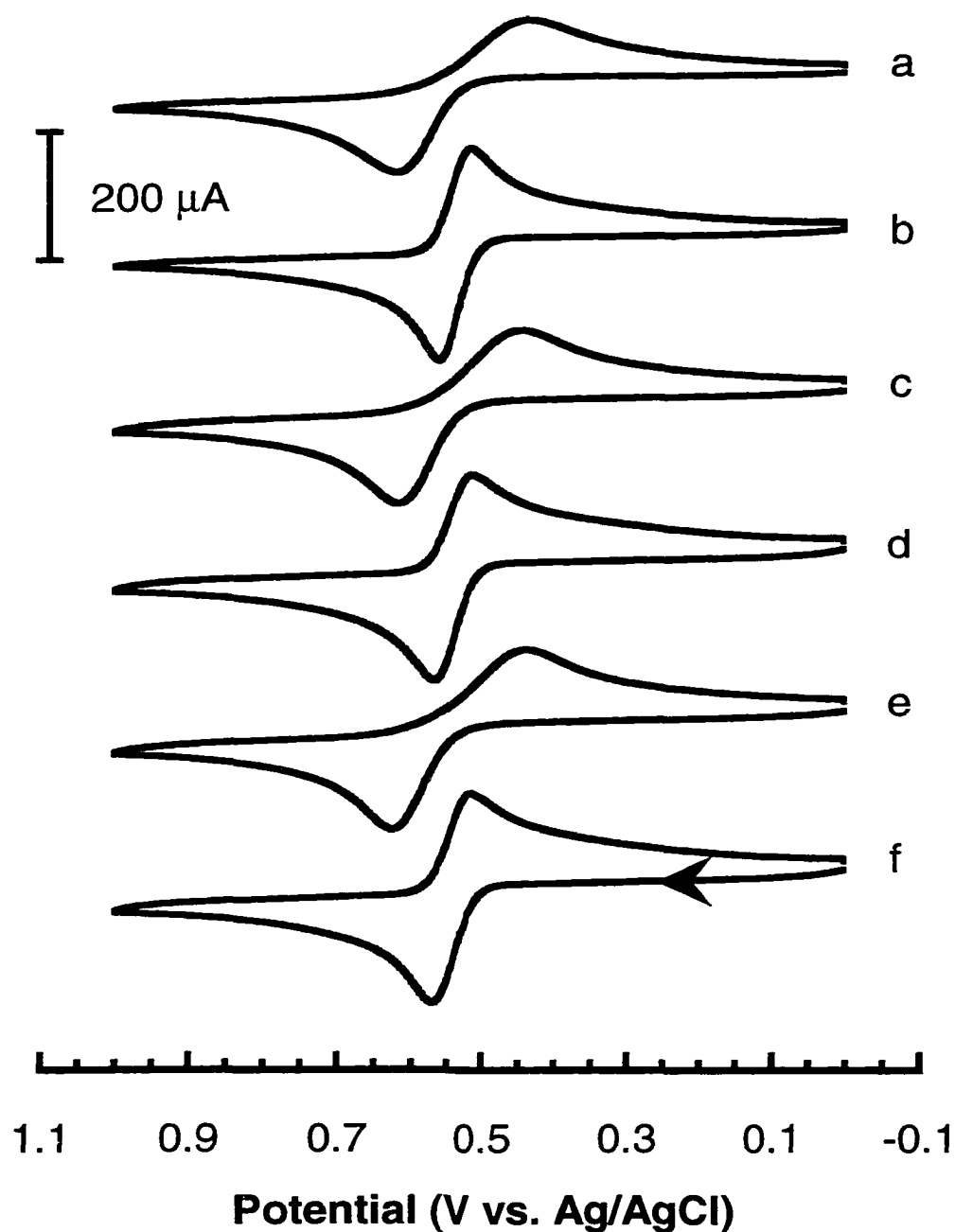


Figure 4.8: Cyclic voltammograms for 1 mM catechol (0.5 M H_2SO_4) on chemically modified gold particles, multiple deposition and modification steps, $\eta = -800$ mV, $[\text{AuCl}_4^-] = 100$ μM , $\nu = 200$ mV/s: (a) oxide free GC, (b) first deposition, (c) first modification, (d) second deposition, (e) second modification, (f) third deposition.

A series of gold particle deposition and modification steps were performed, again using catechol voltammetry as a diagnostic. Gold particles were modified with ODT. Figure 4.8 illustrates the results obtained from these experiments on a single GC electrode and the results are summarized in Table 4.3. As illustrated in Figure 4.8, voltammograms are for (a) oxide free GC, (b) first particle deposition step, (c) particles modified with ODT for 30 min, (d) second particle deposition step, (e) second particles modified with ODT for 30, and (f) third particle deposition step. Three successive deposition and modification steps were performed on a single GC electrode. Each successive gold deposition step was able to activate the GC electrode toward catechol voltammetry. Note that only one set of redox waves is observed after each gold deposition step, unlike Figure 4.7. Each time the gold particles were modified with ODT the voltammetry reverted back to that observed on oxide free GC, indicative of blocking of the gold particles, Table 4.3. This sequence of experiments resulted in cyclic voltammograms that oscillate between quasi-reversible and irreversible catechol electron transfer kinetics. This result demonstrates that it may be possible to employ multiple deposition and modification steps to introduce different functional groups onto GC substrates using a series of deposition and modification steps.

A major disadvantage of this system is that it is not possible to discern whether further gold deposition occurs on the existing modified particles or whether new gold particles are able to nucleate and grow on the GC substrate. Since ODT modified particles are able to block surface oxidation, gold deposition is not expected on ODT modified particles. Because the redox probe we are employing is in solution, an improvement in catechol voltammetry will be observed irrespective of whether further gold deposition proceeds on the ODT modified particles or GC substrate. Ideally, use of a surface bound redox system that can be attached to the supported gold particles is desired. This should be able

to provide more insight into the nature of further gold deposition steps and to determine whether further gold deposition does indeed occur on the modified particles.

Conclusions

Results presented herein demonstrate our ability to employ electrochemical metal deposition and self-assembly methods for the purpose of obtaining supported gold particles that have been chemically modified with alkanethiolate monolayers. The main focus of this research is to be able to employ this method as a means for introducing functional groups onto the surface of carbon electrodes. Modified particles have been studied using IRRAS and electrochemistry. The results of these studies confirm the presence of modified particles supported on a GC substrate.

Herein, the first IRRAS spectrum obtained for self-assembled monolayers on supported gold particles was presented. This result provides spectroscopic evidence that we are able to modify these gold particles by taking advantage of self-assembly methods. It was also demonstrated that these small gold particles provide sufficient surface area to obtain spectra on a relatively nonreflective background substrate such as GC. Examination of the infrared spectrum reveals that the monolayer adopts a relatively disordered structure compared to similar samples prepared on polycrystalline gold films. This observation is attributed to the high density of surface defects or surface roughness of the gold particles. These surface imperfections inhibit the ability of the long alkyl chains to adopt a well packed crystalline geometry.

Electrochemical investigations were also used to evaluate modified gold particles. A series of oxide blocking experiments reveal that self assembled monolayers on gold particles are not able to inhibit surface oxidation as effectively as those formed on polycrystalline gold films. No difference was observed

between the blocking behavior of DDT and ODT, both completely block surface oxidation and the monolayers are stable toward continuous potential cycling. Similar experiments on gold particles show that initially, ODT monolayers display better resistance to gold surface oxidation than DDT or HT. However, upon continuous potential cycling, the ability of these monolayers to block surface oxidation becomes significantly reduced. This result becomes more pronounced for shorter DDT and HT alkyl chains. These observations are attributed to the limited ability of the shorter alkane chains to collapse about surface defects. However, investigation of the blocking of a solution bound redox species reveals that all of the monolayers are able to block voltammetry with equal effectiveness.

Results of multiple deposition and modification steps are also presented. It was demonstrated that it is possible to sequentially activate and deactivate a GC electrode toward catechol voltammetry. Multiple deposition and modification steps were employed on the same electrode to obtain a series of cyclic voltammograms that oscillate between quasi-reversible and irreversible electron transfer kinetics. The significance of this result is that it demonstrates that it may now be possible to employ different adsorbates in a series of deposition and modification steps in an effort to introduce more than one functional group onto a GC substrate. Ideally, we wish to employ adsorbates that will improve the electroanalytical selectivity of the electrode for multiple analytes in solution. However, such a modification scheme must be carefully planned. Monolayer formation is a dynamic process and adsorbates have a tendency to displace one another when in solution, especially when one ligand adsorbs more strongly than another. Modification procedures must be planned such that the strongest adsorbate is adsorbed first. This will prevent the exchange of adsorbates from previously modified particles in further gold particle modification steps.

To better understand the effects of multiple metal deposition steps, modification with electroactive adsorbates may be more suitable. Catechol

voltammetry is not able to reveal whether further gold deposition is occurring on the modified particles. Modifying particles with adsorbates that possess different electroactive groups, it may be possible to address the particles electrochemically once all of the deposition and modification steps have been performed. Electrodes possessing particles that have been modified using different electroactive adsorbates should give rise to voltammograms that display multiple redox waves. Particle modification using electroactive monolayers is investigated in Chapter V.

References

1. R. G. Nuzzo and D. L. Allara, *J. Am. Chem. Soc.*, **105**, 4481, (1983).
2. M. D. Porter, T. B. Bright, D. L. Allara, and C. E. D. Chidsey, *J. Am. Chem. Soc.*, **109**, 3559, (1987).
3. H. O. Finklea, S. Avery, and M. Lynch, *Langmuir*, **3**, 409, (1987).
4. R. G. Nuzzo, F. A. Fusco, and D. L. Allara, *J. Am. Chem. Soc.*, **109**, 2358, (1987).
5. C. D. Bain and G. M. Whitesides, *J. Am. Chem. Soc.*, **110**, 3665, (1988).
6. C. D. Bain, E. B. Troughton, Y. Tao, J. Evall, G. M. Whitesides, and R. G. Nuzzo, *J. Am. Chem. Soc.*, **111**, 321, (1989).
7. R. G. Nuzzo, L. H. Dubois, and D. L. Allara, *J. Am. Chem. Soc.*, **112**, 558, (1990).
8. C. E. D. Chidsey and D. N. Loiacono, *Langmuir*, **6**, 682, (1990).
9. M. A. Bryant and J. E. Pemberton, *J. Am. Chem. Soc.*, **113**, 8284, (1991).
10. P. E. Laibinis, G. M. Whitesides, D. L. Allara, Y. Tao, A. N. Parikh, and R. G. Nuzzo, *J. Am. Chem. Soc.*, **113**, 7152, (1991).
11. C. A. Widrig, C. A. Alves, and M. D. Porter, *J. Am. Chem. Soc.*, **113**, 2805, (1991).

12. C. A. Alves, E. L. Smith, and M. D. Porter, *J. Am. Chem. Soc.*, **114**, 1222, (1992).
13. J. A. M. Sondag-Huethorst and L. G. J. Fokkink, *Langmuir*, **11**, 2237, (1995).
14. C. Jung, O. Dannenberger, Y. Xu, M. Buck, and M. Grunze, *Langmuir*, **14**, 1103, (1998).
15. P. Diao, D. Jiang, X. Cui, D. Gu, R. Tong, and B. Zhong, *J. Electroanal. Chem.*, **464**, 61, (1999).
16. A. Ulman, *An Introduction to Ultrathin Organic Films: From Langmuir-Blodgett to Self-Assembly.*, Academic Press, Inc., Boston, 1991.
17. R. G. Snyder, H. L. Strauss, and C. A. Elliger, *J. Phys. Chem.*, **86**, 5145, (1982).
18. R. G. Snyder, M. Maroncelli, H. L. Strauss, and V. M. Hallmark, *J. Phys. Chem.*, **90**, 5623, (1986).
19. A. Demoz and D. J. Harrison, *Langmuir*, **9**, 1046, (1993).
20. M. Brust, M. Walker, D. Bethell, D. J. Schiffrin, and R. Whyman, *J. Chem. Soc., Chem. Commun.*, 801, (1994).
21. M. Brust, J. Fink, D. Bethell, D. J. Schiffrin, and C. Kiely, *J. Chem. Soc., Chem. Commun.*, 1655, (1995).
22. R. H. Terrill, T. A. Postlethwaite, C. Chen, C. Poon, A. Terzis, A. Chen, J. E. Hutchison, M. R. Clark, G. Wignall, J. D. Londono, R. Superfine, M. Falvo, C. S. Johnson, E. T. Samulski, and R. W. Murray, *J. Am. Chem. Soc.*, **117**, 12537, (1995).
23. C. S. Weisbecker, M. V. Merritt, and G. M. Whitesides, *Langmuir*, **12**, 3763, (1996).
24. M. J. Hostetler, S. J. Green, J. J. Stokes, and R. W. Murray, *J. Am. Chem. Soc.*, **118**, 4212, (1996).
25. M. J. Hostetler, J. J. Stokes, and R. W. Murray, *Langmuir*, **12**, 3604, (1996).

26. A. Badia, W. Gao, S. Singh, L. Demers, L. Cuccia, and L. Reven, *Langmuir*, **12**, 1262, (1996).
27. K. S. Mayya, V. Patil, and M. Sastry, *Langmuir*, **13**, 3944, (1997).
28. S. R. Johnson, S. D. Evans, S. W. Mahon, and A. Ulman, *Langmuir*, **13**, 51, (1997).
29. S. J. Green, J. J. Stokes, M. J. Hostetler, J. Pietron, and R. W. Murray, *J. Phys. Chem. B*, **101**, 2663, (1997).
30. R. S. Ingram, M. J. Hostetler, and R. W. Murray, *J. Am. Chem. Soc.*, **119**, 9175, (1997).
31. C. J. Kiely, J. Fink, M. Brust, D. Bethell, and D. J. Schiffrin, *Nature*, **396**, 444, (1998).
32. M. J. Hostetler, J. E. Wingate, C. Zhong, J. E. Harris, R. W. Vachet, M. R. Clark, J. D. Londono, S. J. Green, J. J. Stokes, G. D. Wignall, G. L. Glish, M. D. Porter, N. D. Evans, and R. W. Murray, *Langmuir*, **14**, 17, (1998).
33. M. J. Hostetler, C. Zhong, B. K. H. Yen, J. Andereg, S. M. Gross, N. D. Evans, M. D. Porter, and R. W. Murray, *J. Am. Chem. Soc.*, **120**, 9396, (1998).
34. M. E. Garcia, L. A. Baker, and R. M. Crooks, *Anal. Chem.*, **71**, 256, (1999).
35. M. J. Hostetler, A. C. Templeton, and R. W. Murray, *Langmuir*, **15**, 3782, (1999).
36. M. D. Porter, *Anal. Chem.*, **60**, 1143A, (1988).
37. U. Oesch and J. Janata, *Electrochimica Acta*, **28**, 1237, (1983).
38. U. Oesch and J. Janata, *Electrochimica Acta*, **28**, 1247, (1983).
39. M. O. Finot, G. D. Braybrook, and M. T. McDermott, *J. Electroanal. Chem.*, **466**, 234, (1999).
40. F. Malem and D. Mandler, *Anal. Chem.*, **65**, 37, (1993).

41. S. Manne, J. Massie, V. B. Elings, P. K. Hansma, and A. A. Gewirth, *J. Vac. Sci. Technol. B*, **9**, 950, (1991).
42. M. M. Walczak, D. D. Popenoe, R. S. Deinhammer, B. D. Lamp, C. Chung, and M. D. Porter, *Langmuir*, **7**, 2687, (1991).
43. C. A. Widrig, C. Chung, and M. D. Porter, *J. Electroanal. Chem.*, **310**, 335, (1991).
44. C. Zhong, J. Zak, and M. D. Porter, *J. Electroanal. Chem.*, **421**, 9, (1997).
45. S. E. Creager, L. A. Hockett, and G. K. Rowe, *Langmuir*, **8**, 854, (1992).
46. A. Hamelin and J. Lipkowski, *J. Electroanal. Chem.*, **171**, 317, (1984).
47. G. E. Cabaniss, A. A. Diamantis, W. R. Murphy, R. W. Linton, and T. J. Meyer, *J. Am. Chem. Soc.*, **107**, 1845, (1985).
48. P. Chen and R. L. McCreery, *Anal. Chem.*, **68**, 3958, (1996).
49. K. R. Brown, A. P. Fox, and M. J. Natan, *J. Am. Chem. Soc.*, **118**, 1154, (1996).
50. I. G. Casella, A. Destradis, and E. Desimoni, *Analyst*, **121**, 249, (1996).

CHAPTER V

MODIFICATION OF SUPPORTED GOLD PARTICLES USING ω -FUNCTIONALIZED ALKANETHIOL SELF ASSEMBLED MONOLAYERS

Introduction

The results presented in Chapter IV demonstrated that it is possible to modify electrochemically deposited gold particles employing self-assembly methods. In these initial studies gold particles were modified using *n*-alkanethiol adsorbates of varying chain length. Work presented in this chapter concentrates specifically on the attachment of a variety of functional groups directly to electrochemically deposited gold particles. The feasibility of multiple deposition and modification steps is also revisited using electroactive adsorbates. Furthermore, the possibility of performing chemical reactions, such as esterification and amidization, with modified particles is explored. Modified gold particles were evaluated using electrochemical and IRRAS methods.

Electroactive self-assembled monolayer systems have recently emerged in a number of electrochemical studies [1-10]. These studies have focused mainly on the investigation of electron transfer through a barrier provided by the monolayer structure of hydrocarbon chains. Determinations of rate constants, tunneling parameters, and reorganization energies have been presented for several diverse systems. Analyses of the data are presented in terms of Butler-Volmer kinetics and Marcus theory to account for reorganization energy in an attempt to relate the observed rate constants to the applied overpotential. Self-assembled monolayer systems have also been used to systematically probe the dependence of electron

transfer rates on distance of the redox center from the electrode surface, and nature of the surrounding medium [1, 3, 10]. It was observed that by diluting the ferrocene terminated adsorbates with *n*-alkanethiols of similar chain length, voltammograms displayed nearly ideal electron transfer behavior. The voltammograms of non-diluted ferrocene monolayers tended to be extremely broadened and not well defined. This behavior is attributed to repulsive interactions between closely packed ferrocenium groups. It was also demonstrated that ferrocene coverage decreases with increasing length of the diluent thiol. This behavior is attributed to the longer adsorbates greater affinity for adsorption and self-assembly due to higher free energy and lower solubility in ethanol.

Electroactive adsorbates have also been used in the modification of gold colloids such that the resulting colloids are rendered electroactive [11-13]. In these preparations, gold colloids are first prepared as monolayer protected clusters (MPCs) of *n*-alkanethiols using the method of Brust and coworkers [14]. Adsorbates containing a ω -terminated functional group are then substituted onto the MPCs by the use of place-exchange reactions [11-13, 15]. Using this method MPCs are exposed to a solution of a ω -terminated alkanethiol that will place-exchange with alkanethiolates already present on the surface of gold colloids. The concentration of the ω -terminated alkanethiol solution can be varied to obtain different "feed ratios". Higher feed ratios give rise to more efficient place-exchange and thus a greater density of functional groups is realized on the colloid surface. This method has been used in the preparation of bromo, nitrile, vinyl, and ferrocene modified gold colloids. These are also referred to as poly-homo- ω -functionalized MPCs [11, 12]. This method has also been used in the preparation of poly-hetero- ω -functionalized MPCs, i.e. clusters that possess multiple functional groups substituted onto their surface [13]. Two approaches have been investigated in the preparation of such MPCs: a simultaneous approach, in which the MPCs are exposed to a mixture of thiols, and a stepwise approach, in which

individual thiols are exchanged onto MPCs employing a series of individual steps. Different degrees of substitution or ratios of functional groups exchanged onto the MPC surface are observed depending on the approach used. The stepwise approach reveals that short bulky adsorbates are more easily displaced than long linear ones. A more comprehensive investigation of the dynamics and mechanism of place-exchange reactions on MPCs has been reported [15].

Colloids modified with ferrocene and anthraquinone redox groups display interesting electroactive behavior [11-13]. Rotating disk voltammograms for these colloids exhibit ferrocene redox waves that are consistent with a system that is under hydrodynamic mass transport control. Clusters that each contain 9 ferrocene groups (on average) display a rotating disk voltammogram wave shape that is consistent with an $n = 1$ reaction [11]. This observation suggests that the ferrocene sites are not electronically coupled, and react more or less independently of each other. It has also been shown that it is possible to calculate diffusion coefficients and hydrodynamic radii for the modified colloids from the limiting current of the rotating disk voltammograms. These voltammograms display sloped regions at potentials that both precede and follow the ferrocene redox wave. The slopes of these regions are proportional to the square root of the electrode rotation rate and thus are also under hydrodynamic control. The sloped regions have been attributed to charging of the electrical double layers of the modified gold colloids. Thus, the authors refer to these colloids as “molecule-sized nanoelectrodes” [11].

Porter was one of the first to take advantage of self-assembled monolayer systems and apply them to specific interfaces designed to improve electroanalytical selectivity [16]. The main advantage of the gold-sulfur system is that an analogous system for the self-assembly of molecules onto a carbon surface does not exist. The long term objective of our work is to exploit and combine electrochemical metal deposition with self assembled monolayer systems in an

attempt to develop a new method of preparing chemically modified electrodes. Ideally, we are interested in producing sites for attaching functional groups to GC, which exhibit analytical selectivity and are located adjacent to electron transfer sites, as illustrated in Figure 1.2.

As previously alluded to in Chapter I, several attempts have been made to control the chemistry of carbon electrodes via attachment of specific functional groups or adsorbates to the carbon surface. These methods include covalent attachment, reduction of diazonium salts, and derivatization of existing functional groups. ECP is often used in conjunction with derivatization in an effort to augment the density of surface functional groups available for derivatization. Kuwana and coworkers have demonstrated that *o*-quinoidal structures, such as catechols, could be attached to GC electrodes via the amidization of dopamine and 3,4-dihydroxybenzylamine with carboxylic acid groups on the GC surface [17, 18]. These groups appear to be rather specific electron transfer mediators for the electrochemical oxidation of NADH. Koval and Anson have also presented a procedure for attaching electroactive pyridine-pentaamineruthenium complexes to graphite electrodes via amidization of surface carboxylic acid groups [19]. Yacynych and Kuwana have used cyanuric chloride as a general linking agent for the attachment of electroactive hydroxy-methylferrocene groups to PG electrodes [20, 21]. Cyanuric chloride attaches to hydroxyl groups on the surface of PG electrodes. These groups are maximized by radiofrequency oxygen plasma treatment followed by reduction with lithium hydride. Hydroxy-methylferrocene is then attached to the electrode surface via an ether linkage.

Derivatization of existing functional groups is not the only method available for the attachment of electroactive groups to carbon electrodes. Recently, Saveant and coworkers have demonstrated that it is possible to attach electroactive 4-nitrophenyl groups to the surface of carbon electrodes by electrochemical reduction of a solution of the corresponding diazonium salt [22,

23]. Belanger and coworkers have also studied the behavior of these 4-nitrophenyl groups attached to GC electrodes using this method [24, 25].

Bourdillon and coworkers have exploited both the methods of covalent attachment and reduction of diazonium salts in an effort to attach biologically important molecules to the electrode surface [26, 27]. ECP of the GC surface, or electrochemical reduction of a solution of 4-phenylacetic acid diazonium fluoroborate can be used to augment the density of carboxylic acid groups on the electrode surface. Glucose oxidase was then immobilized on the surface of these electrodes by amidation using a suitable carbodiimide coupling agent to activate the surface carboxylic acid groups. Similar methods have been used to attach biomolecules to the surface of gold electrodes that have been modified with a monolayer of carboxylic acid terminated adsorbates. Duan and Meyerhoff have used self-assembled monolayers of thioctic acid on the surface of a gold-coated microporous nylon membrane in the development of a separation-free, electrochemical sandwich, enzyme immunoassay [28]. Capture antibodies toward model protein analytes were immobilized on a gold-coated membrane via amidization using EDC as the coupling agent. More recent studies have examined the stepwise self-assembly of multiple layers of thionine and horseradish peroxidase in the development of a hydrogen peroxide biosensor [29]. Modified electrodes used in the quantification of superoxide dismutase (SOD) activity have also been prepared by immobilization of cytochrome c onto carboxylic acid terminated monolayers using similar amidization methods [30].

Our efforts are concentrated on the electrochemical deposition of small gold particles on polished GC substrates. Gold particles are then used as foundations for specific functional group attachment via the self-assembly of thiol molecules. The main advantage of this technique is that it may be possible to employ multiple deposition and modification steps to prepare an electrode that displays improved selectivity for multiple analytes via the attachment of multiple

functional groups. The work presented herein demonstrates that it is possible to attach a number of different functional groups to GC employing this method. We have also demonstrated that it is possible to employ a sequence of deposition and modification steps in the preparation of a chemically modified electrode that possesses more than one electroactive group. It is also possible to subject modified particles to further chemical reactions, such as esterification and amidization, in view of attaching biomolecules to the supported gold particles. These results are significant accomplishments toward achieving our main objective of demonstrating a novel approach toward the preparation of chemically modified electrodes.

Experimental

Chemicals. Potassium tetrachloroaurate, (Aldrich) 4-nitrothiophenol, NTP, (Aldrich), potassium chloride (Anachemia), potassium phosphate di-basic (Caledon), sodium hydroxide (Fisher), sodium dodecylsulfate, SDS (Serva), ethanol (punctilious grade, Millennium Petrochemicals), dimethylformamide, DMF (Caledon), benzene (Fisher), sulfuric acid, (Fisher), perchloric acid, (Caledon) 1-ethyl-3-[(dimethylamino)propyl] carbodiimide, EDC, (Aldrich), cytochrome c (Horse Heart, type IV, Aldrich), and bovine IgG, lyophilized, (ICN) were all used as received. Octadecanethiol, ODT, (Aldrich) was recrystallized three times from ethanol. 11-mercaptoundecanoic acid, MUDA, 11-(ferrocenecarboxy) undecanethiol, FCUT and octadecanethiol- d_{37} were gifts from Marc Porter (Iowa State University).

Electrode Preparation. GC electrodes (Tokai GC-20, Electrosynthesis Company, NY) consisted of 12 mm x 12 mm x 3 mm plates. For infrared measurements, 3 cm x 6 cm x 1 mm GC plates were employed. The backside of these plates was coated with a thick film of poly(ethylene)/poly(vinylacetate)

60:40 (Aldrich) copolymer to block electrochemical activity. Electrode surfaces were prepared by polishing on a glass plate or Micropolish cloth (Buehler) in alumina/water slurries as described in Chapter II. Gold film electrodes consisted of glass slides sputter coated with 500 nm of gold, primed with 30 nm of titanium for adhesion. Supported gold particles were prepared by potential step deposition from solutions of AuCl_4^- in 0.5 M sulfuric acid, as described in Chapter II. Monolayer samples were prepared by immersion of the electrodes into millimolar solutions of the desired thiol in ethanol for a set period of time.

Electrochemical Measurements. Electrochemical experiments were carried out using a Pine Model AFCBP1 bipotentiostat with a coiled platinum wire auxiliary electrode and Ag/AgCl (sat'd KCl) reference electrode. The auxiliary electrode was separated from the bulk solution using a glass frit. All potentials in the text are referred to the Ag/AgCl reference electrode unless stated otherwise. All electrochemical experiments were performed in an inverted three-electrode cell. GC electrodes were mounted into the cell between a viton o-ring and a metal plate and held in place by the use of a metal clip. The geometrical electrode area is defined by the circumference of the o-ring and forms the bottom of the cell. All solutions were purged with prepurified argon prior to use.

Multiple Deposition and Modification. For attachment of electroactive groups: gold particles were first deposited via potential step. Attachment of the first electroactive adsorbate (ferrocene) was then performed in the electrochemical cell by first emptying the inverted three-electrode cell, rinsing with water, rinsing with ethanol, and finally filling the electrochemical cell with a 1 mM solution FCUT in ethanol. All rinsing steps in this procedure were performed in triplicate. Self-assembly was then allowed to proceed for a period of one hour. The cell was then emptied, rinsed with ethanol, rinsed with benzene to remove physisorbed ferrocene, rinsed with ethanol, rinsed with water, and filled with either HClO_4 supporting electrolyte for the purpose of running diagnostic voltammetry, or

AuCl_4^- for further particle deposition. Upon completion of the second particle deposition step the cell was again emptied, rinsed with water, and either filled with supporting electrolyte for the purposes of running diagnostic voltammetry, or rinsed with ethanol, and filled with a 1 mM solution of NTP for modification of the newly deposited gold particles. Again, self-assembly was allowed to proceed for one hour. The cell was then emptied, rinsed with ethanol, rinsed with water, and filled with supporting electrolyte for the purpose of running diagnostic voltammetry.

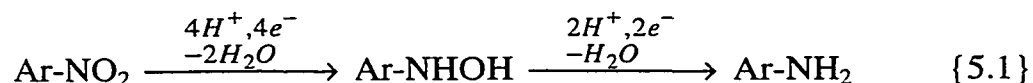
IRRAS Studies. Infrared reflectance spectra were obtained on an ATI Mattson Infinity Series FTIR spectrometer equipped with an external sample module and liquid nitrogen cooled mercury-cadmium-telluride (MCT) detector. Spectra were taken at 2 cm^{-1} resolution with a mirror speed of 40 kHz. Typically, 500 scans and 2000 scans were averaged to yield spectra with acceptable signal-to-noise ratios for bulk gold films and supported gold particles respectively. The interferograms were Fourier transformed using triangular apodization. Reference spectra were obtained on bulk gold films and supported gold particles modified with octadecanethiol- d_{37} under the same conditions.

Attachment of Cytochrome c and IgG. Attachment of cytochrome c and IgG to carboxylic acid modified gold films and particles was accomplished by amidation through the use of an appropriate carbodiimide-coupling agent, such as EDC. Gold substrates were first modified by self-assembly of a carboxylic acid monolayer. The carboxylic acid groups were then activated by exposing them to a 1% solution of EDC in DMF for 4 hours. Upon activation, the substrates were rinsed thoroughly with deionized water, and exposed to a dilute solution of cytochrome c or IgG in 10 mM phosphate buffered saline solution (PBS), pH = 7.0, for 24 hours. These substrates were then rinsed thoroughly with 1% SDS solution before IRRAS analysis.

Results and Discussion

Modification by 4-Nitrothiophenol. In an effort to further probe the use of self-assembly methods as applied to carbon substrates, modification of gold particles with the electroactive adsorbate 4-nitrothiophenol (NTP) was attempted. As both gold and GC are active electrode materials, this approach provides yet another method for distinguishing between the two materials, provided that adsorption of NTP to GC is not a major issue. Voltammetric behavior of NTP modified gold electrodes has previously been studied [31]. The voltammetry of 4-nitrophenyl groups attached to carbon electrodes via reduction of the corresponding diazonium salt [22, 25, 32], and nitrobenzene [33] and *p*-nitrosophenol [34] in aqueous solution has also been studied. The nitro group displays similar voltammetry in each of these cases.

A major drawback of this system is that the voltammetry of NTP is coupled with chemically irreversible reactions. NTP (Ar-NO₂) must be initially reduced to the hydroxylamine species (Ar-NHOH), a four-electron process, before the reversible waves at 400 mV are observed [31]. This behavior is illustrated in Figure 5.1 for NTP on a polycrystalline gold electrode. On the first forward sweep (1F), no current due to reduction of Ar-NHOH to the nitroso species (Ar-NO) is observed. The large cathodic current observed at ~100 mV is attributed to the reduction of Ar-NO₂ to Ar-NHOH and the amine species (Ar-NH₂). This reaction scheme is illustrated below.



On the reverse sweep (1R), an anodic current is observed at ~450 mV, attributed to the oxidation of Ar-NHOH to Ar-NO. On the second, and subsequent potential

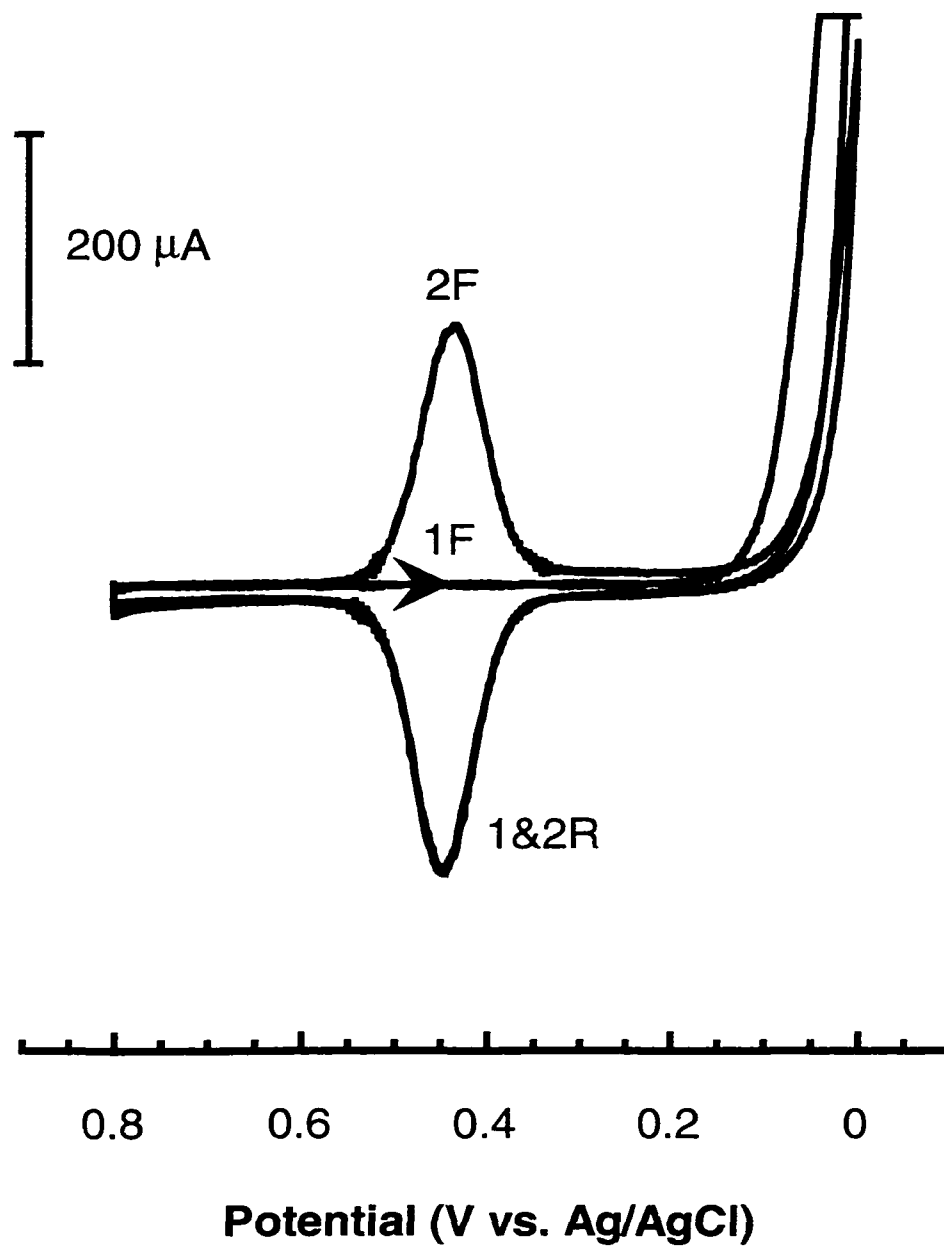


Figure 5.1: Cyclic voltammogram of a NTP modified gold film electrode showing the initial reduction of the nitro group. First two potential cycles, $\nu = 200 \text{ mV/s}$ in 0.5 M HClO_4 .

cycles (2F), a cathodic wave is observed due to the reduction of Ar-NO to Ar-NHOH. A stable wave corresponding to the following redox reaction results.



Excursion to more negative potentials during this initial potential scan results in complete reduction of the nitro group to an amino group, and the voltammetric behavior of interest is not observed. Therefore, careful partial reduction of the nitro group permits brief observation of the reversible two-electron transfer attributed to the hydroxylamine and nitroso redox couple [31].

When NTP is fully reduced to the corresponding amine in acidic aqueous solution, reoxidation back to the nitro group is not observed. Instead, the amino group is oxidized to produce an NH_2^+ radical cation species which participates in further chemical and electrochemical reactions [32, 35]. This behavior leads to a coupling reaction between two adjacent adsorbate molecules [35]. The resulting surface becomes modified with a 4'-mercapto-4-aminodiphenylamine species, basically a dimer of the original adsorbate. This adsorbate remains unstable and further electrochemical and chemical reactions result in a surface bound quinone species. The exact nature of this new redox species is still debated [32, 35]. Figure 5.2 illustrates the complex voltammetric behavior associated with reduction of the amino group on a polycrystalline gold electrode. The second and fourth potential cycles are shown. The redox waves at ~450 mV are attributed to the voltammetry of the nitro group. The redox wave at ~950 mV is attributed to oxidation of the amino group to the radical cation species, a chemically irreversible process. As a result, the redox waves that emerge at ~650 mV are attributed to the resulting quinone species [35]. The redox waves at ~450 mV (due to voltammetry of the nitro group) disappear with time due to coupling of NO_2 adsorbates with the radical cation species.

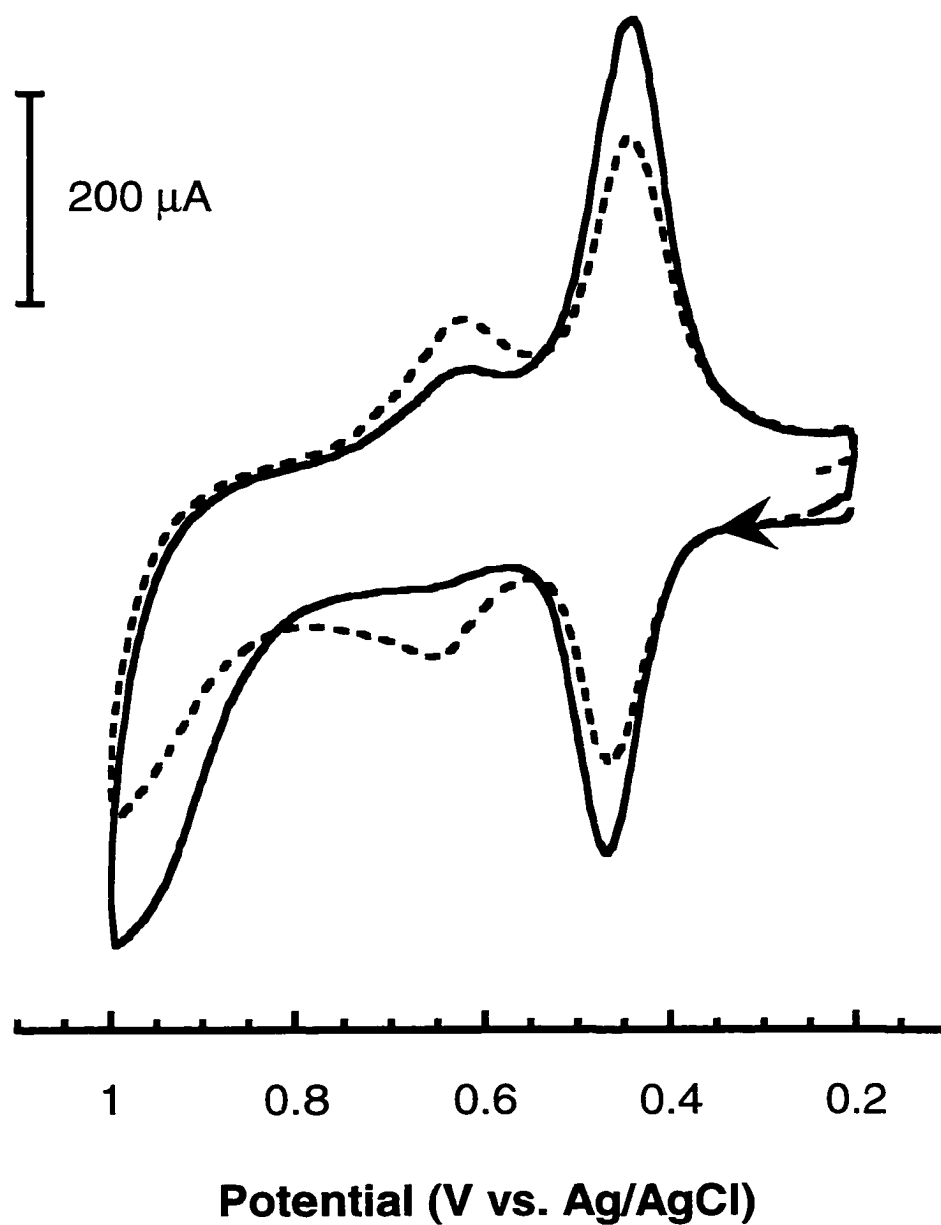


Figure 5.2: Cyclic voltammogram of a NTP modified gold film electrode, further reduction of the amino group. Second and fourth potential cycles, $v = 200 \text{ mV/s}$ in 0.5 M HClO_4 .

Figure 5.3 displays a background subtracted cyclic voltammogram of gold particles modified with NTP. The second potential cycle is shown, obtained after the potential was initially swept to the foot of the wave for NO_2 reduction, similar to that shown in Figure 5.1. Due to the small peak currents observed, background subtraction was employed to eliminate the large double layer charging current and make the redox waves more observable. Control experiments confirm that adsorption of NTP to the GC substrate is negligible. Gold particles were electrochemically deposited from a $500 \mu\text{M AuCl}_4^-$ solution using an overpotential of -800 mV . Characteristic behavior of a surface bound redox species is observed and the redox waves centered at $\sim 400 \text{ mV}$ are attributed to the voltammetry that arises due to reduction of the nitro group: a two-electron transfer between the hydroxylamine and nitroso redox couple. This result confirms that the electroactive adsorbates are bound to the gold particles. Also, gold particles are in good electrical contact with the GC substrate and the adsorbed electroactive groups are easily addressed by application of a potential program.

Further evidence that shows that the gold particles have been modified by self-assembly was obtained by IRRAS. Figure 5.4 displays two reflectance spectra for NTP monolayers on a bulk gold film (Trace a) and on supported gold particles (Trace b). All absorbance bands are attributed to IR active modes of the nitrophenyl group, particularly the N-O stretch at 1362 cm^{-1} and C-N stretch at 869 cm^{-1} [36]. A direct comparison of the two spectra confirms that Trace (b) can be attributed to NTP modified gold particles supported on GC. These observations are consistent with the results of voltammetric studies using NTP as an electroactive probe. Thus, the results of these IRRAS and electrochemical investigations provide confirmation that it is possible to attach functional groups to a GC substrate using electrochemical metal deposition coupled with monolayer self-assembly.

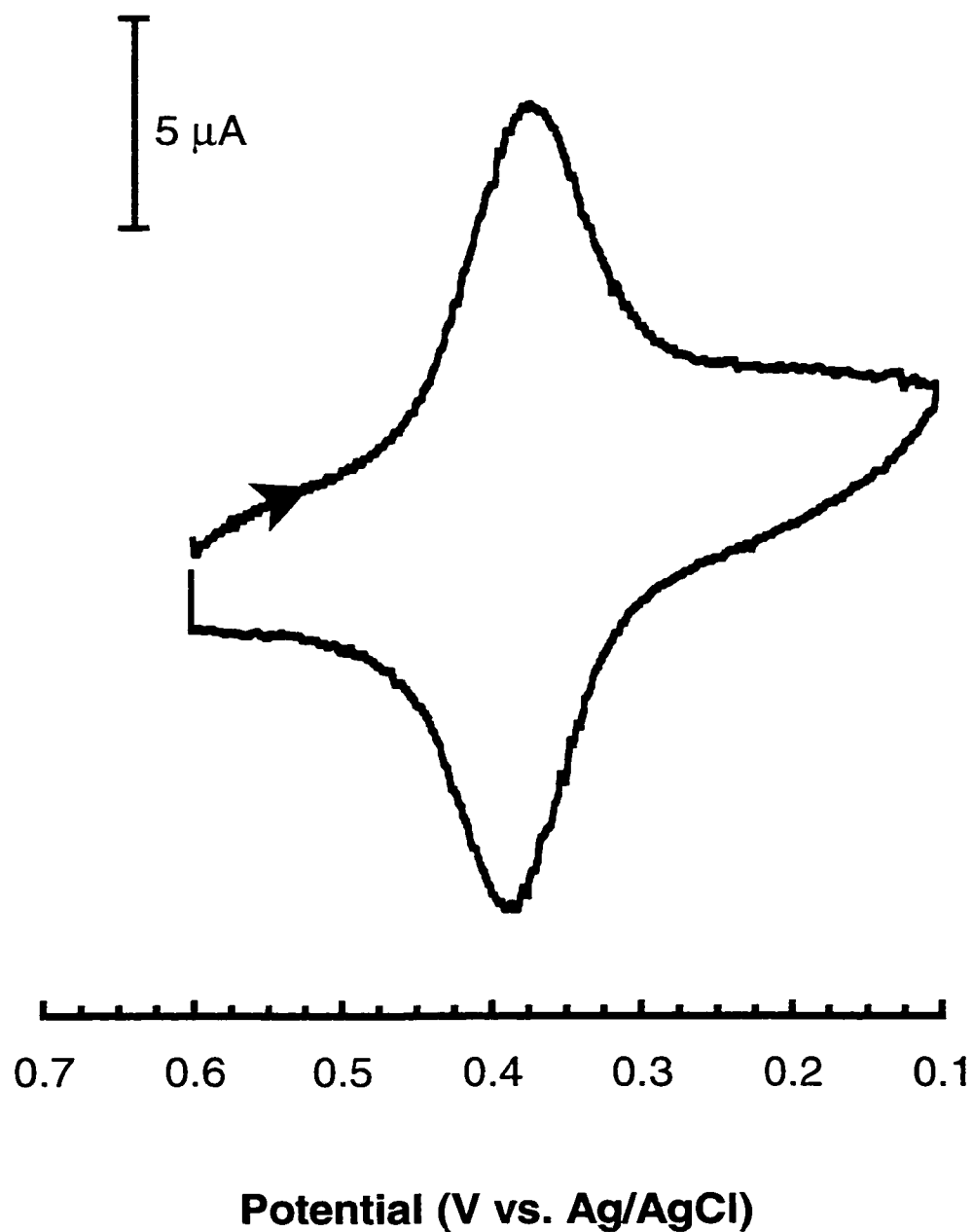


Figure 5.3: Cyclic voltammogram of NTP modified gold particles on GC, background subtracted. $[\text{AuCl}_4^-] = 500 \mu\text{M}$, $\eta = -800 \text{ mV}$, $v = 200 \text{ mV/s}$ in 0.5 M HClO₄.

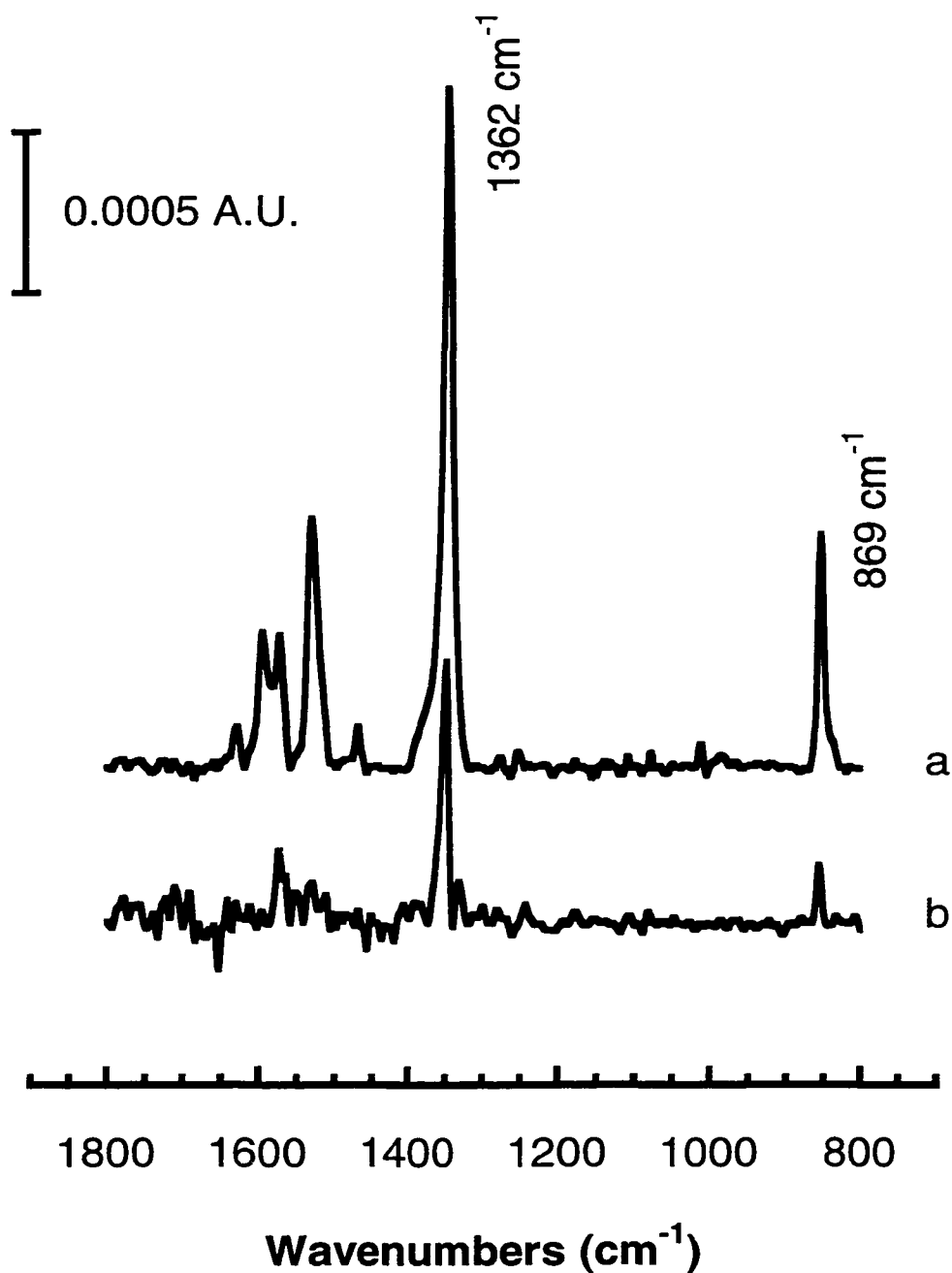


Figure 5.4: IRRAS spectra of (a) a NTP modified bulk gold film, and (b) NTP modified gold particles on GC. $[\text{AuCl}_4^-] = 500 \mu\text{M}$, $\eta = -800 \text{ mV}$.

Given the complex electrochemical behavior of NTP it was concluded that this is not the most desirable electrochemical system to employ in such a study. Any attempts to gain quantitative results would be risky due to the chemical irreversibility of the system. Therefore, a chemically reversible redox system is required before any efforts to gain quantitative results may be attempted. It would be interesting to compare the surface areas of the gold particles obtained by surface oxidation to those obtained using the self-assembly method. Thiol molecules containing a ferrocene or ruthenium pentaamine terminal group would be well suited for such a study as these systems display reversible electrochemical behavior and have been used extensively in previous studies on gold electrodes [1-3, 5-10].

Modification by 11-(Ferrocenecarboxy)undecanethiol (FCUT). Our initial attempts at employing FCUT for particle modification were frustrated by adsorption of the ferrocene group to the GC substrate. Control experiments revealed no difference in the cyclic voltammetry of bare GC substrates and those subjected to gold particle deposition. However, it was discovered that rinsing the modified electrodes in benzene prior to electrochemical investigation is an effective method for removing physisorbed ferrocene from the GC substrate. Figure 5.5 contains cyclic voltammograms for polished GC electrodes (i.e. no gold particles) exposed to a solution of FCUT before and after rinsing in benzene. From these experiments it is reasonable to conclude that rinsing in benzene is effective at removing most of the physisorbed ferrocene.

Figure 5.6 contains cyclic voltammograms for two GC substrates that have been exposed to a solution of FCUT and subsequently rinsed with benzene. The solid trace is for a GC electrode modified with gold particles deposited from a 500 μM AuCl_4^- solution and an overpotential of -800 mV; the dashed trace is for a bare GC electrode. The redox waves centered at 540 mV are attributed to the reversible one electron transfer behavior of the ferrocene-ferrocenium⁺ ion redox

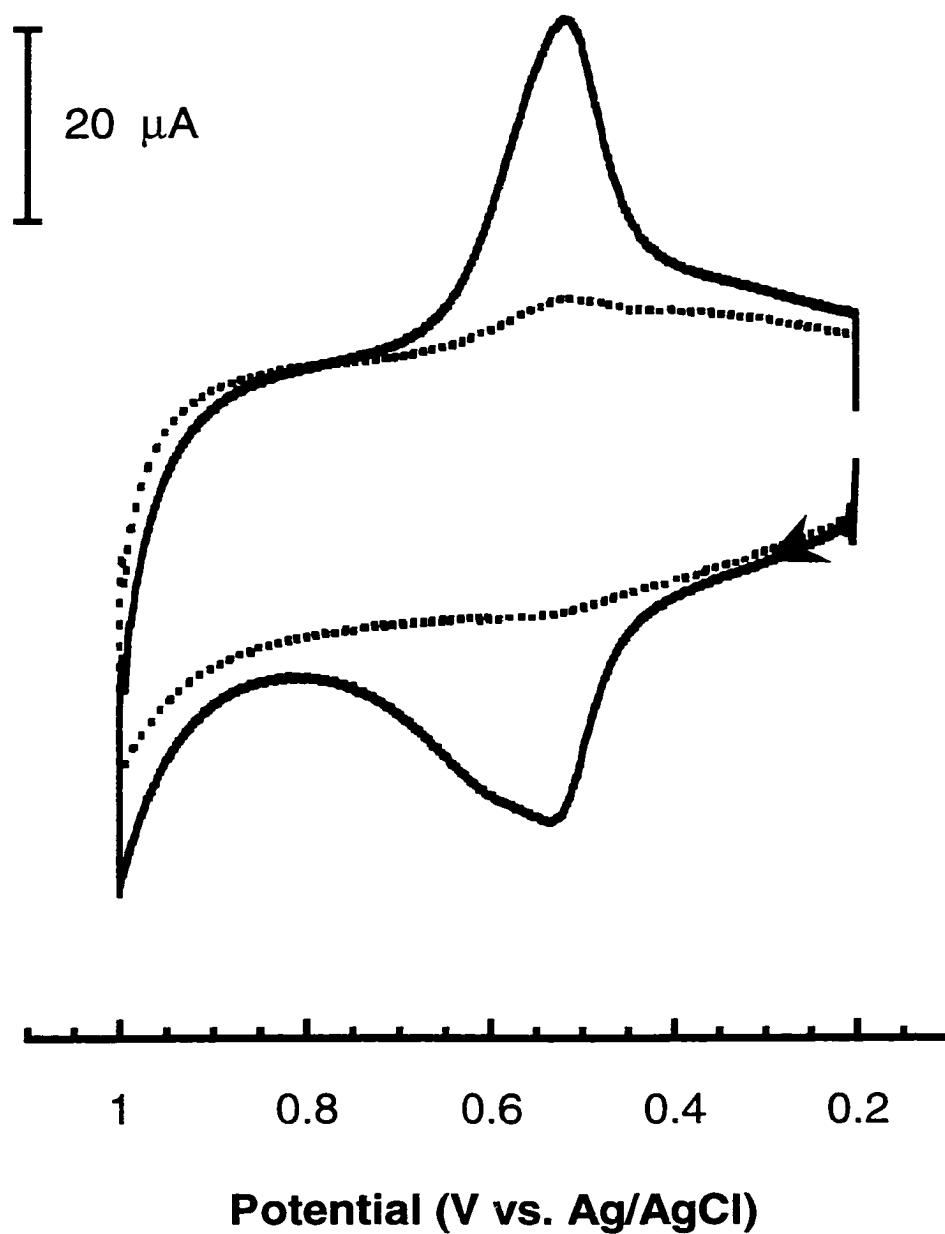


Figure 5.5: Cyclic voltammograms of FCUT adsorbed to polished GC electrodes. Before benzene rinse (solid trace), and after benzene rinse (broken trace), $v = 200 \text{ mV/s}$ in 0.5 M HClO_4 .

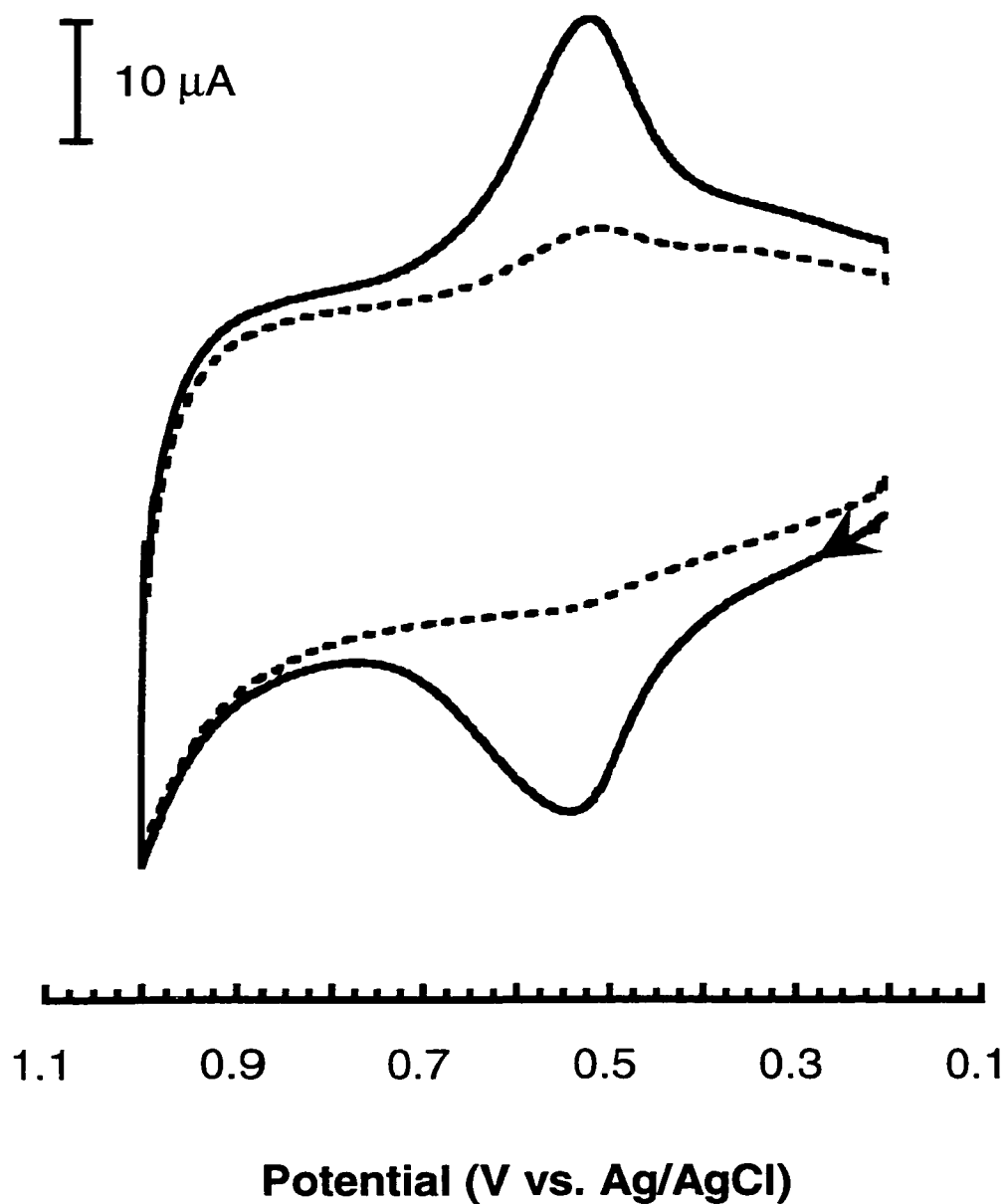


Figure 5.6: Cyclic voltammograms of FCUT modified gold particles, (solid trace), and polished GC, (broken trace), $[\text{AuCl}_4^-] = 500 \mu\text{M}$, $\eta = -800 \text{ mV}$, $\nu = 200 \text{ mV/s}$ in 0.5 M HClO_4 .

couple and are consistent with those observed for similar adsorbates on gold electrodes [1-3, 8]. Only a small residual current, attributed to adsorbed ferrocene, is observed for the bare GC substrate rinsed in benzene. Therefore, the observed voltammetry is attributed mainly to gold particles that have been modified with FCUT. This result provides further evidence that electrochemically deposited gold particles can be modified using the self-assembled monolayer technique

Unlike NTP, FCUT monolayers are stable toward continuous potential cycling; thus, further evaluation can be attempted using this system. Equation {1.17} can be used to describe the peak current of surface bound redox species [37].

$$i_p = \frac{n^2 F^2}{4RT} v A \Gamma^* \quad \{1.17\}$$

Taking the log of both sides of this equation yields an equation of a straight line with a slope equal to one, Equation {5.3}. Different intercepts are observed due to differences in electrode area, and possibly, different values of surface coverage on the gold particles compared to a polycrystalline gold substrate.

$$\log(i_p) = \log(v) + \log \frac{n^2 F^2}{4RT} A \Gamma^* \quad \{5.3\}$$

Figure 5.7 contains a plot of $\log(i_p)$ vs. $\log(v)$ with slopes equal to ~ 1 . This behavior is characteristic of a surface bound redox species. This result provides further evidence that the redox centers are attached to the gold particles.

Due to its well-defined redox behavior an attempt was made to quantify gold surface area employing ferrocene voltammetry. A series of substrates were

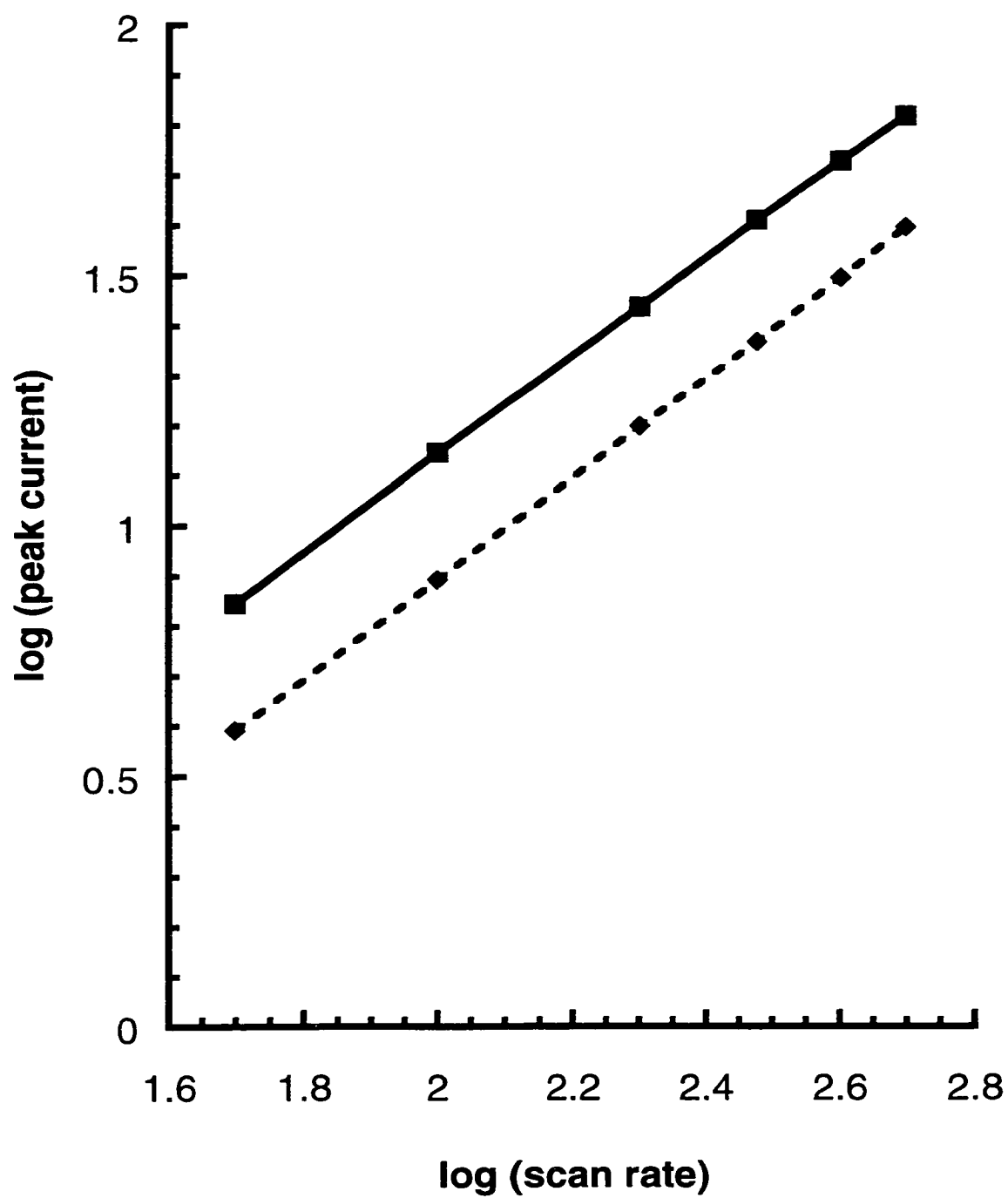


Figure 5.7: Scan rate dependence study for a FCUT modified bulk gold film (solid trace), and supported gold particles (broken trace) in 0.5 M HClO₄.

prepared in which gold particles were deposited from AuCl_4^- solutions ranging in concentration from 100 μM to 1 mM. The area under the redox waves was then integrated to obtain the charge due to ferrocene oxidation. Charge is directly proportional to area, via equation {1.15}. A plot of Q vs. AuCl_4^- concentration in the deposition solution is shown in Figure 5.8. From this plot it is observed that as the AuCl_4^- concentration is increased, charge, and therefore gold surface area also increase, as expected. These results are in agreement with the results obtained in Chapter II for gold oxide reduction and provide compelling evidence that the ferrocene groups are indeed bound to the gold particles.

Observing the shape of the ferrocene redox waves, further conclusions about monolayer structure can be made. Chidsey and coworkers observed broadened voltammetric waves for full monolayers of the ferrocene adsorbate [1]. A cyclic voltammogram of FCUT on a polycrystalline gold substrate is shown in Figure 5.9. Broadening of the waves is attributed to repulsive electrostatic interactions between the closely packed ferrocene groups. The authors demonstrated that upon dilution of the FCUT monolayer with decanethiol the waves become less broadened. The redox waves for FCUT on gold particles in Figures 5.6 are not broadened, suggesting a more loosely packed, less-ordered monolayer structure. This result is consistent with the infrared reflection data presented in Chapter IV that suggests that monolayers formed on supported particles are less ordered than monolayers formed on bulk gold films. Hence, this result provides further evidence that monolayers on particles are less ordered than those obtained on planar gold substrates.

Multiple Deposition and Modification Methods. In order for an adsorbate to be beneficial to our investigations it must be stable toward further gold deposition steps and potential cycling. Thus, the stability of FCUT modified particles was investigated by subjecting these particles to potential step experiments that resemble those used for gold particle deposition. Gold particles

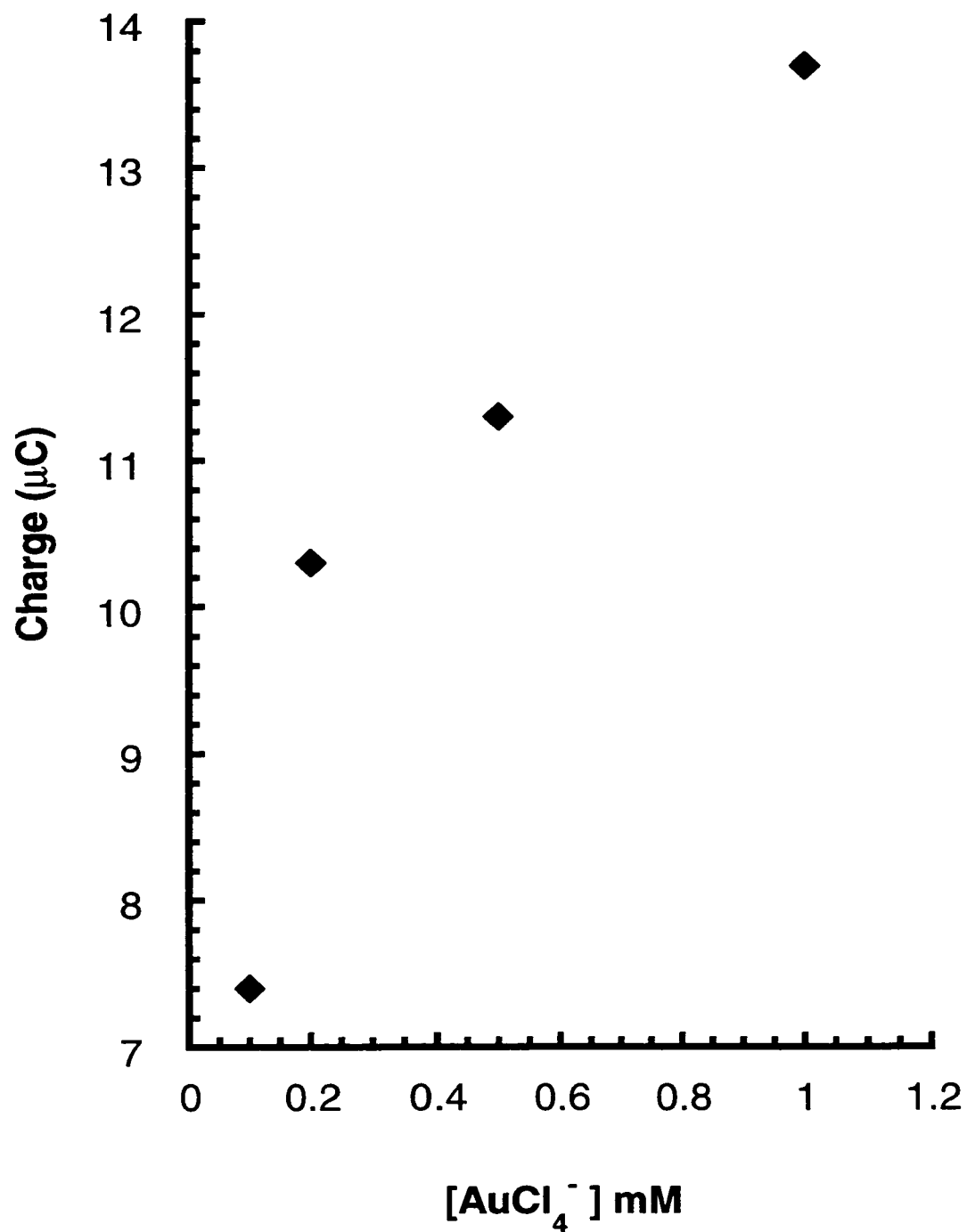


Figure 5.8: Charge due to ferrocene oxidation as a function of AuCl_4^- concentration. $\eta = -800$ mV, $\nu = 200$ mV/s, in 0.5 M HClO_4 .

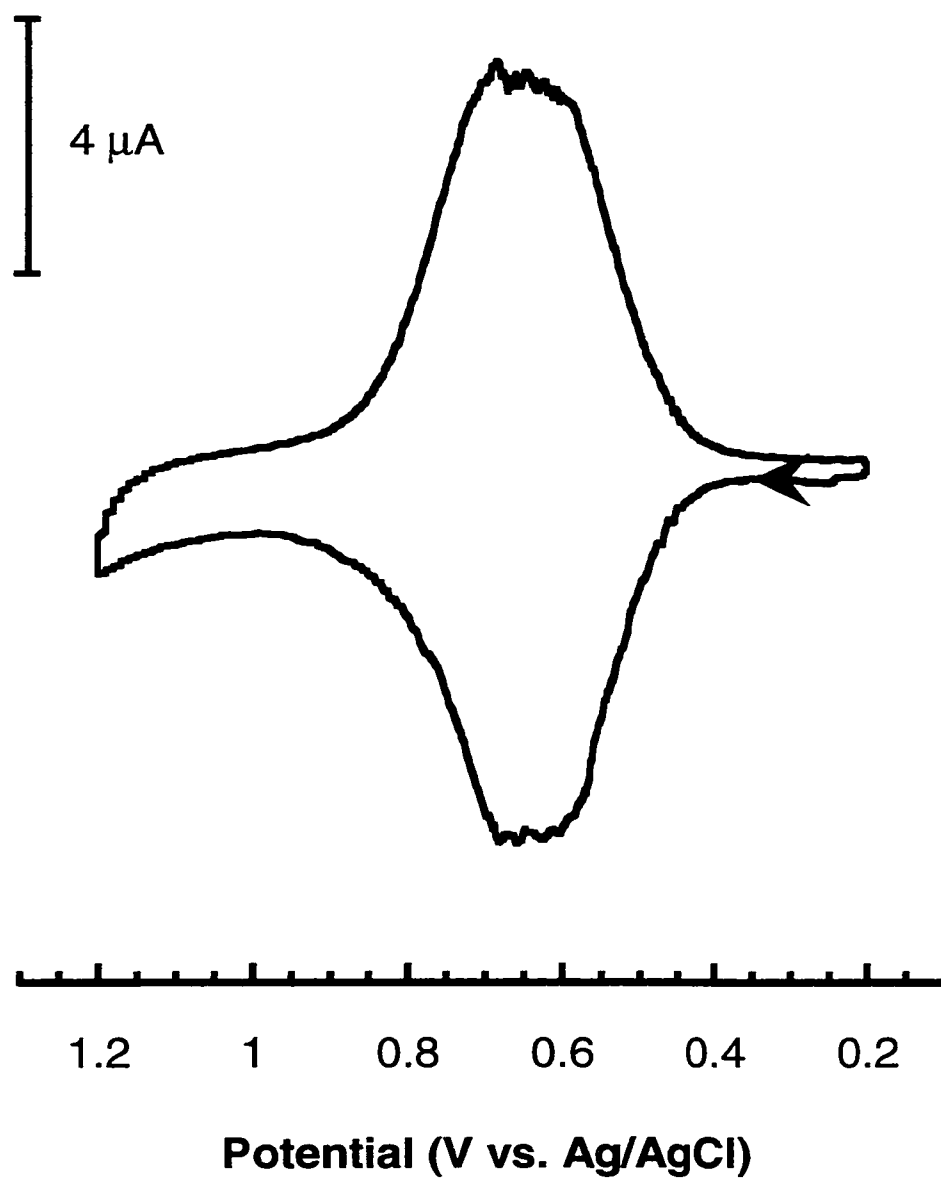


Figure 5.9: Cyclic voltammogram of a FCUT modified gold film electrode. $\nu = 200 \text{ mV/s}$, in 0.5 M HClO_4 .

were deposited from a 500 μM AuCl_4^- solution at an overpotential of -800 mV, modified with FCUT in the usual manner, and subjected to potential step programs in 0.5 M H_2SO_4 supporting electrolyte. Figure 5.10 displays cyclic voltammograms for FCUT modified gold particles before (Trace a) and after (Trace b) exposure to a blank gold deposition step. Results of these control experiments confirm that modified particles display no ill effects or degradation as a result of exposure to potential step programs in supporting electrolyte. Voltammograms obtained before and after exposure to the blank deposition step closely resemble one another and display no significant differences. Thus, it is reasonable to conclude that FCUT modified gold particles are stable upon exposure to potential step programs employed to effect further gold particle deposition.

Another issue which must be addressed is whether the modified particles are able to block further gold deposition. Will new particles nucleate and grow on the exposed GC, or will gold deposition proceed on the modified particles? In Chapter IV we showed that it is possible to employ multiple deposition and modification steps to repeatedly activate and deactivate a GC electrode toward catechol voltammetry. However, from these experiments it is not possible to determine whether gold deposition proceeds on the modified particles, on regions of bare GC substrate, or both. An improvement in catechol voltammetry is observed irrespective of whether gold deposition occurs on GC or not, as long as the newly exposed gold surface area is not passivated by thiol adsorption. A perceived advantage of using a surface bound redox group is that particles modified with electroactive groups may be helpful in determining the result of further gold deposition steps. One would expect to observe a disruption in the voltammetry of the surface bound ferrocene redox group in the event that further gold deposition takes place on the modified particles.

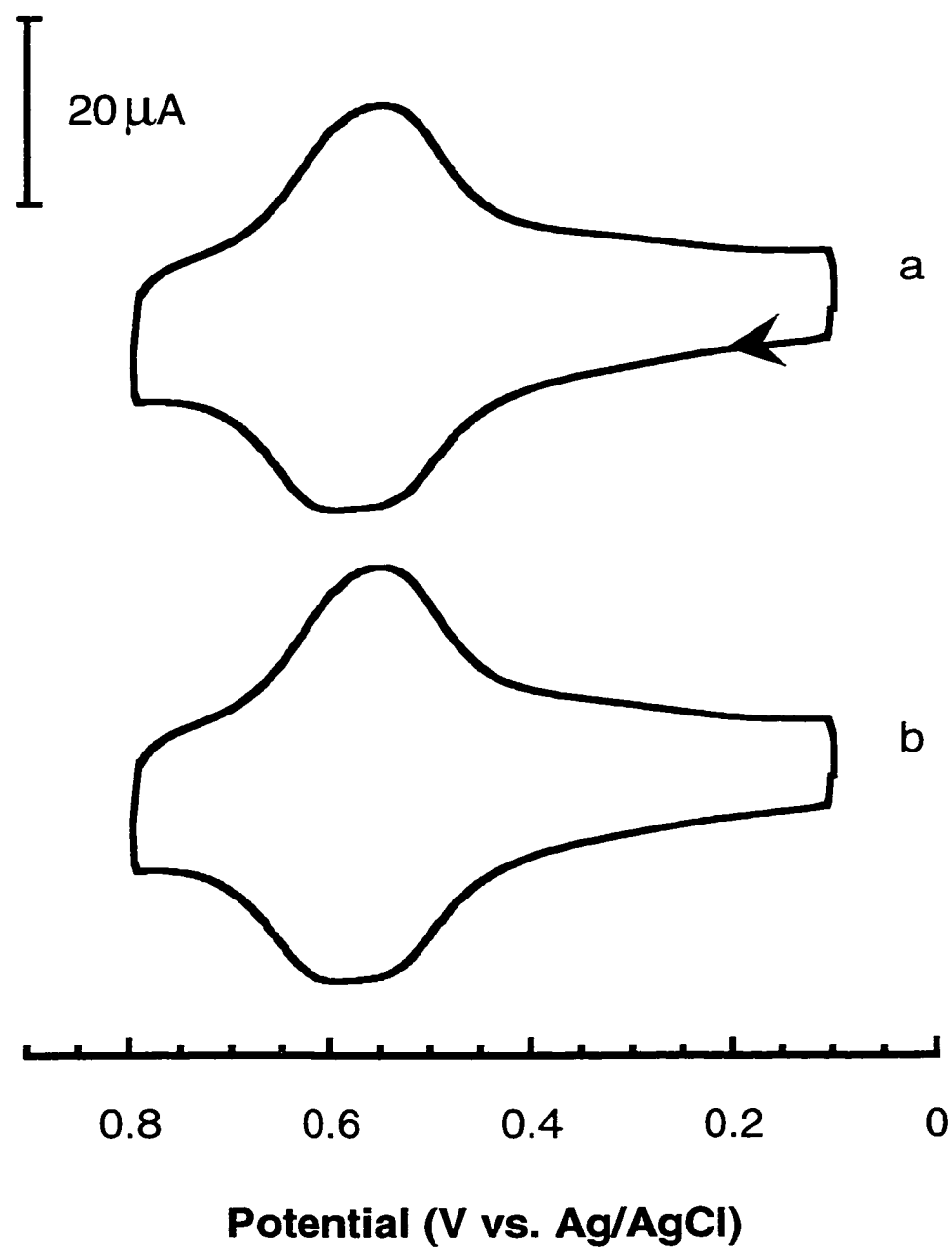


Figure 5.10: Cyclic voltammograms of FCUT modified gold particles on GC. Before (a) and after (b) exposure to a potential step in 0.5 M H_2SO_4 supporting electrolyte. $v = 200 \text{ mV/s}$, in 0.5 M HClO_4 .

Figure 5.11 contains a cyclic voltammogram of FCUT modified gold particles that have been exposed to a second gold deposition step in $500 \mu\text{M AuCl}_4^-$ at an overpotential of -800 mV . Comparing this voltammogram to the ones in Figure 5.10 it is readily observed that something has occurred to the FCUT modified particles as the magnitude of the ferrocene redox waves above the background has been greatly attenuated. Results from control experiments have already established that the modified particles are stable when exposed to the potential program employed for gold deposition in the presence of supporting electrolyte. The only parameter which has been altered in these experiments is the presence of $500 \mu\text{M AuCl}_4^-$ in the deposition solution. Thus, it is concluded that gold deposition is occurring on the FCUT modified particles, to a certain extent.

A possible explanation of this behavior is that the FCUT monolayer on modified particles is not able to completely block gold deposition. In this experiment both deposition steps were performed at an overpotential of -800 mV . Thus, all nucleation sites on the GC substrate may have been exhausted in the first deposition step; therefore, no nucleation sites remain for the second deposition step, and deposition is constrained to the modified particles. Further control experiments were performed such that the overpotential of the first deposition step was set 200 to 400 mV less negative than the second deposition step in an effort to access new nucleation sites. However, no significant differences from previously observed behavior were discerned.

Electrochemical blocking studies presented in Chapter II show that similar alkane chain length adsorbates (DDT) were not able to completely block gold surface oxidation. This suggests that a small fraction of gold surface area remains exposed to the bulk solution. Moreover, as observed in Figure 5.6, the voltammogram suggests that the FCUT adsorbates are not as tightly packed on gold particles as on planar gold substrates. Given these observations, and the fact that ferrocene terminated adsorbates are not able to pack as densely as their non-

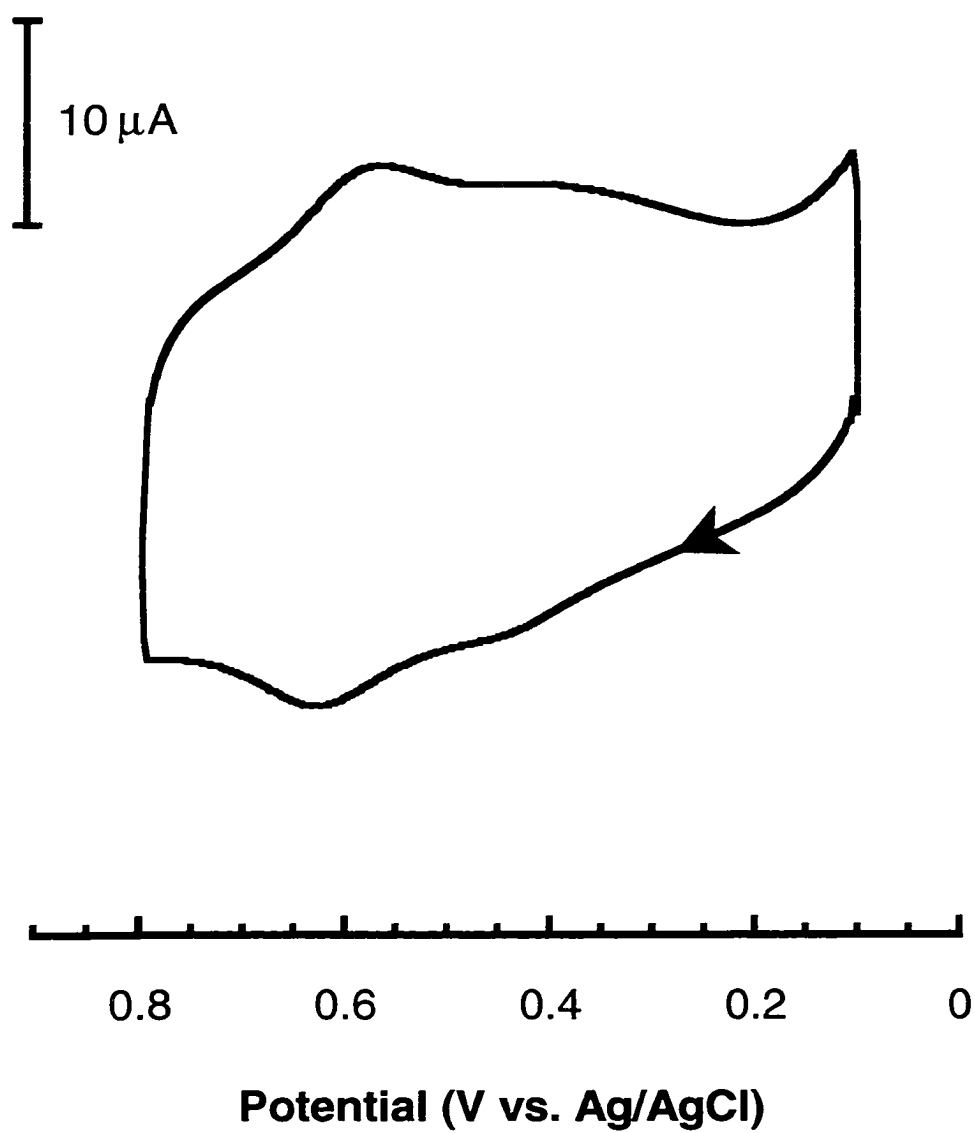


Figure 5.11: Cyclic voltammogram of FCUT modified gold particles on GC after exposure to a second gold deposition step in $500 \mu\text{M AuCl}_4^-$. $\eta = -800 \text{ mV}$, $v = 200 \text{ mV/s}$, in 0.5 M HClO_4 .

substituted alkanethiol analogs [1], it is possible that FCUT modified particles are not able to block further gold deposition from occurring. Consider the fact that a significant overpotential is required for gold deposition on GC compared to that for gold deposition on bulk gold. Then deposition onto modified particles would readily occur if regions of exposed gold surface area were available for further deposition. Other possible explanations for gold deposition onto modified particles include electron tunneling through the monolayer or electron transfer mediation by the ferrocene groups.

Regardless of the fact that gold deposition is occurring on the modified particles, an attempt was made to further modify the newly exposed gold surface area with a different electroactive group. The longstanding goal of this work has been to perform multiple depositions and modifications with different functional groups. Use of electroactive adsorbates allows specific particles to be tagged with electroactive groups that display redox waves at different potentials. Thus, the fate of modified particles generated during earlier modification steps can be monitored by running a cyclic voltammogram and observing the resulting redox waves. Figure 5.12 illustrates a cyclic voltammogram run on the same electrode as Figure 5.11. However, the difference in this case is that the newly deposited gold has been modified using NTP. The redox waves that emerge at 375 mV are attributed to the voltammetry of the hydroxylamine-nitroso redox couple, similar to that in Figure 5.3. Ferrocene voltammetry is not affected by further exposure of these particles to a solution of NTP. This result is expected since an adsorbate such as NTP should not be able to displace or exchange with a long alkane chain adsorbate [13]. In spite of the fact that further gold deposition is occurring on the modified particles, this result demonstrates that it is possible to introduce multiple functional groups onto a GC electrode surface using this method as two sets of redox waves are observed, one for each adsorbate. Although this result is not representative of the ideal result initially sought, the appearance of two sets of

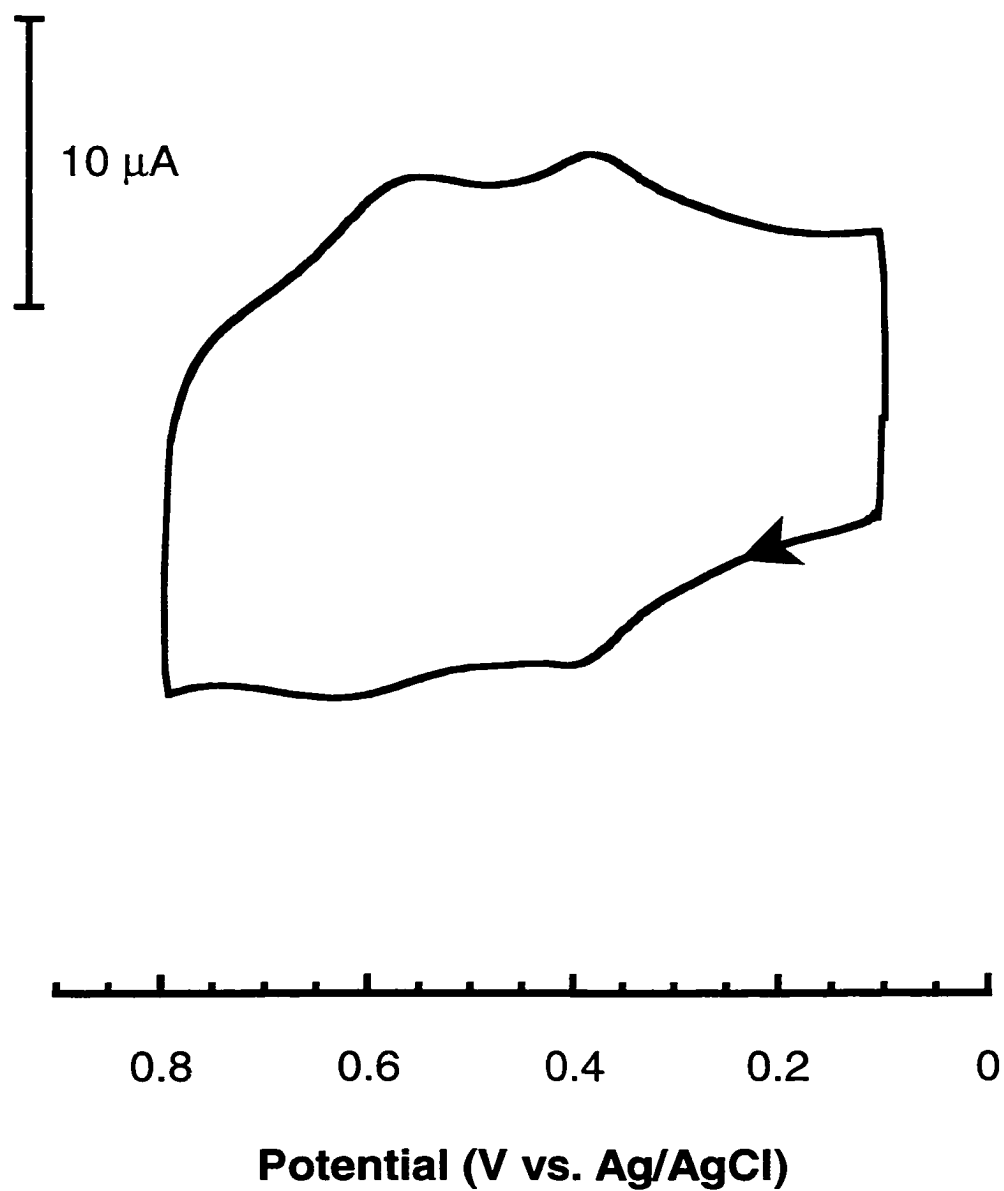


Figure 5.12: Cyclic voltammetry of FCUT modified gold particles after exposure to a second gold deposition step, and subsequent modification with NTP. $[\text{AuCl}_4^-] = 500 \mu\text{M}$, $\eta = -800 \text{ mV}$, $v = 200 \text{ mV/s}$, in 0.5 M HClO_4 .

redox waves in Figure 5.12 confirms that the attachment of two electroactive groups to the GC electrode surface via self-assembly methods is possible, and has been achieved.

IRRAS Studies. As discussed in Chapter IV, it is possible to obtain IRRAS spectra of chemically modified gold particles supported on a GC substrate. Figure 5.13 displays IRRAS spectra of octadecanethiol (ODT, Trace a) and 11-mercaptoundecanoic acid (MUDA, Trace b) modified gold particles on GC. The ODT modified particle spectrum is similar to that shown in Chapter IV. As expected, characteristic symmetric and asymmetric methyl and methylene stretches are observed for the ODT modified gold particles. This observation is consistent with long chain alkanethiolate monolayers on polycrystalline gold films [38-41]. Absorbance peaks are shifted to slightly higher wavenumbers, indicative of a disorder in the monolayer structure, as discussed in Chapter IV. The negative absorbance bands observed between 2000 to 2300 cm^{-1} are representative of the symmetric and asymmetric methyl and methylene stretches of the per-deuterated ODT sample employed for obtaining background spectra. Trace (b) displays an IRRAS spectra of MUDA modified gold particles supported on GC. Symmetric and asymmetric methylene stretches are observed at 2923 and 2854 cm^{-1} , as well as sharp bands at 1742 cm^{-1} and 1598 cm^{-1} , attributed to carbonyl and carboxylate ion absorbance modes [36]. This spectrum is consistent with that of a MUDA monolayer obtained on a polycrystalline gold film.

As an extension of the IRRAS studies, derivatization of carboxylic acid groups with biomolecules was attempted. Figure 5.14 displays IRRAS spectra of cytochrome c modified gold particles (Trace a) and the corresponding MUDA monolayer, activated with EDC (Trace b). A control sample was prepared in the same manner, with the exception of activating the carboxylic acid groups with EDC. A sample containing MUDA modified gold particles was exposed to a one percent solution of 1-ethyl-3-[(dimethylamino)propyl] carbodiimide (EDC) in

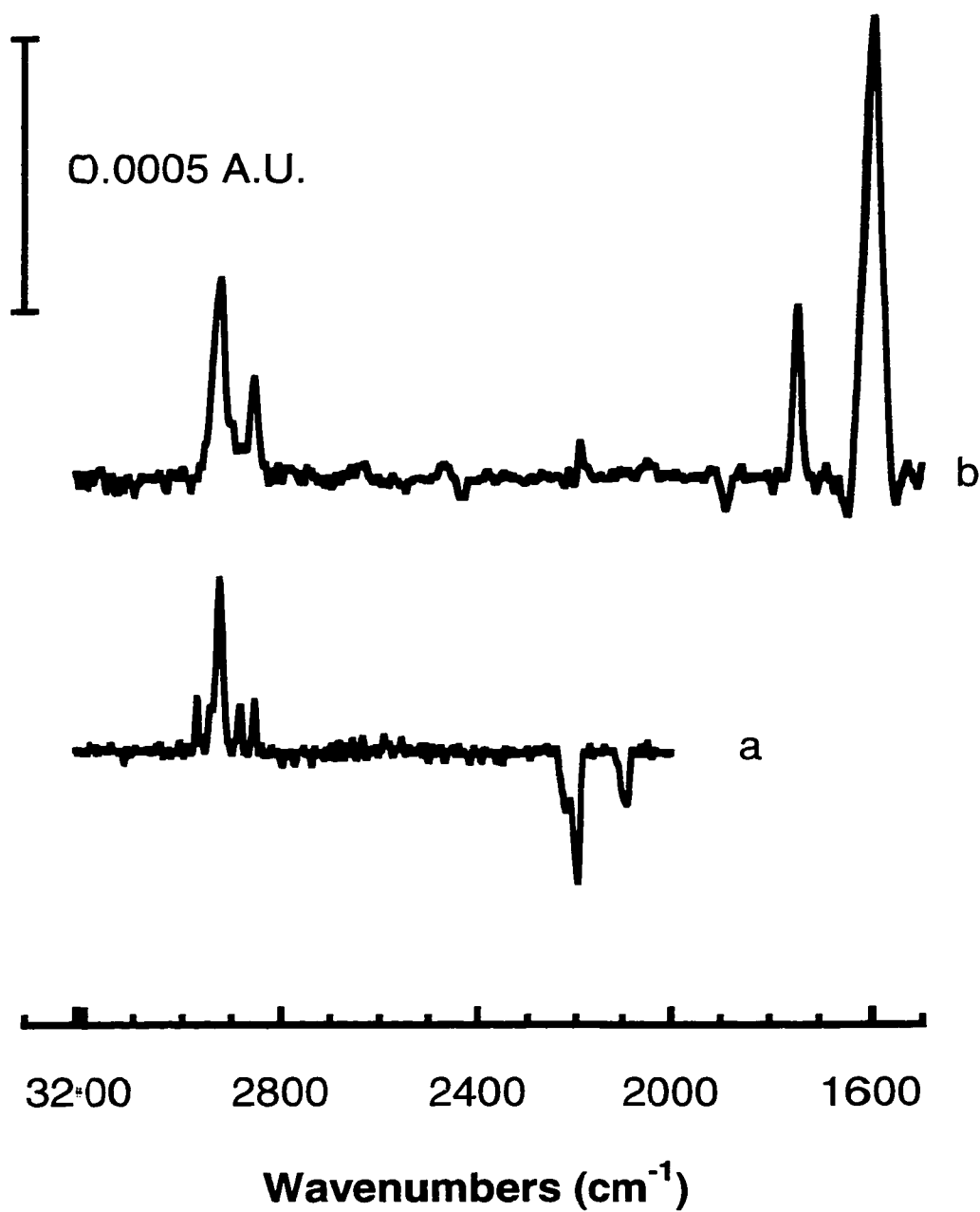


Figure 5.13:: IRRAS spectra of (a) ODT modified gold particles and (b) MUDA modified gold particles on GC. $[\text{AuCl}_4^-] = 1\text{mM}$, $\eta = -800\text{ mV/s}$.

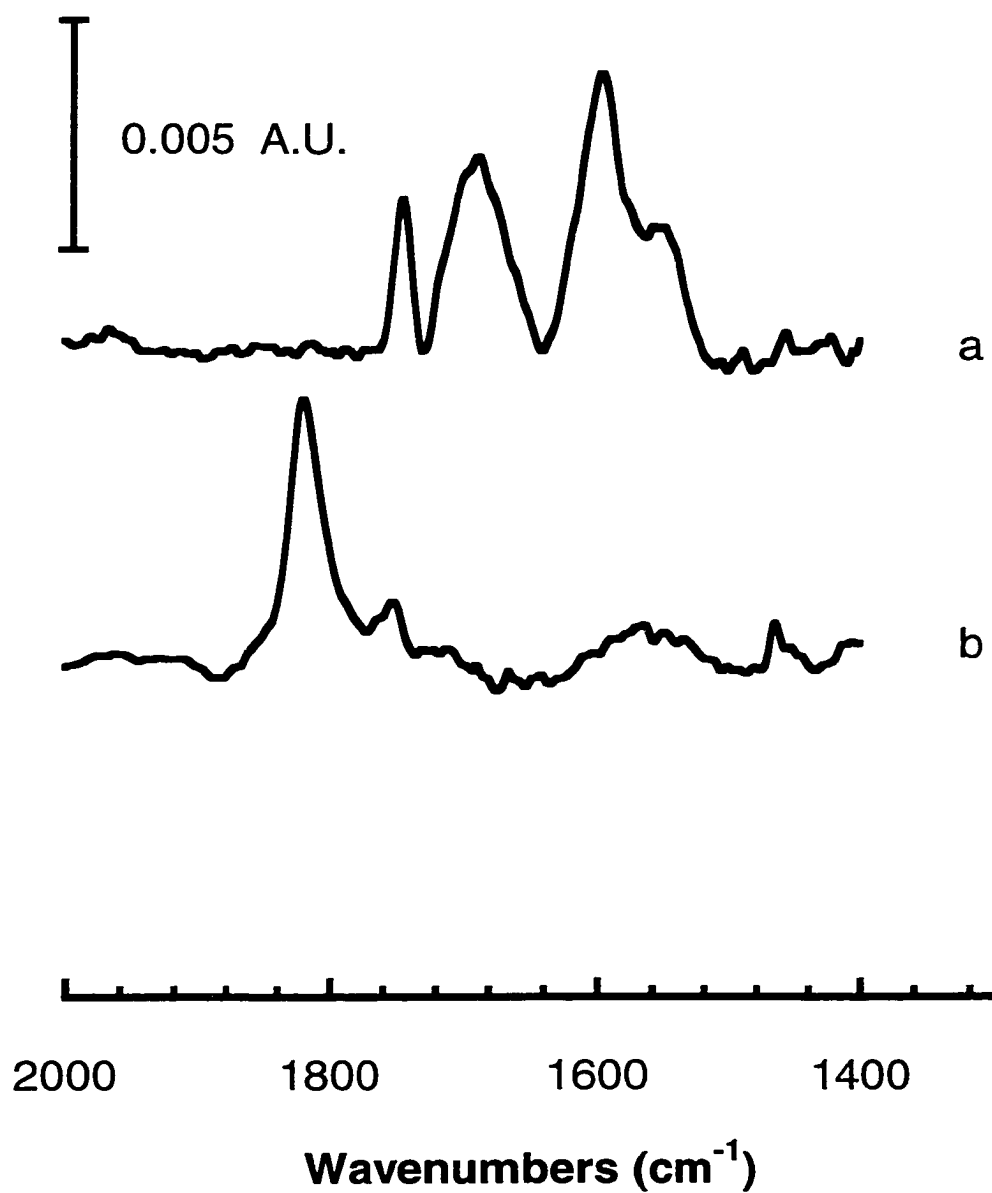


Figure 5.14: IRRAS spectra of (a) cytochrome c attached to MUDA modified gold particles on GC, and (b) activated MUDA monolayer. $[\text{AuCl}_4^-] = 1\text{mM}$, $\eta = 800\text{ mV/s}$.

DMF to activate the carboxylic acid groups [42]. Trace (b) shows that the carboxylic acid groups of the MUDA monolayer have been activated. This is indicated by a shift of the C=O band to higher energy, $\sim 1825\text{ cm}^{-1}$. Exposure of the activated particles to a solution of cytochrome c results in covalent linkage of these molecules to the GC surface via the modified gold particles. Both samples were thoroughly rinsed with a one percent SDS solution to remove any nonspecifically adsorbed protein. Trace (a) displays bands at 1670 cm^{-1} and 1545 cm^{-1} , which are indicative of the Amide I and Amide II bands characteristic of adsorbed proteins [43]. This result is indicative of the immobilization of cytochrome c on modified particles. The control experiment, which consisted of exposing carboxylic acid modified gold particles that had not been activated with EDC, displays very weak absorbance in these regions, due to the presence of nonspecifically adsorbed protein. The band at 1742 cm^{-1} is due to unreacted carboxylic acid groups. These results are consistent with those obtained in similar experiments performed using bulk gold slides, which confirm that immobilization of proteins to activated carboxylic acid monolayers is possible. Hence, this method provides a potentially new route for the attachment of biomolecules to GC substrates.

Conclusions

The results presented herein demonstrate our ability to attach a number of functional groups to GC using metal deposition and self-assembly techniques. This approach has been evaluated using electrochemical and IRRAS methods. The results of these studies indicate that it is possible to attach electroactive groups as well as other functional groups to GC using this approach. Electrochemical investigations reveal that adsorbates display behavior which is characteristic of a surface bound redox group, confirming modification of the gold

particles. This also indicates that supported gold particles are in good electrical contact with the GC substrate. When it has not been possible to use electrochemistry, IRRAS has been successfully employed to evaluate particle modification and the results obtained using these two methods complement one another.

Use of electroactive adsorbates reveal that it is possible to employ multiple deposition and modification steps in an effort to immobilize more than one functional group on the GC surface. While the results indicate that further gold deposition appears to be occurring on particles modified in a previous step, it is possible to modify the newly deposited gold with an electroactive adsorbate that displays a different redox potential than the first. Thus, a cyclic voltammogram displaying two sets of redox waves is obtained.

Derivatization of chemically modified gold particles using simple organic reactions is also possible. It has also been demonstrated using IRRAS that it is possible to attach biomolecules such as cytochrome c to MUDA modified gold particles via amidization using a suitable carbodiimide-coupling agent. This approach provides a potentially new route for the attachment of enzymes and other biologically important molecules to carbon electrode surfaces.

References

1. C. E. D. Chidsey, C. R. Bertozzi, T. M. Putvinski, and A. M. Muzice, *J. Am. Chem. Soc.*, **112**, 4301, (1990).
2. C. E. D. Chidsey, *Science*, **251**, 919, (1991).
3. G. K. Rowe and S. E. Creager, *Langmuir*, **7**, 2307, (1991).
4. M. M. Walczak, D. D. Popenoe, R. S. Deinhammer, B. D. Lamp, C. Chung, and M. D. Porter, *Langmuir*, **7**, 2687, (1991).

5. H. O. Finklea and D. D. Hanshew, *J. Am. Chem. Soc.*, **114**, 3173, (1992).
6. H. O. Finklea, M. S. Ravenscroft, and D. A. Snider, *Langmuir*, **9**, 223, (1993).
7. L. Tender, M. T. Carter, and R. W. Murray, *Anal. Chem.*, **66**, 3173, (1994).
8. K. Weber and S. E. Creager, *Anal. Chem.*, **66**, 3164, (1994).
9. L. A. Hockett and S. E. Creager, *Langmuir*, **11**, 2318, (1995).
10. H. O. Finklea, L. Liu, M. S. Ravenscroft, and S. Punturi, *J. Phys. Chem.*, **100**, 18852, (1996).
11. M. J. Hostetler, S. J. Green, J. J. Stokes, and R. W. Murray, *J. Am. Chem. Soc.*, **118**, 4212, (1996).
12. S. J. Green, J. J. Stokes, M. J. Hostetler, J. Pietron, and R. W. Murray, *J. Phys. Chem. B*, **101**, 2663, (1997).
13. R. S. Ingram, M. J. Hostetler, and R. W. Murray, *J. Am. Chem. Soc.*, **119**, 9175, (1997).
14. M. Brust, M. Walker, D. Bethell, D. J. Schiffrin, and R. Whyman, *J. Chem. Soc., Chem. Commun.*, 801, (1994).
15. M. J. Hostetler, A. C. Templeton, and R. W. Murray, *Langmuir*, **15**, 3782, (1999).
16. C. J. Zhong and M. D. Porter, *Anal. Chem.*, 709A, (1995).
17. D. C. Tse and T. Kuwana, *Anal. Chem.*, **50**, 1315, (1978).
18. C. Ueda, D. C. Tse, and T. Kuwana, *Anal. Chem.*, **54**, 850, (1982).
19. C. A. Koval and F. C. Anson, *Anal. Chem.*, **50**, 223, (1978).
20. A. W. C. Lin, P. Yeh, A. M. Yacynych, and T. Kuwana, *J. Electroanal. Chem.*, **84**, 411, (1977).
21. A. M. Yacynych and T. Kuwana, *Anal. Chem.*, **50**, 640, (1978).

22. M. Delamar, R. Hitmi, J. Pinson, and J. M. Saveant, *J. Am. Chem. Soc.*, **114**, 5883, (1992).
23. P. Allongue, M. Delamar, B. Desbat, O. Fagebaume, R. Hitmi, J. Pinson, and J. M. Saveant, *J. Am. Chem. Soc.*, **119**, 201, (1997).
24. C. Saby, B. Ortiz, G. Y. Champagne, and D. Belanger, *Langmuir*, **13**, 6805, (1997).
25. B. Ortiz, C. Saby, G. Y. Champagne, and D. Belanger, *J. Electroanal. Chem.*, **455**, 75, (1998).
26. C. Bourdillon, J. P. Bourgeois, and D. Thomas, *J. Am. Chem. Soc.*, **102**, 4231, (1980).
27. C. Bourdillon, M. Delamar, C. Demaille, R. Hitmi, J. Moiroux, and J. Pinson, *J. Electroanal. Chem.*, **336**, 113, (1992).
28. C. Duan and M. E. Meyerhoff, *Anal. Chem.*, **66**, 1369, (1994).
29. C. Ruan, F. Yang, C. Lei, and J. Deng, *Anal. Chem.*, **70**, 1721, (1998).
30. F. Lisdat, B. Ge, E. Ehrentreich-Forster, R. Reszka, and F. W. Scheller, *Anal. Chem.*, **71**, 1359, (1999).
31. H. Tsutsumi, S. Furumoto, M. Morita, and Y. Matsuda, *J. Coll. Int. Sci.*, **171**, 505, (1995).
32. W. A. Hayes and C. Shannon, *Langmuir*, **12**, 3688, (1996).
33. I. Rubenstein, *J. Electroanal. Chem.*, **183**, 379, (1985).
34. R. S. Nicholson and I. Shain, *Anal. Chem.*, **37**, 190, (1965).
35. J. Lukkari, K. Kleemola, M. Meretoja, T. Ollonqvist, and J. Kankare, *Langmuir*, **14**, 1705, (1998).
36. R. M. Silverstein, G. C. Bassler, and T. C. Morrill, *Spectrometric Identification of Organic Compounds*, John Wiley & Sons, Inc., New York, (1991).

37. A. J. Bard and L. R. Faulkner, *Electrochemical Methods: Fundamentals and Applications*, John Wiley & Sons, Inc., New York, (1980).
38. M. D. Porter, T. B. Bright, D. L. Allara, and C. E. D. Chidsey, *J. Am. Chem. Soc.*, **109**, 3559, (1987).
39. R. G. Nuzzo, F. A. Fusco, and D. L. Allara, *J. Am. Chem. Soc.*, **109**, 2358, (1987).
40. R. G. Nuzzo, L. H. Dubois, and D. L. Allara, *J. Am. Chem. Soc.*, **112**, 558, (1990).
41. C. E. D. Chidsey and D. N. Loiacono, *Langmuir*, **6**, 682, (1990).
42. I. Willner and A. Riklin, *Anal. Chem.*, **66**, 1535, (1994).
43. B. Leidberg, B. Ivarsson, and I. Lundstrom, *J. Biochem. Biophys. Met.*, **9**, 233, (1984).

CHAPTER VI

HIGH-RESOLUTION CHEMICAL MAPPING OF SURFACE-BOUND FUNCTIONAL GROUPS WITH TAPPING-MODE SCANNING PROBE MICROSCOPY

Introduction

The work presented in this chapter was performed in my first summer as a graduate student at the University of Alberta, and is not necessarily related to the work presented in Chapters I through V.

One of the recent, exciting advancements in scanning probe microscopy (SPM) is the development of contrast mechanisms which yield surface compositional information. Efforts toward this goal are driven by fundamental and technological interests in mapping interfaces chemically with nanometer scale lateral resolution. Recently, several groups have demonstrated the chemical sensitivity of scanning force microscopy (SFM) in both a single-point contact mode [1-5] and in an imaging mode [6-13]. Studies concerned with chemical imaging have mainly involved the use of contact mode SFM imaging with frictional force contrast [6-11], although contrast mechanisms based on adhesion [12, 13] and elastic compliance [7, 9] have been successfully employed. We report here our initial results which demonstrate for the first time the ability of tapping-mode SFM (TM-SFM) [14] to distinguish between segregated domains of functional groups. We show that the phase shift of an oscillating cantilever is sensitive to the surface functional groups that are interacting with the tip. The efforts here are motivated by our interest in the compositional mapping of chemically modified electrodes and polymer interfaces, a challenging prospect in contact mode SFM (i.e., friction contrast) because of tip-induced sample

deformation and topographic convolution in frictional signals. The advantages of phase contrast TM-SFM are discussed in this context.

The ability of TM-SFM to distinguish between regions of varying chemical composition was assessed by imaging surfaces composed of spatially segregated domains of methyl ($-\text{CH}_3$) and carboxylic acid ($-\text{CO}_2\text{H}$) groups. The samples utilized can be described as partial bilayer structures formed by exposing gold substrates to an ethanolic solution containing both mercaptohexadecanoic acid (MHDA, $\text{HS}(\text{CH}_2)_{16}\text{CO}_2\text{H}$) and steric acid (SA, $\text{CH}_3(\text{CH}_2)_{16}\text{CO}_2\text{H}$) as previously described [11]. A schematic of the bilayer formed from MHDA and SA is shown in Figure 6.1. As shown by friction force imaging, a surface exposing segregated domains of $-\text{CH}_3$ and $-\text{CO}_2\text{H}$ groups to the interface can be formed by allowing the second layer to only partially assemble [11]. This provides us with a test sample where the regions of differing functionality also exhibit a difference in height which allows for direct comparison between chemical imaging and topography.

In these studies we demonstrate that TM-SFM can distinguish between regions of varying chemical composition. Phase contrast TM-SFM is used to map chemically a partially formed bilayer structure composed of segregated $-\text{CH}_3$ and $-\text{CO}_2\text{H}$ moieties. The contrast derived from these samples is shown to be due solely to chemical differences, with negligible contribution from variations in surface mechanical properties. We also demonstrate that the chemical contrast in TM-SFM is unaffected by significant topographic variations, which illustrates the utility of phase contrast imaging for the compositional mapping of rough surfaces. This result, combined with reduced sample deformation as a consequence of the intermittent contact between the tip and sample, leads us to believe that phase contrast TM-SFM will be more applicable than contact mode SFM for the chemical imaging of technologically relevant materials. Our results are presented in this context.

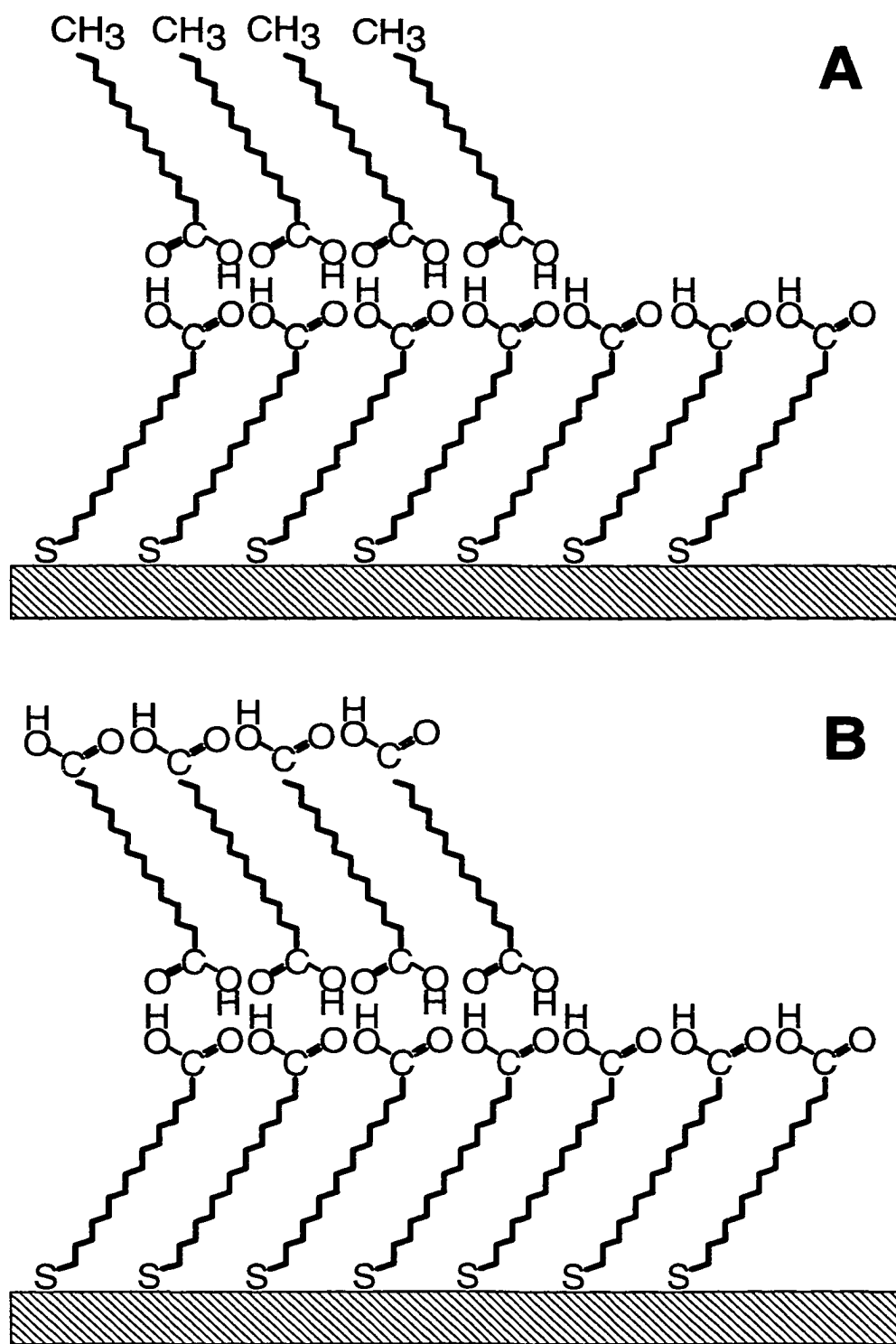


Figure 6.1: Schematic diagram of partial bilayers formed at Au(111). SA partial bilayer (A), and a HDDA partial bilayer (B).

Experimental

Chemicals. Ethanol (punctilious grade, Millennium Petrochemicals), stearic acid (SA), and hexadecanedioic acid (HDDA) were used as received, (Aldrich), 16-mercaptohexadecanoic acid, MHDA, was a gift from Marc Porter (Iowa State University).

Gold Substrates. Gold substrates were prepared by the resistive evaporation of 300 nm of gold onto Tempax glass. These gold films were then annealed in a H₂ flame.

Bilayer Sample Preparation. Bilayer samples were prepared by immersing annealed gold samples into dilute solutions of MHDA and SA or HDDA in ethanol. The degree of formation of the second layer can be manipulated by controlling the SA or HDDA concentration and immersion time. Typical formation conditions were as follows, [MHA] = 10 μM, [SA], [HDDA] = 1 mM, immersion time = 16 to 20 hrs.

TM-SPM Imaging. All images in this work were collected with a Nanoscope III MultiMode SPM (Digital Instruments, Santa Barbara, CA) operated in the ambient. Microfabricated silicon tapping-mode cantilevers were also provided by Digital Instruments. Images were collected with the cantilever oscillating slightly below the its resonance frequency (f_0) at an amplitude of 50 to 70 nm. In Figures 6.2, 6.3, and 6.4 the imaging amplitude (IA) corresponds to a 60% damping of the free oscillation amplitude (FOA). The FOA was determined from force-distance plots (i.e., force curves) in which the oscillation amplitude is plotted as a function of tip-sample distance. From these plots, the distance the sample is translated to completely damp the cantilever relative to the point of initial contact represents one-half the FOA. Typical FOAs used in this work ranged between 100 and 120 nm.

Results and Discussion

The ability of TM-SFM to distinguish between regions of varying chemical composition was assessed by imaging surfaces composed of spatially segregated domains of methyl ($-\text{CH}_3$) and carboxylic acid ($-\text{CO}_2\text{H}$) groups. The samples utilized can be described as partial bilayer structures formed by exposing gold substrates to an ethanolic solution containing both MHDA and SA as previously described [11]. A schematic of the bilayer formed from MHDA and SA is shown in Figure 6.1A. As shown by friction force imaging, a surface exposing segregated domains of $-\text{CH}_3$ and $-\text{CO}_2\text{H}$ groups to the interface can be formed by allowing the second layer to only partially assemble [11]. This provides us with a test sample where the regions of differing functionality also exhibit a height difference which allows for direct comparison between chemical imaging and topography.

Several different samples of partially formed bilayers of MHDA and SA at Au(111) were characterized with TM-SFM. Figures 6.2 presents 600×600 nm constant amplitude topographic (Image A) and phase contrast (Image B) TM-SFM images that are representative of >100 images from 5 different samples. The images in Figure 6.2 were collected simultaneously at a location on top of a flat Au(111) terrace. As illustrated in the image and in the cross-sectional profile of Image A, the topography of these samples is comprised of segregated domains exhibiting heights that range from 1.5 to 2.0 nm consistent with the height expected for a fully extended layer of SA [15, 16].

Image B provides the initial evidence for chemical sensitivity in phase contrast TM-SFM of partial bilayer interfaces. With regard to image interpretation, the contrast observed in Image B reflects phase angle differences ($\Delta\phi$) of the oscillating cantilever as the tip interacts with the surface relative to its phase while oscillating freely. As shown in both the image and the cross sectional profile in Image B, a significant change in $\Delta\phi$ is detected between the different

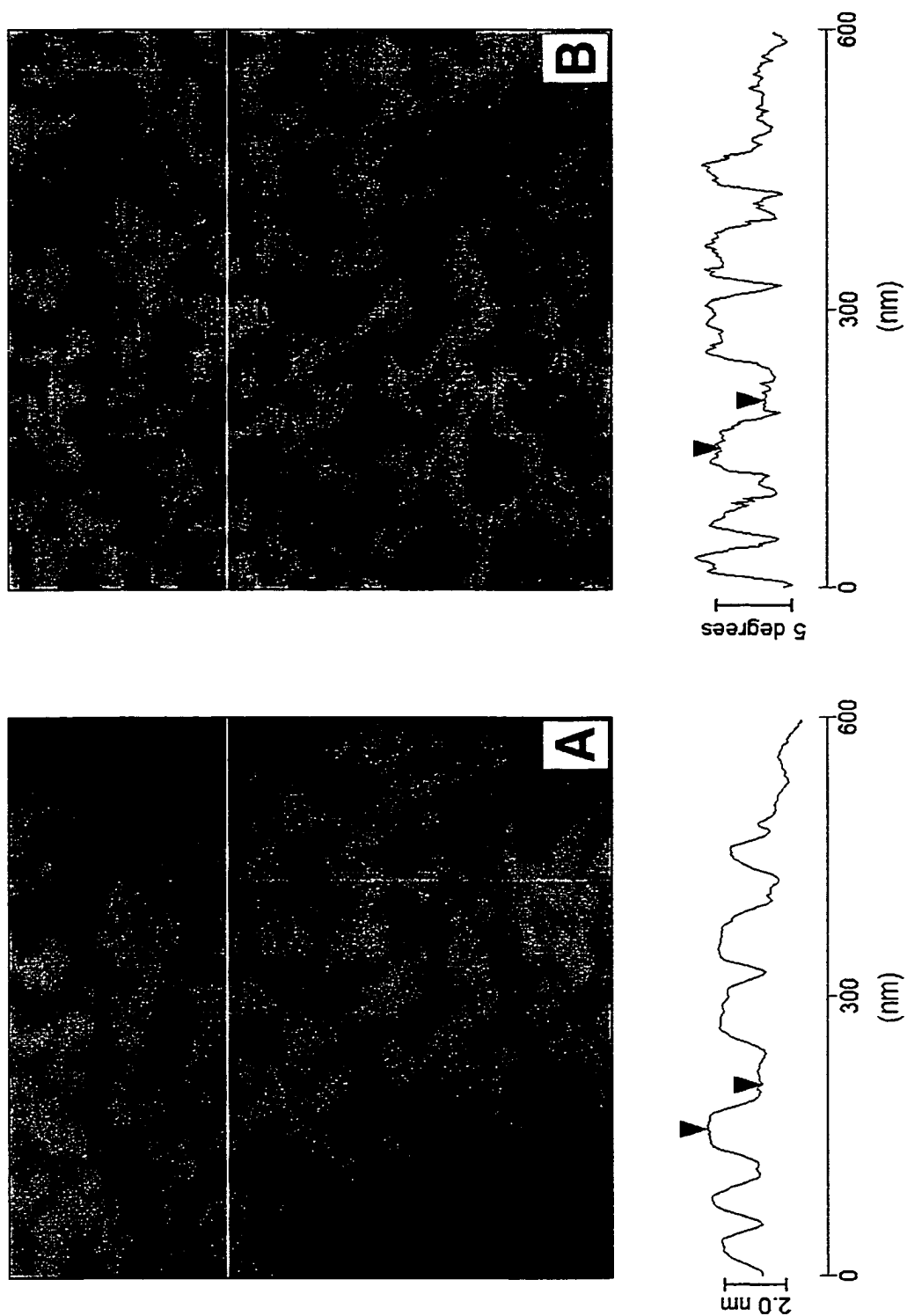


Figure 6.2: Topographic (A, z-scale = 10 nm) and phase contrast (B, z-scale 20°) tapping-mode SFM images of a MHDA/SA partial bilayer.

domains of the partial bilayer samples. Quantitatively, $\Delta\phi$ at the top of the SA layer is typically 2 to 5 degrees higher than that at the top of the MHDA layer for imaging amplitudes (IA) of 50 to 60% of the FOA. While the magnitude of the contrast increases to 20 degrees for low IA (e.g., 10% of FOA), its direction remains constant. We estimate a lateral resolution of 15 nm in terms of both the smallest domain resolved and the distance clearly separating two regions of different phase. It is tempting, because of the controlled design of our samples, to correlate the contrast in Image B with differences in the functional groups exposed at each region (i.e., $-\text{CH}_3$ and $-\text{CO}_2\text{H}$). However, because a number of recent reports have linked contrast in phase images to surface mechanical properties [16-18], the observations in Image B alone are insufficient to associate the contrast solely with chemical composition.

Recent experimental [19-23] and theoretical [16] investigations have demonstrated the dependence of phase shifts in TM-S-FM on sample elasticity and viscoelasticity. We thus designed control samples in order to ensure the contrast observed in Image B was not based on variations in the mechanical properties of the bilayer as a result of, for example, differences in packing between the first and second layers. In these samples a partial second layer was formed at a MHDA/Au(111) monolayer from hexadecanedioic acid (HDDA, $\text{HO}_2\text{C}(\text{CH}_2)_{14}\text{CO}_2\text{H}$). As depicted in Figure 6.1B, this type of surface consists of segregated regions of different heights but identical interfacial chemistry. Figure 6.3, Images C and D respectively, presents 600×600 nm topographic and phase contrast images of a partial MHDA/HDDA bilayer. Similar to the MHDA/SA system, the topographic profile reveals domains differing in height by 1.8 to 2.2 nm. However, relative to Image B, Image D exhibits negligible phase contrast between the top of the second layer relative to the top of the first. A small variation in $\Delta\phi$ is apparent at the edges of the HDDA domains, likely as a result of torsional bending of the cantilever at the step between layers. Importantly, the

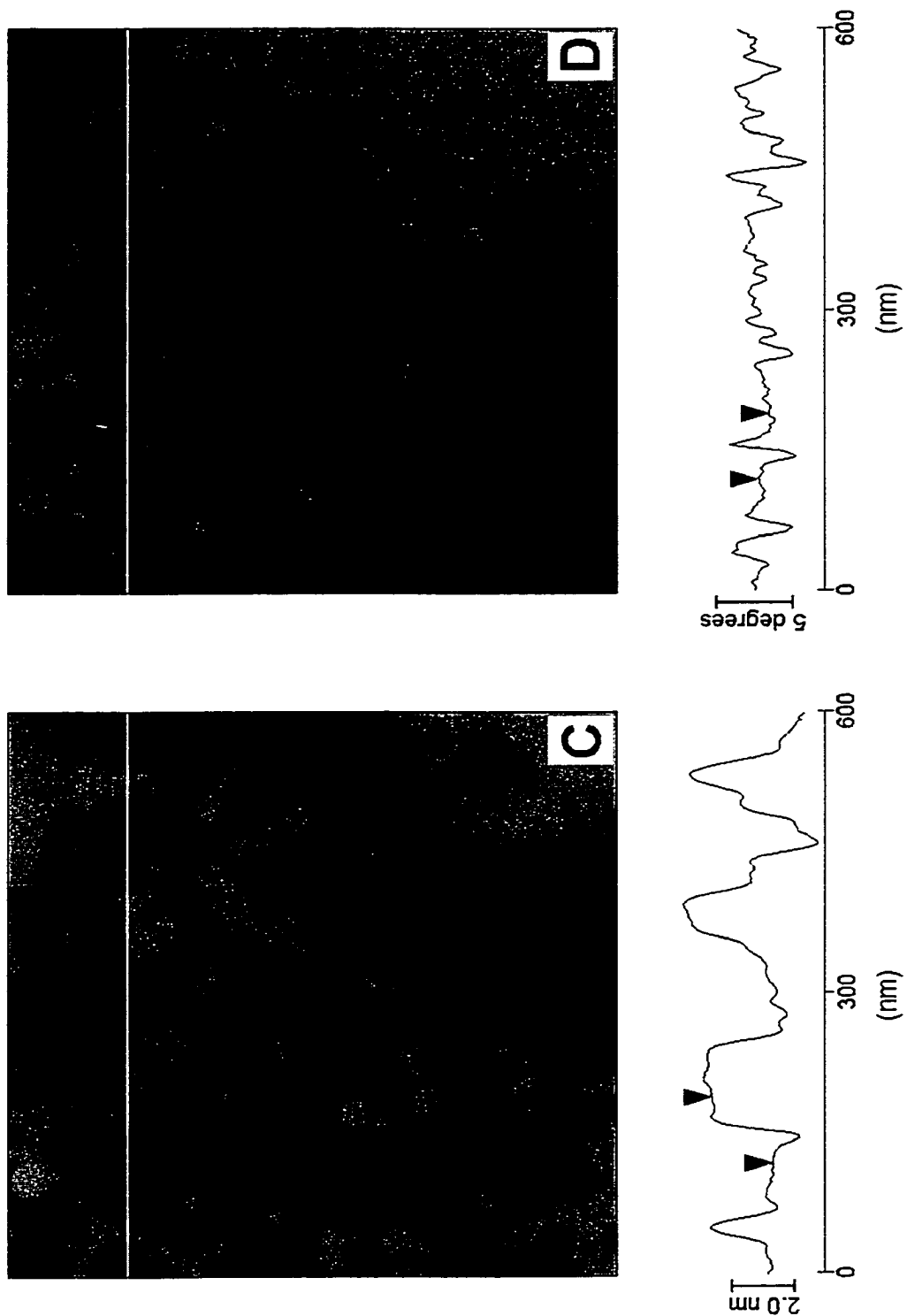


Figure 6.3: Topographic (C, z-scale = 15 nm) and phase contrast (D, z-scale 20°) tapping-mode SFM images of a MHDA/HDDA partial bilayer.

lack of contrast in Image D argues that any variations in mechanical properties between the top and bottom layers in our partial bilayers is negligible in terms of generating phase differences. Thus, the images of our control sample in Images C and D provide compelling evidence that the phase contrast observed at the MHDA/SA system (Image B) is predominantly due to differences in surface chemistry.

Confining the image areas in Figures 6.2 and 6.3 to atomically flat Au(111) terraces permits the assessment of chemical mapping without the influence of substrate topography. However, we believe the real utility of chemically sensitive SPM techniques will be demonstrated by their ability to probe technologically relevant materials (e.g., polymers and electrodes) which often exhibit surfaces with rough, ill-defined topography. The influence of topographic variations on SFM frictional signals has been demonstrated [24, 25], and may ultimately limit the applicability of chemical mapping with contact mode SFM. Our results show that compositional contrast can easily be obtained with phase imaging in the presence of significant variations in topography. Figure 6.4 is a $5 \times 5 \mu\text{m}$ TM-SFM topographic image of a partial bilayer sample assembled on a gold film sputter coated onto mica at room temperature. The observed topographic variations arise from the randomly sized gold crystallites in the substrate resulting from the deposition process. At this lateral length scale, the topography of bilayer domains cannot be observed. The phase image in Figure 6.4, Image B, reveals contrast apparently unrelated to gross substrate topography. Images at lower lateral scales indicate that the regions in Image B exhibit an increased $\Delta\phi$ correspond to areas covered by the SA layer (i.e., $-\text{CH}_3$ groups) and that the regions of lower $\Delta\phi$ correspond to $-\text{CO}_2\text{H}$ moieties. Note that this is the expected contrast based on the results in Figure 6.2. Figure 6.4 thus demonstrates that significant topographic variations contribute little to chemical contrast in

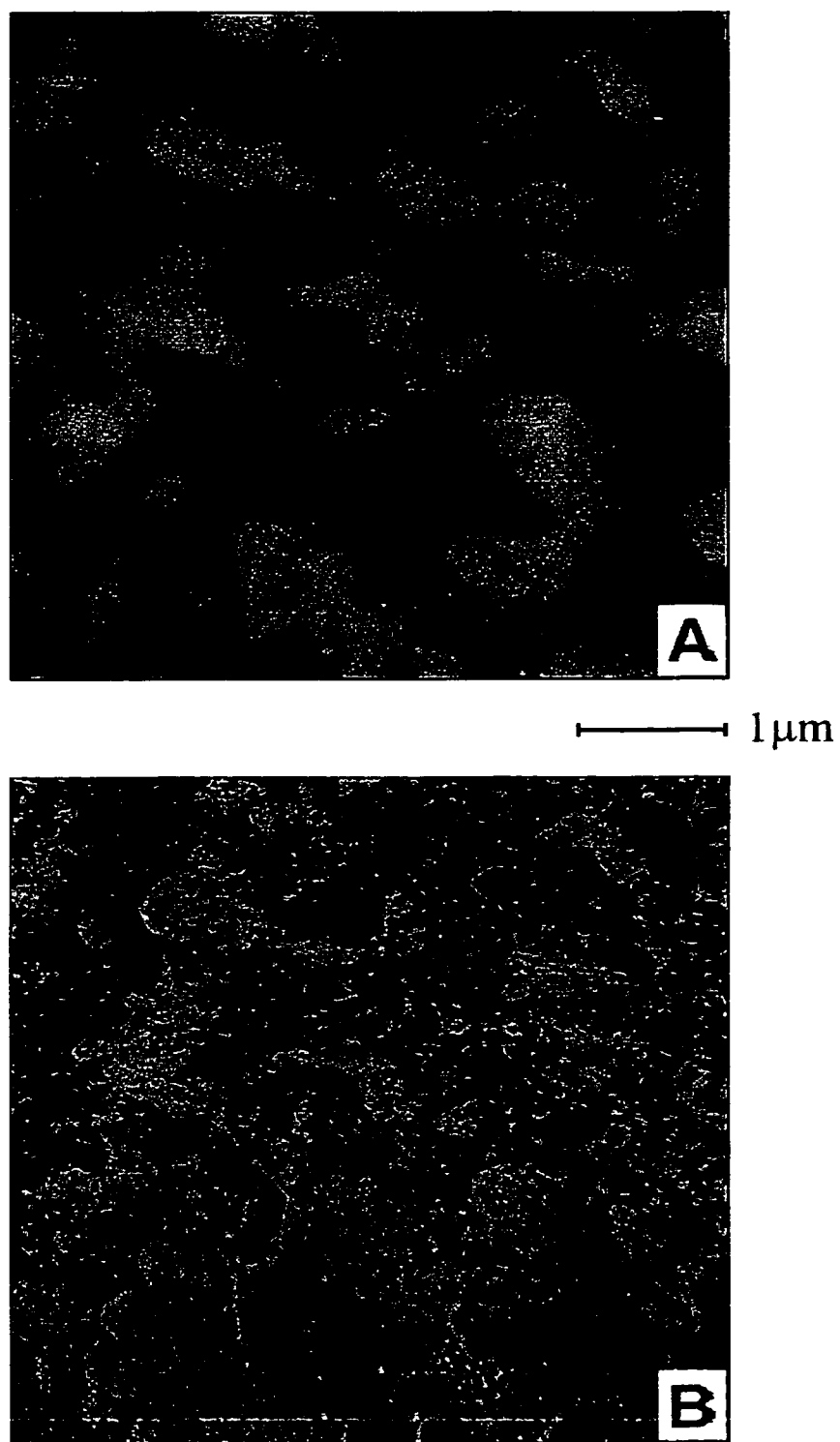


Figure 6.4: Topographic (A, z-scale = 30 nm) and phase contrast (B, z-scale 30°) tapping-mode SFM images of a MHD/SA partial bilayer.

TM-SFM and illustrates the applicability of phase contrast TM-SFM for the chemical imaging of relatively rough surfaces.

We believe the ability of phase contrast imaging to discriminate between the functional groups of our samples involves a mechanism based on adhesive differences between the Si tip and each functional group [16]. Considering surface free energy arguments and recent reports, the adhesion between the hydrophilic Si-OH groups on the tip and $-\text{CO}_2\text{H}$ groups is expected to be higher than that between the tip and $-\text{CH}_3$ groups [3, 5, 8, 10]. Studies which treat a tapping tip/cantilever assembly as a damped oscillator predict that adhesive interactions will result in lower phase shifts and darker contrast in phase images [16, 23, 26]. An adhesion mechanism is further supported by our observed dependence of $\Delta\phi$ on IA stated above. The tip-sample contact time (t_c) is directly related to the IA where lower amplitudes correspond to higher t_c . In the limit of the short contact times involved in TM-SFM (μs range) the number of adhesive interactions between the tip and sample is expected to increase the longer the tip is in contact. Consistent with the proposed adhesion mechanism, we observe an increase in the magnitude of $\Delta\phi$ between $-\text{CH}_3$ and $-\text{CO}_2\text{H}$ groups as t_c is increased.

Conclusions

Our continuing efforts are focused on further elucidating the mechanism of chemically sensitive phase contrast and in developing quantitative descriptions by manipulating adhesive interactions via the use of chemically modified probe tips. In addition, we are applying this methodology to the study of modified electrodes and polymer surfaces. Preliminary results indicate that tip induced surface perturbations limit the use of frictional force imaging for the chemical mapping of electrochemically pretreated GC electrodes. However, the intermittent contact of TM-SFM overcomes such difficulties [27].

References

1. N. A. Burnham, D. D. Dominguez, R. L. Mowery, and R. J. Colton, *Phys. Rev. Lett.*, **64**, 1931, (1990).
2. R. C. Thomas, P. Tangyunyong, J. E. Houston, T. A. Michalske, and R. M. Crooks, *J. Phys. Chem.*, **98**, 4493, (1994).
3. S. K. Sinniah, A. B. Steel, C. J. Miller, and J. E. Reutt-Robey, *J. Am. Chem. Soc.*, **118**, 8925, (1996).
4. J. B. Green, M. T. McDermott, and M. D. Porter, *J. Phys. Chem.*, **100**, 13342, (1996).
5. D. V. Vezenov, A. Noy, L. F. Rozsnyai, and C. M. Lieber, *J. Am. Chem. Soc.*, **119**, 2006, (1997).
6. R. M. Overny, E. Meyer, J. Frommer, D. Brodbeck, R. Luthi, L. Howald, H. J. Guntherodt, M. Fujihira, H. Takano, and Y. Gotoh, *Nature*, **359**, 133, (1992).
7. R. M. Overny, E. Meyer, J. Frommer, H. J. Guntherodt, M. Fujihira, H. Takano, and Y. Gotoh, *Langmuir*, **10**, 1281, (1994).
8. C. D. Frisbie, L. F. Rozsnyai, A. Noy, M. S. Wrighton, and C. M. Lieber, *Science*, **265**, 2071, (1994).
9. J. L. Wilbur, H. A. Biebucyk, J. C. MacDonald, and G. M. Whitesides, *Langmuir*, **11**, 825, (1995).
10. A. Noy, C. D. Frisbie, L. F. Rozsnyai, M. S. Wrighton, and C. M. Lieber, *J. Am. Chem. Soc.*, **117**, 7943, (1995).
11. J. B. Green, M. T. McDermott, M. D. Porter, and L. M. Siperko, *J. Phys. Chem.*, **99**, 10960, (1995).
12. M. Radmacher, M. Fritz, J. P. Cleveland, D. A. Walters, and P. K. Hansma, *Langmuir*, **10**, 3809, (1994).
13. C. E. H. Berger, K. O. van der Werf, R. P. H. Kooyman, B. G. de Grooth, and J. Greve, *Langmuir*, **11**, 4188, (1995).

14. Q. Zhong, D. Innis, K. Kjoller, and V. B. Elings, *Surf. Sci. Lett.*, **290**, L688, (1993).
15. Y. T. Tao, *J. Am. Chem. Soc.*, **115**, 4350, (1993).
16. J. Tamayo and R. Garcia, *Langmuir*, **12**, 4430, (1996).
17. B. Anczykowski, D. Kruger, and H. Fuchs, *Phys. Rev. B*, **53**, 15485, (1996).
18. R. G. Winkler, J. P. Spatz, S. Sheiko, M. Moller, P. Reineker, and O. Marti, *Phys. Rev. B*, **54**, 8908, (1996).
19. S. N. Magonov and M. G. Heaton, *American Laboratory*, **April**, 59, (1996).
20. P. Leclere, R. Lazzaroni, J. L. Bredas, J. M. Yu, P. Dubois, and R. Jerome, *Langmuir*, **12**, 4317, (1996).
21. S. N. Magonov, V. B. Elings, and V. S. Papkov, *Polymer*, **38**, 297, (1997).
22. R. Viswanathan, J. Tian, and D. W. M. Marr, *Langmuir*, **13**, 1840, (1997).
23. S. N. Magonov, V. B. Elings, and M. H. Whangbo, *Surf. Sci.*, in press,.
24. D. R. Baselt and J. D. Baldeschwieler, *J. Vac. Sci. Tech. B*, **10**, 2316, (1992).
25. G. Haugstead, W. L. Gladfelter, E. B. Weberg, R. T. Weberg, and T. D. Weatherill, *Langmuir*, **10**, 4295, (1994).
26. D. A. Chernoff, *Proc. Microscop. Microanal.*, 888, (1995).
27. G. K. Kiema, G. Fitzpatrick, and M. T. McDermott, *Anal. Chem.*, **71**, 4306, (1999).

CHAPTER VII

SUMMARY, CONCLUSIONS, AND FUTURE WORK

Summary and Conclusions

The purpose of this research focused on the investigation of a new method for the preparation of chemically modified electrodes. This approach makes use of metal deposition and self-assembly techniques as a method for attaching specific functional groups to GC electrodes. Self-assembly of sulfur-containing molecules onto gold substrates has become a popular method for controlling surface chemistry. Unfortunately, an analogous method which could be applied to carbon substrates does not exist. The preparation of arrays of small, well-dispersed gold particles on GC substrates via electrochemical metal deposition was investigated as a means of attaching functional groups to GC electrodes using self-assembly methods, as illustrated in Figure 1.1. The work presented herein discusses the preparation of gold particle arrays, and their modification with a variety of thiol molecules possessing different terminal functional groups.

The focus of this research can be divided into two phases. The first phase concentrated on the development of a standard method for the production of small, well dispersed, supported gold particle arrays on GC. Gold particles were electrochemically deposited on GC substrates by taking advantage of the nucleation and growth behavior of gold on GC. This behavior is highly dependent on deposition solution concentration and deposition overpotential. We have demonstrated that it is possible to control the size and number density of gold particles by careful choice of these two parameters. The resulting gold deposits were characterized by scanning electron microscopy and electrochemical techniques, such as oxide stripping voltammetry and underpotential deposition of

lead. A method for the determination of gold surface area was developed by integrating the charge under the oxide stripping waves. During the course of these studies it was also discovered that different electrode pretreatment/activation methods have a profound effect on the nucleation and growth behavior of gold on GC, as well as the adhesion of these small metal particles to the underlying GC substrate.

The second phase of this research focused on chemical modification of electrochemically deposited gold particles using self-assembly methods. Initial experiments concentrated on modification of gold particles using long chain alkanethiol adsorbates. A series of alkanethiols of varying chain length were employed. The initial objective of these experiments was to confirm that it is feasible to modify supported gold particles using this method. Modification of gold particles was confirmed using infrared reflection absorption spectroscopy (IRRAS) and electrochemistry. Further studies were aimed at probing the structure of the obtained monolayers. Oxide and catechol blocking experiments were among the methods used to probe the ability of these monolayers to block electrochemical activity at gold particles. It was observed that monolayers formed from longer alkanethiols are more effective at blocking electron transfer at gold particles. The blocking behavior of these monolayers was compared to that of similar monolayers on planar gold films. Finally, multiple deposition and modification steps were attempted in order to assess their feasibility.

The success of these experiments prompted us to extend these studies to include modification using ω -terminated alkanethiols. A variety of functional groups were used including carboxylic acid ($-\text{CO}_2\text{H}$), ethylester ($-\text{CO}_2\text{CH}_2\text{CH}_3$), nitro ($-\text{NO}_2$), and ferrocene ($-\text{Fc}$). As ferrocene and nitro groups are electroactive this provides additional evidence that confirms chemical modification of the gold particles. Cyclic voltammetry experiments demonstrate that it is possible to use this method to attach multiple functional groups to the GC surface by employing

multiple deposition and modification steps. IRRAS was also used to confirm successful attachment of the various functional groups to GC. The results obtained from these experiments complement the results of cyclic voltammetry studies. The significance of these results is that we now have a method for attaching a variety of functional groups to GC substrates. Finally, it was demonstrated that it is possible to subject modified particles to further modification steps such as covalent attachment of a protein or antibody. This method may be used in future experiments for the attachment of enzymes or electron transfer mediators to previously modified particles in the preparation of novel sensor elements.

The results presented herein demonstrate that it is possible to attach functional groups to GC using electrochemical metal deposition and self-assembly methods. However, this method may not be ideal or practical for preparing chemically modified electrodes to be used in routine electroanalysis. One shortcoming of this approach is the adhesion of the gold particles to the GC substrate. Adhesion studies demonstrate that it is difficult to obtain gold particles that display good adhesion to the GC electrode. As a consequence, modified particles may be lost or dislodged from the electrode surface during normal use of the modified electrode. Regardless, this method may still be useful for attaching functional groups to GC surfaces in an effort to evaluate their use as electron transfer mediators or receptors. An advantage of this approach is that it may be possible to prepare segregated domains of specific surface chemistry are created on a conductive electrode substrate. These domains may be located adjacent to electron transfer sites on the GC substrate. A consequence of using self-assembly methods on polycrystalline gold films is that some important electron transfer features or characteristics of the functional group of interest may be missed or overlooked due to blocking of the gold electrode surface by alkane chains used to tether functional groups to the electrode surface. Electron tunneling through the

monolayer may not become an issue when using supported gold particles. Another shortcoming of this technique is that the fate of multiple gold deposition steps remains unresolved. Results indicate that gold deposition on existing modified particles appears to disrupt the existing monolayer.

Suggestions for Future Work

Suggestions for future experiments that can be pursued as a continuation of this research will now be discussed. As previously alluded to in Chapter III, several experiments have been suggested for further investigation of the effects of electrochemical pretreatment (ECP) on the nucleation and growth behavior of electrochemically deposited metals. These suggestions include SEM analysis as a function of pretreatment time, and the effects of employing a cathodization step immediately following ECP. Such investigations may reveal gold particles that display superior adhesion to gold particles on polished GC.

Another avenue that may be explored is the attachment of biomolecules, such as enzymes and proteins, and other suitable electron transfer mediators to GC electrode surfaces by covalent attachment to chemically modified gold particles. Kuwana and coworkers have shown that covalent attachment of dopamine to carbon electrodes produces an electrode that is useful for NADH analysis [1, 2]. It should be possible to immobilize dopamine on the surface of 11-mercaptoundecanoic acid (MUDA) modified gold particles via amidization. It would be interesting to observe the properties of such an electrode as applied to the electrochemical analysis of NADH.

References

1. D. C. Tse and T. Kuwana, *Anal. Chem.*, **50**, 1315, (1978).
2. C. Ueda, D. C. Tse, and T. Kuwana, *Anal. Chem.*, **54**, 850, (1982).